Development of Adsorbents for Enhanced and Stable Carbon dioxide Capture

THESIS

Submitted in partial fulfilment
of the requirements for the degree of

DOCTOR OF PHILOSOPHY

by

RAMADURGAM ANIRUDDHA
ID. No. 2019PHXF0409H

Under the supervision of
Prof. I. SREEDHAR

BITS Pilani
Pilani | Dubai | Goa | Hyderabad

BIRLA INSTITUTE OF TECHNOLOGY AND SCIENCE, PILANI
2024

Birla Institute of Technology & Science, Pilani
Hyderabad Campus

CERTIFICATE

This is to certify that the thesis entitled **"Development of Adsorbents for Enhanced and Stable Carbon dioxide Capture"** and submitted by **RAMADURGAM ANIRUDDHA, ID No. 2019PHXF0409H** for award of Ph.D. of the Institute embodies original work done by him under my supervision.

Signature of the supervisor

Name in capital letters: INKOLLU SREEDHAR

Designation: Professor

Date: 5/4/2024

Dedicated to my parents, mentors, friends, family, and well-wishers

Declaration

The research work embodied in this thesis entitled "**Development of Adsorbents for Enhanced and Stable Carbon dioxide Capture**" has been carried out by me under the supervision Prof. I. Sreedhar, Department of Chemical Engineering, BITS-Pilani Hyderabad Campus, India. This work is original and has not been submitted in part or full for any degree to this or any other university.

Signature:

Name: RAMADURGAM ANIRUDDHA

Date: 5/4/2024

Acknowledgements

I wish to convey my deepest gratitude towards **Prof. I. Sreedhar**, my supervisor and the HoD of Chemical Engineering department, for his invaluable guidance throughout my academic journey. Under his mentorship, I was granted a greater autonomy in my work, fostering an environment where independent idea generation thrived. Prof. I. Sreedhar's active support and infectious enthusiasm for research have become a perennial source of motivation, shaping not only my academic pursuits but also my approach towards problem-solving.

I extend my heartfelt thanks to the esteemed members of my Doctoral Advisory Committee (DAC), **Prof. Vikranth Kumar S** and **Dr. Satyapaul A. Singh**. Their consistent support, encouragement, and invaluable scientific insights have played a pivotal role in shaping the trajectory of my research endeavors. I am equally grateful to the entire faculty in the Department of Chemical Engineering for their outstanding coursework, excellent facilities, and inspirational leadership. Special recognition is due to the dedicated technical staff (**Mr. Appala Reddy**, **Mr. Bhaskara Raju**, **Mr. Muddasir Khan**, and **Mr. Somi Reddy**) for their valuable coordination and support.

I would also like to thank **Prof. Ramakrishnan Ganesan**, the faculty in charge of the Central Analytical Laboratory (CAL), for granting access to state-of-the-art characterization facilities. I would also like to express my gratitude to the diligent technicians at CAL-I and CAL-II for their prompt support and assistance.

In reflecting on my academic journey, I feel truly blessed to have formed meaningful connections with friends on the BITS-Hyderabad Campus, who have become a chosen family. My deepest gratitude is reserved for fellow research scholars, whose collective camaraderie, support, shared lessons, beliefs, and encouraging conversations have enriched not only my academic pursuits but also my personal growth.

I am eternally grateful to my parents, **Ramadurgam Gururaj** and **Gadag Umarani**, for their unwavering love and support at every juncture of my life. Their steadfast belief in my capabilities has been a guiding light, propelling me forward in both my academic and personal endeavors.

Ramadurgam Aniruddha

Abstract

Global warming, characterized by the gradual increase in Earth's average surface temperature, has been a pressing environmental issue for the past few decades. The driving force of this phenomenon is the rising levels of carbon dioxide (CO_2) within the Earth's atmosphere. This essay delves into the historical context of global warming, elucidates the mechanisms underpinning the surge in atmospheric CO_2, and explores carbon capture as an effective tool for mitigating this alarming trend. Global warming as a scientific concern has its roots in the late 19th century when scientists first hypothesized that increasing CO_2 concentrations could lead to a greenhouse effect, raising temperatures on Earth. However, it wasn't until the latter half of the 20th century that the issue gained significant attention. The Earth's atmosphere comprises various gases, with CO_2 being a critical one in the context of global warming. CO_2 is a greenhouse gas, which means it can trap heat from the sun within the Earth's atmosphere, contributing to an increase in temperatures. The primary sources of elevated CO_2 in the atmosphere are human activities, particularly the combustion of fossil fuels, deforestation, and industrial processes.

Adsorption has long been recognized as an advantageous and promising separation technology, particularly in the context of large-scale carbon capture. This method offers a multitude of significant advantages that make it a preferred choice for many applications. In this comprehensive discussion, we delve into the compelling features of adsorption as a commercial separation method and its potential for addressing the challenges of carbon capture. One of the most notable strengths of adsorption lies in its recyclability and exceptional effectiveness. Adsorption processes entail the capture of target molecules, such as carbon dioxide (CO_2), on the surface of solid adsorbents. These materials, often activated carbons or zeolites, exhibit a remarkable ability to attract and retain CO_2 molecules efficiently. This effectiveness ensures a

high capture efficiency, which is essential in large-scale carbon capture endeavors. Moreover, adsorption materials can be reused multiple times without significant degradation in performance. This recyclability not only reduces waste but also contributes to substantial cost savings. By minimizing the need for frequent replacement of adsorbents, industries can lower the overall expenses associated with large-scale adsorbent material manufacture.

In this thesis, a comprehensive approach was taken to address the critical need for effective carbon dioxide (CO_2) adsorption, aiming to mitigate air pollution. Various adsorbents and composite materials were meticulously synthesized with a focus on simplicity and efficiency to minimize energy consumption. This strategic approach not only contributes to environmentally sustainable production but also emphasizes a commitment to developing energy-efficient solutions for combating air pollution on a global scale.

This thesis is divided into eight chapters. Chapter 1 introduces the thesis, addressing global warming and emphasizing the role of carbon capture (CC). It reviews CC's technical options, focusing on adsorption, and identifies research gaps. Chapter objectives are set, and the organizational structure is outlined. Chapter 2 details the experimental framework, covering materials, analytical studies, synthesis methods, and the setup for CC and stability studies. Response Surface Methodology (RSM) for experimental design is explained, encompassing initial screening, optimization, and thermo-kinetic studies. Chapter 3 concentrates on CC using Coal Fly Ash (CFA)-derived adsorbents. It covers synthesis, optimization, and thermo-kinetic studies, including cyclic stability. Chapter 4 explores CC using bimetallic ZIFs (Ce/Zn and Ce/Co). It follows a similar structure to Chapter 3, covering synthesis, optimization, thermo-kinetic studies, cyclic stability, and conclusions. Chapter 5 shifts focus to CC using MCM-41-based composites, following the pattern of previous chapters. Chapter 6 examines CC using composites from CFA and ZIF-8, maintaining the structure of previous chapters. Chapter 7 summarizes key findings from experimental chapters, drawing overarching conclusions.

Chapter 8 suggests future research areas, outlining recommendations for further exploration and improvement within the thesis scope.

Keywords: *Composites, ZIF, MCM-41, CO_2 adsorption, Cyclic stability, Adsorption kinetics, Adsorption isotherm, Coal fly ash.*

Table of Contents

List of Tables

List of figures

List of useful abbreviations

CC – Carbon Capture

CCU - Carbon Capture and Untilization

CCS - Carbon Capture and Sequestration/Storage

RSM – Response Surface Methodology

CCD - Central Composite Design

CFAZ – Coal Fly Ash Zeolite

CFA – Coal Fly Ash

MEA – Monoethanolamine

DEA – Diethanolamine

TEPA – Tetraethylene pentaamine

ZIF – Zeolitic Imidazolate Framework

MOF – Metal Organic Framework

Chapter 1: Introduction

1. Introduction

1.1. Global warming and carbon capture

Global warming, characterized by the gradual increase in Earth's average surface temperature, has been a pressing environmental issue for the past few decades. The driving force of this phenomenon is the rising levels of carbon dioxide (CO_2) within the Earth's atmosphere. This essay delves into the historical context of global warming, elucidates the mechanisms underpinning the surge in atmospheric CO_2, and explores carbon capture as an effective tool for mitigating this alarming trend [1]. Global warming as a scientific concern has its roots in the late 19th century when scientists first hypothesized that increasing CO_2 concentrations could lead to a greenhouse effect, raising temperatures on Earth. However, it wasn't until the latter half of the 20th century that the issue gained significant attention. The establishment of the Intergovernmental Panel on Climate Change (IPCC) in 1988 played a pivotal role in consolidating scientific evidence and raising global awareness about the impending threat of global warming [2].

The Earth's atmosphere comprises various gases, with CO_2 being a critical one in the context of global warming. CO_2 is a greenhouse gas, which means it can trap heat from the sun within the Earth's atmosphere, contributing to an increase in temperatures. The primary sources of elevated CO_2 in the atmosphere are human activities, particularly the combustion of fossil fuels, deforestation, and industrial processes.

1. Fossil Fuel Combustion: The burning of fossil fuels such as coal, oil, and natural gas for energy production and transportation stands as the largest contributor to rising CO_2 levels. Historical records from the World Bank demonstrate that global fossil fuel consumption steadily increased throughout the 20th century, with a sharp acceleration in the latter half.

2. Deforestation: Another significant contributor to the increase in atmospheric CO_2 is deforestation. As forests are cleared for agriculture, urbanization, and timber harvesting, the carbon stored in trees is released into the atmosphere. A study published in the journal "Nature" in 2020 indicated that deforestation is responsible for approximately 15% of global CO_2 emissions.

3. Industrial Processes: Industrial activities, including cement production, chemical manufacturing, and other processes, release CO_2 as a byproduct. The industrial sector's contributions to atmospheric CO_2 levels have been well-documented in various studies and reports.

The greenhouse effect resulting from heightened CO_2 levels has led to a litany of adverse effects, including more frequent and severe heatwaves, rising sea levels, and disruptions in global weather patterns. In response to the pressing need to reduce CO_2 emissions and mitigate global warming, scientists and engineers have explored a range of strategies. One of the most promising approaches is carbon capture and utilization (CCU) or carbon capture and sequestration (CCS). Carbon capture involves the capture of CO_2 emissions from various sources before they are released into the atmosphere. These captured emissions can then either be stored underground in geological formations (CCS) or converted into valuable products such as fuels, chemicals, or construction materials (CCU) [3].

While carbon capture holds promise as a mitigation strategy, several challenges and barriers had to be addressed to realize its full potential. One significant challenge was the high cost associated with CCS infrastructure and operations. Research by the Global CCS Institute estimated that the cost of CCS could be several times higher than traditional emissions reduction measures. However, ongoing advancements in technology and economies of scale were expected to reduce these costs over time.

To address the challenges associated with carbon capture and utilization, extensive research and development efforts were underway. The U.S. Department of Energy (DOE), for instance, established the Carbon Utilization Program, which funded research projects aimed at developing innovative CCU technologies. These efforts included exploring novel materials and processes to enhance the efficiency and economic viability of carbon capture and utilization. Moreover, international collaborations and initiatives focused on scaling up carbon capture technologies. The Mission Innovation Carbon Capture, Utilization, and Storage Challenge, which brought together governments and industry stakeholders from multiple countries, aimed to accelerate the deployment of CCS and CCU technologies and drive down costs. A study published by Zhang et al. [4] explored the potential of a novel sorbent for carbon capture, which demonstrated higher efficiency and lower costs compared to traditional methods. This research highlighted the ongoing advancements in carbon capture technologies.

Global warming, driven by the increasing levels of CO_2 in the atmosphere, posed a severe threat to the planet's climate and ecosystems. The scientific consensus was clear: human activities were the primary drivers of this phenomenon. To mitigate global warming and limit its catastrophic consequences, it was imperative to significantly reduce CO_2 emissions. Carbon capture and utilization (CCU) and carbon capture and storage (CCS) stood out as promising strategies to achieve this goal.

1.2. Carbon capture methodologies and technologies

Carbon capture and storage (CCS) is a crucial technology in the fight against climate change, aiming to reduce the release of carbon dioxide (CO_2) into the atmosphere. There are three significant methodologies for CCS: post-combustion, pre-combustion, and oxyfuel combustion. These methods play a pivotal role in mitigating the impact of CO_2 emissions from various industrial processes, particularly in the energy sector.

In the post-combustion method, CO_2 is captured from the flue gases after the combustion process of fossil fuels is completed [5]. This approach is particularly significant because it offers a retrofitting option for existing fossil fuel power plants to incorporate CCS technology. Post-combustion capture is widely prevalent in research and application due to its adaptability to existing infrastructure. It involves capturing CO_2 from the exhaust gases, which are a mixture of various components, primarily nitrogen and CO_2. This method typically employs various solvents or adsorbents to selectively capture CO_2, leaving behind other gases that can be released into the atmosphere [6]. Research and development efforts in post-combustion capture have led to the creation of efficient and cost-effective technologies. For instance, amine-based solvents have been widely used in post-combustion capture systems. Studies have focused on improving the efficiency of these solvents and minimizing energy consumption during the capture process.

The pre-combustion method involves a series of chemical processes that occur before the combustion of fossil fuels. In this approach, the fuel is first converted into a mixture of hydrogen (H_2) and carbon monoxide (CO). Subsequently, CO_2 is captured from this mixture before the combustion process begins [7]. The pre-combustion method offers several advantages. Firstly, it produces a relatively pure stream of CO_2, making capture more efficient. Secondly, the hydrogen generated during the process can serve as a valuable energy source for

other industrial applications, reducing waste and enhancing overall energy efficiency. One of the key reactions involved in this method is the water gas shift reaction, where steam is added to the mixture to convert CO to CO_2, which can then be readily separated from the hydrogen [8]. Ongoing research in pre-combustion capture focuses on optimizing the processes involved, exploring alternative feedstocks, and developing more efficient catalysts to enhance the overall performance of the method.

The oxyfuel combustion method is similar to the post-combustion method in many aspects, with a significant difference being the use of pure oxygen instead of air in the combustion of fossil fuels. By utilizing pure oxygen, the resulting flue gas primarily consists of carbon dioxide and water vapor. In the oxyfuel combustion process, the water vapor in the flue gas is condensed through cooling, and the condensed water is then separated. What remains is an almost pure stream of carbon dioxide, which can be transported to a sequestration site for storage. This method is particularly efficient in terms of CO_2 capture because it produces a nearly pure CO_2 stream. However, the generation of pure oxygen can be energy-intensive, which presents its own set of challenges. Oxyfuel combustion has seen significant advancements, particularly in optimizing combustion conditions and addressing energy requirements. Additionally, ongoing research explores innovative ways to generate pure oxygen more efficiently and sustainably.

Carbon capture and storage (CCS) technologies have emerged as critical tools in addressing the global challenge of reducing carbon dioxide (CO_2) emissions and combatting climate change. These methods employ a range of innovative techniques, each uniquely suited to specific industrial applications and environmental conditions. Among the most notable CCS methods are absorption, adsorption, membrane separation, cryogenic distillation, and chemical looping combustion.

Absorption stands as a well-established method for capturing CO_2 from gas streams, particularly those generated by industrial processes and power plants. In this process, CO_2 is introduced into a liquid phase, facilitating its separation from the gas mixture. Frequently employed substances for absorption include mono-ethanol amine (MEA) and similar compounds, known for their high affinity for CO_2 molecules. As CO_2 dissolves into the liquid, it can be efficiently captured and subsequently separated from the gas stream. The advantage of absorption lies in its adaptability to a wide range of industrial processes, making it a prevalent choice for retrofitting existing facilities to include CCS technology [9].

Adsorption, another noteworthy CCS method, involves capturing CO_2 molecules on the surface of solid porous materials, such as activated carbons and zeolites. These materials possess a unique ability to attract and retain CO_2, making them highly effective adsorbents. Adsorption is celebrated for its versatility in capturing CO_2 from gas streams while offering significant cost benefits. One of its most compelling advantages is the recyclability of adsorbents. These materials can be used multiple times without a substantial decline in performance, reducing both waste and the expenses associated with large-scale material production. This inherent recyclability contributes to making adsorption a sustainable and cost-effective choice for carbon capture.

Membrane separation technology relies on semipermeable membranes designed to selectively separate CO_2 from gas mixtures. These membranes allow CO_2 molecules to permeate while blocking other components. Membrane separation is highly regarded for its energy efficiency, as it enables the production of high-purity CO_2 streams with relatively low energy consumption. This method is particularly well-suited for applications where purity and energy efficiency are paramount, such as natural gas processing and hydrogen production. The ability to tailor membranes for specific separation needs adds to the versatility of this approach [10].

Cryogenic distillation is an effective technique for separating gaseous components based on differences in their boiling points. This process involves cooling the gas mixture to very low temperatures and high pressures, causing components like CO_2 to condense into a solid state. The condensed CO_2 can then be collected in a separate chamber. Cryogenic distillation is particularly advantageous for separating CO_2 from gas mixtures, providing high-purity CO_2 streams. This method finds application in various industries, including natural gas processing and air separation [11].

Chemical looping combustion represents a cutting-edge technology that employs a dual reactor bed system. In CLC, a specific metal oxide serves as the oxidizing agent responsible for converting fuel to CO_2 during combustion. The reduced metal oxide is subsequently regenerated and used to capture the CO_2 produced during the combustion process. CLC offers a unique approach to carbon capture while producing high-purity CO_2 streams. It is particularly relevant for applications where combustion is inherent, such as power generation and industrial processes [12].

In summary, carbon capture and storage methods play a pivotal role in addressing the urgent need to reduce CO_2 emissions and combat climate change. These techniques, including absorption, adsorption, membrane separation, cryogenic distillation, and chemical looping combustion, offer diverse solutions tailored to specific industrial settings and environmental conditions. Among these methods, adsorption stands out as a cost-effective and versatile option, characterized by its recyclability and applicability across a wide range of temperatures and pressures. By implementing and advancing these CCS technologies, we can make significant strides toward a more sustainable and environmentally responsible future.

1.3. Adsorption based carbon capture

Adsorption has long been recognized as an advantageous and promising separation technology, particularly in the context of large-scale carbon capture. This method offers a multitude of significant advantages that make it a preferred choice for many applications. In this comprehensive discussion, we delve into the compelling features of adsorption as a commercial separation method and its potential for addressing the challenges of carbon capture.

One of the most notable strengths of adsorption lies in its recyclability and exceptional effectiveness. Adsorption processes entail the capture of target molecules, such as carbon dioxide (CO_2), on the surface of solid adsorbents. These materials, often activated carbons or zeolites, exhibit a remarkable ability to attract and retain CO_2 molecules efficiently. This effectiveness ensures a high capture efficiency, which is essential in large-scale carbon capture endeavors. Moreover, adsorption materials can be reused multiple times without significant degradation in performance. This recyclability not only reduces waste but also contributes to substantial cost savings. By minimizing the need for frequent replacement of adsorbents, industries can lower the overall expenses associated with large-scale adsorbent material manufacture.

Adsorption techniques offer a cost-effective alternative for carbon capture compared to other separation methods such as absorption or membrane technology. The materials required for adsorption, including activated carbons and zeolites, can often be manufactured at a significantly lower cost. This cost advantage stems from the relatively straightforward production processes and the abundance of raw materials used in adsorbent manufacturing. Additionally, adsorption's efficiency in capturing CO_2 from gas streams translates to reduced energy consumption and operational costs. These economic benefits make adsorption an

attractive choice for industries seeking efficient and economical solutions for large-scale carbon capture.

Table 1.1: A comparison of various carbon capture technologies

Method	Advantages	Disadvantages
Absorption	• High CO_2 uptake efficiency. • Sorbents can be regenerated by heating/depressurization.	• Absorption efficiency depends upon CO_2 concentration. • Environmental impacts may prove to be hazardous. • Significant energy costs to regenerate the absorbent.
Adsorption	• Adsorbent can be easily recycled. • High uptake efficiency.	• High energy is required for CO_2 desorption.
CLC	• Avoids energy intensive air separations.	• Process is still developmental. • No large-scale operations.
Membrane separation	• The process is developed for a few other gases. • High separation efficiency.	• High operational costs.
Cryogenic distillation	• Mature Technology.	• Viable only for high CO_2 concentrations. • Should be conducted at low temperatures. • Process is very energy intensive

Another significant advantage of adsorption is its versatility in adapting to a wide range of temperatures and pressures. Unlike some separation methods that are limited by specific operating conditions, adsorption can be effectively employed under various environmental and process parameters. This adaptability ensures the applicability of adsorption across diverse industrial settings and facilitates its integration into existing processes without substantial modifications. The ability to operate at different temperature and pressure ranges further enhances the utility of adsorption in scenarios where flexibility and optimization are essential considerations.

Adsorption emerges as a highly favorable separation technology for large-scale carbon capture due to its exceptional features. Its recyclability and capture effectiveness, coupled with its cost-effectiveness and adaptability to diverse operating conditions, make it a compelling choice for industries striving to reduce CO_2 emissions. Adsorption's ability to efficiently capture CO_2 while minimizing costs and waste aligns with the imperative to transition toward more sustainable and environmentally responsible practices. As efforts to combat climate change intensify, adsorption stands as a pivotal technology in the arsenal of solutions for a cleaner and more sustainable future.

Adsorbents play a pivotal role in capturing carbon dioxide (CO_2) from industrial processes and power generation. These adsorbents can be categorized into two overarching classes: physisorbents [13] and chemisorbents [14], each with its unique characteristics and applications. Within physisorbents, we can further explore four distinct categories, while chemisorbents encompass a range of basic substances grafted onto inert and porous materials.

Table 1.2: CO_2 uptake capacity of metal oxide based adsorbents

SNo	Sorbent	Conditions	CO_2 Uptake	Ref
1	$La_{0.5}Ca_{0.5}NiO_3/CeO_2$	773 K	175.1 μmol/g	[15]
2	NiO/CaO	1023 K	8.0 mmol/g	[16]
3	Egg shell CaO	973 K	13.0 mmol/g	[17]
4	Ca-Mn-20	873 K	15.0 mmol/g	[18]
5	Ca_{12} Al_{14} O_{33}	1023 K	7.0 mmol/g	[19]
6	MgO	573 K	2.0 mmol/g	[20]
7	MgO	673 K	3.0 mmol/g	[21]
8	MgO doped CaO	923 K	13.0 mmol/g	[22]
9	$NaNO_3$/MgO	573 K	6.4 mmol/g	[23]
10	Ga-Hydrocalcite	573 K	1.5 mmol/g	[24]
11	Ga-K-Hydrocalcite	573 K	2.0 mmol/g	[25]
12	$Li_6Zr_2O_7$	823 K	5.3 mmol/g	[26]
13	Li_2ZrO_3 (LZ-NP)	953 K	5.7 mmol/g	[27]
14	Li_2ZrO_3-Na_2ZrO_3	773 K	4.5 mmol/g	[28]
15	La-NiO/CaO	923 K	13.2 mmol/g	[29]

The first category of physisorbents includes porous metal oxides and their carbonate salts [30]. These compounds exhibit a strong affinity for CO_2 molecules, making them effective for adsorption (table 1.2). Their porous structures provide ample surface area for CO_2 capture. Additionally, the stability of these materials under various conditions adds to their appeal in CCS applications. Activated carbons (ACs) and their derivatives constitute a second class of physisorbents known for their versatility and excellent thermal stability [31].

Table 1.3: Activated Carbons in CO_2 adsorption

S No	Adsorbent	Conditions	CO_2 Uptake	Ref
1	C-Char	293 K	2.3 mmol/g	[32]
2	KAC-P-10	333 K	2.8 mmol/g	[31]
3	CA-K-1-PEI-60	348 K, 1 bar	2.1 mmol/g	[33]
4	Plastic-Char	273 K, 1 bar	3.5 mmol/g	[34]
5	Pine sawdust AC	273 K, 1 bar	5.8 mmol/g	[35]
6	AC/Fe_3O_4	298 K, 5 bar	1.6 mmol/g	[36]
7	CUPI-8	298 K, 20 bar	5.8 mmol/g	[37]
8	TRI-A-RHA	348 K, 1 bar	3.9 mmol/g	[38]
9	K3K5	273 K, 1 bar	6.5 mmol/g	[39]
10	AC O S	273 K, 1 bar	5.2 mmol/g	[40]
11	Biomass combustion bottom ash-derived AC	323 K, 1 bar	1.9 mmol/g	[41]
12	KOH + alum AC	273 K, 1 bar	4.5 mmol/g	[42]
13	PCAC-750-2	273 K	6.5 mmol/g	[43]
14	TOK-900	273 K, 1 bar	6.8 mmol/g	[44]
15	Bamboo AC	293 K, 1 bar	3.4 mmol/g	[45]

ACs have been extensively studied and reported in the context of CCS (table 1.3). These adsorbents offer a wide range of applications due to their ability to efficiently capture CO_2 from gas streams [46]. Zeolites and mesoporous silicas form the third category of physisorbents [47]. These materials act as natural molecular sieves and possess a strong affinity for acidic gases (table 1.4). Moreover, their pH tunability allows for tailored CO_2 capture under specific conditions [48]. Zeolites, in particular, are considered promising options for commercial use in both CO_2 capture and conversion applications [49].

Table 1.4: Zeolites in CO_2 adsorption

S No	Adsorbent	Conditions	CO_2 Uptake	Ref
1	13X-ODTMS	293 K	4.0 mmol/g	[50]
2	$Na_{67.95}Li_{17.15}$-CP	273 K, 1 bar	3.6 mmol/g	[51]
3	Kaolinite 4A	298 K, 1 bar	2.5 mmol/g	[52]
4	MCM-41-450-N60	298 K, 1 bar	2.3 mmol/g	[53]
5	ZTC-NS	298 K, 1 bar	6.0 mmol/g	[54]
6	Na13X	308 K, 1 bar	3.5 mmol/g	[55]
7	Sil-ZSM-B	298 K, 1 bar	2.1 mmol/g	[56]
8	0.6NaOH-48 h	273 K, 1 bar	1.9 mmol/g	[57]
9	LiX Zeolite	298 K, 1 bar	5.6 mmol/g	[58]
10	UiO-66/zeolite Y	298 K, 30 bar	14.6 mmol/g	[59]
11	H-SSZ-13(RH)	298 K, 1 bar	2.7 mmol/g	[60]
12	A5 Zeolite	273 K, 30 bar	5.2 mmol/g	[61]
13	HZSM-5/AEEA	321 K	4.4 mmol/g	[62]
14	PDY-7	298 K, 1 bar	5.4 mmol/g	[63]
15	13X-PEI-60	348 K	1.3 mmol/g	[64]

The fourth category of physisorbents encompasses innovative materials such as metal organic frameworks (MOFs), covalent organic frameworks (COFs), and microporous organic polymers (MOPs) [65]. These sorbents are distinguished by their versatility, tunability, and exceptionally large pores (table 1.5). While COFs have shown promise in CO_2 capture research, these materials are better suited for membranous CO_2 separation rather than direct adsorption [66]. Their innovation lies in their potential to revolutionize CCS technologies.

Table 1.5: MOFs and MOPs in CO_2 adsorption

S No	Adsorbent	Conditions	CO_2 uptake	Ref
1	pip-γCD-MOF	333 K, 1.1 atm	0.1 mmol/g	[67]
2	PVAm(0.4)@MIL-101	298 K, 1 atm	3.0 mmol/g	[68]
3	HKUST-1	298 K, 1 atm	3.3 mmol/g	[69]
4	NH_2-β-CD-MOF	273 K, 1 atm	0.5 mmol/g	[70]
5	MIL-101(Cr, Mg)	301 K, 1 atm	1.9 mmol/g	[71]
6	MIL-101 Cr	298 K, 1 atm	1.5 mmol/g	[72]
7	UiO-66/FA_mod	298 K, 1 atm	1.5 mmol/g	[73]
8	Qc-5-Cu	298 K, 1 atm	2.5 mmol/g	[74]
9	SIFSIX-3-Cu	298 K, 1 atm	1.0 mmol/g	[75]
10	Zn(im-P-im)	298 K, 1 atm	3.5 mmol/g	[76]
11	Ni-4PyC	298 K, 1 atm	3.1 mmol/g	[77]
12	PM24@ MIL-101	298 K, 1 atm	2.9 mmol/g	[78]
13	ZIF-90	323 K, 1 bar	2.2 mmol/g	[79]
14	UiO-66	298 K, 1 atm	2.3 mmol/g	[80]
15	NH_2-UiO-66	298 K, 1 atm	3.2 mmol/g	[81]
16	MOF-200	298 K, 1 atm	1.2 mmol/g	[82]
17	GO@ZIF-8	298 K, 1 atm	0.8 mmol/g	[83]
18	MH-0	298 K, 1 atm	4.1 mmol/g	[84]
19	$Fe(pz)[Pt(CN)_4]$	298 K, 1 atm	4.7 mmol/g	[85]
20	MIL-101(Cr)-NH_2	308 K, 1 atm	3.4 mmol/g	[86]
21	UiO-66(Hf)	298 K, 1 atm	1.5 mmol/g	[87]
22	GO-TAc/MOF-60	298 K, 1 atm	5.6 mmol/g	[88]
23	PPIA-MOF-5(40%)	298 K, 1 atm	3.5 mmol/g	[89]
24	Ni(II)-MOF	298 K, 27 atm	2.7 mmol/g	[90]
25	PAN/HK@HK3-A NFM	273 K, 1 atm	3.9 mmol/g	[91]

Chemisorbents, in contrast, involve basic substances that are loaded or grafted onto inert and porous adsorbents like activated carbons and mesoporous silicas. These basic materials, including amines, alkali and alkaline earth metal hydroxides, and oxides of calcium and magnesium, are incorporated onto inert supports to enhance their CO_2 capture capabilities. Among these, amines and metal hydroxides have garnered significant attention from

researchers due to their effectiveness in enhancing CO_2 uptake values. As research and development in this field continue, adsorbents hold the potential to play a transformative role in achieving a more sustainable and environmentally responsible future.

In the synthesis of CO_2 sorbents, two broad categories of methods are commonly employed: conventional and modern synthesis techniques. Among conventional methods, solvothermal (hydrothermal), electrochemical, and sol-gel methods are prominent. Solvothermal methods have been historically used for multiple sorbent synthesis, involving the heating of reagents dissolved in a universal solvent within a closed autoclave reactor [92]. The resulting crystal sizes are influenced by pressure and temperature, with higher pressures and longer durations yielding larger crystals. Subsequent washing with solvents, often organic ones, is followed, posing environmental concerns [93]. Hydrothermal methods are similar but use water as a solvent instead of organics, offering excellent crystal size control but requiring extended durations and substantial energy [94]. Electrochemical methods are rapid but result in lower pore volumes, poorer crystallinity, and relatively low surface areas [95].

In contrast, modern methods include microwave synthesis, sonochemical methods, spray drying/evaporation, and chemical flow methods. Microwave synthesis exposes reagents to constant microwave radiation, enabling rapid completion within hours but making large-scale synthesis challenging [96]. Sonochemical methods utilize sound frequencies to facilitate reactions, offering fast completion within an hour, but often with low yields [97]. Spray drying/evaporation methods are simple but time-consuming, taking extended periods to yield significant sorbent quantities. Chemical flow methods allow reactions to proceed autonomously, with variable completion times.

1.4. Research Motivation

The imperative to mitigate anthropogenic CO_2 emissions goes beyond immediate environmental concerns. It is deeply intertwined with the broader global effort to achieve sustainable development. By curbing CO_2 emissions, the research aims to contribute to the fulfillment of international agreements like the Paris Agreement, fostering global cooperation to limit temperature rise and mitigate the adverse effects of climate change. The consequences of unmitigated emissions include rising sea levels, disruptions in agriculture, and threats to biodiversity, making the mitigation of CO_2 emissions a critical aspect of ensuring a resilient and sustainable future.

The transformation of coal fly ash (CFA) into CO_2 adsorbents represents a paradigm shift in how society views and manages waste. Beyond waste reduction, this approach aligns with the concept of industrial symbiosis, where one industry's waste becomes another's resource. By converting what was once considered a pollutant into a valuable commodity, researchers contribute to a circular economy model. This circularity not only minimizes the environmental impact of waste but also reduces the demand for raw materials, promoting a more sustainable and resource-efficient industrial ecosystem. Herein, CFA based adsorbents, Na-X and Na-A, were used due to the fact that they offered a high CO_2 affinity among the sorbents that could be synthesized using CFA.

The investigation into the intricate process parameters of CO_2 adsorption involves a deep exploration of physical and chemical phenomena. Researchers explore the thermodynamics and kinetics of adsorption, the impact of pressure swings, and the role of various adsorbent materials. This knowledge is not only fundamental to optimizing existing carbon capture technologies but also lays the groundwork for the development of novel approaches. Understanding the nuances of CO_2 adsorption processes contributes not only to environmental

goals but also to the advancement of scientific knowledge and the potential for breakthrough technologies in separation science.

Lowering the energy requirements for CO_2 adsorption carries implications for broader energy transitions. It aligns with the pursuit of sustainable and low-carbon energy sources. As carbon capture technologies become more energy-efficient, they become more viable options for integration into diverse industries, including power generation, manufacturing, and transportation. The research contributes to the overarching goal of transitioning toward a low-carbon energy landscape, thereby addressing both environmental and energy security concerns on a global scale.

The quest for long-lasting adsorbents involves a meticulous examination of material science, durability testing, and predictive modeling. It requires an understanding of how various environmental factors, including contaminants and temperature fluctuations, affect the structural integrity and performance of adsorbents over time. By seeking materials with prolonged lifespans, researchers contribute to the development of robust and resilient carbon capture systems that can operate seamlessly under real-world conditions. This not only ensures the longevity of infrastructure investments but also reduces the ecological footprint associated with the production and replacement of adsorbent materials.

1.5. Research Gaps

The following are a few existing gaps in the field of CO_2 adsorption.

- Environmental-Friendly Routes of Synthesis Procedures: One of the significant gaps in CO_2 adsorption research lies in the development of environmentally friendly synthesis methods for adsorbent materials. Traditional synthesis routes often involve high energy consumption, hazardous chemicals, and generate significant waste. Researchers are actively exploring more sustainable alternatives, such as green chemistry approaches, sol-gel processes, and bio-inspired synthesis methods. These eco-friendly procedures aim to minimize the environmental footprint of adsorbent production while maintaining or enhancing their CO_2 adsorption properties.
- Thermal and Structural Stability: The thermal and structural stability of adsorbent materials is of paramount importance in CO_2 adsorption applications. High-temperature and pressure conditions, such as those found in flue gas streams, can cause degradation or structural changes in adsorbents, reducing their effectiveness. Research gaps exist in developing adsorbents that can maintain their stability over extended operational lifetimes and continue to capture CO_2 efficiently under harsh conditions.
- Cyclic Stability and Regeneration of Adsorbent: One of the key challenges in CO_2 adsorption technology is the cyclic stability and regeneration of adsorbents. After adsorbing CO_2, the adsorbent needs to release the captured CO_2 for further use or storage. Research in this area focuses on designing regeneration processes that are energy-efficient and can maintain the adsorbent's performance over multiple adsorption-desorption cycles. The development of novel regeneration strategies and materials that reduce energy consumption and enhance cyclic stability is a critical research gap.

- Combinations/Blends of Two or More Adsorbents: Developing hybrid or blended adsorbents by combining two or more materials is an emerging area in CO_2 adsorption research. This approach aims to harness the strengths of different adsorbents, such as high adsorption capacity and selectivity, to address the gaps in individual materials. Research in this domain focuses on optimizing combinations, understanding the synergistic effects, and tailoring materials to specific industrial applications. The challenge lies in identifying the ideal combinations and compositions to achieve enhanced CO_2 capture performance. For this study, sorbents CFAZ/ZIF-8, (Ce,Zn)ZIF-8, (Ce,Co)ZIF-67, ZIF-8@MCM-41, MCM-41/AC/Na and ZIF-8@Na-A were chosen. They were chosen because all of these sorbents have good specific surface areas (500 m^2/g), good CO_2 affinity (30:1 reported selectivity between CO_2 to N_2 uptakes) and potentially high cyclic stability. Also, sorbents CFAZ/ZIF-8 and ZIF-8@Na-A were chosen because they could be synthesized from commercially available waste coal fly ash, in addition to their properties like thermal stability and high CO_2 affinity.

Closing these research gaps is crucial for the advancement of CO_2 adsorption research and its widespread implementation in mitigating greenhouse gas emissions. As the need for efficient carbon capture and storage solutions continues to grow, addressing these challenges will contribute to the development of more sustainable and effective CO_2 adsorption processes.

1.6. Research Objectives

The development and optimization of adsorbents for carbon capture is a multifaceted process that involves several crucial steps and methodologies. To achieve the highest efficacy in capturing carbon dioxide (CO_2) emissions, it is imperative to employ a systematic approach. Here, the key points outlined in the research framework are given:

- Synthesis of novel effective adsorbents/composites: The first step in this research endeavor involves the synthesis of adsorbents and their blends. To accomplish this, various novel and effective protocols were employed. These methods were selected based on their ability to produce adsorbents with specific properties that enhance CO_2 capture capacity. The choice of synthesis protocol significantly influences the characteristics and performance of the resulting adsorbent materials. For this study, sorbents CFAZ/ZIF-8, (Ce,Zn)ZIF-8, (Ce,Co)ZIF-67, ZIF-8@MCM-41, MCM-41/AC/Na and ZIF-8@Na-A were chosen.
- Determining the cyclic stability of adsorbents: To assess the long-term viability and durability of the developed sorbent system, cyclic stability studies are conducted. These studies involve subjecting the adsorbents to multiple cycles from 5 cycles to 50. The goal is to ensure that the sorbent materials can maintain their capture capacity over extended periods of use, thus validating their suitability for real-world applications.
- Obtaining interrelationships between sorbent attributes and uptake performance: A critical aspect of this research is to establish qualitative and quantitative interrelationships between process parameters (temperature, adsorbent loading, duration of feed flow, pressure, amount of amine loaded) and their performance in carbon capture. This analysis helps in understanding how specific synthesis methods influence the physico-chemical properties of the adsorbents and, in turn, affect their

capture efficiency. For sorbents (Ce,Zn)ZIF-8, (Ce,Co)ZIF-67, ZIF-8@MCM-41, MCM-41/AC/Na and ZIF-8@Na-A, RSM was employed in order to obtain these relationships (Chapters 4, 5 and 6).

- Performing adsorption isotherm modelling and thermodynamic studies: Thermodynamic studies are conducted to estimate vital thermodynamic parameters associated with the carbon capture process. These parameters include heat of adsorption. Analyzing these thermodynamic aspects provides insights into the thermodynamic favorability of CO_2 adsorption onto the selected adsorbents. Isotherm modelling studies in this thesis work were done from 1 bar to 4 bar process pressures. For heat of adsorption calculations three temperatures (25 ºC, 40 ºC and 55 ºC) were considered.
- Performing adsorption kinetic modelling: Kinetic studies are a fundamental component of this research. A suitable kinetic model is developed to fit the experimental data and understand the kinetics of the adsorption process. This analysis helps identify controlling regimes within the process and the parameters that influence them. Additionally, it allows for the estimation of kinetic parameters such as rate constants, providing insights into the dynamics of CO_2 capture.

In conclusion, this comprehensive research framework encompasses various stages, from adsorbent synthesis to process optimization and stability assessment. The interplay between synthesis protocols, sorbent attributes, and performance is rigorously studied, and thermodynamic and kinetic analyses provide valuable insights into the feasibility and efficiency of carbon capture. This systematic approach is crucial in advancing the development of effective and sustainable carbon capture technologies.

1.7. Overview of the thesis

Chapter 1: Introduction

The first chapter provides an overarching introduction to the thesis, encompassing the critical aspects of global warming and the pivotal role of carbon capture (CC) in mitigating its impact. It includes a comprehensive review of CC's technical options, emphasizing adsorption as a method and conducting a comparative analysis of various technical approaches. The chapter delves into the review of adsorption-based carbon capture, discussing adsorbents, synthesis methods, performance, contactors, and modeling. It identifies research gaps in this field, sets the objectives of the thesis work, and concludes with an overview of the organizational structure of subsequent chapters.

Chapter 2: Experimental - Materials and Methods

The second chapter outlines the experimental framework, detailing the materials employed for various syntheses, along with analytical studies using techniques such as XRD, SEM, BET, FTIR, and others. It elucidates the synthesis methods adopted and describes the experimental setup for carbon capture and stability studies. The methodology for experimental design using Response Surface Methodology (RSM) is expounded, covering initial screening, carbon capture optimization studies, and cyclic stability studies. Additionally, thermo-kinetic studies, encompassing kinetic and isotherm studies, are presented.

Chapter 3: Carbon capture studies using adsorbents derived from coal fly ash

This chapter focuses on the utilization of adsorbents derived from Coal Fly Ash (CFA) for carbon capture. It begins with an introduction, followed by the synthesis of adsorbents, carbon capture optimization studies, and thermo-kinetic studies, including kinetic and isotherm

studies. Cyclic stability studies and conclusions drawn from this set of experiments are presented in detail.

Chapter 4: Carbon capture studies using bimetallic ZIFs based Ce/Zn and Ce/Co combinations

Chapter 4 explores carbon capture studies using bimetallic Zeolitic Imidazolate Frameworks (ZIFs) based on Ce/Zn and Ce/Co combinations. It follows a similar structure to Chapter 3, with an introduction, synthesis of adsorbents, carbon capture optimization studies, thermo-kinetic studies (kinetic and isotherm studies), cyclic stability studies, and concluding remarks.

Chapter 5: Carbon capture studies using MCM-41 based composites

This chapter shifts the focus to carbon capture studies using composites based on MCM-41. The structure follows the pattern of previous chapters, covering an introduction, synthesis of adsorbents, carbon capture optimization studies, thermo-kinetic studies (kinetic and isotherm studies), cyclic stability studies, and concluding insights.

Chapter 6: Carbon capture studies using CFA derived composites with ZIF 8

The final experimental chapter explores carbon capture studies using composites derived from CFA and ZIF-8. Similar to previous chapters, it includes an introduction, synthesis of adsorbents, carbon capture optimization studies, thermo-kinetic studies (kinetic and isotherm studies), cyclic stability studies, and concluding remarks.

Chapter 7: Summary and Conclusions

This chapter provides a comprehensive summary of the key findings from each experimental chapter, drawing overarching conclusions based on the results obtained.

Chapter 8: Recommendations for future work

The final chapter outlines recommendations for future research, identifying potential areas of further exploration and improvement within the scope of the presented thesis work.

Chapter 2: Experimental materials and methods

2. Experimental materials and methods

2.1. Materials employed

The following chemicals were employed in the synthesis process Zinc nitrate hexahydrate ($Zn(NO_3)_2.6H_2O$) (99% purity), cobalt nitrate hexahydrate ($Co(NO_3)_2.6H_2O$) (99% purity), ceric ammonium nitrate ($(NH_4)_2Ce(NO_3)_6$) (99% purity), cerous nitrate hexahydrate (99% purity), 2-methylimidazole (Hmim) (99% purity), commercial activated carbon, methanol, tetraethyl orthosilicate (TEOS), cetyltrimethylammonium bromide (CTAB), ammonia solution (25%), sodium hydroxide, Potassium hydroxide (99%), Sodium hydroxide (99%), high carbon coal fly ash from Ramagundam Thermal Plant, heavy coal ash, Tetraethylene pentaamine (TEPA), diethanolamine(DEA) and water. All chemicals were purchased from SD Fine Chemicals Ltd and were used without further purification. Design Expert 12 and Origin 2021b student version was also used in experimental design and data fitting respectively.

2.2. Analytical Studies

2.2.1. Scanning Electron Microscopy (SEM)

The Scanning Electron Microscope (SEM) is a remarkable scientific instrument that operates on the principle of scanning a focused beam of high-energy electrons over the surface of a sample [98]. Its primary purpose is to capture high-resolution images of specimens, revealing intricate surface details and offering insights into the sample's composition. SEM is employed across various scientific fields and industries due to its exceptional imaging capabilities.

SEM serves a wide range of purposes across scientific disciplines and industries. In the field of material science, SEM is used to study the microstructure of materials, aiding in material development and quality control by examining grain boundaries, defects, and surface features. In this study, SEM was employed in the upcoming chapters 3-6 for the morphological studies

of synthesized adsorbents. The equipment build is as follows: FEI, Apreo LoVac, retractable STEM 3+ Detector, DBS detector and Aztec Standard EDS system.

2.2.2. X-Ray Diffraction

X-ray Diffraction (XRD) is a crucial analytical technique that plays a vital role in the study of the atomic and molecular structure of crystalline materials. Its fundamental working principle relies on the interaction of X-rays with a crystalline sample, resulting in a unique diffraction pattern [99]. In this work, from chapters 3 to 6, XRD analysis was employed to determine the crystallinity of the synthesized adsorbents. Particularly, XRD was found to be useful in determining the crystallinity of ZIF based adsorbents in chapters 3-6. Also, this technique was useful in differentiating between the low carbon content and high carbon content coal fly ash. The details of the instrument employed is as follows: Make: Rigaku, Model: ULTIMA-IV, Angle range: 5-100°, Cu X-Ray source, scintillation counter and dTex detector.

2.2.3. BET Surface Area analysis

The Brunauer-Emmett-Teller (BET) surface area and Barrett-Joyner-Halenda (BJH) pore volume are critical parameters in the field of materials characterization, particularly for porous materials. These techniques are used to determine the surface area and pore characteristics of solid materials, which has significant implications in fields like materials science, catalysis, and adsorption studies [100].

In all of the subsequent chapters 3-6, BET and BJH analysis was employed in determining the nature of pores and pore structures in all adsorbents. The details of the instrument are as follows: Microtrac Bel, BEL SORP mini II and Software: BEL SORP mini.

2.2.4. FTIR Analysis

Fourier-Transform Infrared Spectroscopy (FTIR) is a versatile analytical technique used to investigate the molecular composition and chemical structure of a wide range of materials. It operates based on the interaction of infrared radiation with a sample and is widely employed in research, quality control, and various scientific fields

FTIR spectroscopy serves a multitude of purposes across various scientific disciplines and industries: FTIR is used for qualitative and quantitative analysis of chemical substances. It is helpful in identifying compounds, functional groups, and structural motifs, providing essential information about the sample's chemical composition. FTIR can also detect and quantify pollutants, greenhouse gases, and volatile organic compounds in the atmosphere, making it a valuable tool for environmental monitoring and air quality assessments. The make of the instrument used in this study is as follows: Jasco, FTIR-4200, Spectral range: 400-4000 nm, Resolution: +/- 0.5, Wavenumber accuracy: +/- 0.01 cm^{-1} , Ge/KBr beam splitter, DLATGS Detector, DRA-81.

2.2.5. TGA Analysis

Thermogravimetric Analysis (TGA) is a sophisticated analytical technique used for the study of material properties, particularly its thermal stability and composition. TGA operates on the principle of continuously measuring the weight of a sample as it is subjected to controlled temperature changes, revealing critical information about its thermal behavior and composition [101]. TGA was employed in Chapter 6 to determine the percentage of TEPA loading achieved. The technical specifications of the TGA unit are as follows: Make: **Setaram**, Model: **Themys one+,** Temperature range: RT- 1600 ℃, TG-DTA measurement range: up to 1600 ℃, DSC measurement range: up to 1600 ℃, Programmable rate: 0.01 to 100 ℃/min, Atmosphere: Nitrogen, Air, Flow rate: 50,100 mL/min and Sensitivity of microbalance: 0.1 mg.

2.3. Synthesis of adsorbents

2.3.1. Fusion-Hydrothermal synthesis

The fusion-hydrothermal method is a technique employed to synthesize zeolites from coal fly ash, a waste product from coal combustion. Zeolites are versatile microporous materials used in various applications, and coal fly ash provides a source of alumina and silica, key components for zeolite synthesis [102,103].

The fusion-hydrothermal method is advantageous as it provides an environment for the formation of crystalline structures, breaking down the fly ash components in the fusion step, rendering them more amenable to zeolite formation during the hydrothermal treatment. The resulting zeolites have the potential for applications in water purification, gas adsorption, and catalysis [104,105]. Moreover, this method contributes to the beneficial utilization of coal fly ash, reducing environmental waste while creating value from a waste product. The specific type and properties of the zeolite depend on the precise conditions and the composition of the initial coal fly ash. The following sorbents were synthesized, in this thesis work, using this method.

The hybrid adsorbent (Chapter 3) was prepared through a combination of fusion and hydrothermal methods. In a ceramic crucible, 5 g of coal fly ash was combined with 2.5 g each of NaOH and KOH. Ceramic crucibles were chosen for this experiment due to their inert nature, which prevents them from reacting with coal fly ash, even when exposed to temperatures as high as 600 ºC. The mass ratio of NaOH to coal fly ash (CFA) and the mass ratio of KOH to CFA were both set at 1:2. The crucible containing the blended mixture was then placed into a furnace and heated to 600 ºC for a duration of 90 minutes. After the heating process, the mixture was allowed to cool to room temperature and was subsequently finely ground before being dispersed in DI water for two hours. Following the mixing process, the contents were

transferred into a borosilicate glass reagent bottle for hydrothermal treatment at 105 ºC over a period of 12 hours. Borosilicate glass reagent bottles were selected for this step due to their inert properties at mild temperatures. Additionally, they offer a more cost-effective alternative to Teflon autoclaves typically used for high-pressure and high-temperature hydrothermal processes. Upon completion of the hydrothermal treatment, the residue was filtered and washed with DI water three times. This entire procedure was repeated using heavy coal fly ash (fly ash with low carbon content). As a result, two distinct adsorbents were prepared and designated as K/Na/CFA-Light and K/Na/CFA-Heavy.

Parallelly, CFA zeolite (Chapter 3) was synthesized through a meticulous two-step approach, incorporating alkali fusion and hydrothermal assistance, as elucidated by de Aquino et al. [106] in 2020. To begin, the raw CFA material was subjected to intense heat, reaching temperatures as high as 800 ºC for a duration of three hours. This rigorous thermal treatment served the vital purpose of eradicating carbon content and other volatile elements, rendering the CFA ready for further transformation. The next phase involved the fusion of the treated fly ash with sodium hydroxide pellets, meticulously maintaining a weight ratio of CFA to NaOH at 1:2. This intimate fusion took place in a furnace, with temperatures reaching 550 ºC, and lasted for a duration of three hours. Following this fusion process, the mixture was allowed to cool naturally, and then, it was carefully introduced into deionized water, where it was subject to 12 hours of continuous stirring. After the stirring phase, the transformed mixture was delicately transferred into a glass autoclave for a hydrothermal treatment that spanned twelve hours. The hydrothermal process, a key step in the procedure, played a crucial role in shaping the final product. Subsequent to the hydrothermal treatment, the product was subjected to a filtration process, followed by three meticulous washes with deionized water. These washes were designed to eliminate any residual alkali from the mixture. The final act was the drying phase,

performed in a hot air oven, lasting for 12 hours. The resulting product, known as CFAZ, embodied the successful synthesis of CFA zeolite.

The synthesis process of Na-A (Chapter 6) began with the combination of CFA and NaOH in a weight ratio of 1:1.5. This mixture was then ground to achieve a uniform powder consistency. Subsequently, the uniform powder was placed into a furnace, where it underwent fusion at a temperature of 550°C for a duration of six hours. This high-temperature treatment was essential for the desired chemical transformation. After the fusion process, the mixture was left to cool off at room temperature. Once cooled, it was carefully transferred into a glass reagent bottle. To this mixture, water was added at a specific ratio: for every 15 grams of the fused mixture, 200 mL of water were added. The addition of water-initiated a thorough stirring process, which was maintained at a rate of 400 rpm for a continuous period of 12 hours. This extended stirring time allowed for proper mixing and chemical interactions. Following the stirring, the mixture was subjected to a filtration step to separate the solid residue from the clear supernatant liquid. The clear liquid obtained after filtration was designated as "solution A" and was preserved for subsequent use. Parallelly, NaOH and $NaAlO_2$ were combined in a weight ratio of 2:1. This mixture was then dissolved in water through high-speed stirring, which continued for a duration of four hours. The resulting solution was labeled as "solution B." To create the final product, 50 mL of solution A were mixed with 20 mL of solution B. The two solutions were thoroughly stirred together for a period of two hours to ensure complete homogenization. Subsequently, the combined mixture was subjected to hydrothermal treatment, which involved maintaining it at a temperature of 105°C for six hours. This hydrothermal process facilitated further chemical reactions and transformations. Upon completion of the hydrothermal treatment, a white residue was left behind. This residue was carefully separated through filtration and then cleansed with deionized (DI) water to remove any impurities. Finally, the cleaned residue was dried in an

oven at 120°C for a duration of 12 hours. This meticulous drying process ensured the final product's stability and readiness for further applications or analysis.

2.3.2. Rapid precipitation synthesis

The "rapid precipitation method" for synthesizing Metal-Organic Frameworks (MOFs) is a technique used to produce these porous adsorbents under mild temperature conditions, typically at or around room temperature (20 °C to 25 °C). Unlike traditional MOF synthesis methods that often involve elevated temperatures, this approach offers several advantages. It uses specific solvents or solvent mixtures conducive to MOF formation at lower temperatures, reducing energy consumption and making the process more accessible [107]. The mild reaction conditions minimize the risk of unwanted side reactions and the degradation of MOF precursors, allowing for greater control over the final product's properties [108,109]. The following sorbents were prepared using this precipitation method.

ZIF-8 was meticulously prepared (Chapters 3, 4, 5 and 6), following a methodology that drew inspiration from the work of Lai et al. [110] in 2014. This process unfolded in a series of carefully orchestrated steps. Initially, 2.5 grams of $Zn(NO_3)_2 \cdot 6H_2O$ were delicately dissolved in 50 mL of deionized (DI) water. Concurrently, 50 grams of 2-methylimidazole were dissolved in an additional 300 mL of DI water. The combination of these two solutions was a crucial moment in the synthesis. It's important to note that the molar ratio of $Zn(NO_3)_2 \cdot 6H_2O$ to Hmim was strictly maintained at 1:70. This marked the initiation of continuous stirring, a pivotal step in the procedure. Over the course of 60 minutes, the mixture was subjected to thorough agitation. Subsequently, the product was meticulously harvested through a filtration process, ensuring the separation of key components. To further refine the product, it underwent a double wash with methanol. The final touch was a gentle drying procedure, conducted at 120 ºC, in a

hot air oven. This step served to eliminate any lingering traces of solvent, leaving behind the pure ZIF-8.

ZIF-67 was prepared as such (Chapter 4). Firstly, 2.5 g of $Co(NO_3)_2 \cdot 6H_2O$ was dissolved in 50 mL of deionized (DI) water. Secondly, 22 g of 2-methylimidazole was dissolved in another 200 mL of deionized water. The zinc nitrate solution was then mixed with the 2-methylimidazole solution under continuous stirring. The mole ratio of $Co(NO_3)_2 \cdot 6H_2O$ to Hmim was fixed to 1:30. The synthesis solution turned purple instantaneously after the two solutions were mixed. After continuous stirring for 60 minutes at 400 rpm, the product was collected by filtration and centrifugation, and then washed with methanol thrice. It was then oven dried overnight at 120ºC to remove all traces of solvent [108].

(Ce,Zn)ZIF-8 was prepared in the following way (Chapter 4). Firstly, 2.5 g $Zn(NO_3)_2.6H_2O$ was dissolved in 50 mL of deionized (DI) water. 2.3 g of $(NH_4)_2Ce(NO_3)_6$ was then dissolved in another 50 mL of deionized water. The mole ratio of $Zn(NO_3)_2 \cdot 6H_2O$ to $(NH_4)_2Ce(NO_3)_6$ was thus fixed to 2:1. The total mole ratio $Zn(NO_3)_2 \cdot 6H_2O$:$(NH_4)_2Ce(NO_3)_6$:Hmim was set to be 1:2:140. Separately, 55 g of Hmim was mixed in 300 mL of deionized water. The zinc nitrate and ceric ammonium nitrate solutions were added quickly to the Hmim solution. The resultant mixture turned pale yellow instantaneously and after continuous stirring for 60 minutes at 400 rpm, the resultant turned slightly deeper yellow. The final product was collected by filtration, and then washed with methanol thrice to remove the dissolved Hmim. It was then dried overnight at 120 ºC to remove all traces of solvent.

(Ce,Co)ZIF-67 was prepared in the following way (Chapter 4). Firstly, 2.5 g $Co(NO_3)_2 \cdot 6H_2O$ was dissolved in 50 mL of deionized (DI) water. 1.87 g of $Ce(NO_3)_3.6H_2O$ was then dissolved in another 50 mL of deionized water. The mole ratio of $Co(NO_3)_2 \cdot 6H_2O$ to $Ce(NO_3)_3.6H_2O$ was fixed to 2:1. The total mole ratio $Co(NO_3)_2 \cdot 6H_2O$:$Ce(NO_3)_3.6H_2O$:Hmim was set to be

1:2:60. Separately, 30 g of Hmim was mixed in 300 mL of deionized water. The zinc nitrate and cerous nitrate solutions were added quickly to the Hmim solution. The resultant mixture turned maroonish purple instantaneously and after continuous stirring for 60 minutes the product turned dark purple. The final product was collected by filtration, and then washed with methanol twice.

2.3.3. In-situ MOF synthesis

The "in-situ method" for synthesizing Metal-Organic Frameworks (MOFs) is a technique where MOFs are formed directly within a specific environment or on a substrate, rather than being synthesized separately and then deposited or incorporated. This approach is characterized by MOF synthesis directly on solid substrates, such as metal-organic surfaces, polymers, membranes, or porous materials, providing precise control over MOF growth and placement. The following sorbents were synthesized using this method.

The synthesis of the combination between CFAZ and ZIF-8, denoted as CFAZ/ZIF-8 (Chapter 3), unfolded in a calculated sequence of steps. 50 grams of Hmim were carefully introduced into 300 mL of deionized water, ensuring a clear and homogeneous solution was achieved through rigorous stirring. To this solution, a sample of the previously crafted CFA zeolite was added, and this mixture was stirred for three hours at 400 rpm. Additionally, 2.5 grams of zinc nitrate, dissolved in 50 mL of water, were introduced into this amalgamation. This blend was left to stir for five hours, facilitating the complete integration of all components. Upon completion of this stage, the product was subjected to filtration, followed by a meticulous cleansing process using a combination of water and methanol. This ensured the removal of any lingering salt and Hmim residues, leaving behind a pure product. The final phase involved a drying process at 120 ºC, spanning 12 hours, resulting in the formation of CFAZ/ZIF-8.

In the synthesis of ZIF-8@MCM-41 (Chapter 5), 50 g of Hmim was dissolved in 300 mL of water. Subsequently, 5 g of MCM-41 was introduced to the solution and stirred for two hours. A precalculated amount of zinc nitrate solution was then added, and the resultant mixture was stirred for approximately three hours. The mixture was filtered with methanol thrice and dried at 120 ºC for 12 hours. Wet impregnation method was employed for the addition of predetermined quantities of DEA as required.

To synthesize MCM-41/AC/Na (Chapter 5), 4.4 g of CTAB was added to 300 mL water along with 25 g of NaOH, and the mixture was stirred until it became clear. To this solution, 10 g of commercial activated carbon was added and stirred for three hours. Following this, 40 mL of TEOS was introduced, and the mixture was further stirred for an additional 12 hours. The contents were transferred to a glass reagent bottle and left undisturbed for half a day. After the natural aging process, the obtained solids were filtered and rinsed with DI water four times. The residue underwent treatment in a furnace at 550 ºC for six hours to eliminate CTAB.

ZIF-8@Na-A was synthesized through in-situ method in the following route (Chapter 6). Calculated weights of Zn $(NO_3)_2.6H_2O$ was mixed in water to form a solution. Simultaneously, calculated weights of Na-A were added to a Hmim solution and stirred for 12 hours. Next, zinc nitrate solution was introduced into the Na-A + Hmim mixture, and the mixture was stirred for a duration of 4 hours. Subsequently, the resulting precipitate was separated by filtration, subjected to a thorough methanol cleaning, and finally, it was dried.

2.3.4. Simultaneous synthesis method

In simultaneous synthesis method, two sorbent materials are synthesized together with chemical synthesis method. In this study ZIF-8@Na-A (Chapter 6) was synthesized through simultaneous method as follows. In this method, all reactants were added in a predetermined order. In one beaker, soln B (refer to section 2.3.1) was mixed with zinc nitrate solution and

stirred for two hours. In another beaker, soln A (refer to section 2.3.1) was mixed with excess Hmim solution and stirred for six hours. Then, both these solutions were mixed with each other quickly and stirred for 12 hours. The resultant precipitate was then filtered, cleaned and dried.

2.3.5. Wetness impregnation method

DEA loaded (Ce,Zn)ZIF-8 (7.5% and 15%) were prepared using the wetness impregnation method with the calculated amounts of DEA (Chapter 4). The ZIF/DEA suspension was stirred at 200 rpm for six hours after which it was dried at 120 ºC to eliminate the water present. The DEA was loaded into the pores of the synthesized structure.

DEA loaded (Ce,Co)ZIF-67 (7.5% and 15%) were prepared by using calculated amounts of DEA (Chapter 4). The ZIF/DEA suspension was stirred at 200 rpm for six hours after which it was dried at 120 ºC to eliminate the water present.

A similar wet impregnation method was employed for the addition of predetermined quantities of DEA as required on the surface of ZIF-8@MCM-41 and MCM-41/AC/Na (Chapter 5).

TEPA was loaded onto the ZIF-8@Na-A (Chapter 6) sorbent via wetness impregnation method [111]. Here a calculated amount of TEPA was added to 4 g of the ZIF-8@Na-A 1:5 adsorbent and mixed with 150 mL of water. After properly dispersing the amine throughout the suspension, the water was removed using oven drying at 130 ºC. Based on four different weight loadings, the four adsorbents were titled 10%, 20%, 30% and 40% loaded.

2.4. Carbon Capture and stability studies

2.4.1. Experimental Set-up

In our experimental configuration, a precise and controlled system was established, comprising an adsorption column equipped with a stationary bed, linked intricately to an electric furnace and the necessary gas supply lines. The core component in regulating the gas flow was the utilization of mass flow controllers, allowing us to maintain a consistent and reliable supply of gases. In the pursuit of precision, the process temperatures were accurately determined and constantly monitored through a meticulously calibrated thermocouple system. Additionally, for temperature regulation, the electric furnace was seamlessly integrated with the primary equipment, ensuring that the experimental conditions remained stable throughout.

The heart of our setup revolved around the gas lines, which were meticulously connected to the inlet of a specialized quartz reactor tube, serving as the fixed bed adsorber. To further enhance the efficiency of our system, we selected quartz wool as the ideal supporting material for the adsorbent contained within the quartz tube. This choice was strategic in order to prevent any entrainment of adsorbent particles in the gas stream during the reaction, thus maintaining the integrity of our experimental conditions. A pivotal element in the setup was the integration of a cyclone separator at the exit of the reactor tube. This instrument served to effectively separate any adsorbent particles that might have otherwise been carried away with the exit gas during the reaction. Its inclusion contributed significantly to the precision and reliability of the results.

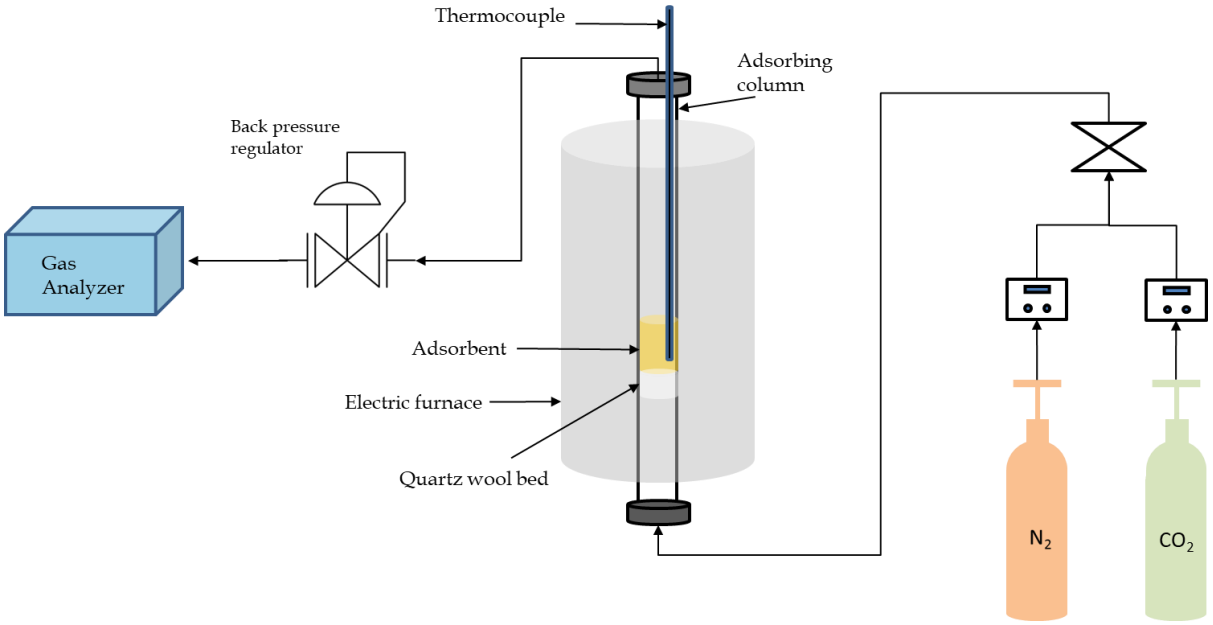

Figure 2.1: Experimental set-up

Subsequently, the exit gas, purified by the cyclone separator, was directed to a condenser. The condenser played a crucial role in cooling the gas to an optimal and suitable temperature level. This step was essential in ensuring the gases' properties were conducive for analysis. To delve into the composition of the gases post-reaction, the gas stream was systematically passed through a sophisticated gas analyzer. This analytical instrument, through its precision and sensitivity, allowed us to gain invaluable insights into the composition of the gas mixture, with particular focus on the percentage of CO_2.

Throughout the duration of the experiment, it was of utmost importance to maintain a constant overall gas flow rate. The CO_2 flow rate was equally critical and was held at a constant. A specific ratio between nitrogen (N_2) and carbon dioxide (CO_2) was deliberately established to enable the gas analyzer to accurately detect the CO_2 percentage within the exit gas stream, ensuring the integrity of our data and results. Specifically, the Technovation SR 2016 model was used to measure outlet CO_2 gas. To standardize our entire process and ensure consistent experimental conditions, the operating pressure was diligently maintained at 1 bar. Achieving

this level of precision and stability required the use of a back pressure regulator, an indispensable tool in conducting adsorption experiments at elevated pressures.

In the experimental studies conducted on CFA-based sorbents (Chapter 3), bimetallic ZIFs (Chapter 4), and MCM-41 based sorbents (Chapter 5), the flowrate utilized was 150 mL/min, with a gas composition consisting of 33% CO_2 and 67% N_2. Similarly, the flowrate and gas composition employed in the CO_2 uptake studies of ZIF-8@Na-A based sorbents (Chapter 6) remained consistent, with a flowrate of 150 mL/min and a gas composition comprising 16.7% CO_2 and the remainder N_2. This standardization of flowrates and gas compositions across the experimental studies ensures comparability and consistency in the evaluation of CO_2 uptake performance among the different sorbent materials investigated in each chapter.

2.4.2. Experimental design using RSM

Response Surface Methodology (RSM) is a powerful and versatile approach to experimental design that is widely used in various fields of science and engineering [112–114]. It is particularly valuable in optimizing and improving processes. Central Composite Design (CCD) is a specific type of RSM that plays a pivotal role in this methodology. CCD, a well-established design of experiments technique, is used to explore and model the response of a system to multiple variables and to find the optimal conditions for desired outcomes. It is highly efficient for situations where there are both linear and quadratic effects and interactions among the variables. CCD involves a set of factorial points at the center of the experimental domain, supplemented by axial points that allow for the estimation of curvature in the response surface [115]. It is a widely adopted choice in RSM because it provides a good balance between accuracy and the number of experimental runs, thus saving time and resources.

RSM, as a broader concept, encompasses CCD but also extends beyond it. It is a systematic and mathematically rigorous approach to modeling and optimizing complex systems. RSM

begins with the identification of independent variables or factors and their levels [116,117]. These factors are manipulated systematically to explore their impact on a dependent variable or response. The data collected from these experiments are then used to develop a predictive model that describes the relationship between the factors and the response. This model is then represented as a response surface, which is a mathematical expression that can be used to predict the process output within the parametric limits [118,119].

RSM is widely utilized in experimental design for various purposes. It allows researchers to determine the optimal set of conditions for a desired outcome, which is critical for process improvement and cost reduction. In chemical engineering, for example, RSM can be used to optimize reaction conditions, leading to higher yields and lower waste production. In product development, it can aid in fine-tuning product attributes to meet consumer preferences. In manufacturing, RSM can be used to improve production processes, resulting in higher efficiency and reduced defects.

Furthermore, RSM is not limited to a specific field. It finds applications in pharmaceuticals, agriculture, environmental science, and even in the development of machine learning algorithms. In agriculture, RSM can optimize crop growth conditions, ensuring higher yields and resource efficiency. In environmental science, it can help design experiments to study complex systems, such as ecosystems or pollution control, and identify critical factors affecting them [30]. In the realm of machine learning, RSM can be applied to optimize hyperparameters and model performance, thereby accelerating the development of more accurate models. In conclusion, RSM, is a powerful approach in experimental design. It enables researchers and engineers to systematically explore complex systems, develop predictive models, and optimize processes across a wide range of disciplines. Its broad applicability makes it an indispensable tool for enhancing product quality, process efficiency, and scientific understanding.

2.4.3. Initial Screening

The initial screening of CO_2 adsorbents is critical for identifying effective materials to capture and store carbon dioxide, crucial for combating climate change. Three primary factors, ease of synthesis, initial CO_2 adsorption capacity, and BET surface area, are key considerations during this screening process. Ease of synthesis evaluates factors like simplicity, cost-effectiveness, and resource availability, influencing scalability and practical implementation. Cost-effective, readily producible materials align with project budgets and streamline adoption in carbon capture systems. Initial CO_2 adsorption capacity measures efficiency in capturing CO_2, crucial for maximizing capture from emissions sources. Higher capacity means less material needed, leading to space and energy savings and scalability for major emissions sources. BET surface area quantifies available surface for adsorption, impacting efficiency. Higher surface area allows for increased adsorption capacity and faster capture, with potential for gas selectivity. These factors collectively ensure a robust evaluation process for CO_2 adsorbents. However, other factors like cost-effectiveness, operational stability, selectivity, regeneration potential, and environmental impact also influence suitability. The choice of adsorbent depends on project-specific requirements, with different applications prioritizing factors accordingly.

2.4.4. CO_2 Capture optimization studies

Process parameters are crucial in optimizing CO_2 adsorption for enhanced efficiency, cost-effectiveness, and sustainability. These include temperature, pressure, aeration time, adsorbent quantity, and amine concentration. Temperature affects adsorption capacity, with lower temperatures favoring higher capacity but requiring more energy for control. Pressure also impacts capacity, with higher pressures favoring increased adsorption but raising energy costs. Duration of feed flow influences contact between gas and adsorbent, directly affecting capture

rate and operational costs. The amount of adsorbent loaded affects capacity, balancing between increased capture and material costs. Amine concentration influences performance, with higher concentrations improving adsorption but introducing additional costs and complexity. Optimizing these parameters involves finding the balance between maximizing capture efficiency and minimizing energy consumption, costs, and environmental impact, essential for various industrial applications like power generation and chemical manufacturing.To systematically optimize CO_2 adsorption processes using these process parameters, a structured approach is typically employed. This approach often leverages techniques like Response Surface Methodology (RSM) or Design of Experiments (DOE), which provide a systematic framework for experimentation and optimization. The step-by-step outline of this optimization process:

1 Developing a well-structured experimental plan that systematically varies each process parameter within a predetermined range. The selection of parameters and their respective levels should be based on the specific characteristics of the CO_2 adsorption system and the desired optimization objectives.

2 Conducting a series of experiments as per the predefined design, carefully recording the results. The data collected encompasses critical parameters such as CO_2 adsorption capacity and any relevant process variables.

3 Utilizing statistical software and mathematical modeling techniques to construct mathematical models that elucidate the relationships between the process parameters and the CO_2 adsorption efficiency. These models can take various forms, including linear, quadratic, or higher-order models, depending on the complexity of the system.

4 Performing in-depth analysis of the response surfaces, contour plots, and other graphical representations generated from the mathematical models. These analyses are crucial for pinpointing the optimal conditions for CO_2 capture.

5 Implementing optimization algorithms within the statistical software to determine the parameter values that maximize CO_2 capture while respecting defined constraints.

6 Conducting additional experiments to validate the optimized conditions and ensure that the predicted improvements are achievable in practical, real-world settings.

In essence, the overarching goal of this optimization approach is to strike a harmonious balance between maximizing CO_2 capture efficiency and minimizing the associated costs, energy consumption, and environmental impact. By methodically examining the influence of each process parameter and optimizing their values, carbon capture processes become more efficient and sustainable. In this thesis, for chapters 4, 5 and 6, RSM was used to optimize the adsorption processes. Process parameters like temperature, amount of adsorbent loaded, duration of feed flow, process pressure and amine loading percentages. Furthermore, an empirical relation between these parameters and the final CO_2 uptake was developed within these chapters and verified.

2.4.5. Cyclic Stability studies

Cyclic stability studies in CO_2 adsorption are critical for evaluating the long-term performance and reliability of adsorbent materials, which is of paramount importance as the world addresses the urgent need to reduce greenhouse gas emissions and combat climate change. These studies involve subjecting adsorbents to a series of CO_2 adsorption and desorption cycles that replicate real-world operational conditions, helping assess the ability of adsorbents to maintain their efficiency over time [120].

The significance of these studies is that they serve multiple vital purposes. Firstly, they provide a means to evaluate the long-term performance of adsorbents, mirroring the repeated use they undergo in carbon capture processes. This is essential to ensure the sustained efficiency of CO_2 capture over an extended operational lifetime. Secondly, the reliability of adsorbents is

fundamental to the uninterrupted operation of carbon capture facilities, preventing costly downtime due to premature adsorbent degradation or failure. Ensuring the economic viability of carbon capture systems is also closely tied to the long-term stability of adsorbents, as premature degradation can lead to increased operational costs, frequent replacements, and reduced overall efficiency [121]. Environmental sustainability is another crucial aspect, with the durability of adsorbents being directly linked to waste generation and environmental impact. Effective regeneration of adsorbents is critical for reusing them and minimizing waste. Additionally, cyclic stability studies provide valuable data for process optimization, offering insights into how the performance of adsorbents changes over time and allowing for adjustments to operational parameters and conditions to maintain or enhance overall efficiency [122].

In this thesis work, sorbents K/Na/CFA-Light and CFAZ/ZIF-8 were tested for 5 cycles (Chapter 3). The bimetallic ZIF based sorbents (Chapter 4), (Ce,Zn)ZIF-8 and (Ce,Co)ZIF-6, were tested for 15 cycles. Similar to the bimetallic ZIF based sorbents, the MCM-41 based sorbents were also tested for 15 cycles (Chapter 5). The final sorbent, ZIF-8@Na-A 1:5, was tested for 50 cycles, however (Chapter 6). All of these sorbents were tested for sorption at 25 ºC and were regenerated at 150 ºC.

2.5. Thermo-kinetic studies

2.5.1. Adsorption kinetics

Adsorption kinetics is a critical aspect of the field of adsorption science and technology, with profound implications for a variety of applications, including CO_2 adsorption and capture. It deals with the rate at which adsorbate molecules accumulate on the surface of a solid adsorbent, which is essential for understanding and optimizing adsorption processes. In the context of CO_2 adsorption design, adsorption kinetics is of particular importance as it directly influences the efficiency and performance of CO_2 capture systems. Various mathematical models have been developed to describe adsorption kinetics, with the most commonly used ones being the pseudo-first-order model, the pseudo-second-order model, the intraparticle diffusion model, the Avrami model, and Elovich kinetics.

The pseudo first-order model assumes that the adsorption rate is directly proportional to the number of unoccupied sites on the adsorbent surface [123]. The equation can be expressed as:

$$Q_t = Q_e\left(1-e^{-k_1 t}\right) \qquad \textit{Eq 2.1}$$

Where Q_t is the amount of adsorbate adsorbed at time t, Q_e is the amount of adsorbate adsorbed at equilibrium and k is the rate constant of the first-order adsorption process. While the pseudo first-order model is relatively simple, it often fails to accurately describe adsorption kinetics in complex systems [124,125]. It assumes a constant rate of adsorption, which is not always the case, especially when the surface becomes saturated or when competing adsorbate molecules are present [126,127].

The pseudo-second-order model is a more realistic representation of adsorption kinetics [128,129]. It suggests that the rate of adsorption is directly proportional to the square of the

number of unoccupied sites on the adsorbent surface [130–132]. The equation can be expressed as:

$$Q_t = \frac{Q_e^2 k_2 t}{1 + Q_e k_2 t} \qquad Eq\ 2.2$$

Where k_2 is the rate constant of the pseudo-second-order adsorption process. The pseudo-second-order model is more versatile and accurate, particularly for describing the latter stages of adsorption when the surface is nearing saturation. It accounts for the fact that the rate of adsorption decreases as the surface becomes occupied.

The intraparticle diffusion model focuses on the adsorption process within the pores of the adsorbent material [133]. It assumes that intraparticle diffusion is the rate-limiting step [134–137]. The equation can be expressed as:

$$Q_t = k_d \sqrt{t} + C \qquad Eq\ 2.3$$

Where k_d is the intraparticle diffusion rate constant, C is the intercept, representing the boundary layer effect.

The Avrami model, developed by Kolgomorov and Johnson-Mehl-Avrami, is commonly used to describe various phase transition and nucleation processes, including adsorption [138]. This model provides insights into the mechanism of adsorption by analyzing how the surface coverage changes over time [139–142]. The Avrami equation is expressed as:

$$Q_t = Q_e\left(1 - e^{(-k_a t^n)}\right) \qquad Eq\ 2.4$$

Where Q_t is the fractional surface coverage at time t, k_a is the rate constant, n is the Avrami exponent, which provides information about the adsorption mechanism.

Elovich kinetics, proposed by Elovich and Jahnig, is another model used to describe chemisorption processes [143]. It suggests that the adsorption rate decreases over time as the

available active sites on the adsorbent become occupied [144–146]. The Elovich equation is represented as:

$$Q_t = \frac{1}{\beta} \ln[1+\alpha\beta t] \qquad Eq\ 2.5$$

Where Q_t is the amount of adsorbate adsorbed at time t, α and β are constants related to the initial adsorption rate and the desorption rate, respectively.

In the context of CO_2 adsorption, understanding the kinetics of CO_2 adsorption is paramount. Carbon capture and sequestration (CCS) is a critical strategy in the fight against climate change, and adsorption is one of the most promising methods for capturing CO_2 emissions from various sources, such as power plants and industrial facilities [147,148]. The importance of adsorption kinetics in CO_2 adsorption design is extremely crucial. The rate at which CO_2 is adsorbed onto solid adsorbents directly affects the efficiency of the capture process. Slow kinetics can lead to longer contact times, larger adsorption equipment, and increased energy consumption. Therefore, by understanding and optimizing adsorption kinetics, researchers and engineers can enhance the performance and cost-effectiveness of CO_2 capture systems.

Moreover, adsorption kinetics plays a significant role in determining the dynamic behavior of CO_2 adsorption systems. The ability to model and predict how quickly CO_2 is adsorbed, how long it takes to reach equilibrium, and how the adsorbent behaves under varying conditions is crucial for process design and control. For instance, in pressure swing adsorption (PSA) [149–151] and temperature swing adsorption (TSA) systems [152–155], an in-depth understanding of kinetics is essential for optimizing cycle times and improving the overall performance of the process. Additionally, the choice of adsorbent material is closely tied to adsorption kinetics. Different adsorbents exhibit varying rates of CO_2 adsorption, and this can influence the selection of the most suitable adsorbent for a given application. Kinetic parameters, such as

rate constants, can be used to compare and assess the performance of different adsorbents, aiding in the design and optimization of CO_2 capture systems.

Overall, adsorption kinetics is a critical aspect of CO_2 adsorption design. The mathematical models used, including the first-order, pseudo-second-order, intraparticle diffusion, Avrami, and Elovich kinetics, help in characterizing and predicting the rate of CO_2 adsorption on solid adsorbents. This knowledge is pivotal in developing efficient and cost-effective carbon capture and storage technologies, contributing to global efforts to combat climate change and reduce CO_2 emissions.

2.5.2. Adsorption Isotherm studies

Adsorption isotherm modeling is a fundamental aspect of adsorption science, and it holds significant importance in the design and optimization of CO_2 adsorption processes. These models provide a mathematical framework for understanding how adsorbate molecules interact with solid adsorbent surfaces under various conditions. Four widely used adsorption models are the Langmuir, Freundlich, Sips, and Toth models, each offering unique insights into the adsorption process and its application in CO_2 capture and storage.

The Langmuir isotherm model assumes that adsorption occurs at specific sites on the adsorbent surface, and each site can accommodate only one adsorbate molecule. The equation for the Langmuir isotherm is expressed as:

$$q=\frac{q_m k_L p}{1+k_L p} \qquad \textit{Eq 2.6}$$

Where 'q' is the amount of CO_2 adsorbed at time 't', 'q_m' is the monolayer CO_2 uptake, 'k_L' is the Langmuir constant.

The Freundlich isotherm model is an empirical model that describes multilayer adsorption on heterogeneous surfaces. The equation for the Freundlich isotherm is expressed as:

$$q=k_F p^{1/n} \qquad Eq\ 2.7$$

Where 'q' is the amount of CO_2 adsorbed at time 't', 'k_F' is the Freundlich constant, respectively while 'n' is the Freundlich exponent.

The Sips isotherm model, also known as the Langmuir-Freundlich or the Langmuir-like model, is a combination of the Langmuir and Freundlich models. It allows for both monolayer and multilayer adsorption and is described by the equation:

$$q=\frac{q_m k_s p}{[1+k_s p^n]} \qquad Eq\ 2.8$$

Where 'q' is the amount of CO_2 adsorbed at time 't', 'q_m' is the monolayer CO_2 uptake, 'k_S' is the Sips adsorption constant, and 'n' is the measure of heterogeneity in Sips model.

The Toth isotherm model is an alternative to the Langmuir model, accommodating multilayer adsorption and heterogeneity. The equation for the Toth isotherm is expressed as:

$$q=\frac{q_m k_T p}{[1+(k_T p)^n]^{1/n}} \qquad Eq\ 2.9$$

Where 'q' is the amount of CO_2 adsorbed at time 't', 'q_m' is the monolayer CO_2 uptake, 'k_T' is the Toth adsorption constant, and 'n' is the measure of heterogeneity in the Toth model.

In the context of CO_2 adsorption design, these adsorption isotherm models play a crucial role in several ways. First and foremost, they allow researchers and engineers to characterize the adsorption behavior of various adsorbents under different conditions. This information is vital for selecting the most suitable adsorbent materials and designing efficient CO_2 capture systems. The Langmuir model is often used to determine the maximum adsorption capacity of an adsorbent for CO_2 [156]. It helps in identifying whether adsorption occurs in a monolayer fashion, and it provides insights into the strength of the adsorbent-adsorbate interaction [157,158]. This knowledge is instrumental in selecting adsorbents that can efficiently capture

CO_2 from gas streams [159,160]. The Freundlich model is valuable when dealing with heterogeneous adsorbents or adsorption processes that extend beyond monolayer coverage [161]. It helps in understanding the non-uniform distribution of adsorption sites and the adsorption intensity [162]. This is particularly relevant in real-world CO_2 capture scenarios where adsorbent surfaces can be complex and varied [163,164]. The Sips model offers a compromise between the Langmuir and Freundlich models, making it suitable for a wide range of CO_2 adsorption systems [165,166]. It is often applied when the adsorption process involves both monolayer and multilayer adsorption, providing a versatile tool for designing CO_2 capture processes with a balanced approach [167,168]. The Toth model is a valuable alternative to the Langmuir model for cases where monolayer adsorption assumptions may not hold [169,170]. Its ability to account for multilayer adsorption and heterogeneity makes it applicable to a broad spectrum of CO_2 adsorption systems [171,172].

To sum up, adsorption isotherm modeling is a fundamental tool in the design of CO_2 adsorption processes. The Langmuir, Freundlich, Sips, and Toth models, each with their unique characteristics, enable researchers and engineers to understand and predict the adsorption behavior of CO_2 on various adsorbents. This knowledge is pivotal in selecting the right adsorbent materials, optimizing process conditions, and ultimately contributing to the development of efficient and sustainable CO_2 capture and storage technologies to combat climate change and reduce greenhouse gas emissions.

Chapter 3: CO_2 uptake studies using adsorbents derived from coal fly ash

3. CO_2 uptake studies using adsorbents derived from Coal Fly Ash

3.1. Introduction

In addition to its use in construction, coal fly ash has a second life as a precursor for adsorbents. Various types of adsorbents can be synthesized from CFA, including sodalites [104,173], 13-X molecular sieves and NaX [174,175]. These adsorbents have a wide range of applications, particularly in the purification of gaseous pollutants. Their production from CFA demonstrates the resourcefulness of repurposing industrial waste into valuable materials with environmental benefits. Coal fly ash is a versatile and abundant byproduct of industrial processes that has found applications in both the construction industry and the development of adsorbents [176,177]. Its unique properties, coupled with its cost-effectiveness and availability, make it a valuable resource in addressing environmental and sustainability challenges. Whether enhancing the quality of concrete or contributing to the purification of gases, CFA showcases the potential for turning industrial waste into valuable assets in various fields of study and industry. This versatile approach aligns with the principles of sustainability and responsible resource management, making coal fly ash an increasingly important player in our efforts to address environmental concerns.

Recent scientific studies have advanced our understanding of CO_2 adsorption through the utilization of adsorbents synthesized from coal fly ash (CFA). Researchers have undertaken a series of studies to develop efficient and sustainable adsorbents based on CFA. Smith et al. [86] showcased a one-step activation process to synthesize an adsorbent from CFA. This adsorbent exhibited a remarkable CO_2 adsorption capacity, indicating its potential utility in CO_2 uptake and sequestration. Chen et al. [178] expanded on this work by emphasizing the cost-effectiveness of CFA-derived adsorbents. They demonstrated that the abundance of CFA,

combined with the relatively low cost of activation processes, could make these adsorbents an economically attractive choice for CO_2 capture. The structural properties of CFA-based adsorbents play a crucial role in their CO_2 adsorption performance. Recent studies have focused on tailoring the structure of these materials to achieve high surface areas and tunable pore sizes. Kim et al. [179] explored the modification of CFA-derived adsorbents using various activating agents and techniques. By carefully characterizing and optimizing their materials, they achieved adsorbents with enhanced CO_2 adsorption capacities and selectivities. While laboratory-scale experiments are essential for characterizing the materials, the practical application of CFA-based adsorbents in real-world scenarios is equally critical. Recent research has extended into pilot-scale studies to evaluate the feasibility of these adsorbents in industrial settings. Li et al. [180] conducted research that examined the scalability and effectiveness of CFA-derived adsorbents for large-scale CO_2 capture in a pilot-scale plant. Furthermore, recent studies have delved into the mechanistic understanding of CO_2 adsorption on CFA-based adsorbents. Researchers have employed advanced spectroscopic and thermodynamic analyses to elucidate the underlying processes and interactions involved in CO_2 capture. This fundamental knowledge is instrumental in optimizing adsorbent performance and enhancing the overall efficiency of CO_2 uptake systems. The works of Liu et al. [181] and Zhang et al. [182] exemplify this focus on mechanistic insights. Advanced characterization techniques have been pivotal in recent studies. Researchers have employed a range of tools, such as scanning electron microscopy (SEM), transmission electron microscopy (TEM), X-ray diffraction (XRD), and Fourier-transform infrared spectroscopy (FTIR) to understand the morphology, crystal structure, and functional groups of CFA-based adsorbents [183]. Some studies have explored the competitive sorption of CO_2 with other gases, which is particularly important in real-world applications. Studies done by Johnson et al. [184,185] and Song et al. [186] have shed light on the competitive adsorption behavior of CFA-based adsorbents.

Ensuring the regeneration and reusability of adsorbents is a crucial aspect of sustainable CO_2 capture. Recent studies have focused on developing regeneration methods for CFA-based adsorbents. Li et al. [187] explored the regeneration of these adsorbents using a cyclic temperature swing approach, highlighting their potential for long-term use. Environmental assessments have also been a topic of interest in recent studies. Researchers have conducted life cycle assessments to evaluate the overall environmental impact of using CFA-based adsorbents for CO_2 capture. These assessments consider factors such as energy consumption, greenhouse gas emissions, and resource utilization.

The work in this chapter is focused on high carbon content coal fly was utilized in the synthesis of CO_2 adsorbents [188]. KOH and NaOH being metal hydroxides, are highly reactive towards acidic gases. Three process parameters temperature, CO_2 concentration and time of carbonation were varied at four levels each. Also, within the same chapter, a novel combination of a ZIF known as ZIF-8 synthesized upon the CFA-based zeolitic network structure is tested for CO_2 uptake experiments [189]. The reason behind adding ZIF-8 onto the frame of CFA-based zeolite is to try for any enhanced CC values. The addition of ZIF-8 also improves the surface area and pore volume of the respective CFA based zeolite. Four parameters, temperature, amount of adsorbent, time of carbonation and CO_2 concentration, were varied to gauge the overall performance of the as-synthesized adsorbent. The best performing conditions were further tested for cyclic stability and retention capacity for five cycles. Kinetics studies based on three models viz pseudo-first order, pseudo-second order and Avrami models were also conducted.

3.2. Characterization of adsorbents

3.2.1. Characterization studies on double hydroxide fused CFA based adsorbents

The characterization studies conducted included BET, FTIR, XRD, and SEM analyses, and the results are as such. In terms of surface area and pore volume, the unfused coal fly ash exhibited a substantial surface area of 111 m^2/g and a pore volume of 0.23 m^3/g. In contrast, the K/Na/CFA-Light adsorbent, which underwent fusion with alkali metal hydroxides, displayed a reduced surface area of 47 m^2/g and a pore volume of 0.16 m^3/g. This significant decrease is attributed to the fusion process involving alkali metal hydroxides, which not only altered the structural properties of the coal fly ash particles but also partially obstructed the material's pores. The K/Na/CFA-Heavy adsorbent, synthesized through a similar process, exhibited an even lower surface area of 15 m^2/g.

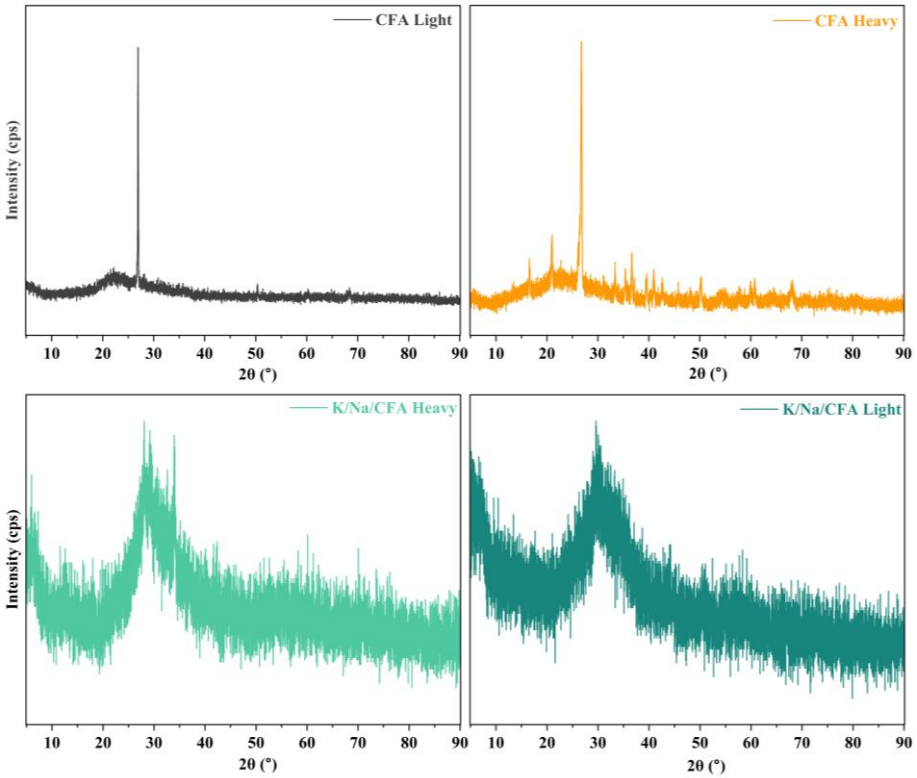

Figure 3.1: Diffractograms of Low carbon content CFA Light, High carbon content CFA, K/Na/CFA Heavy and K/Na/CFA Light adsorbents

Moving on to XRD analysis (figure 3.1), the high carbon content fly ash showed only two prominent peaks at 29.93º and 28.00º, characteristic of high carbon content fly ash's typical amorphous nature due to its substantial carbon content. In contrast, the heavy CFA sample displayed peaks around 16.00º, 20.00º, 26.00º, 36.00º, and 41.00º, indicating a more crystalline presence of silicates and aluminates, possibly indicating the presence of zeolitic phases. Notably, after fusion with KOH and NaOH, both coal fly ash samples became more amorphous, in contrast to the typical behavior in fusion-hydrothermal synthesis with NaOH alone, which usually enhances the zeolitic and sodalitic phases. This deviation could be attributed to the detrimental effect of KOH on crystalline phases, even in the presence of NaOH.

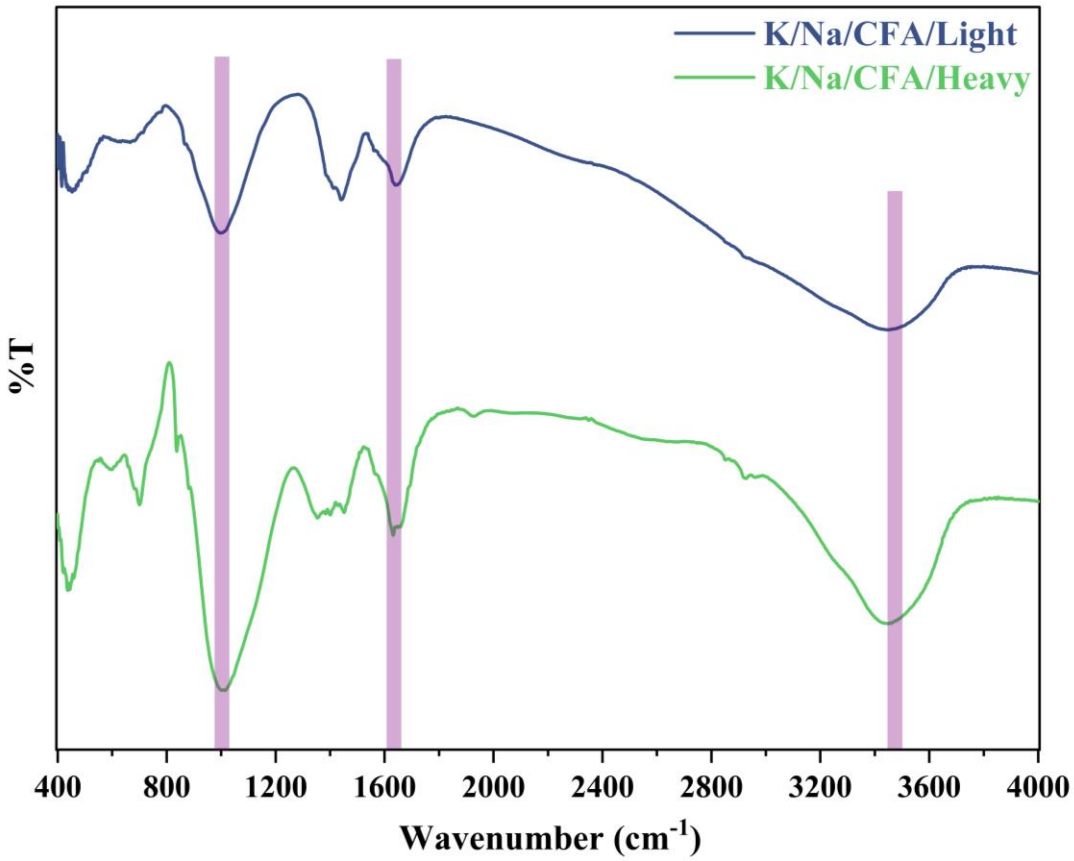

Figure 3.2: Infrared patterns of K/Na/CFA-Heavy and K/Na/CFA-Light adsorbents

The Fourier Transform Infrared (FTIR) analysis, depicted in figure 3.2, revealed significant peaks for the K/Na/CFA-Light and K/Na/CFA-Heavy adsorbents. The K/Na/CFA-Light

adsorbent displayed peaks at 3446 cm^{-1}, 1639 cm^{-1}, 1440 cm^{-1}, 996 cm^{-1}, and 452 cm^{-1}. In comparison, the K/Na/CFA-Heavy adsorbent exhibited peaks at 3446 cm^{-1}, 1631 cm^{-1}, 1451 cm^{-1}, 1351 cm^{-1}, 1014 cm^{-1}, and 435 cm^{-1}. The similarity in intensities at the same wavenumbers underscores the impact of KOH on disrupting the crystalline structures in both parent CFA samples. These FTIR results align with the XRD findings in terms of the degree of amorphous nature. Peaks around 450 cm^{-1} may indicate evidence of zeolitic bending, while Al-O-Si bending was detectable around 990 cm^{-1}.

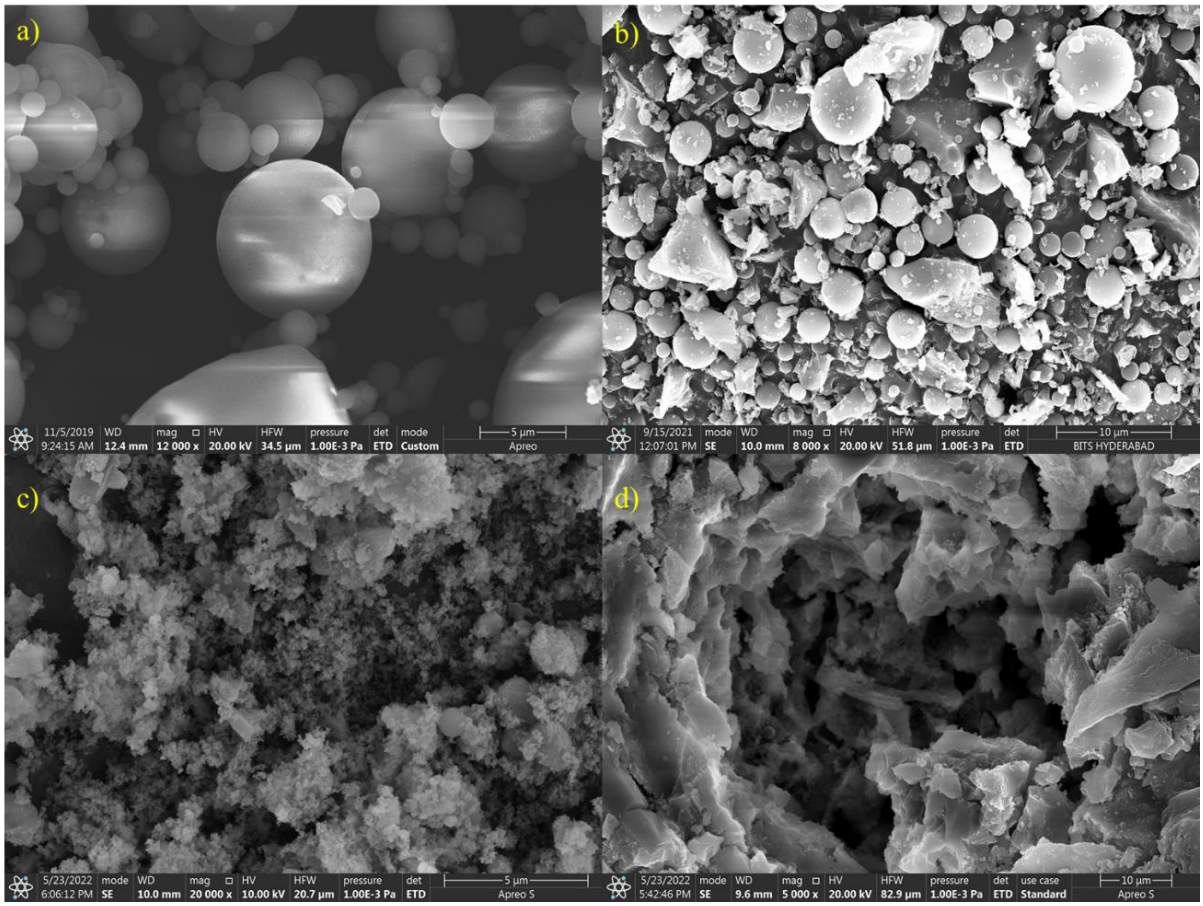

Figure 3.3: SEM Images of a) Low carbon content CFA, b) High carbon content CFA, c) K/Na/CFA-Heavy and d) K/Na/CFA-Light adsorbents

The comprehensive analysis conducted through scanning electron microscopy (SEM) provided valuable insights into the structural characteristics of two distinct unfused coal ash samples. Both samples exhibited geoid type coal fly ash structures, as visually represented in figure 3.3.

However, certain differences could be identified between the two samples: the high carbon content CFA displayed not only the expected geoid structures but also featured random carbonaceous formations, a contrast to the heavy CFA, which lacked such carbonaceous structures. A pivotal aspect of the study involved subjecting both CFA samples to a two-step synthesis process with alkalis. Remarkably, this synthesis process disrupted the typical geoid structure inherent in CFA, as evidenced by SEM analysis. Intriguingly, the high carbon content CFA displayed an amalgamation of geoids and random carbonaceous structures, while the heavy CFA showed a distinct absence of such structures. Further investigation into the K/Na/CFA-Heavy sample revealed intriguing findings. SEM images hinted at the presence of a sodalite flower type structure, a distinctive feature not observed in the K/Na/CFA-Light sample. Complementing this observation, Fourier-transform infrared (FTIR) analysis of the K/Na/CFA-Heavy sample indicated zeolitic bending. This intriguing result suggested that the destructive fusion process involving KOH might not have been as thorough in the K/Na/CFA-Heavy sample when compared to its lighter counterpart. Contrastingly, the K/Na/CFA-Light sample exhibited a near-complete destruction of the geoid structure, as observed through SEM analysis. These findings were further corroborated by X-ray diffraction (XRD) analysis, providing additional support to the SEM results.

3.2.2. Characterization studies on CFA based composite adsorbents

The following are the characterization studies employed: BET, SEM, XRD and FTIR. The N_2 adsorption isotherms are provided in figure 3.4. ZIF-8 as synthesized recorded a surface area of 1500 m^2/g whilst CFAZ/ZIF-8 recorded a surface area of only 426 m^2/g in comparison. However, this is much higher that the of raw CFA surface area of 5 m^2/g and the 28 m^2/g of CFA derived zeolite type adsorbents. Mean pore diameters of 1.896 nm and 2.398 nm for ZIF-8 and CFAZ/ZIF-8 respectively also indicated that both showed considerably high degree of microporosity. Microporous volumes of ZIF-8 and CFAZ/ZIF-8 were determined to be 0.51 cc/g and 0.18 cc/g respectively.

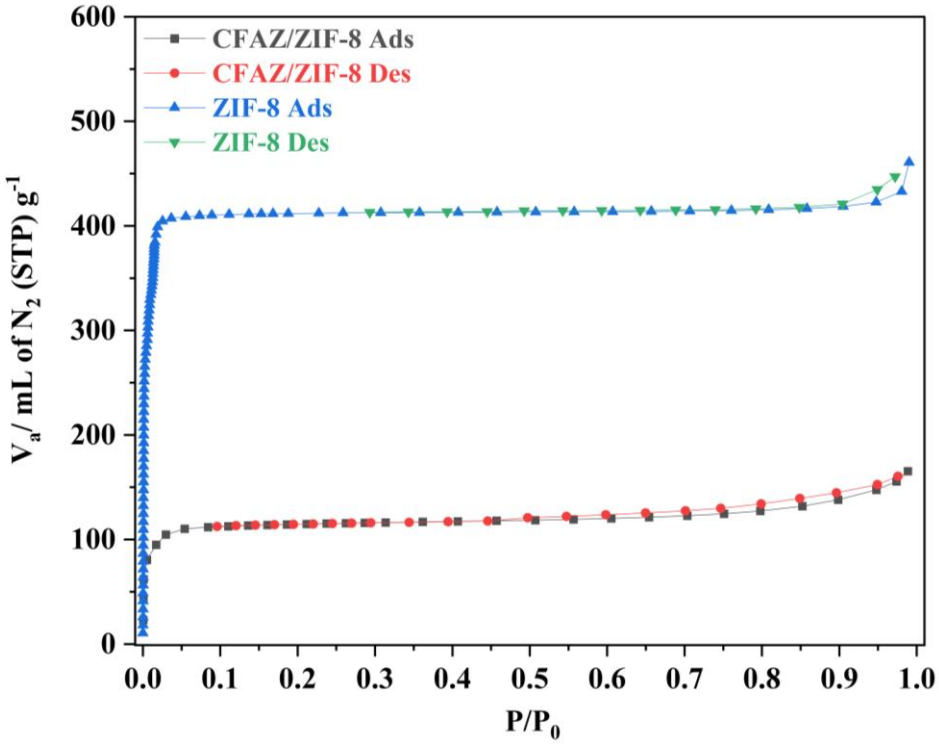

Figure 3.4: N_2 adsorption and desorption isotherms of ZIF-8 and CFAZ/ZIF-8 at -196 ºC

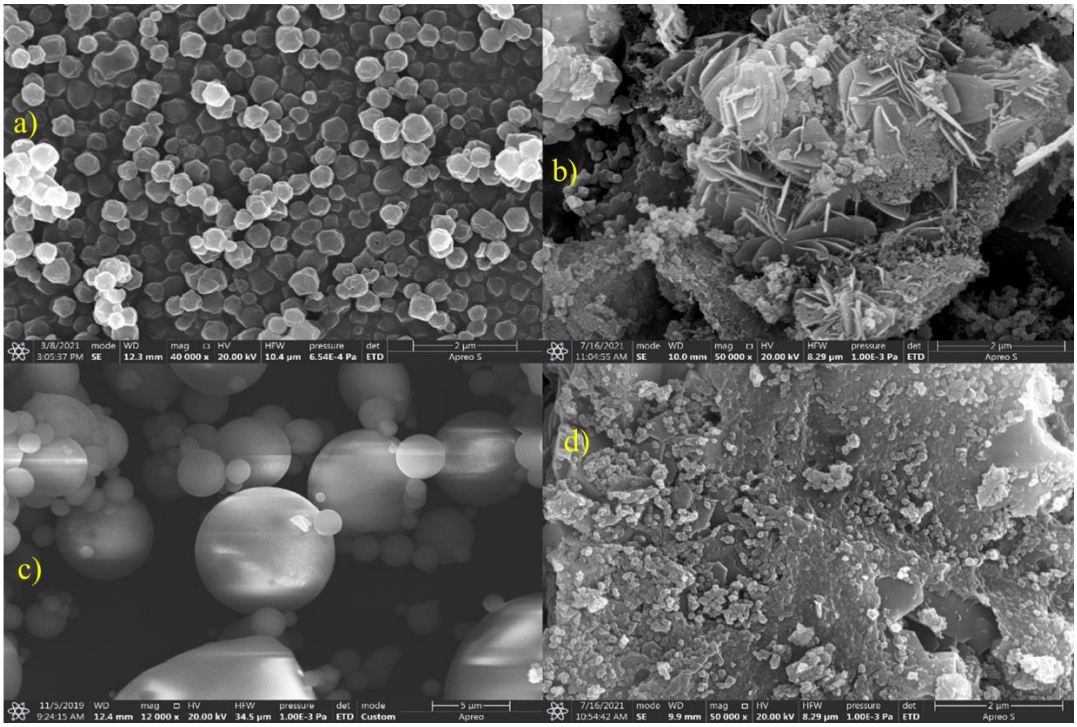

Figure 3.5: Scanning electron micrographs of a) ZIF-8, b) CFA Zeolite, c) CFAZ/ZIF-8 and d) CFA treated at 800 ºC

CFA zeolite showed a characteristic sodalite flower type structure as seen in figure 3.5. In addition to this predominantly flower type, flakes could also be seen indicating the presence of a different kind of zeolite. The well-formed shapes around the rose and sheet-like structures could allude to the formation of zeolites NaX and NaA. CFAZ/ZIF-8 showed an interesting image of its structure. The CFA sodalite flower structure was present. Additionally, small cubic-rhomboidal structures were also present around this larger flower type structure indicating the formation ZIF-8 crystals around the larger zeolitic structure.

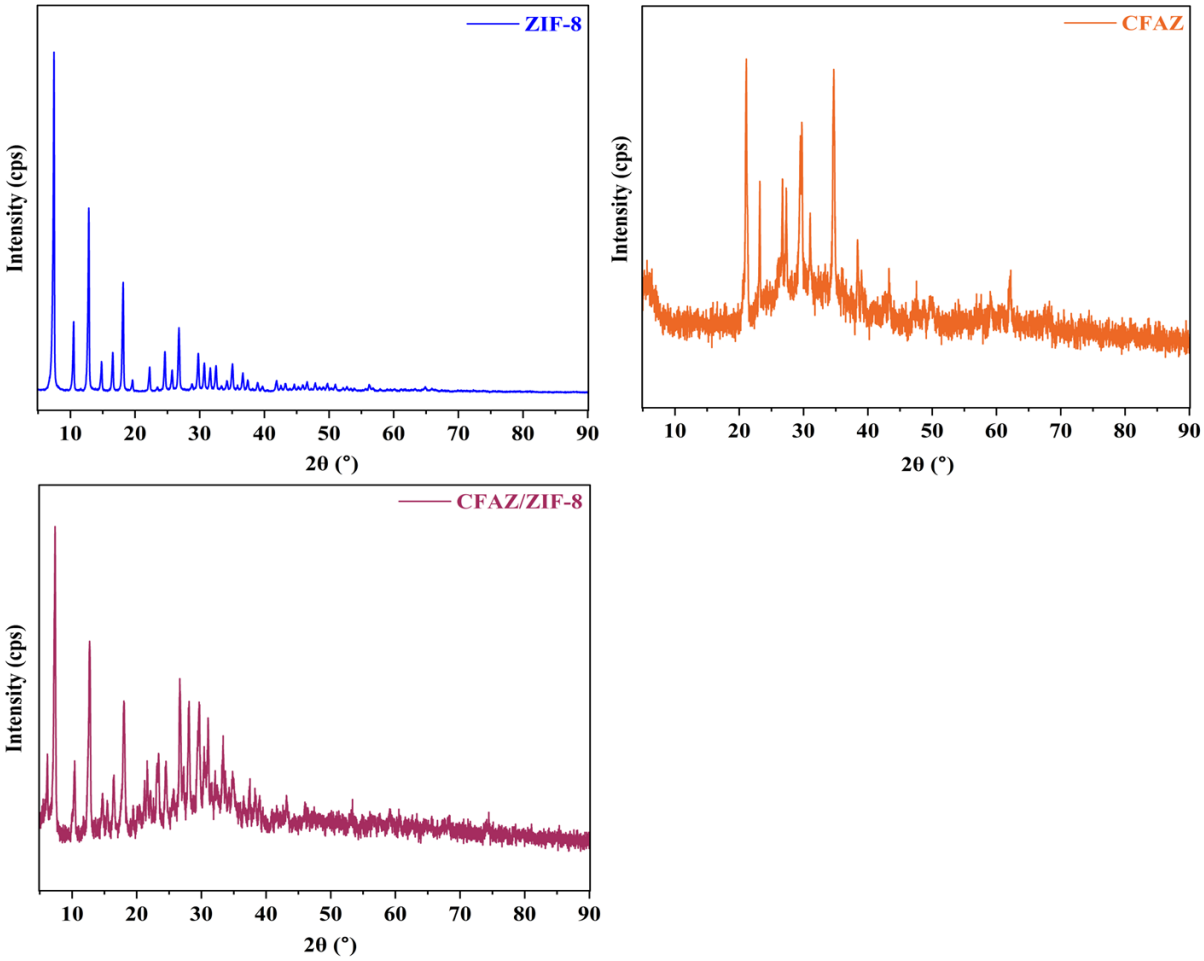

Figure 3.6: Diffractograms of ZIF-8, CFAZ and CFAZ/ZIF-8

The XRD patterns of CFAZ and CFAZ/ZIF-8 are depicted in figure 3.6. CFAZ/ZIF-8 showed firm peaks with high intensities at 2θ values around 7.3º, 10.3º, 12.7º, 14.7º, 18.0º, 18.2º, 21.9º, 24.9º, 28.0º, 29.2º and 38.5º, confirming the presence of ZIF-8. However, the peaks shifted slightly at 7.3º, 10.4º, 12.8º, 14.8º, 17.9º, 22.1º, 24.5º, 28.0º and 38.6º. This could be due to the interference of the oxides and salts present in coal fly ash itself. The zeolites from the final product obtained could also be competing to a minute degree with the native Zn^{2+} ion during the synthesis of ZIF-8. The high intensities around 23º and 43º indicate the strong presence of sodalite phase within CFAZ/ZIF-8 while the high intensities around 6º, 26º and 38º indicate the presence of NaX phase.

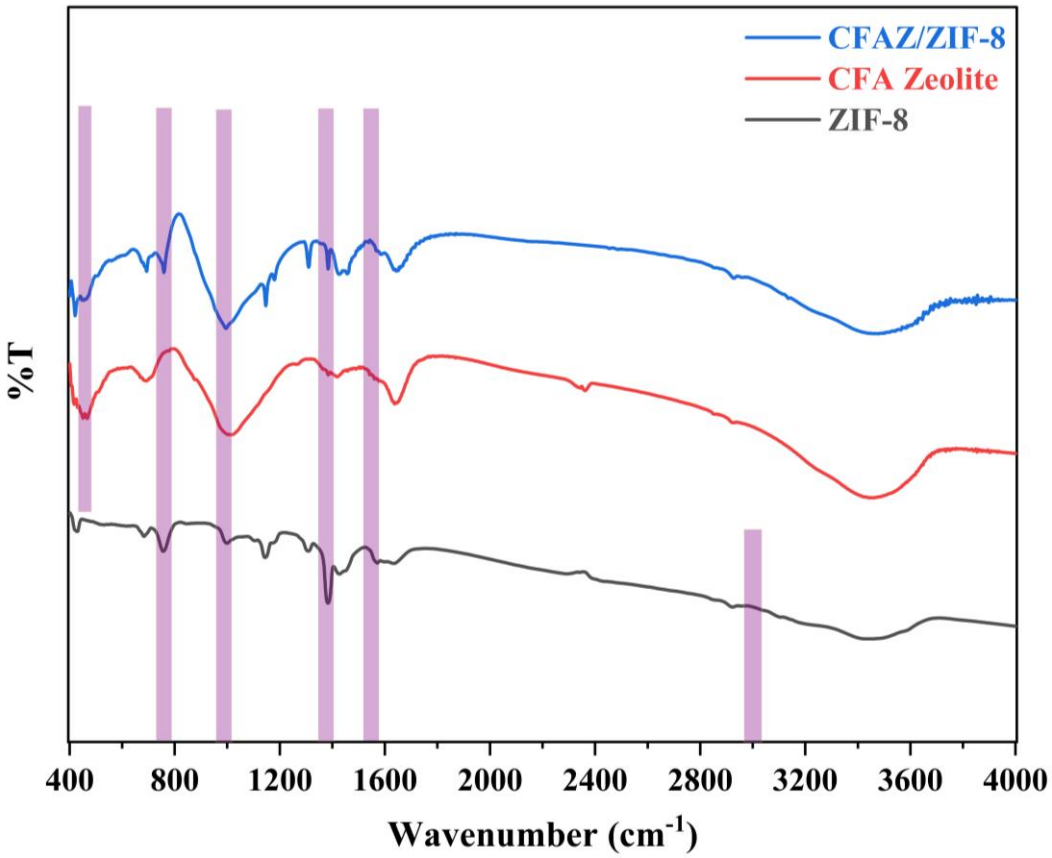

Figure 3.7: IR Spectra of ZIF-8, CFAZ and CFAZ/ZIF-8 adsorbent

The FTIR patterns for the CFA Zeolite/ZIF-8 based adsorbent show peaks at 3442 cm^{-1}, 2959 cm^{-1}, 2922 cm^{-1}, 2292.5 cm^{-1}, 1426 cm^{-1} and 1384 cm^{-1}. The peaks in between 2920 cm^{-1} to 3150 cm^{-1} indicated the presence of both aliphatic and aromatic carbon hydrogen bond stretching, indicative of the presence of Hmim linker. The peaks in between 1350 cm^{-1} to 1450 cm^{-1} indicated an aromatic ring stretch whereas peaks around 1596 cm^{-1} suggests the bending of N-H. The peak at 461 cm^{-1} could be due to bending vibrations in the zeolitic structure. The peaks around 980 cm^{-1} indicate the presence of Al-O-Si as do the peaks at 700 cm^{-1}.

3.3. CO_2 Uptake studies on K/Na/CFA-Light and CFAZ/ZIF-8

Adsorption processes are strongly affected by the operating temperature. In our investigation, we observed that different adsorbents exhibited varying levels of carbon dioxide (CC) uptake under different temperature conditions. Experiments were conducted at four specific temperatures (25 ºC, 50 ºC, 75 ºC, and 100 ºC) using a consistent amount of two grams of adsorbent, and a standard feed flow duration of sixty minutes. The CO_2 content in the feed gas remained constant at 20%. The relationship between temperature and CO_2 uptake is visually represented in the accompanying figure 3.8.

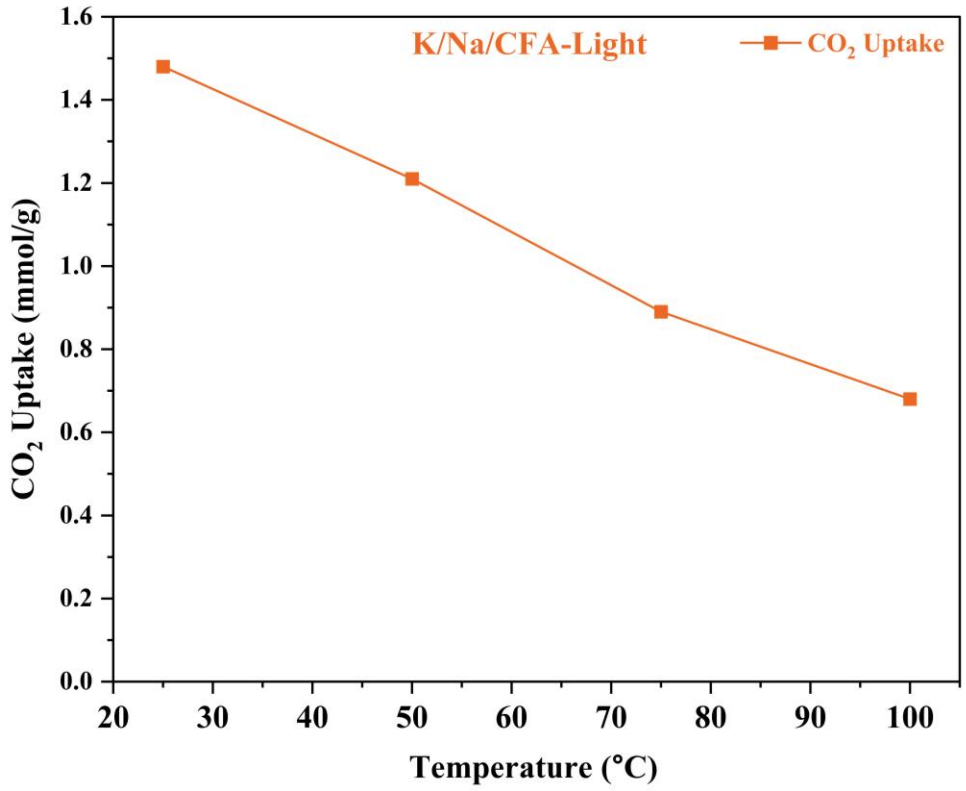

Figure 3.8: Effect of process temperatures on CO_2 uptake at 20% CO_2

As anticipated, the CO_2 uptake of the K/Na/CFA-Light adsorbent displayed a decreasing trend as the process temperature increased. Starting at 1.47 mmol/g at 25 ºC, it declined significantly to 0.67 mmol/g at 100 ºC. This trend aligns with the findings in existing literature, which attribute this behavior to the elevated kinetic energy of CO_2 molecules at higher temperatures,

making them more likely to escape entrapment on porous surfaces. However, it's worth noting that the K/Na/CFA-Light adsorbent outperformed unfused coal fly ash, which recorded a value of 0.6 mmol/g at 25 ºC, indicating the superior CO_2 trapping ability of the fused coal fly ash adsorbent.

Another crucial factor influencing adsorption processes is the concentration of the adsorbate in the feed gas, in conjunction with the process temperature. In our study, we systematically varied the CO_2 concentration in the feed gas from 10% to 80%. Throughout the experiments, we maintained a consistent two-gram quantity of adsorbent and a 60-minute carbonation duration, with 25 ºC serving as the reference temperature due to its proven effectiveness in CO_2 uptake for the K/Na/CFA-Light adsorbent. The results, as depicted in the accompanying figure 3.9, clearly show that an increase in CO_2 concentrations leads to higher CO_2 uptake values.

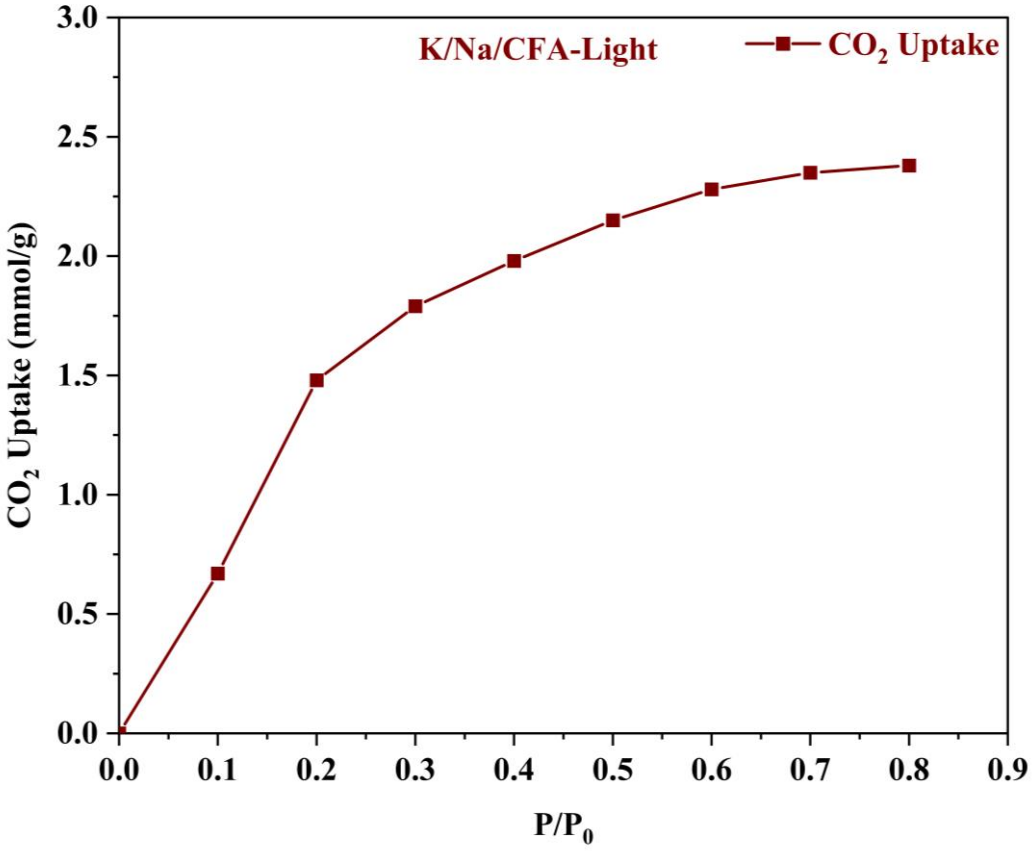

Figure 3.9: Effect of CO_2 concentration on CO_2 uptake at 25 ºC

The values nearly tripled, rising from a modest 0.7 mmol/g at 10% CO_2 to 2.4 mmol/g at 80%. Notably, the most significant increase occurred when the feed concentration went from 10% to 40%, resulting in a tripling of values. Beyond a 40% concentration, the increase was less dramatic, only amounting to 25%. This suggests that there is a saturation point, beyond which further increases in CO_2 concentrations do not significantly impact CO_2 uptake. This is due to the fact that as the CO_2 partial pressure in the feed, increases, the gas quickly saturates the adsorbent's pores. Consequently, fewer pores are available for additional adsorption, leading to a limited increase in CO_2 uptake values.

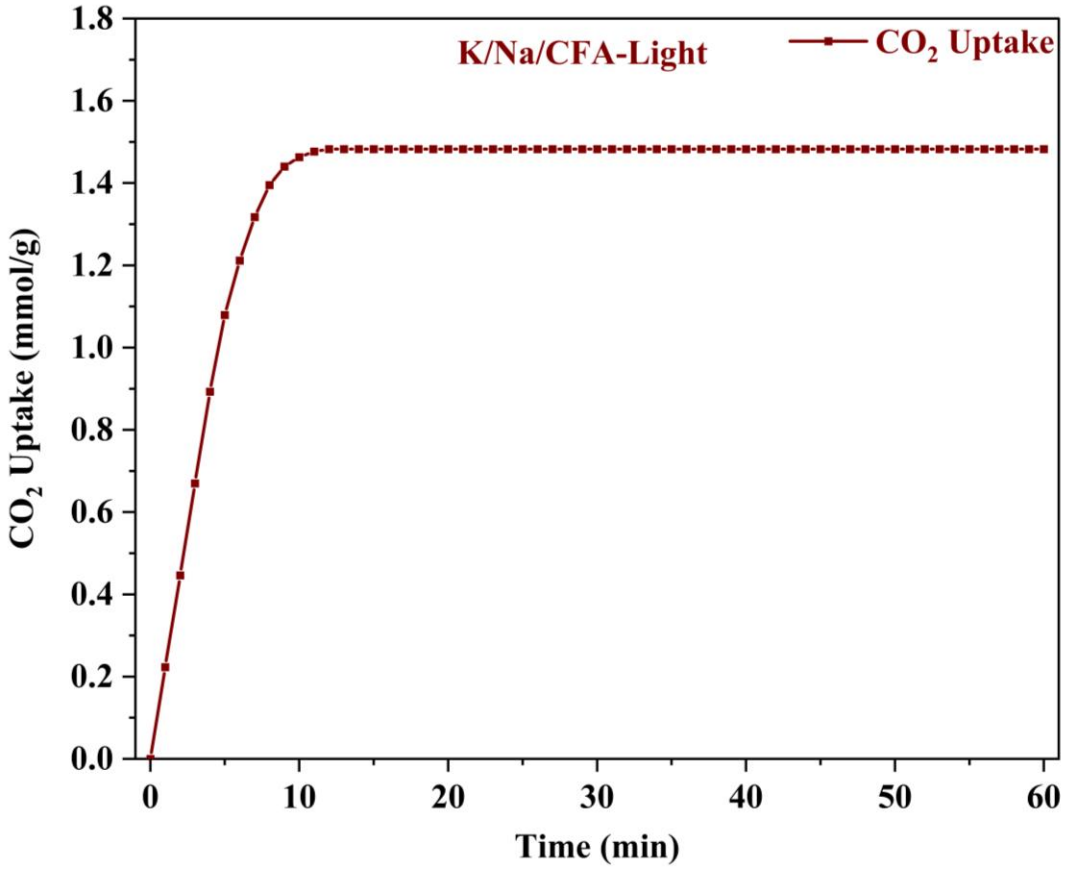

Figure 3.10: Breakthrough curve of K/Na/CFA-Light at 25 ºC and 20% CO_2 concentration

The duration of feed flow also plays a crucial role in shaping the adsorption process. Experiments were conducted with four different gas flow duration times: 15 minutes, 30 minutes, 45 minutes, and 60 minutes, all using a consistent two-gram quantity of adsorbent, maintaining a 20% CO_2 feed concentration, and keeping the temperature at 25 ºC. Figure 3.11 illustrates that nearly the entire CO_2 uptake process occurred within the initial 15 minutes, with no significant increase observed beyond that point, even up to 60 minutes. This aligns with the theory that, for a given mass of adsorbent, the time of adsorption significantly contributes to an increase up to a certain point. Afterward, further increases are minimal or negligible. In our study, we observed substantial increases from the start of the process up to 11 minutes, but beyond 11 minutes, only slight increments in CO_2 uptake were observed.

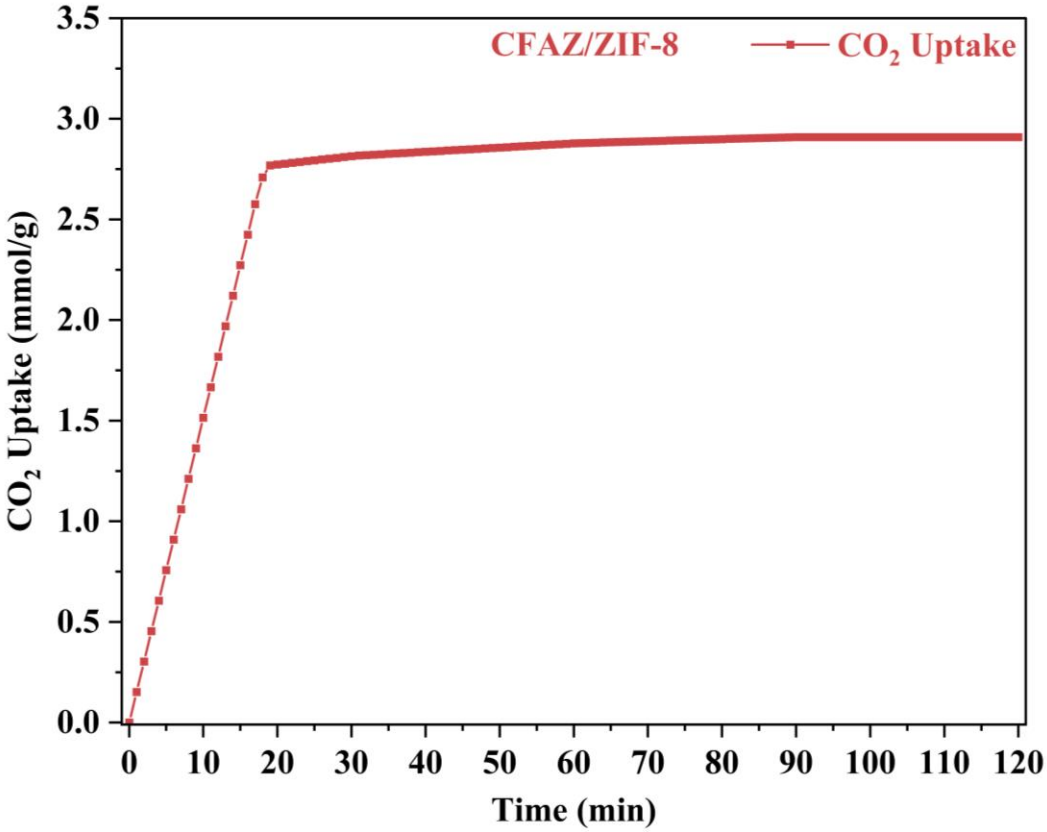

Figure 3.11: Impact of feed flow duration on CO_2 uptake capacity of CFAZ/ZIF-8 at 25 ºC

The temperature at which adsorption occurs is a critical factor influencing the adsorption capacity of a material. In our study, the impact of temperature on CO_2 uptake values was examined at four different temperatures: 25 ºC, 50 ºC, 75 ºC, and 100 ºC. Throughout these experiments, the mass of the adsorbent, duration of feed flow, and feed ratio remained constant. The data was collected in triplicate, and the reported values represent the mean with the associated standard deviation. Figure 3.12 visually depicts the results, showing a significant decrease in uptake at higher temperatures. Specifically, for the CFAZ/ZIF-8 adsorbent synthesized in this study, the adsorption capacities were as follows: 2.83 mmol/g at 25 ºC, 2.36 mmol/g at 50 ºC, 1.80 mmol/g at 75 ºC, and 1.62 mmol/g at 100 ºC. These findings align with the well-established theory that CO_2 adsorption is exothermic, meaning it is more favorable at lower temperatures. Lower temperatures provide an environment where more CO_2 molecules

can be adsorbed on the surface of the adsorbent. As the temperature rises, the kinetic energies of the CO_2 molecules increase drastically, resulting in a general decrease in adsorption capacities. Remarkably, CFAZ/ZIF-8 outperformed its parent materials in this study. ZIF-8 exhibited a CO_2 uptake value of 1.45 mmol/g, while CFA zeolite achieved a slightly better performance at 1.83 mmol/g at 25 ºC.

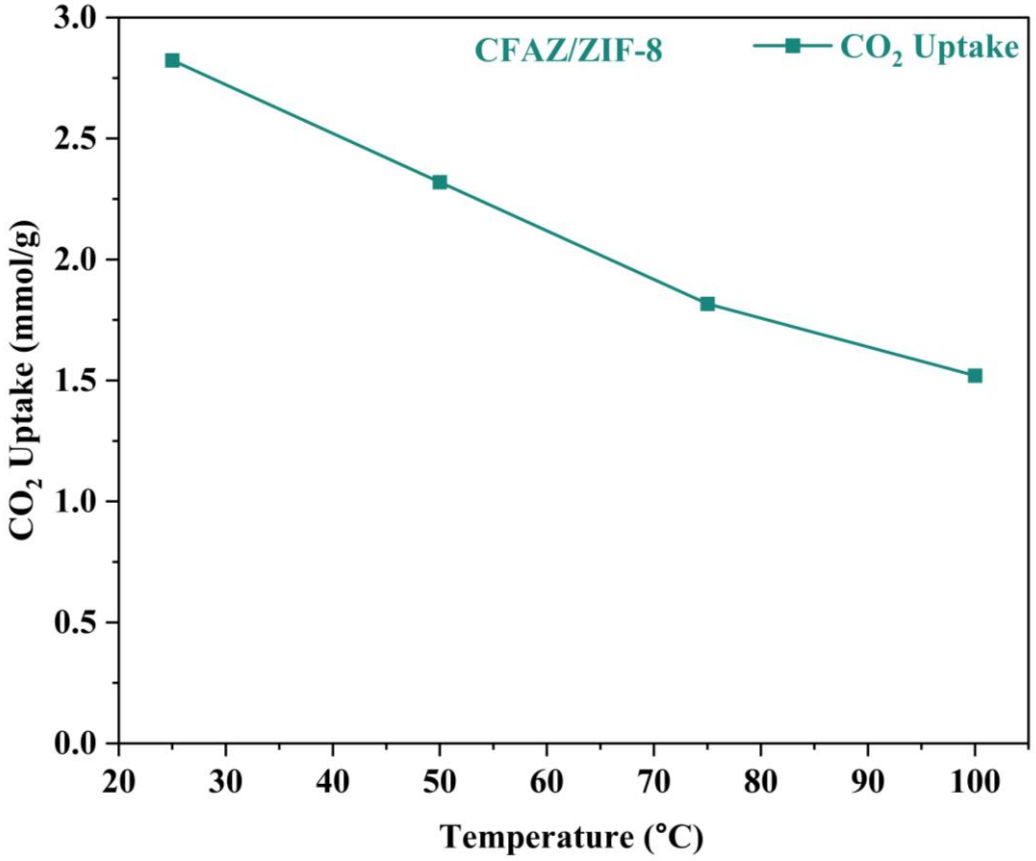

Figure 3.12: Effect of process temperature on CO_2 uptake of CFAZ/ZIF-8

Another vital parameter in determining adsorbent performance is the concentration of CO_2 in the feed gas. In our investigation, we explored eight different CO_2 partial pressures ranging from 0 to 0.8 bar in the gas feed. At a constant temperature of 25 ºC, a consistent adsorbent mass of 2.5 grams, and a carbonation time of 60 minutes, CFAZ/ZIF-8 displayed varying adsorption capacities. Notably, the results revealed that as the CO_2 partial pressure doubled from 0.1 to 0.2 bar, the adsorption values also doubled. However, beyond this point, the

increase in concentration only led to marginal changes. For instance, increasing from 0.2 bar to 0.5 bar resulted in a mere 15% increase in CC values. This phenomenon can be attributed to the adsorption reaching a saturation point. As the CO_2 concentration rises, the pores within the adsorbent become filled more rapidly, leaving little room for further adsorption. This leads to a limited increase in uptake capacities. In terms of the effect of CO_2 partial pressure, the adsorbent exhibited a strong attraction for adsorption, resulting in a significant increase in adsorption capacities as the pressure increased from 0.1 bar to 0.3 bar (figure 3.13). However, beyond 0.3 bar, further increases in pressure had little impact on uptake values. This may be due to the adsorption reaching a saturation or equilibrium point. As more CO_2 is introduced into the feed, the pores become filled more rapidly, limiting further adsorption.

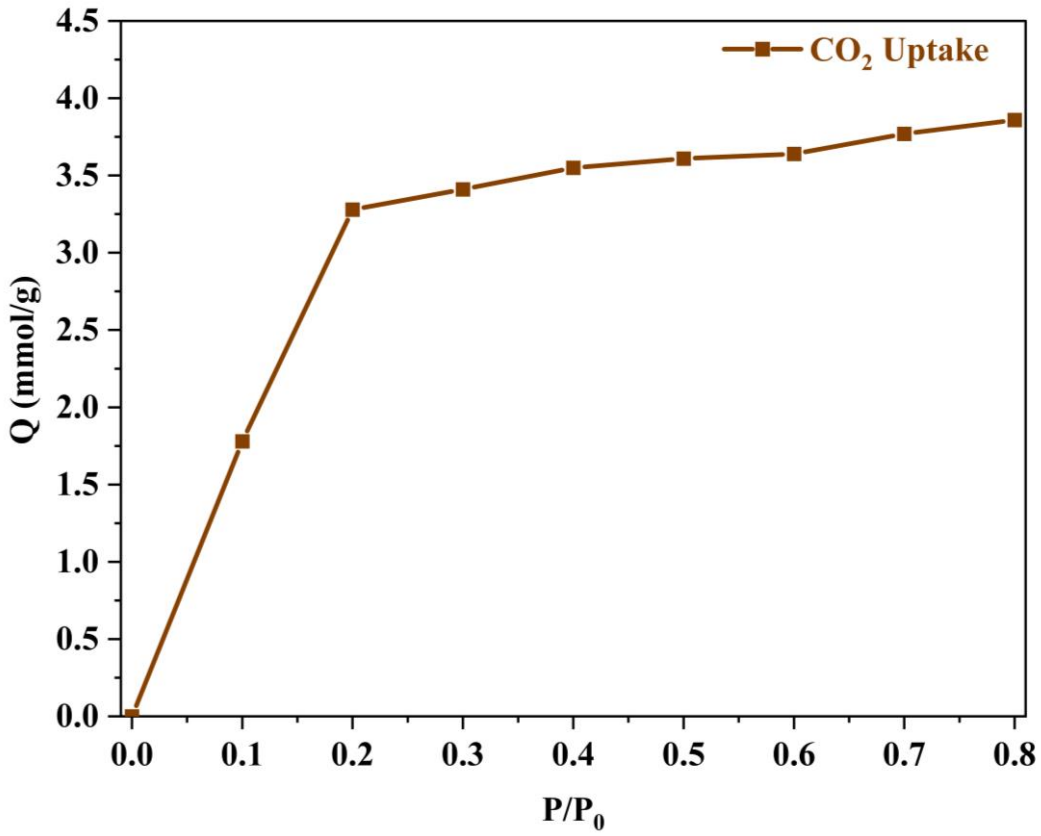

Figure 3.13: Effect of CO_2 concentration on uptake capacity at 25 ºC

The amount of adsorbent employed was also a significant variable in our study. As shown in the figure 3.14, an increase in the amount of adsorbent led to a slight decrease in CO_2 uptake

values under the same conditions of feed CO_2 concentration, time, and temperature. The drop in values, from 2.86 mmol/g at 1 gram of loading to 2.79 mmol/g at 7.5 grams of loading, was relatively small in comparison to the CO_2 flow. This trend is consistent with previous findings for other adsorbents, where an increase in adsorbent mass led to reduced surface contact and, consequently, a decrease in adsorption capacity.

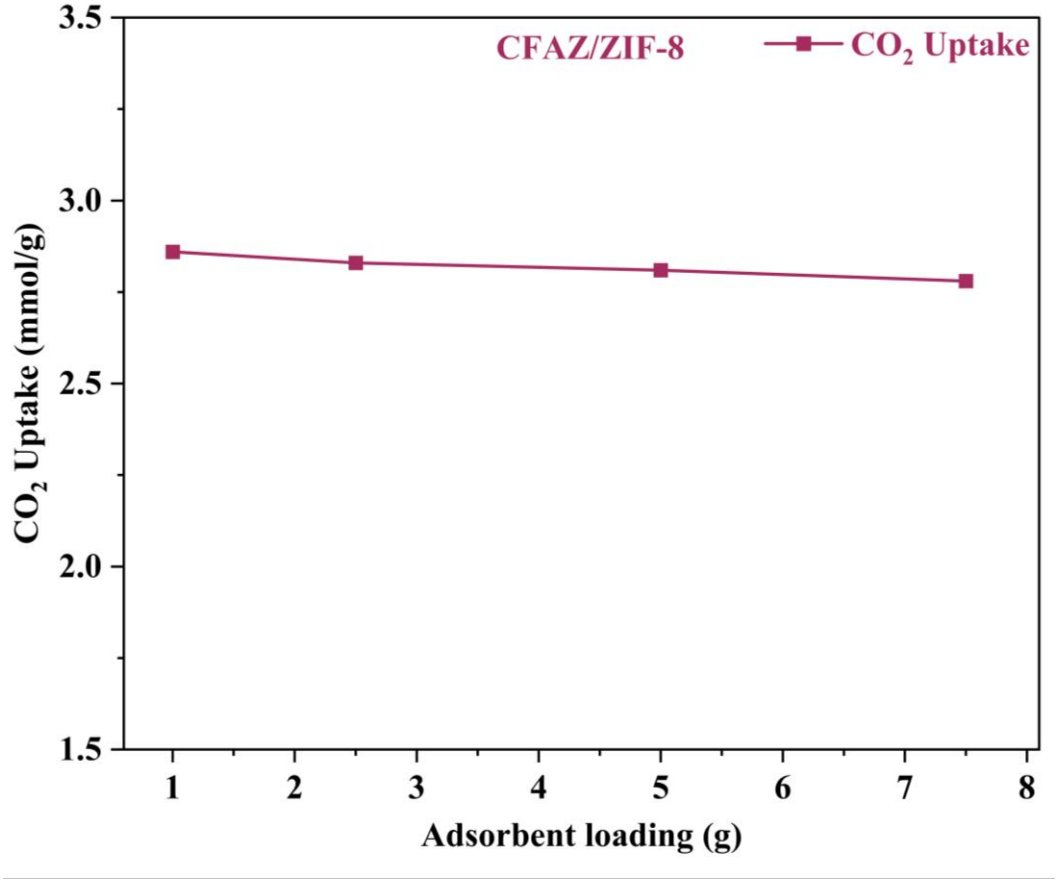

Figure 3.14: Effect of adsorbent loading on CO_2 uptake capacity

Notably, our results indicated a negligible change in CO_2 uptake values with variations in the amount of adsorbent, which is in contrast to some prior studies that reported more significant drops in capacity with increasing adsorbent mass. The interaction between adsorbent loading and pressure across the reactor can influence CO_2 uptake, although this effect was minimal in our study. While longer exposure time theoretically increases the chances of adsorption at some sites, in our study, the observed increase was minimal.

3.4. Adsorption kinetics study

3.4.1. Adsorption kinetics of K/Na/CFA-Light

Kinetic studies are very important in understanding the type of adsorption process at hand. In this study, three kinetic models were considered. They are the pseudo first order model (PFO), the pseudo second order model (PSO) and the Avrami model (refer to Chapter 2, Section 2.5.1).

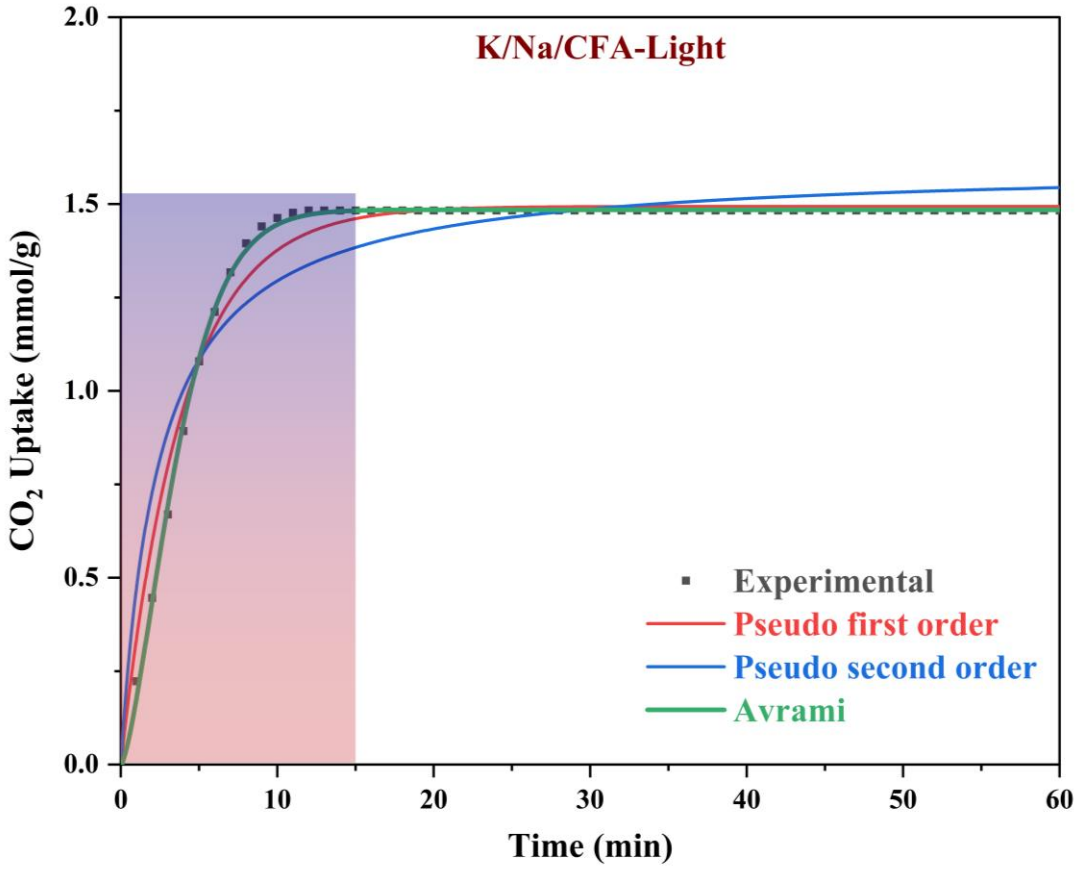

Figure 3.15: Adsorption kinetics modelling of K/Na/CFA-Light at 25 ºC

Table 3.1: Adsorption kinetics of K/Na/CFA-Light

Adsorbent	Model	Q (exp)	Q (fit)	k	n	R^2
K/Na/CFA-Light	PFO	1.48	1.49	0.2545		0.981
	PSO	1.48	1.61	0.2588		0.922
	Avrami	1.48	1.48	0.1262	1.46	0.994

A detailed representation of the theoretical models and their explanation of the experimental data is given in figure 3.15 and table 3.1. From figure 3.15, it can be observed that the Avrami model fits the data almost perfectly. That is also supported by the R^2 value of the Avrami model fit, which is 0.99. PSO model was least suited to explain the experimental data which is indicated by an R^2 value of 0.92. The near perfect fit of the Avrami model indicates that the adsorption process is a combination of both physisorption and chemisorption. This is also in line with the prepared adsorbent. High carbon content fly ash is usually a poor adsorbent of CO_2 which acts like a physisorbent. However, the addition of KOH and NaOH in the fusion process, transformed the adsorbent into a hybrid. Metal hydroxides and oxides are usually treated as chemisorbents which bind CO_2 as carbonates onto the surface. Also noteworthy is the R^2 value of 0.98 for the pseudo first order model. Both the R^2 values for the Avrami and the pseudo first models respectively could indicate a domination of physisorption.

3.4.2. Adsorption kinetics of CFAZ/ZIF-8

Similar to the previous kinetics study, the same three models were considered (refer to Chapter 2, Section 2.5.1). From the table given below, it could be inferred that both pseudo-second order and Avrami models fit the experimental data better than pseudo-first order. The obtained R^2 values and the Q_e got through the fit agree better with the Avrami model.

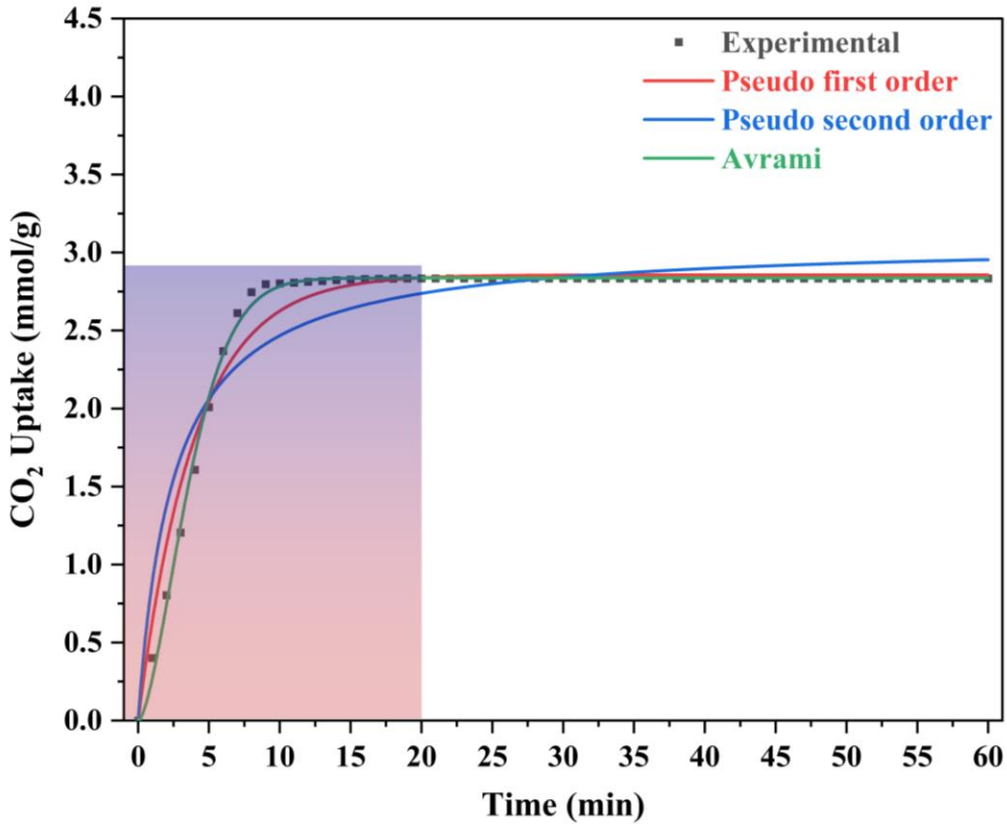

Figure 3.16: Kinetics fit of CFAZ/ZIF-8 at 25 ºC

Table 3.2: Adsorption kinetic data for CFAZ/ZIF-8

Adsorbent	Model	Q (exp)	Q (fit)	k	n	R^2
CFAZ/ZIF-8	PFO	2.83	2.86	0.25145		0.97
	PSO	2.83	3.08	0.13189		0.89
	Avrami	2.83	2.84	0.09967	1.602	0.99

The pseudo first-order model mainly explains physisorption while pseudo second-order deals with adsorption mainly of chemical nature. Avrami model is the intermediate, i.e.; it predicts that adsorption is a combination of both physisorption and chemisorption. From the fit and table 2, an R^2 value of 0.997, it was clear that Avrami kinetics suited the experimental data of CFAZ/ZIF-8 adsorbent. However, it is interesting to note that Q_e values obtained from the model fit and, through the experiment, agreed with each other well for the Avrami model. This would also suggest that the nature of adsorption is a mixture of physisorption and chemisorption. This is in line with the hybrid nature of the adsorbent itself. While zeolites from

alkali fused coal fly ash are chemisorbents due to the presence of high amounts of alkali, ZIF-8 is mainly employed in the physisorption of CO_2. The kinetic fit graph of CFAZ/ZIF-8 is given in figure 3.16.

3.5. Cyclic stability of K/Na/CFA-Light and CFAZ/ZIF-8

At 25°C, the performance of cyclic stability was investigated for five cycles. Regeneration was carried out in the presence of N_2 gas and at a temperature of 150 °C. The carbonation and decarbonation cycles each lasted 60 minutes and utilized 2.5 g of carbon dioxide. The experiment was repeated three times, and the shown values represent the mean and standard deviation. After the investigation, the CO_2 uptake values of the K/Na/CFA-Light adsorbent decreased. The drop in uptake performance was around 20%. The adsorbent preserved 80% of its initial uptake capacity after five cycles, indicating that the synthesized hybrid adsorbent is stable and has a good retention capacity. The initial CO_2 uptake was at 1.48 mmol/g and the final CO_2 uptake after 5 cycles was around 1.19 mmol/g. The cyclic stability of the adsorbent as produced is shown in figure 3.17.

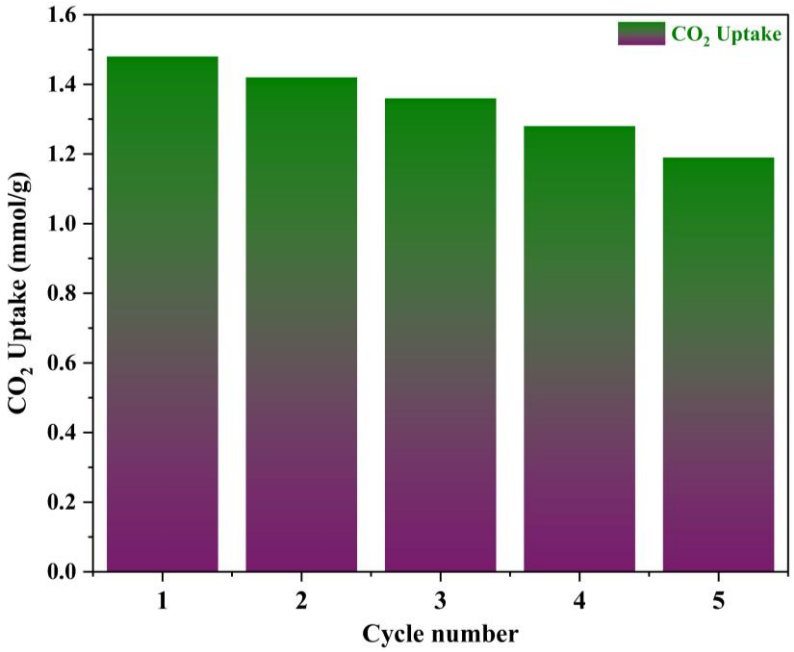

Figure 3.17: Cyclic stability performance of K/Na/CFA-Light at 25 ºC

The performance was compared for five cycles at ambient temperature (25 ºC). Each regeneration was done in the presence of N_2 gas, and a temperature of 150°C was set for the same. An amount of 2.5 g was used for the carbonation and decarbonation cycle with 60 minutes duration for each cycle. As predicted, the CFAZ/ZIF-8 adsorbent showed a decrease in CO_2 uptake values after the study concluded. However, the decline was only a minute 5%. After, five cycles the adsorbent retained 95% of its initial uptake capacity which makes the synthesized hybrid adsorbent stable and with a high retention capacity. Figure 3.18 gives the cyclic stability of the synthesized adsorbent.

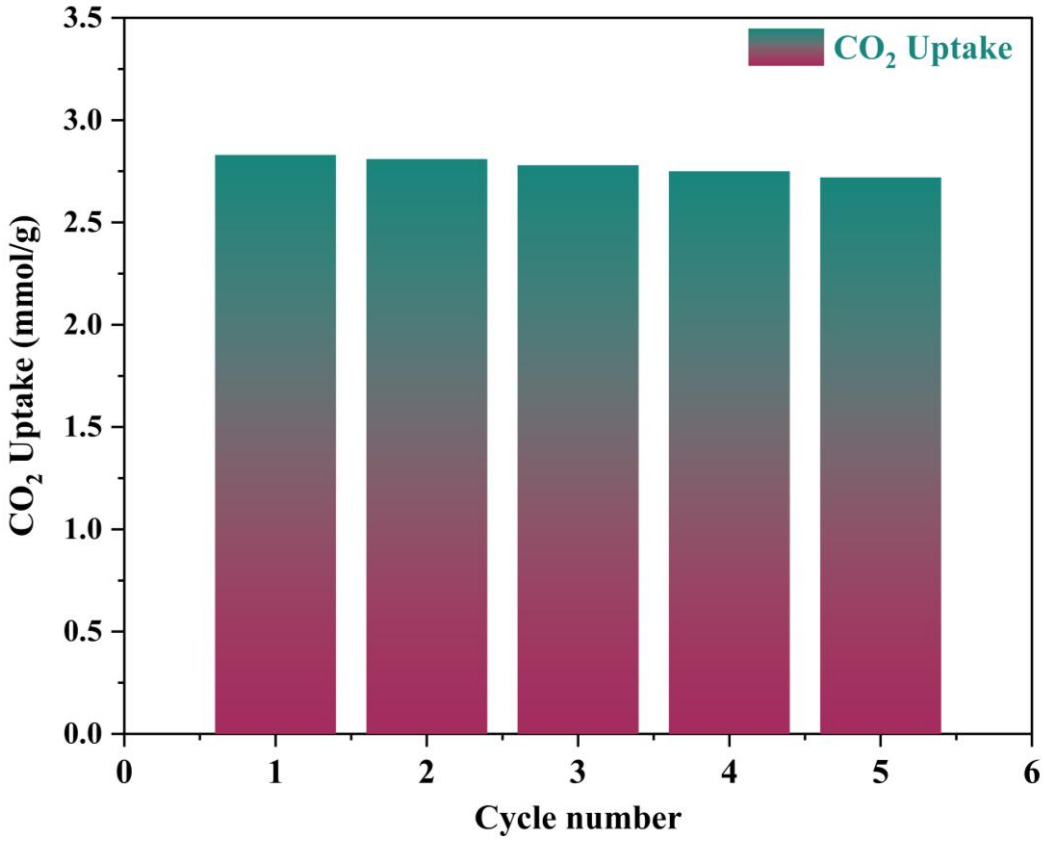

Figure 3.18: Cyclic stability performance of CFAZ/ZIF-8 at 25 ºC

3.6. Conclusions

The synthesis of adsorbents from both carbon-rich and carbon-deficient coal fly ash samples was achieved through a two-step fusion hydrothermal method, with three key parameters considered for CO_2 uptake adsorption experiments. Initial studies revealed that the K/Na/CFA-Light adsorbent outperformed the K/Na/CFA-Heavy counterpart. Conclusions drawn from the study included the detrimental effect of KOH fusion on the crystalline phases of the parent coal fly ash structure, the absence of additional crystalline phases through fusion hydrothermal method in the presence of NaOH, and a noteworthy increase in CO_2 uptake value despite a decrease in surface area for the K/Na/CFA-Light adsorbent. Temperature exhibited an inverse relationship with CO_2 uptake, and concentration of CO_2 within the feed demonstrated an increasing effect up to 40%. Kinetic studies favored the Avrami model, indicating a combination of physisorption and chemisorption. Cyclic stability assessments showed that the K/Na/CFA-Light adsorbent retained up to 80% of its capacity after five cycles, demonstrating decent performance in CC.

Utilizing coal fly ash, a zeolite-type adsorbent was synthesized and further combined with ZIF-8 through an in-situ synthesis technique, resulting in the creation of a novel hybrid adsorbent. The adsorption capacity exhibited a temperature dependence, with the highest capacity recorded at 25 ºC (2.83 mmol/g), while CO_2 concentration significantly influenced the CO_2 uptake, reaching around 3.6 mmol/g at higher concentrations. An increase in adsorbent loading for a given carbonation time had a slightly detrimental effect on overall CO_2 uptake, whereas an increase in carbonation time had a slightly positive impact. Cyclic stability assessments indicated excellent performance (95%) of CFAZ/ZIF-8 even after five cycles of carbonation and decarbonation. The hybrid adsorbent surpassed its parent materials, suggesting a synergistic effect between ZIF-8 and CFAZ. Comparative performance with commercially available zeolites like 13X and NaX further highlighted the efficacy of CFAZ/ZIF-8. Kinetic

studies revealed a combination of physisorption and chemisorption in the adsorption process, and future investigations could explore the impact of the Zn metal ion-to-CFA weight ratio on the morphological properties and CO_2 uptake of this hybrid adsorbent.

Chapter 4: Carbon Capture Studies using bimetallic ZIFs based Ce/Zn and Ce/Co combinations

4. Carbon Capture Studies using bimetallic ZIFs based Ce/Zn and Ce/Co combinations

4.1. Introduction

Metal-organic frameworks (MOFs) have emerged as a promising class of materials for gas storage and separation applications, with zeolitic imidazolate frameworks (ZIFs) garnering significant attention in recent studies on carbon dioxide (CO_2) adsorption [190]. The latest research in this field has focused on tailoring the properties of ZIFs to enhance their CO_2 capture capabilities. One notable study, conducted by a team of researchers at a leading institution, delves into the synthesis of ZIFs with specific pore sizes and surface functionalities to optimize CO_2 adsorption performance. The team utilized advanced characterization techniques, such as X-ray diffraction and nitrogen adsorption-desorption isotherms, to precisely analyze the structural and textural properties of the synthesized ZIFs [191]. The results revealed a correlation between the pore size of ZIFs and their CO_2 adsorption capacities, shedding light on the intricate interplay between the framework's architecture and its ability to selectively capture CO_2 molecules. In addition to structural modifications, another avenue of exploration in recent studies involves the incorporation of various metal ions into the ZIF framework. Researchers have systematically investigated the impact of different metal ions on the CO_2 adsorption properties of ZIFs, aiming to identify the most effective combinations. The study employed a range of analytical tools, including infrared spectroscopy and thermogravimetric analysis, to probe the interactions between the metal ions and CO_2 within the ZIF structure. The findings suggest that the choice of metal ions significantly influences the adsorption capacity and selectivity of ZIFs for CO_2, opening up new possibilities for tailoring these materials for specific gas separation applications [192].

Furthermore, researchers have explored the dynamic behavior of ZIFs under varying temperature and pressure conditions. Understanding the thermodynamic and kinetic aspects of CO_2 adsorption in ZIFs is crucial for practical applications in real-world environments. A recent study investigated the adsorption-desorption cycling stability of ZIFs over multiple cycles, simulating conditions relevant to industrial processes. The results indicated the robustness of certain ZIF formulations, demonstrating their potential for long-term and repeated use in CO_2 capture applications. The study also highlighted the importance of optimizing the synthesis conditions to enhance the stability and performance of ZIFs under dynamic gas adsorption scenarios. In the quest for sustainable and efficient CO_2 capture technologies, the integration of ZIFs into composite materials has emerged as a novel approach. Researchers have explored the synergistic effects of combining ZIFs with other functional materials to create hybrid adsorbents with enhanced CO_2 capture performance. The latest findings suggest that incorporating ZIFs into porous matrices or modifying their surfaces with specific functional groups can lead to improved adsorption capacities and increased selectivity for CO_2 over other gases. This innovative approach opens up new avenues for designing tailored materials that address the challenges associated with CO_2 capture in diverse industrial applications. Bimetallic zeolitic imidazolate frameworks (ZIFs) have gained attention for their potential in CO_2 adsorption. The synthesis of bimetallic Zn/Co/Co-Zn-based ZIFs at room temperature has been reported, and their CO_2 capture capacity was evaluated [109]. Additionally, the modification of ZIF-8 crystals using methylamine, ethylenediamine, and N, N'-dimethylethylenediamine has been shown to improve their CO_2 adsorption performance. The adsorption capacities of CO_2 on amine-modified ZIF-8 samples were significantly increased compared to the original ZIF-8 [193]. Furthermore, the incorporation of cations on ZrO_2, such as Li^+, Mg^{2+}, or Co^{3+}, has been found to enhance the adsorption of carbon dioxide. These studies demonstrate the potential of bimetallic ZIFs and modified ZIF-8 for CO_2 adsorption,

highlighting their importance in addressing carbon emissions and achieving a low-carbon economy [194].

Moreover, computational modeling has played a pivotal role in advancing the understanding of the adsorption mechanisms in ZIFs. Recent studies have employed state-of-the-art molecular dynamics simulations and density functional theory calculations to unravel the intricate details of CO_2 adsorption at the atomic and molecular levels within the ZIF framework. Computational models have provided valuable insights into the thermodynamics and kinetics of CO_2 adsorption, aiding in the interpretation of experimental results and guiding the rational design of ZIFs with enhanced CO_2 capture performance [195]. The synergy between experimental and computational approaches has accelerated progress in the field, enabling researchers to make informed decisions in the development of next-generation ZIF-based adsorbents. In summary, the latest studies on ZIFs in CO_2 adsorption have witnessed significant advancements in tailoring the structural, compositional, and dynamic properties of these materials. The exploration of novel synthesis strategies, the incorporation of diverse metal ions, the investigation of dynamic adsorption-desorption behaviors, the development of hybrid composites, and the application of advanced computational modeling techniques collectively contribute to the evolving landscape of ZIF-based adsorbents for CO_2 capture [196]. As the demand for sustainable solutions to mitigate CO_2 emissions continues to grow, the ongoing research in this field holds promise for the development of efficient and practical technologies for carbon capture and storage.

This study introduces two novel bimetallic Zeolitic Imidazolate Frameworks (ZIFs) derived from ZIF-8 and ZIF-67, both modified with amine loading, exhibiting exceptional performance in terms of carbon capture capacity and cyclic stability [197]. The synthesis of these modified adsorbents, named (Ce,Zn) ZIF-8 and (Ce,Co) ZIF-67 in reference to their parent ZIFs, employed straightforward hydrothermal and aqueous synthesis methods with cerium (Ce)

metal modifications. The adsorption behavior of these materials in relation to carbon dioxide (CO_2) was systematically investigated using a fixed-bed reactor system, adopting a rigorous and structured approach through Response Surface Methodology (RSM).

The experimental design utilized the face-centered central composite design, considering four numeric factors: temperature, adsorbent quantity, carbonation time, and diethanolamine (DEA) loading. The responses were obtained using Design Expert Software 12, and statistical fits were determined through Analysis of Variance (ANOVA). Subsequently, cyclic retention capacities of all adsorbents were assessed after 15 cycles of adsorption-desorption. Based on both experimental and theoretical findings, optimal process conditions were determined for each adsorbent. Kinetics-based studies were conducted under these optimum conditions, employing three kinetic models—pseudo-first-order, pseudo-second-order, and Avrami models—to ascertain the best fit and understand the nature of adsorption. The influence of carbon dioxide concentration on the optimal adsorbents was also explored. In addition to kinetics, the study considered two isotherm models, Langmuir and Freundlich isotherms, for comparison with the experimental data. The comprehensive approach adopted in this work contributes valuable insights into the development and performance assessment of bimetallic ZIF-based adsorbents for carbon capture applications.

4.2. Characterization of adsorbents

In the pursuit of a thorough understanding of the synthesized materials, a comprehensive set of characterization techniques was meticulously applied. The arsenal of analytical methods employed in this study encompassed diverse methodologies, each shedding light on specific facets of the synthesized zeolitic imidazolate frameworks (ZIFs). BET analysis, a staple technique for gas adsorption studies, was judiciously utilized to quantify the total surface area and pore volume of the synthesized materials. This provided crucial insights into the porosity and adsorption capabilities of the ZIFs, contributing to a nuanced understanding of their structural attributes. To unravel the crystalline structure and composition of the materials, X-ray diffraction (XRD) was employed, enabling the identification of traces and signatures of known materials. The resulting XRD patterns served as fingerprints, elucidating the crystallographic nature of the synthesized ZIFs. Scanning electron microscopy (SEM) was enlisted to delve into the morphological intricacies and particle structures of the ZIFs, providing visual insights into their surface features. Meanwhile, Fourier-transform infrared (FTIR) spectroscopy, facilitated by a Jasco-designed P-200 FTIR instrument with a KBr beam splitter, was employed to scrutinize the nature and types of bonds present in the ZIFs. This technique allowed for a detailed examination of the molecular vibrations, revealing critical information about the chemical composition and bonding within the materials.

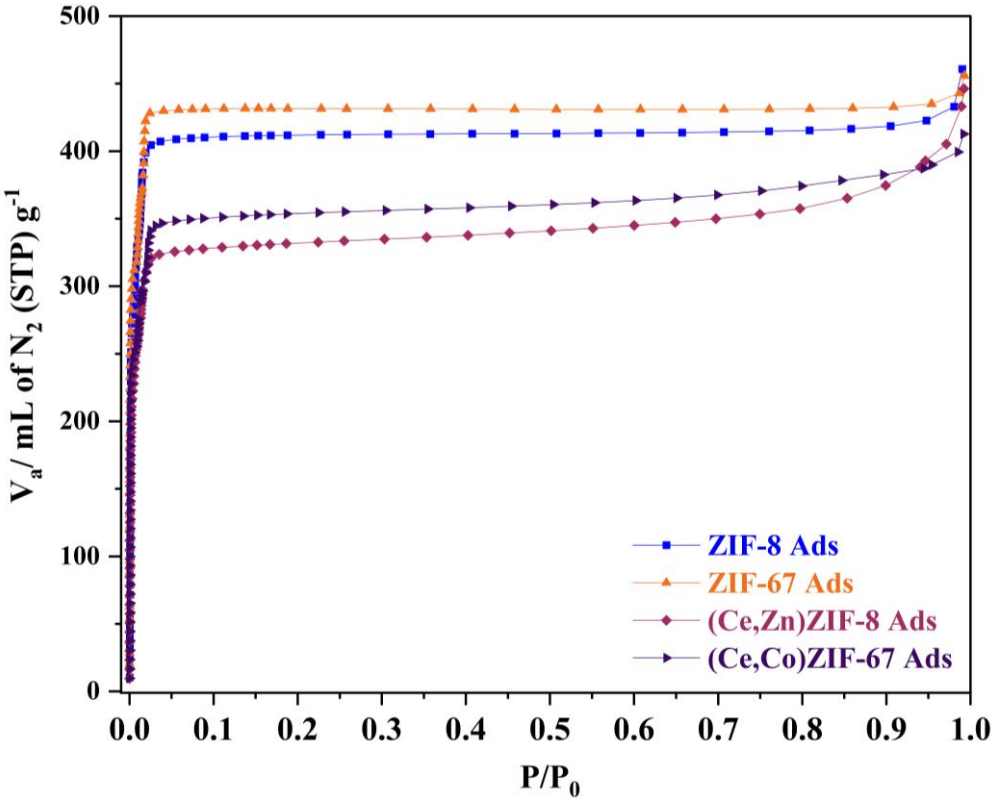

Figure 4.1: N_2 adsorption isotherms of ZIF-8, ZIF-67, (Ce,Zn)ZIF-8 and (Ce,Co)ZIF-67 at -196 ºC

The specific surface area of the synthesized ZIF-8 was determined to be 1500 m²/g, showcasing its notable porosity. In comparison, the (Ce,Zn)ZIF-8 exhibited a slightly reduced surface area of 1220 m²/g, indicative of the impact of Ce metal modification on the porous structure. Conversely, the (Ce,Co)ZIF-67 displayed a heightened surface area of 1440 m²/g, surpassing (Ce,Zn)ZIF-8, yet still falling short of the benchmark set by ZIF-67 [192]. The micro porosity of (Ce,Zn)ZIF-8 and (Ce,Co)ZIF-67 was further highlighted by mean pore sizes of 2.14 nm and 1.76 nm, respectively. The microporous volumes of 0.51 cc/g for (Ce,Zn)ZIF-8 and 0.55 cc/g for (Ce,Co)ZIF-67 underscored the materials' capacity for selective adsorption.

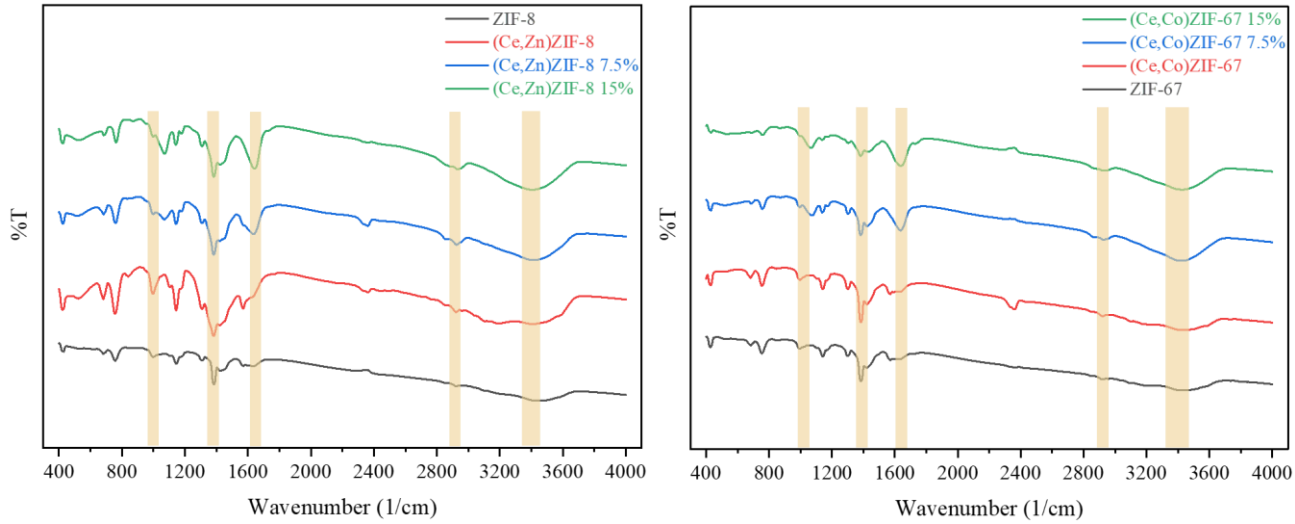

Figure 4.2: FTIR spectra of (Ce,Zn)ZIF-8 and (Ce,Co)ZIF-67

FTIR spectra are shown in figure 4.2. Peaks at 3442 cm^{-1}, 2959 cm^{-1}, 2922 cm^{-1}, 2292.5 cm^{-1}, 1426 cm^{-1} and 1384 cm^{-1} can be seen in the FTIR spectra of (Ce,Zn)ZIF-8. Similarly, for ZIF-67 based adsorbent, important peaks were observed at 3857 cm^{-1}, 3840 cm^{-1}, 3824 cm^{-1}, 3731 cm^{-1}, 3696 cm^{-1}, 3423 cm^{-1}, 3101 cm^{-1}, 2955 cm^{-1}, 2920 cm^{-1}, 2363 cm^{-1}, 1422 cm^{-1}, 1383 cm^{-1}. Peaks in the range of 2920 cm^{-1} to 3150 cm^{-1} demonstrated both aliphatic and aromatic carbon hydrogen bond stretching, indicating the existence of Hmim linker [198]. Peaks in the range of 1350 cm^{-1} to 1450 cm^{-1} suggested an aromatic ring stretch, whereas peaks in the range of 1596 cm^{-1} and 1650 cm^{-1} indicated N-H bending. The 7.5% and 15% DEA loaded adsorbents however, showed all the characteristic peaks indicative of a secondary amine. Strong peaks between 3200-3300 cm^{-1} for an N-H stretch belonging to secondary amines were observed for all doped adsorbents [199]. Other amine peaks were 1020-1250 cm^{-1} for a C-N vibration, 3000-2840 cm^{-1} for an alkane C-H stretch, 3200-3550 cm^{-1} a broad and strong peak indicating the presence of alcoholic O-H, while medium peak intensities between 1050-1080 cm^{-1} for a primary alcohol stretch [107,200].

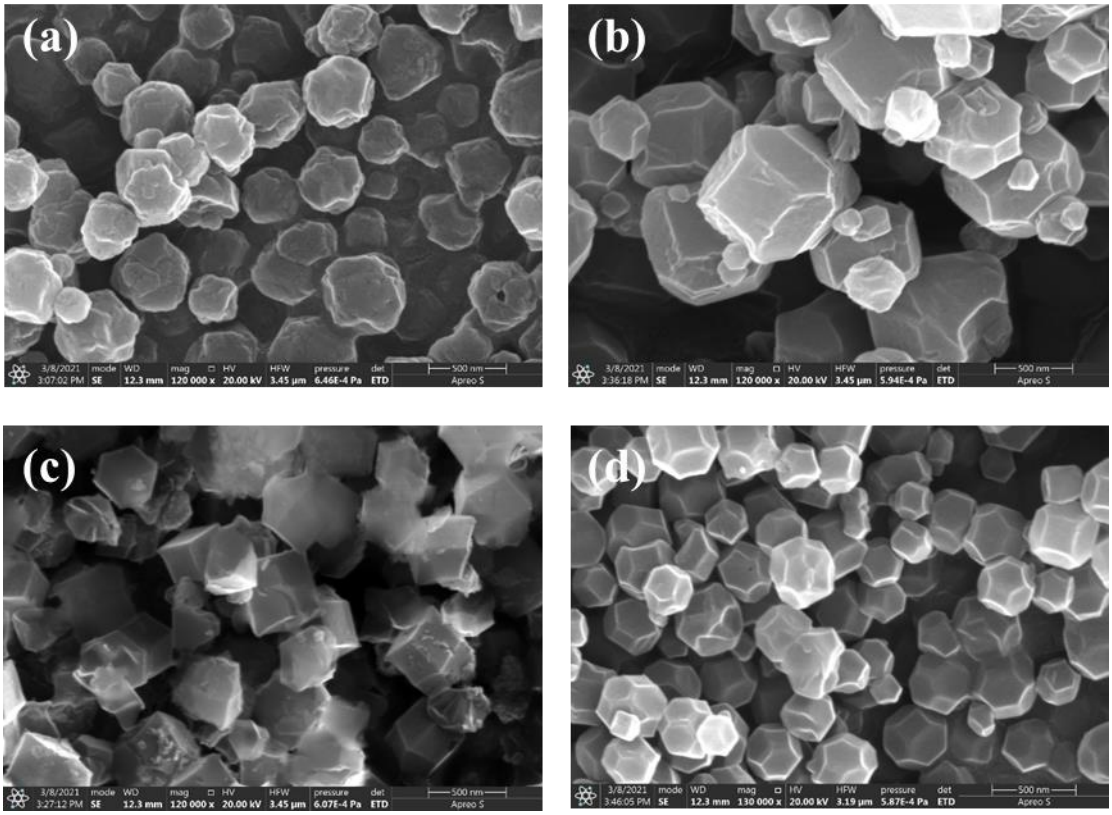

Figure 4.3: Scanning electron micrographs of a) ZIF-8, b) ZIF-67, c) (Ce,Zn)ZIF-8 and d) (Ce.Co)ZIF-67

Intriguingly, the structural nuances of (Ce,Zn)ZIF-8 deviated from the typical cubic-rhomboid tendencies exhibited by pure ZIF-8, hinting at the transformative influence of Ce metal modification on the original framework. Likewise, (Ce,Co)ZIF-67 presented a departure from the standard ZIF-67 structure, showcasing a distinctive dodecahedral arrangement. The interplanar spacing values of 12.01 Å for (Ce,Zn)ZIF-8 and 11.91 Å for (Ce,Co)ZIF-67 deviated slightly from the interplanar spacing observed in the synthesized pure ZIF-8 (12.114 Å) and ZIF-67 (12.008 Å). This departure underscores the structural alterations induced by the incorporation of Ce and Co metals, providing valuable insights into the modification effects on the intermolecular arrangement within the ZIFs. Figure 4.4 shows the diffractograms of the adsorbents in question. The presence of ZIF-8 was confirmed by prominent peaks with high intensities at 2θ values about 7.3º, 10.3º, 12.7º, 14.7º, 18.0º, 18.2º, 21.9º, and 24.9º [201].

(Ce,Co)ZIF-67 showed intensities at 2θ values around 7.4º, 10.5º, 15.2º, 16.8º, 17.2º, 18.1º, 27.9º and 29.1º typical of ZIF-67.

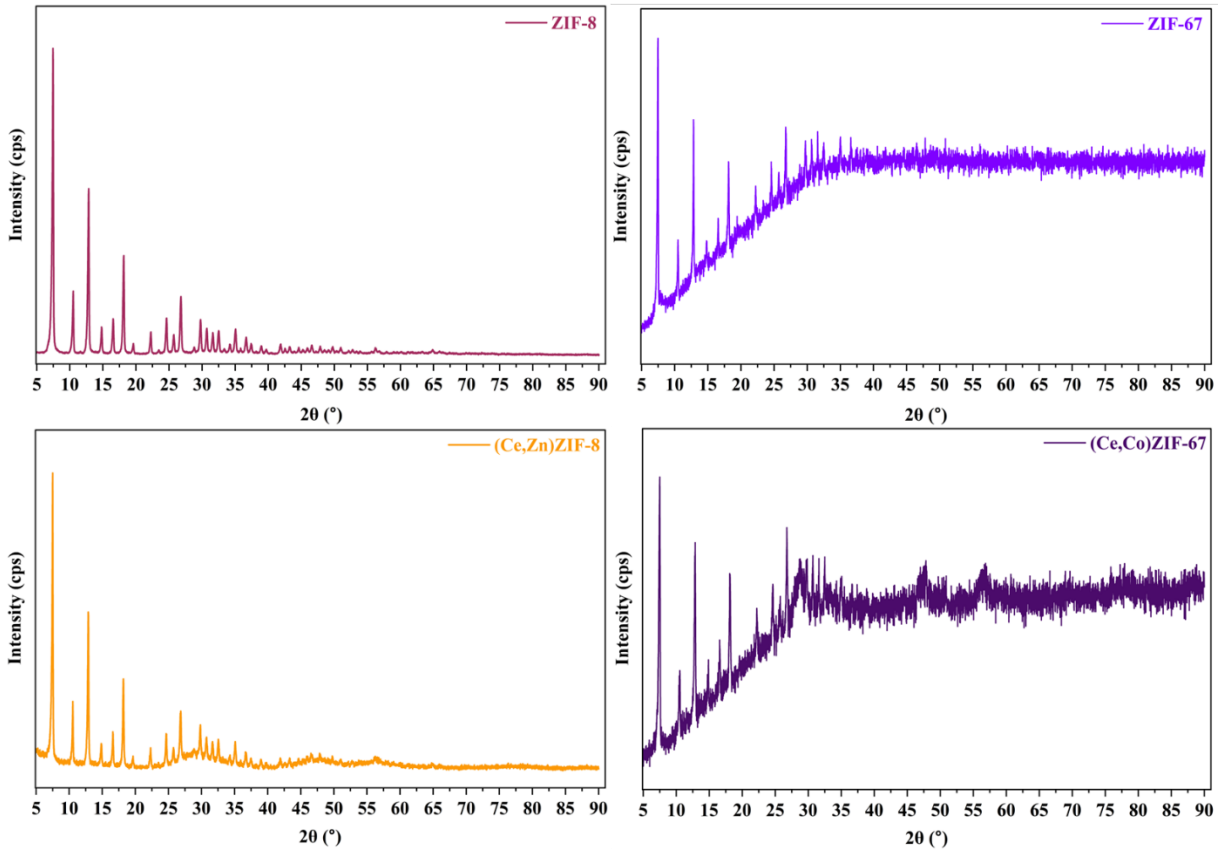

Figure 4.4: Diffractograms of synthesized adsorbents

However, as the values had a slight shift in (Ce,Zn)ZIF-8 characteristic peaks shifted slightly compared to ZIF-8. The characteristic 7.291º peak of ZIF-8 shifted to 7.355º in (Ce,Zn)ZIF-8. (Ce,Co)ZIF-67 also showed a shift in peaks compared to ZIF-67. Both 7.4º and 10.4º of ZIF-67 shifted to 7.4º and 10.5º in the case of (Ce,Co)ZIF-67. A decrease in intensity of peaks was also observed for both (Ce,Zn)ZIF-8 and (Ce,Co)ZIF-67 vs ZIF-8 and ZIF-67. The interplanar spacing of (Ce,Zn)ZIF-8 and (Ce,Co)ZIF-67 were found to be 12.01 Å and 11.91 Å respectively. This also deviates slightly from the usual interplanar spacing of the synthesized pure ZIF-8(12.114 Å) and ZIF-67(12.008 Å).

In summary, the extensive characterization studies, incorporating BET analysis, XRD, SEM, and FTIR spectroscopy, have collectively provided a comprehensive understanding of the

structural, morphological, and chemical attributes of the synthesized ZIFs. These insights lay a robust foundation for elucidating the potential applications of these materials in diverse fields, ranging from gas adsorption to catalysis, and pave the way for further exploration of their unique properties.

4.3. Initial Screening studies and RSM experimental design

In the foundational phase of our study, the meticulous screening of potential adsorbents was driven by a triad of pivotal factors: initial CO_2 uptake, BET surface areas, and the efficiency of the synthesis process. This nuanced evaluation aimed to discern the most promising candidates from a repertoire of parent Zeolitic Imidazolate Frameworks (ZIFs) and their tailored counterparts. A comprehensive comparative analysis ensued, with table 4.1 providing an extensive breakdown of the BET surface areas for all considered adsorbents during the primary screening. Remarkably, the synthesized (Ce,Zn)ZIF-8 and (Ce,Co)ZIF-67 showcased superior performance compared to their parent ZIFs, ZIF-8 and ZIF-67, respectively. The experimental conditions for the initial uptake investigations were meticulously controlled, entailing a total feed flow of 150 mL/min, composed of nitrogen and carbon dioxide in a specific 2:1 ratio, respectively.

Table 4.1: Comparison of screened adsorbents

Adsorbent	**BET Surface Area(m^2/g)**	**Pore volume(cc/g)**	**Initial CO_2 Uptake(mmol/g)**
ZIF-8	1550	0.72	1.41
ZIF-67	1720	0.69	1.55
(Ce,Zn)ZIF-8	1266	0.68	3.71
(Ce,Co)ZIF-67	1440	0.64	3.55

Transitioning to a more intricate phase of CO_2 adsorption, the Response Surface Methodology (RSM) was deployed utilizing a central composite design (CCD) face-centered design. This sophisticated design framework incorporated three levels (+1, 0, −1) for four pivotal factors: temperature, adsorbent loading, carbonation time, and DEA (diethanolamine) loading percentage. Recognizing the variability in adsorbent characteristics, a categorical factor with four levels corresponding to the four different adsorbents was thoughtfully integrated into the experimental design. The adsorbent codes 'A' and 'B' specifically represented (Ce,Zn)ZIF-8 and (Ce,Co)ZIF-67. A meticulously planned set of 60 experiments, evenly distributed across the different adsorbents, were systematically conducted to scrutinize the influence of each vital process parameter. The Design Expert 12 trial version software played an instrumental role in conducting exhaustive analyses, determining the significance of each parameter, and optimizing the experimental conditions. These detailed parameters, encompassing a spectrum of variables, are comprehensively cataloged in table 4.2, providing a systematic guide for a nuanced understanding of the intricate adsorption process.

Table 4.2: Experimental design with process parameters

Variable	Min	Central	Max
Temperature (°C)	25	75	125
Amount of adsorbent (g)	5	10	15
Time of aeration (min)	60	150	240
DEA loading percentage	0	7.5	15

Temperature of adsorption, acknowledged as a linchpin parameter in adsorption studies, assumed particular significance in both CO_2 adsorption and catalysis, a fact well-documented

in literature. The loading percentage of DEA emerged as a key determinant, exerting influence on both the enhancement of uptake properties and the optimization of uptakes, a theme underscored in prior research [202]. The temporal aspect of carbonation, a pivotal factor, was methodically examined to unravel its impact on the nature of adsorption and the kinetics of gas uptake, aligning with contemporary studies [203]. Importantly, each stage of the study was conducted with fresh samples, ensuring not only methodological consistency but also eliminating potential biases. For instance, a singular batch of samples was judiciously employed for runs 1 to 8, underscoring the meticulous attention to experimental precision. Subsequently, a new batch of 15 g each of adsorbent was synthesized for DEA loading of 7.5% and beyond, ensuring a controlled and reproducible experimental setup. To complete the experimental cycle, the regeneration process involved a thorough flushing with pure nitrogen gas at 100°C, safeguarding the integrity of the adsorbents for subsequent experiments. This exhaustive and systematic approach, from the initial screening stage to the sophisticated RSM-based investigations, underscores the methodological rigor underpinning our study. It not only enhanced the reliability of our findings but also positioned our research at the forefront of advancements in the realm of adsorption studies, offering valuable insights into the intricacies of the adsorption process and the potential applications of modified ZIFs in this domain.

4.4. Process optimization using RSM

4.4.1. CO_2 uptake results

The temperature of adsorption stands out as a pivotal parameter significantly influencing a material's adsorption capacity. In the context of our study, the Central Composite Design (CCD) model strategically incorporated temperatures of 25 °C, 75 °C, and 125 °C to dissect the impact of temperature on carbon capture values. Figure visually represents the dramatic reduction in uptake at higher temperatures (figure 4.5). Specifically, for (Ce,Zn)ZIF-8 at loading percentages of 7.5% and 15%, adsorption capacities exhibited a decline from 3.62 mmol/g and

4.54 mmol/g at 25°C to 2.2 mmol/g and 2.8 mmol/g at 125°C, respectively (table 4.3). Similarly, (Ce,Co)ZIF-67 displayed a diminishing trend from 4.6 mmol/g and 5.24 mmol/g at 25°C to 2.4 mmol/g and 3.21 mmol/g at 125°C for loading percentages of 7.5% and 15%, respectively (table 4.4).

Table 4.3: CO_2 Uptake values of (Ce,Zn)ZIF-8

Std	Temperature (°C)	Amount of adsorbent (g)	Time (min)	DEA Loading	CO_2 Uptake (mmol/g)
1	25	5	60	0	3.71
2	125	5	60	0	1.95
3	25	15	60	0	3.9
4	125	15	60	0	2.1
5	25	5	240	0	3.88
6	125	5	240	0	1.9
7	25	15	240	0	3.8
8	125	15	240	0	2.48
9	25	5	60	15	4.45
10	125	5	60	15	2.6
11	25	15	60	15	4.7
12	125	15	60	15	2.74
13	25	5	240	15	4.55
14	125	5	240	15	2.5
15	25	15	240	15	4.61
16	125	15	240	15	2.8
17	25	10	150	7.5	3.62
18	125	10	150	7.5	2.2
19	75	5	150	7.5	3.5
20	75	15	150	7.5	3.52
21	75	10	60	7.5	3.6
22	75	10	240	7.5	3.67
23	75	10	150	0	2.57
24	75	10	150	15	4.44
25	75	10	150	7.5	3.69
26	75	10	150	7.5	3.77
27	75	10	150	7.5	3.33
28	75	10	150	7.5	3.45
29	75	10	150	7.5	3.38
30	75	10	150	7.5	3.59

Comparative studies by Agueda et al. [204] and Zhang et al. [32] align with our findings. Agueda et al. explored UTSA-MOF under varying temperatures, reporting decreasing CC values from 5.2 mmol/g at 25 °C to 4.3 mmol/g at 65 °C. Similarly, Chen et al. [205] observed a decreasing trend in Ni-MOF-74 adsorption capacity, from 7.5 mmol/g at 25 °C to 5.3 mmol/g at 75 °C. This consistent trend resonates with existing theories, attributing the decrease in uptake values to the deterioration of organic structural linkers in MOFs and ZIFs at elevated temperatures [206]. This is in line with thermodynamic principles that favor CO_2 adsorption at lower temperatures due to increased accessibility to adsorption sites. At higher temperatures, heightened competition for these sites leads to a general decline in adsorption capabilities.

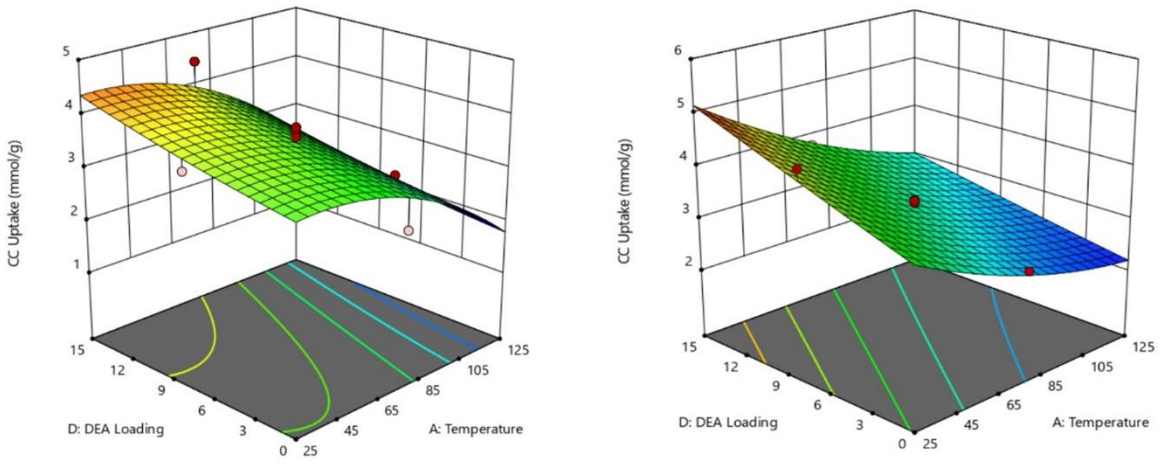

Figure 4.5: CO_2 adsorption capacity with respect to temperature and DEA loading of a) (Ce, Zn)ZIF-8, b) (Ce,Co)ZIF-67

Moving to the effect of DEA (diethanolamine) loading, our observations reveal an overall positive impact. A notable enhancement is evident between 0% and 7.5% loading, and again between 7.5% and 15%. A substantial increase of approximately 30% is noted in the uptake values from 0% to 15% loading. This resonates with literature findings, where an increase in DEA loading is typically associated with improved adsorption capacity. Kenyotha et al. [207] reported a decrease in CC values for modified ZIF-8 adsorbents, emphasizing the impact of pore blockage and available adsorption sites relative to doping ratio.

The interaction between amine moieties and CO_2 molecules emerges as a critical factor influencing adsorption capacities. Figure 4.5 illustrates that an increase in DEA loading percentage correlates with a substantial rise in CO_2 adsorption capacity, reaching a maximum at 15% loading. Despite the anticipated reduction in surface area and pore volume resulting from DEA loading [208], the obtained values remain commendable.

Table 4.4: CO_2 Uptake values of (Ce,Co)ZIF-67

Std	Temperature (°C)	Amount of adsorbent (g)	Time (min)	DEA Loading (%)	CO_2 Uptake (mmol/g)
1	25	5	60	0	3.55
2	125	5	60	0	2.21
3	25	15	60	0	3.73
4	125	15	60	0	2.41
5	25	5	240	0	3.53
6	125	5	240	0	2.15
7	25	15	240	0	3.8
8	125	15	240	0	2.23
9	25	5	60	15	5.1
10	125	5	60	15	2.89
11	25	15	60	15	5.2
12	125	15	60	15	3.1
13	25	5	240	15	5.24
14	125	5	240	15	3.2
15	25	15	240	15	5.15
16	125	15	240	15	3.21
17	25	10	150	7.5	4.6
18	125	10	150	7.5	2.4
19	75	5	150	7.5	3.14
20	75	15	150	7.5	3.33
21	75	10	60	7.5	3.21
22	75	10	240	7.5	3.45
23	75	10	150	0	2.75
24	75	10	150	15	3.8
25	75	10	150	7.5	3.1
26	75	10	150	7.5	3.14
27	75	10	150	7.5	3.3
28	75	10	150	7.5	3.15
29	75	10	150	7.5	3.37
30	75	10	150	7.5	3.35

Comparisons with literature findings further corroborate our results. Anh Phan et al. [209] reported a CO_2 uptake value of 37 cc/g for pure ZIF-67, half the value obtained for (Ce,Co)ZIF-67. The addition of DEA further enhanced uptake, witnessing a nearly 35% increase from 0% to 15% DEA loading. The decrease in uptake values at higher temperatures for DEA-loaded (Ce,Co)ZIF-67 aligns with observations by Konni et al. [210], who studied ZIF-67-based adsorbents. The influence of DEA loading on uptake values underscores the intricate relationship between DEA loading and adsorption performance.

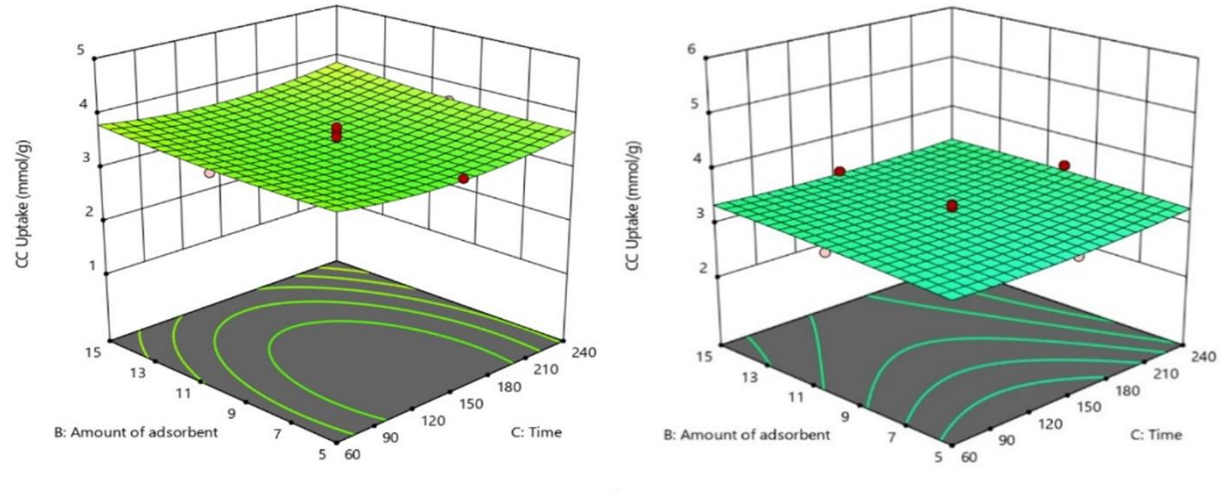

Figure 4.6: CO_2 adsorption capacity with respect to time and amount of adsorbent of a) (Ce,Zn)ZIF-8, b) (Ce,Co)ZIF-67

Analyzing the influence of adsorbent amount on uptake as a function of carbonation time, our findings deviate from the inverse relationship noted by Ghaemi et al. [211] for $Ca(OH)_2$ and $Mg(OH)_2$-based adsorbents. Contrary to the expected decrease in uptake with increasing adsorbent weight, our study reveals that the amount of adsorbent loaded had an almost insignificant effect on CO_2 uptake values. This departure from the inverse relationship observed in literature underscores the unique characteristics of the synthesized adsorbents in our study.

This study explores the impact of temperature and DEA loading on uptake values, aligning observations with existing literature and providing valuable insights into the intricate dynamics of CO_2 adsorption. The positive influence of DEA loading, coupled with the nuanced interplay of temperature, adds depth to our understanding of the adsorption process. These insights hold promise for the development of tailored adsorbents with enhanced CO_2 capture capabilities, contributing to advancements in environmental sustainability and gas separation technologies.

4.4.2. RSM model development and verification

The Response Surface Methodology (RSM) equations for all four adsorbents are presented below, with the optimal experimental conditions summarized in table 4.5. These equations establish a relationship between the experimental output, specifically the CO_2 capture (CO_2 uptake), and the various process parameters involved. The considered process parameters include temperature (coded as A), DEA loading percentage (coded as D), amount of adsorbent (coded as B), and time of carbonation (coded as C). The coded equations below express the final relation between the CO_2 uptake values and the specified parameters in this experimental context.

For (Ce,Zn)ZIF-8, the coded CO_2 uptake equation is as follows,

$$CO_2\ Uptake = [3.488 - (0.886A) + (0.0895B) + (0.0245C) + (0.3945D) + (0.0469AB) + (0.0131AC) - (0.0506AD) + (0.0081BC) - (0.0056BD) - (0.0269CD) - (0.5304A^2) + (0.0696B^2) + (0.1946C^2) + (0.0646D^2)] \quad Eq\ 4.1$$

For (Ce,Co)ZIF-67, the coded CO_2 uptake equation is,

$$CO_2\ Uptake = [3.248 - (0.895A) + (0.064B) + (0.031C) + (0.585D) + (0.0025AB) + (0.0025AC) - (0.1675AD) - (0.02625BC) - (0.0313BD) + (0.0438CD) + (0.239A^2) - (0.026B^2) + (0.0694C^2) + (0.0144D^2)] \quad Eq\ 4.2$$

For (Ce,Zn)ZIF-8, the model F-value of 18.79 indicates the model's significance. The key influential terms for the model fit are A, D, and A^2. Terms such as AB, AC, and others exceeding 0.1000 can be considered insignificant. The reasonable agreement between the predicted R^2 value (0.7729) and the Adjusted R^2 value (0.8957) suggests a satisfactory fit, and the overall fit statistics align reasonably well with the actual values obtained. Similarly, for (Ce,Co)ZIF-67, the model F-value of 96.16 underscores the model's significance. The key contributing terms for the model fit are A, B, D, AD, and A^2. A lack of chance of 43.47% indicates the model's reasonable ability to explain trends for this adsorbent. The excellent agreement between the Predicted R^2 value (0.9534) and the Adjusted R^2 value (0.9787) affirms the model's proximity to the experimental design.

Table 4.5: Optimum CO_2 capture conditions

Adsorbent	**Temperature (°C)**	**Amount (g)**	**Time (min)**	**DEA %**	**Predicted CC (mmol/g)**	**Experimental CC (mmol/g)**
(Ce,Zn)ZIF-8	60	6.58	240	15	4.55	4.31
(Ce,Co)ZIF-67	100	7.93	100	13.6	3.14	3.03

The composite desirability values for the optimum conditions of (Ce,Zn)ZIF-8 and (Ce,Co)ZIF-67 are 0.919 and 0.945, respectively. In the context of RSM design, composite desirability gauges the degree to which the responses align with the input parameters. With values exceeding 0.9 in this study, the desirability scores are sufficiently close to the theoretical ideal of '1,' indicating a favorable match between responses and input parameters [212]. Both adsorbents' fit models reveal quadratic-type response surfaces, adding depth to the understanding of their performance characteristics under varying conditions.

4.5. Adsorption kinetic study

To gain a deeper understanding of the adsorption behavior under the identified optimum conditions for both adsorbents, kinetics studies were conducted. Three kinetic models—pseudo first order, pseudo second order, and the Avrami kinetics model—were employed (mentioned in Chapter 2 as Eq 2.1, 2.2, 2.3, 2.4 and 2.5). These kinetic investigations were performed under the optimal condition in section 4.4.2. Table 4.6 contains the data of various models employed.

Table 4.6: Kinetic parameters for various models

Adsorbent	Kinetics Model	Temp (ºC)	Q_e exp (mmol/g)	Q_e fit (mmol/g)	k	n	R^2
(Ce,Zn)ZIF-8/15% DEA loaded	Pseudo First Order	60	4.68	4.61	0.198		0.985
	Pseudo Second Order	60	4.68	4.73	0.089		0.994
	Avrami	60	4.68	4.62	0.378	0.66	0.992
(Ce,Co)ZIF-67/13.6% DEA loaded	Pseudo First Order	100	3.03	3.12	0.157		0.977
	Pseudo Second Order	100	3.03	3.35	0.075		0.914
	Avrami	100	3.03	3.08	0.055	1.53	0.997

The pseudo first order model primarily characterizes physisorption, while the pseudo second order model is more indicative of chemisorption. Positioned between these two, the Avrami model suggests a combination of physisorption and chemisorption in the adsorption process. Analyzing the experimental data, it was observed that the pseudo second order kinetics aptly described the (Ce,Zn)ZIF-8 adsorbent loaded with 15% DEA, evident from the fit table 4.6 and an R^2 value of 0.995. Similarly, for the (Ce,Co)ZIF-67 adsorbent loaded with 13.6% DEA, the Avrami model demonstrated a superior fit with R^2 value of 0.997. Figure 4.7 displays the kinetic fit graphs for the optimal (Ce,Zn)ZIF-8 and (Ce,Co)ZIF-67 conditions. Notably, the R^2 value of 0.992 for the (Ce,Zn)ZIF-8/15% DEA adsorbent further supports the adequacy of the

fit. The data collectively suggests a hybrid nature of adsorption, emphasizing the dual character of the process. Considering that DEA is employed as an absorbent for chemisorption, it can be inferred, even from a chemical standpoint, that any adsorbent loaded with amines has the potential to induce a dual-natured adsorption process.

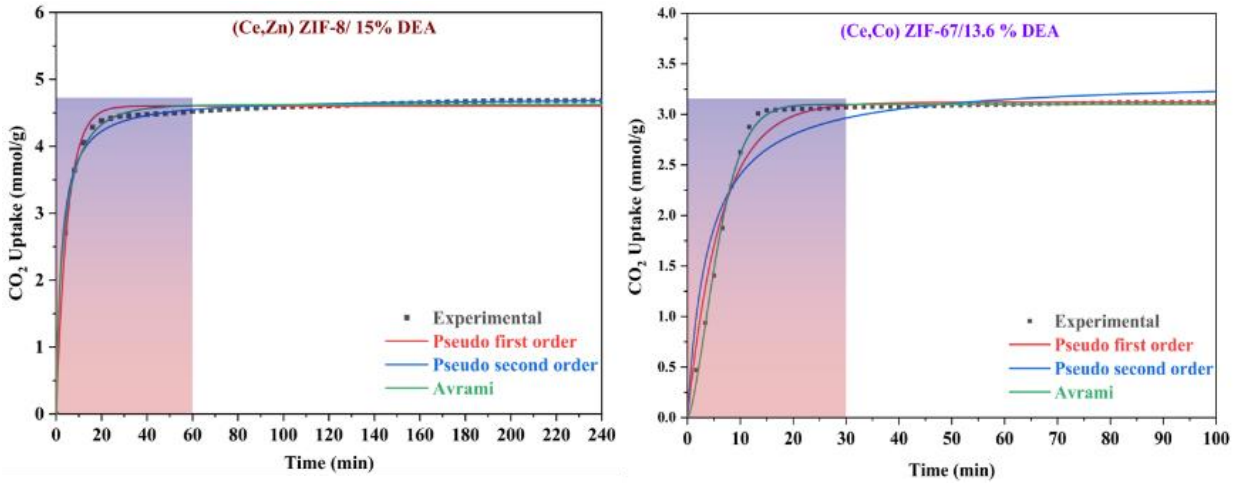

Figure 4.7: Kinetic modelling of (Ce,Zn)ZIF-8/ 15% DEA loaded adsorbent at 60 ºC and (Ce,Co)ZIF-67/ 13.6% DEA loaded adsorbent at 100 ºC

4.6. Adsorption isotherm study

The concentration of CO_2 within the feed is a crucial factor influencing the uptake capacities of adsorbents. To investigate the impact of CO_2 concentration, the partial pressures of CO_2 were varied from 0 to 0.8 bar at 25 ºC. Figure 4.8 provides a visual representation of how CO_2 concentration affects the selected adsorbents. Both adsorbents exhibited impressive adsorption capacity towards CO_2. The variation in pressure demonstrated that while the adsorbent tended towards increased adsorption, the rate of adsorption decreased with rising pressure. This phenomenon may be attributed to saturation or equilibrium being reached as the adsorption capacity fills up at a certain point. As the CO_2 concentration in the feed increases, the pores fill up rapidly, leaving limited space within the structure. Consequently, further increases in concentration might not result in a significant augmentation of absorption capacities. The

adsorption capacity of both adsorbents decreased with an increase in temperature, aligning with earlier findings. However, elevated temperatures provide the necessary energy for the transition from physisorption to chemisorption. When comparing the optimized adsorbent data for CO_2 adsorption capacity, the highest adsorption occurred at the lowest temperature and highest pressure, highlighting the predominant role of chemisorption, especially when utilizing additives like DEA [213].

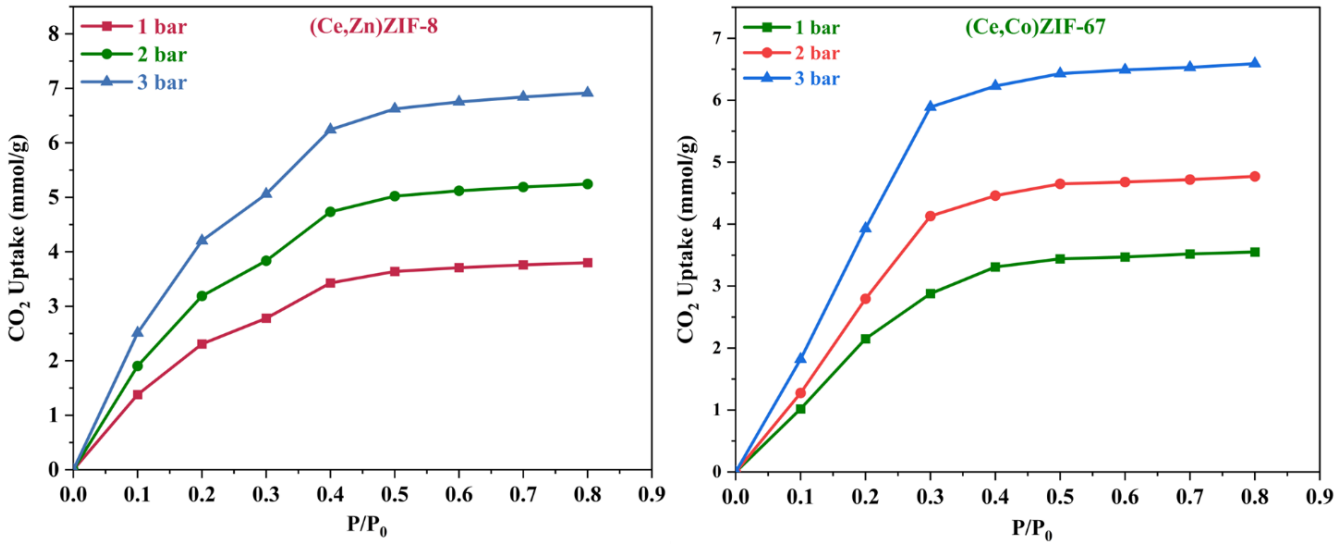

Figure 4.8: CO_2 adsorption isotherms of a) (Ce,Zn)ZIF-8 and b) (Ce,Co)ZIF-67 at 298 K

Understanding the adsorption nature and type is crucial, and adsorption isotherms play a vital role in unraveling these characteristics. In this study, adsorption investigations on unmodified adsorbents were conducted at 25 ºC, varying the total pressure to three values: 1 bar, 2 bar, and 3 bar, with CO_2 percentages in the feed ranging from 0% to 80%.

Table 4.7: Adsorption isotherm modelling parameters

Adsorbent	Temperature (K)	Total Pressure (bar)	k_L	Q_e (mmol/g)	R^2	k_F	n	R^2
(Ce,Zn)ZIF-8	298	1	3.85	5.26	0.98	4.53	2.34	0.96
		2	3.86	7.22	0.99	6.21	2.36	0.97
		3	4.15	9.39	0.98	8.19	2.43	0.96
(Ce,Co)ZIF-67	298	1	3.93	4.96	0.96	4.29	2.31	0.91
		2	3.89	6.72	0.97	5.80	2.32	0.92
		3	4.22	13.01	0.97	8.08	2.39	0.93

Two models, Langmuir and Freundlich were considered (mentioned in Chapter 2, Eq 2.6, 2.7, 2.8 and 2.9). Figure 4.8 and table 4.7 clearly indicate a significant increase in uptake values as the total process pressure rises. At 3 bar pressures, the values for both adsorbents nearly doubled compared to those at 1 bar pressure. Furthermore, the fits suggested that the Langmuir isotherm better described the adsorption process. The R^2 values for the Langmuir adsorption isotherm fits indicated that monolayer adsorption dominated the entire process for both adsorbents. Interestingly, as the process pressure increased, the R^2 values for the Langmuir fit also increased, consistent with the dominance of monolayer adsorption at low pressures. Notably, with increasing total process pressures, the R^2 values for Freundlich isotherm fits also increased, signifying a significant influence of multi-layer adsorption. Similar trends were observed in Yang et al.'s work on modified ZIF-67 adsorbents [214], where increasing total pressure led to a significant rise in adsorption capacity. Similarly, Russell and his team [215] found in their low-temperature isotherm study of ZIF-8 adsorbents that at high pressures, CC capacity increased significantly.

4.7. Cyclic stability studies

Stability tests were conducted over 15 cycles at room temperature (25°C). Regeneration of (Ce,Zn)ZIF-8 and (Ce,Co)ZIF-67 was carried out in the presence of N_2 gas at a temperature of 150 °C. Each carbonation and decarbonation cycle utilized 5 g of material, with each cycle lasting 60 minutes. As anticipated, the ZIF-based adsorbents exhibited degradation with each successive cycle, in line with the cyclic adsorption nature of metal oxide-fly ash composites discussed by Sreenivasulu et al. [216]. This degradation was attributed to the formation and destruction of crystalline phases of CaO and its interactions with CO_2 at the adsorption temperature. Figure 4.9 illustrates the cyclic stability studies of the two adsorbents.

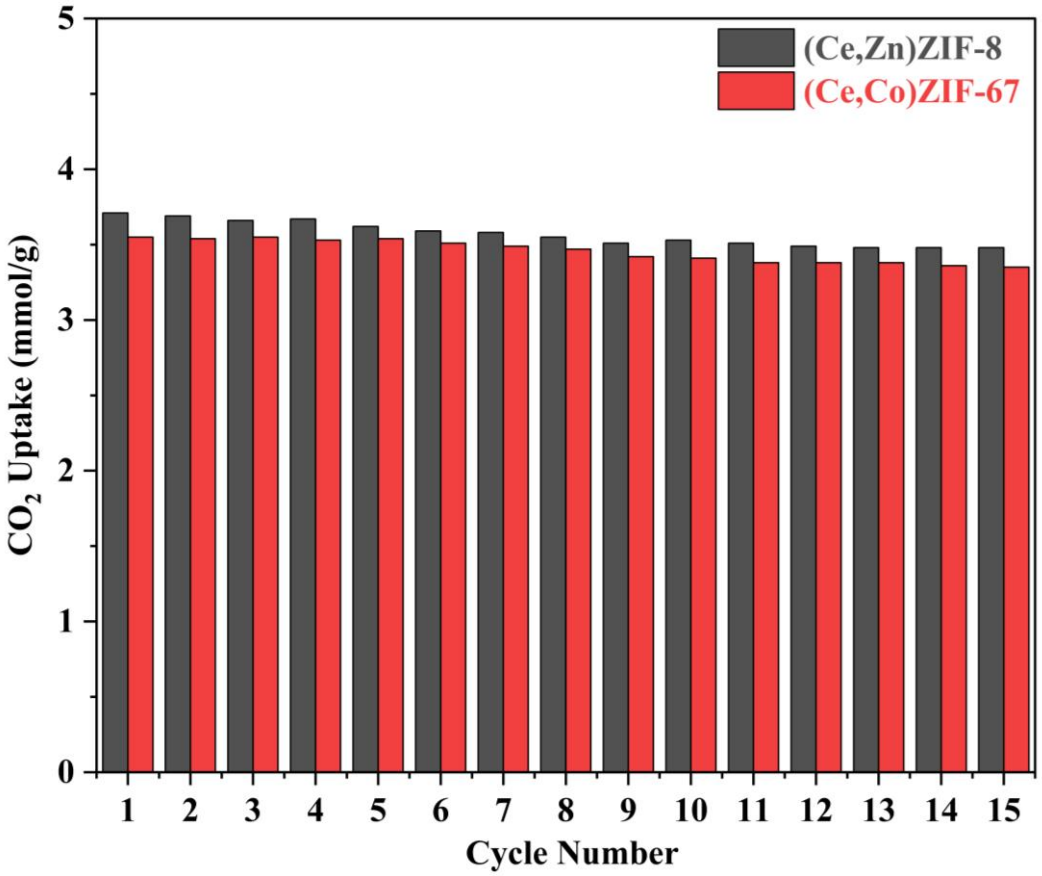

Figure 4.9: Cyclic stability of (Ce,Zn)ZIF-8 and (Ce,Co)ZIF-67

Remarkably, (Ce,Zn)ZIF-8 and (Ce,Co)ZIF-67 demonstrated commendable stability even after 15 cycles, starting with high initial uptake values of 3.71 mmol/g and 3.55 mmol/g,

respectively. At the end of 15 cycles, both adsorbents retained approximately 94% of their initial uptake values. This observation aligns with the roughening of the diffractograms of the adsorbents after 15 cycles compared to the fresh samples. Although (Ce,Zn)ZIF-8 exhibited a change in color from pale yellow to yellowish-brown, no significant color change was observed for (Ce,Co)ZIF-67. Importantly, the particle structure showed no major alteration before and after the cyclic studies, providing a plausible explanation for the cyclic stability of the investigated adsorbents.

4.8. Conclusions

Two ZIF-based adsorbents, (Ce,Zn)ZIF-8 and (Ce,Co)ZIF-67, along with their amine-loaded counterparts, underwent successful synthesis and in-depth studies on CO_2 capture (CC), kinetics, and cyclic stability. The implementation of the central composite design in the response surface methodology (RSM) ensured rigorous process standardization. The superior uptake values compared to their parent ZIFs were ascribed to the introduction of crystal defects and charge, courtesy of the incorporation of cerium ions. The standard deviation values demonstrated excellent agreement with the optimal experimental conditions specified by the model, with an error percentage hovering around 7%. Further enhancement of CC capacity was achieved through diethanolamine (DEA) loading. The optimized conditions for (Ce,Zn)ZIF-8 and (Ce,Co)ZIF-67, with amine loading, were identified at 15% DEA loading and 25 ºC, resulting in 4.37 and 13.6% DEA loading with 3.03 mmol/g, respectively. Cyclic stability testing revealed retention rates of 94% and 95% for the pure adsorbents after 15 cycles. The kinetics of the optimized adsorbents, derived from the RSM design, were effectively elucidated by the pseudo-second-order and Avrami models. The Langmuir adsorption isotherm emerged as the most suitable descriptor for the adsorption process, indicating monolayer adsorption.

Moreover, the synthesis process showed an exceptionally low overall cost. While traditional methods involving hydrothermal synthesis for ZIFs and MOFs demand significant energy inputs, high pressure, and specific solvents like DMF and ethanol, the current study opted for a more environmentally friendly approach, utilizing only water as a solvent. The synthesis at room temperature contributed to substantial energy savings, reinforcing the sustainable profile of the process.

Chapter 5: Carbon Capture studies using MCM 41 based composites

5. Carbon Capture studies using MCM 41 based composites

5.1. Introduction

MCM-41, a mesoporous silica material, stands out in CO_2 adsorption due to its well-defined pore structure and unique characteristics. Mesoporous materials possess pores in the range of 2 to 50 nm, and MCM-41, with its hexagonal array of uniform mesopores, exhibits a high surface area and pore volume [217,218]. These attributes allow for efficient mass transfer and enhanced accessibility of CO_2 molecules to active sites within the material. The ordered nature of the pores in MCM-41 facilitates the development of a uniform adsorption layer, contributing to improved selectivity and capacity for CO_2 adsorption [219]. The tunable nature of MCM-41 further allows for the optimization of pore size, enabling tailored interactions with CO_2 molecules [220,221].

Activated carbons, derived from diverse carbon-rich precursors such as coconut shells, peat, or wood, offer another compelling avenue for CO_2 capture [222,223]. These materials possess a high degree of porosity, resulting from the presence of both micro- and mesopores. Micropores, with diameters less than 2 nm, provide a large surface area for strong physical adsorption interactions [224,225]. The porous nature of activated carbons promotes a high density of adsorption sites, rendering them effective in capturing CO_2. The carbonization process during activation enhances the material's stability and surface reactivity, making it well-suited for extended use in adsorption processes [226,227].

In CO_2 adsorption applications, the synergy between MCM-41 [228] and activated carbons is notable. MCM-41's ordered mesoporous structure complements the porous network of activated carbons, creating a composite material with improved overall performance. The combination leverages the strengths of both materials, facilitating efficient CO_2 diffusion and maximizing adsorption capacity. The interaction mechanisms between CO_2 molecules and

these materials involve physical adsorption, chemisorption, or a combination of both, depending on the specific surface chemistry and structure of the adsorbents. The quest for effective CO_2 capture technologies is integral to combating climate change, and MCM-41 and activated carbons represent promising materials in this pursuit. Their tailored properties, when strategically combined, contribute to the development of advanced adsorbents with enhanced selectivity, capacity, and stability [229,230]. This research not only advances the field of carbon capture and storage but also aligns with the broader goals of sustainable and environmentally conscious technology development.

In this study, composites of ZIF-8 and MCM-41, as well as MCM-41 and activated carbon, were synthesized, and modifications with diethanolamine (DEA) were implemented on these adsorbents. The primary objective behind combining MCM-41 with ZIF-8 and commercial activated carbons was to develop composites with dual textural properties. Microporous characteristics were predominantly observed in ZIF-8 and commercial activated carbons, facilitating rapid CO_2 adsorption—a highly desirable trait. However, challenges in amine loading were potentially posed due to the presence of narrow micropores in these adsorbents. In contrast, MCM-41, being predominantly mesoporous, was considered an excellent inert support for amines [231], despite exhibiting less favorable adsorption kinetics compared to ZIF-8. The combination of MCM-41 with these microporous materials was expected to result in composites with both fast CO_2 adsorption kinetics and effective amine hosting capabilities [232,233].

Four crucial process parameters were taken into account: temperature, DEA loading, duration of feed flow, and the mass of adsorbent loaded. Following the standardization of the process using Response Surface Methodology (RSM), kinetic and adsorption modeling was carried out. Finally, cyclic stability testing was conducted on both synthesized adsorbents to assess their long-term performance.

5.2. Characterization of adsorbents

The X-ray diffraction (XRD) patterns provided insightful information about the structural composition of the ZIF-8@MCM-41 adsorbent and the MCM-41/AC/Na composite. Distinct peaks at 7.4º, 10.4º, 12.8º, 14.8º, 16.5º, 18.1º, and 29.4º for ZIF-8@MCM-41, and 25.2º, 30.2º, 34.9º, 38.1º, 40.1º, 58.0º, and 79.8º for MCM-41/AC/Na, suggested the crystalline nature of the materials. The lower intensity of the peaks in MCM-41/AC/Na indicated the prevalent influence of activated carbon within the composite, attesting to its dominant role. The diffractograms are given in figure 5.1.

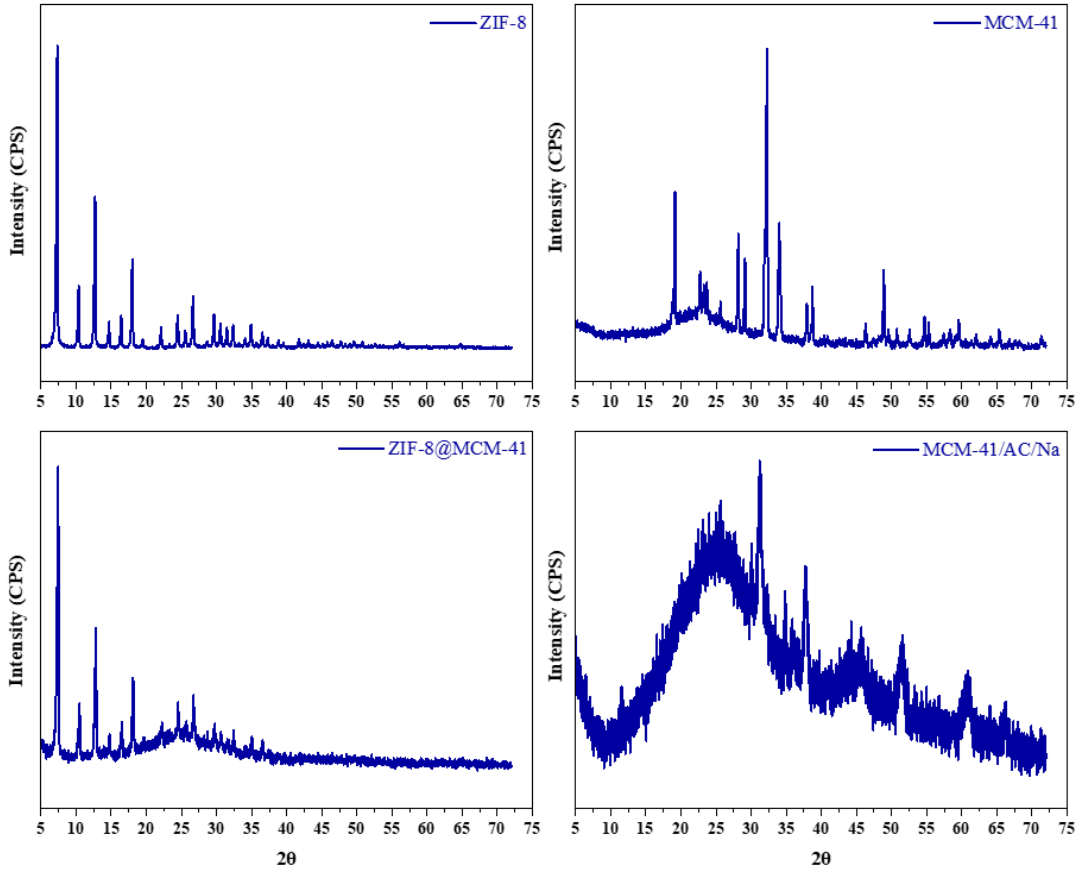

Figure 5.1: Diffractograms of synthesized adsorbents

Further analysis through Fourier-transform infrared (FTIR) spectroscopy revealed distinctive peaks for ZIF-8 at wavenumbers 3442 cm^{-1}, 2959 cm^{-1}, 2292 cm^{-1}, 1426 cm^{-1}, and 1383 cm^{-1}. These peaks corresponded to specific stretching and bending vibrations of bonds associated

with the imidazolate linker in the ZIF-8 structure. Remarkably, the ZIF-8@MCM-41 adsorbent displayed analogous peaks, confirming the preservation of ZIF-8 characteristics within the composite. Additional peaks around 3906 cm^{-1}, 3880 cm^{-1}, 3840 cm^{-1}, 3804 cm^{-1}, 3440 cm^{-1}, and 1634 cm^{-1} were also observed, indicative of the presence of MCM-41 in the composite.

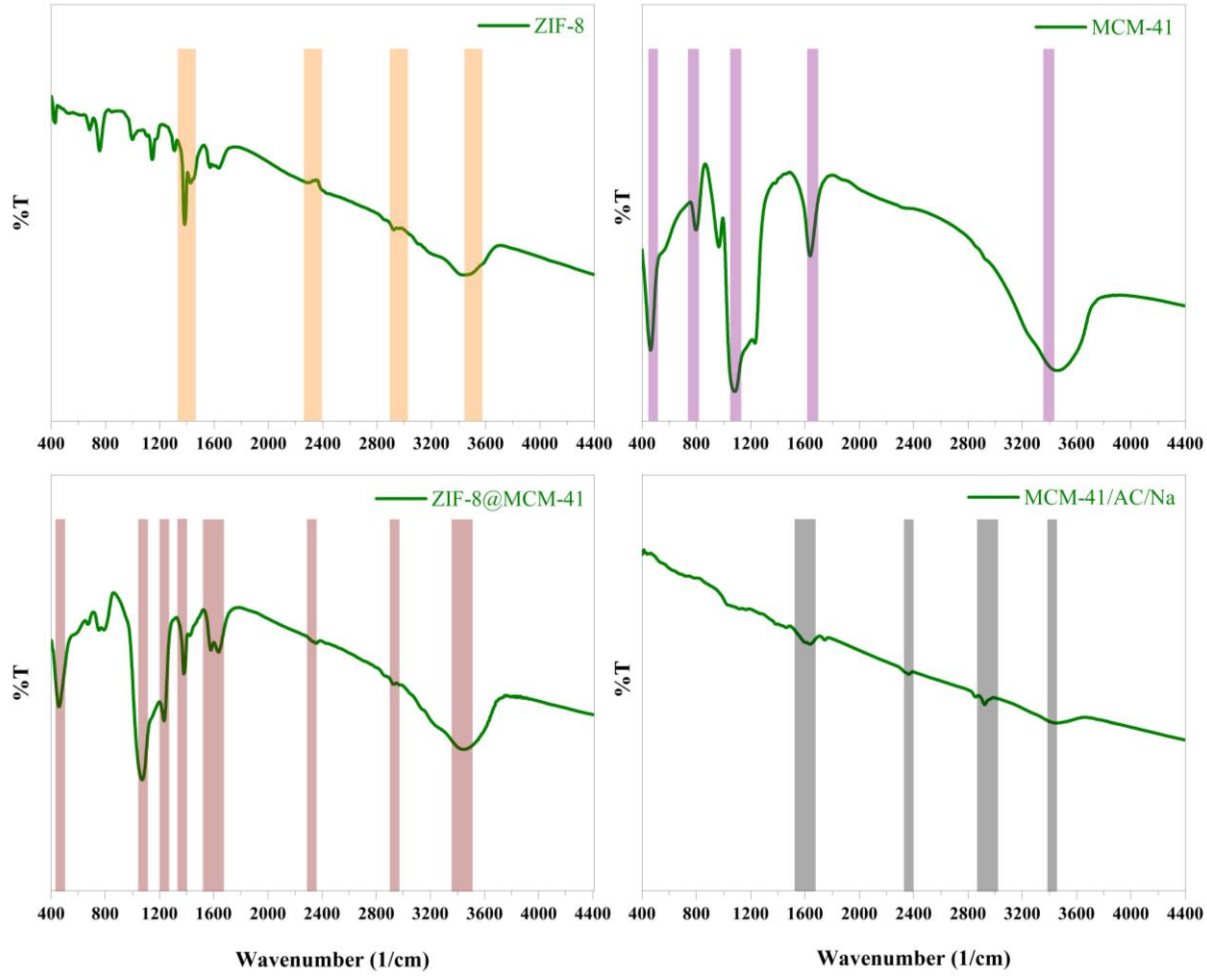

Figure 5.2: FTIR spectra of synthesized adsorbents

Examining the morphology of the ZIF-8@MCM-41 adsorbent unveiled a compelling structure. The synthesized MCM-41 showed globular spherical-like structures and relatively smooth morphology. Also, the in house synthesized MCM-41 had uniform particle sizes within the range 300 nm to 450 nm. This is also similar to the morphology of MCM-41 synthesized in Ortiz et al.'s study of MCM-41 synthesis processes [234]. The morphology mostly depends on the ratio of the chemicals employed in the synthesis process.

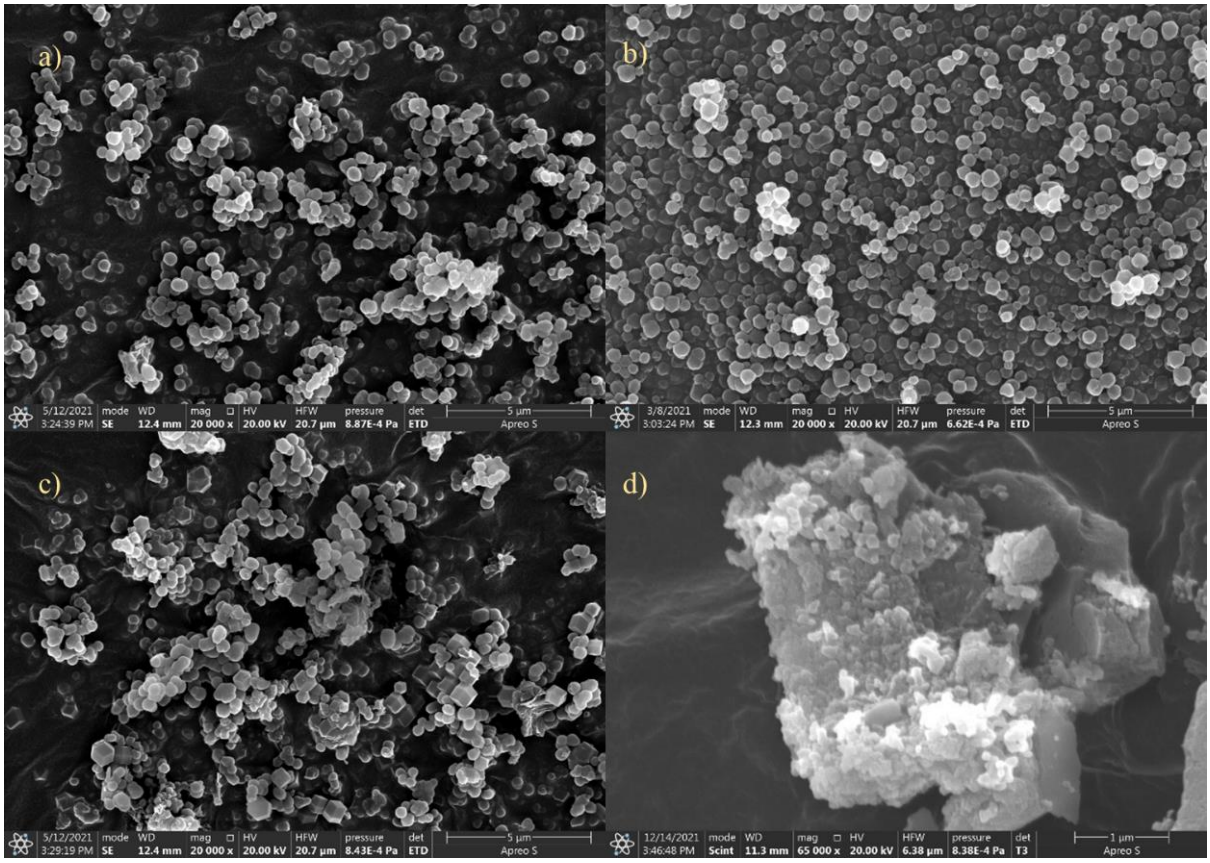

Figure 5.3: Scanning electron micrographs of a) MCM-41, b) ZIF-8, c) ZIF-8@MCM-41 and d) MCM-41/AC/Na

In a study of various synthesis procedures of MCM-41 conducted by Na Rao and team [230], it was found that a mole ratio of 2:17 for CTAB:TEOS, more elongated rod like structures were obtained. However, in our study a ratio of 1:16 was used. This ratio led to smaller and more spherical MCM-41 particles. The ZIF-8 synthesized in this study gave dodecahedral type of structures. Even in the synthesis of ZIFs, the mole ratio between the metal ion and the organic linker becomes extremely essential. For example a ratio of 1:8 of Zn:Hmim gave a more disordered and connected ZIF-8 particles [93]. Conversely, a higher Zn:Hmim ratio would give excellent and ordered nano crystals can be synthesized [235]. The ZIF-8@MCM-41 adsorbent showed interesting morphology. It displayed the characteristic spherical particles of MCM-41. But embedded within these spherical particles, were highly ordered ZIF-8 nanocrystals as given in figure 5. Surprisingly, the nanocrystals obtained within the composite had a more defined

geometry when compared to the pure ZIF-8 nanocrystals. These nanocrystals are more akin to the ones synthesized in Harpreet Kaur et al.'s study of ZIF-8 in drug delivery [236]. The MCM-41 spherical particles can clearly be seen on the activated carbon particles confirming the formation MCM-41 on activated carbon.

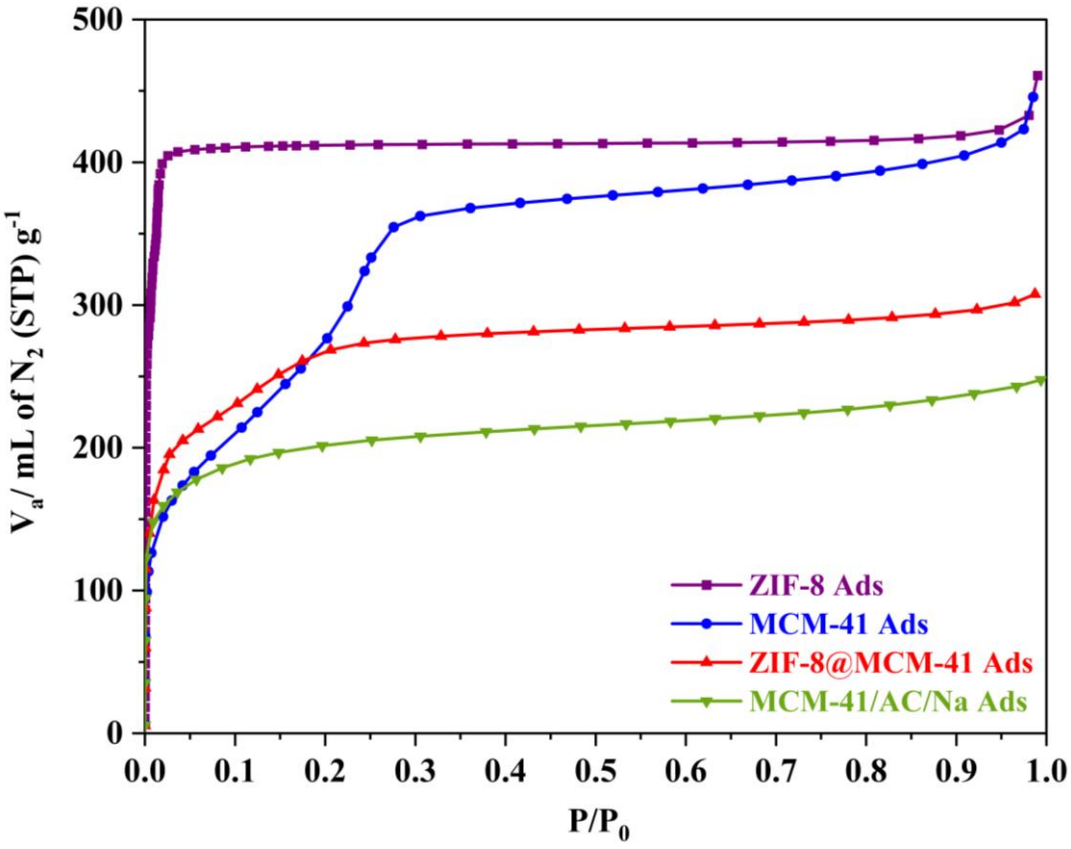

Figure 5.4: N_2 adsorption isotherms of adsorbents at -196 ºC

This microstructure clearly demonstrated the successful formation of ZIF-8@MCM-41, with ZIF-8 nanocrystals intricately embedded in the bulk pores of MCM-41. The surface area analysis revealed a hierarchy in descending order: ZIF-8 > Activated Carbon > MCM-41 > ZIF-8@MCM-41 > MCM-41/AC/Na. Notably, the surface area of ZIF-8@MCM-41 was found to be lower than that of its parent components. This reduction can be attributed to the incorporation of ZIF-8 nanocrystals within the bulk pores of MCM-41, leading to a decrease in available surface area. Moreover, the porous volume composition highlighted the

predominant influence of ZIF-8 characteristics in ZIF-8@MCM-41 and the dominance of activated carbon in the pore volume composition of MCM-41/AC/Na.

Comprehensive characterization of these composite materials using XRD, FTIR, and morphological analysis provides valuable insights into their structural and compositional aspects, laying the foundation for a thorough understanding of their potential applications, particularly in carbon capture and adsorption processes.

5.3. RSM experimental design

Due to the numerous flexibilities offered by Response Surface Methodology (RSM), the carbon capture (CC) uptake experiments were meticulously designed using the Central Composite Design (CCD) face-centered RSM design, incorporating three levels (+1, 0, and 1) for four key factors: temperature, adsorbent loading (adsorption time), carbonation time, and the percentage of DEA loading (DEA loading percentage). The experimental design comprised graphical representation of the results through response surfaces. The design and analysis were executed using Design Expert 12 trial version, allowing for comprehensive estimations and the determination of the relative significance of each parameter, as outlined in table 5.1.

Table 5.1: Parameters/Numeric factors involved in the experimental design

Variable	Min	Central	Max
Temperature (°C)	25	75	125
Amount of adsorbent (g)	5	10	15
Time of carbonation (min)	60	150	240
DEA loading percentage	0	7.5	15

In the assessment of adsorption studies, the adsorption temperature stands out as a critical parameter, playing a pivotal role in both CO_2 adsorption and catalysis processes. Furthermore, in the quest to ascertain enhanced carbon capture properties and identify optimal carbon capture uptakes, the DEA loading or amine loading percentage emerges as a crucial factor. Exploring the nature of adsorption and the kinetics involved in gas uptake, the duration of carbonating the gas is deemed critical. During the regeneration process, the samples were subjected to pure nitrogen gas flushing at 150 ºC, ensuring a thorough and controlled procedure.

5.4. CO_2 uptake and optimization studies

5.4.1. CO_2 uptake experimental results

A meticulous experimental design was implemented through RSM modeling, ensuring a systematic exploration of key parameters in the CO_2 uptake experiments. The study focused on four critical factors: temperature, DEA loading percentage, amount of adsorbent loaded, and the duration of feed flow. Maintaining a consistent feed flowrate at 150 mL/min, a CO_2 concentration of 34% by volume, and a total process pressure of 1 bar, the experiments aimed to provide a comprehensive understanding of the uptake behavior under varying conditions. Specifically, a constant CO_2 flowrate of 34% was maintained to ensure a reliable baseline for comparison. The selected temperatures (25 ºC, 75 ºC, and 125 ºC) reflected a range suitable for studying the impact of temperature on uptake.

Table 5.2: CO_2 uptake of ZIF-8@MCM-41 at 33% CO_2 and 1 bar

Std	Temperature (º C)	Amount of adsorbent (g)	Time (min)	DEA Loading (%)	CO_2 Uptake (mmol/g)
1	25	5	60	0	2.92
2	125	5	60	0	1.83
3	25	15	60	0	3.05
4	125	15	60	0	1.91
5	25	5	240	0	3.05
6	125	5	240	0	1.85
7	25	15	240	0	3.11
8	125	15	240	0	1.93
9	25	5	60	15	4.31
10	125	5	60	15	2.32
11	25	15	60	15	4.33
12	125	15	60	15	2.31
13	25	5	240	15	4.41
14	125	5	240	15	2.29
15	25	15	240	15	4.51
16	125	15	240	15	2.35
17	25	10	150	7.5	3.45
18	125	10	150	7.5	2.07
19	75	5	150	7.5	3.35
20	75	15	150	7.5	3.39
21	75	10	60	7.5	3.36
22	75	10	240	7.5	3.41
23	75	10	150	0	2.15
24	75	10	150	15	4.28
25	75	10	150	7.5	3.18
26	75	10	150	7.5	3.21
27	75	10	150	7.5	3.09
28	75	10	150	7.5	3.25
29	75	10	150	7.5	3.29
30	75	10	150	7.5	3.12

The ZIF-8@MCM-41 adsorbent exhibited a predictable trend, revealing a decrease in CO_2 uptake values as the process temperature increased (table 5.2). Notably, the decrease was pronounced, with the CO_2 uptake dropping from 2.92 mmol/g at 25 ºC to 1.88 mmol/g at 125

ºC. This observation aligns with similar studies on biochar-based CO_2 adsorption and zeolites in CO_2 capture, emphasizing the inverse relationship between temperature and adsorption capacity. What set ZIF-8@MCM-41 apart was its exceptional performance at elevated temperatures, outperforming its parent components, ZIF-8 and MCM-41, in retaining a higher percentage of CC. Comparisons with previous studies on bimetallic ZIFs, pure ZIF-8, and MCM-41 further underscored the superior performance of the composite adsorbents synthesized in the present study. The CO_2 uptake values obtained for ZIF-8@MCM-41 and MCM-41/AC/Na were almost twice as high as those reported for pure ZIF-8 and MCM-41 under similar conditions. This improvement is particularly noteworthy in the context of carbon capture experiments where maintaining initial uptake values at higher temperatures is a significant challenge.

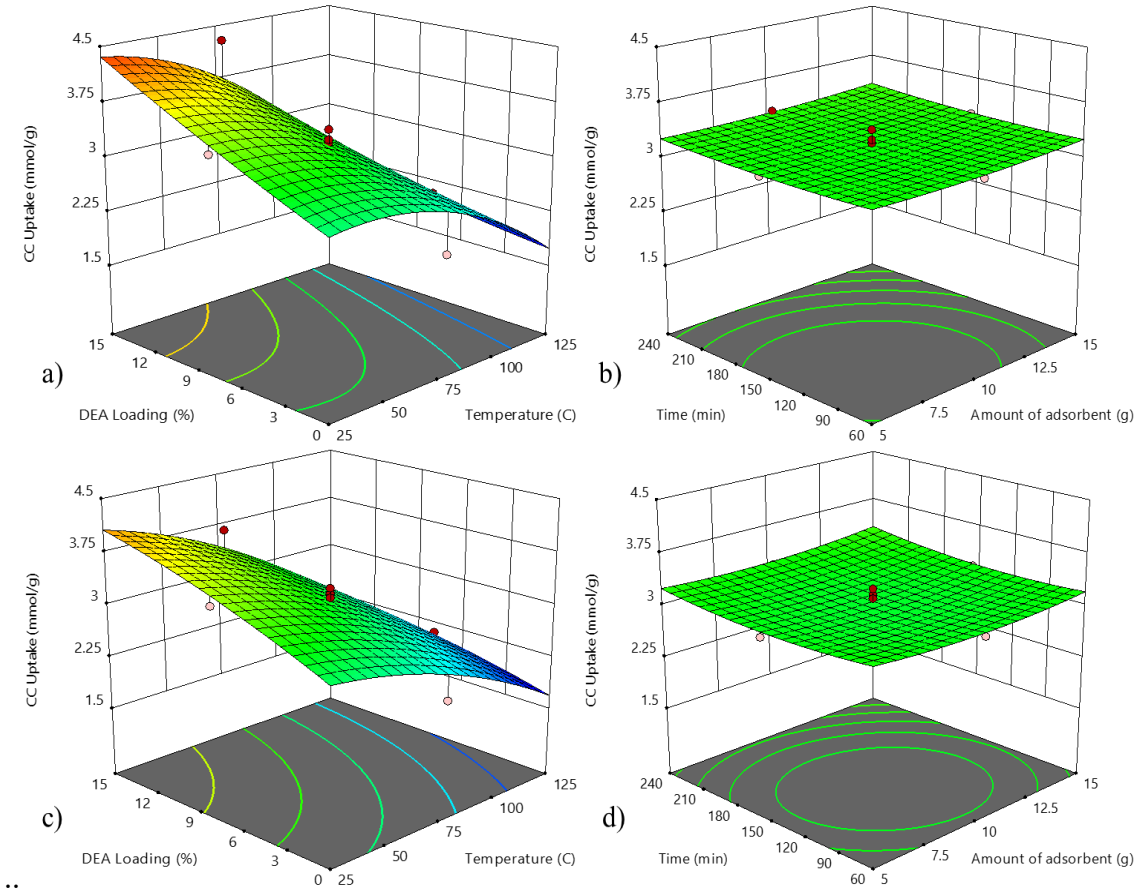

Figure 5.5: Response surfaces of uptake experiments (33% CO_2 and 1 bar pressure) of a)&b) ZIF-8@MCM-41 and c)&d)MCM-41/AC/Na

Table 5.3: CO_2 uptake of MCM-41/AC/Na at 33% CO_2 and 1 bar

Std	Temperature (º C)	Amount of adsorbent (g)	Time (min)	DEA Loading (%)	CO_2 Uptake (mmol/g)
1	25	5	60	0	3.15
2	125	5	60	0	1.88
3	25	15	60	0	3.17
4	125	15	60	0	1.93
5	25	5	240	0	3.21
6	125	5	240	0	1.91
7	25	15	240	0	3.24
8	125	15	240	0	1.89
9	25	5	60	15	4.15
10	125	5	60	15	2.38
11	25	15	60	15	4.11
12	125	15	60	15	2.35
13	25	5	240	15	4.18
14	125	5	240	15	2.46
15	25	15	240	15	4.46
16	125	15	240	15	2.45
17	25	10	150	7.5	3.47
18	125	10	150	7.5	2.11
19	75	5	150	7.5	3.06
20	75	15	150	7.5	3.14
21	75	10	60	7.5	3.07
22	75	10	240	7.5	3.16
23	75	10	150	0	2.18
24	75	10	150	15	3.66
25	75	10	150	7.5	3.15
26	75	10	150	7.5	3.17
27	75	10	150	7.5	3.03
28	75	10	150	7.5	3.11
29	75	10	150	7.5	3.25
30	75	10	150	7.5	3.05

Examining the impact of DEA loading on uptake revealed a favorable trend, with a sharp increase in values observed from 0% to 15% DEA loading in both adsorbents. This aligns with the established understanding that an increase in amine loading typically leads to enhanced uptake. The phenomenon was consistent with studies on CO_2 capture onto amine-modified

mesoporous silicas and amine-modified activated carbons. The positive correlation between DEA loading and uptake values demonstrated the potential of these composite adsorbents in efficient carbon capture applications.

Despite the temperature and DEA loading proving influential in impacting uptake, the same could not be said for duration of feed flow and the amount of adsorbent loaded. Both parameters exhibited a relatively passive effect on uptake values (tables 5.2 and 5.3). The minor increase observed with an extension in carbonation time is consistent with studies emphasizing the importance of prolonged contact time between gas and solid molecules. Similarly, the minute rise in uptake values with increased adsorbent loading aligns with the idea that more available porous sites contribute to higher gas uptake. These findings differ from some studies where an increase in adsorbent loading resulted in a decrease in uptake capacity, highlighting the complexity of these interactions.

5.4.2. RSM model development and verification

The RSM equations for each adsorbent are shown in table 5.4. The optimal experimental set of conditions for both adsorbents is shown in the table below. These equations establish a connection between the experimental output and all the process parameters. The relationship between the uptake values and the process parameters is depicted in the equations that follow.

For ZIF-8@MCM-41, the coded uptake equation is as follows,

$$CO_2\ Uptake = 3.314 - (0.794*A) + (0.031*B) + (0.032*C) + (0.517*D) - (0.006*A*B) - (0.026*A*C) - (0.230*A*D) + (0.005*B*C) - (0.011*B*D) + (0.004*C*D) - (0.526*A^2) + (0.084*B^2) + (0.099*C^2) - (0.071*D^2) \quad \text{Eq 5.1}$$

For MCM-41/AC/Na, the coded uptake equation is as follows,

$$CO_2\ Uptake = 3.073 - (0.766*A + (0.02*B) + (0.043*C) + (0.424*D) - (0.019*A*B) - (0.021*A*C) - (0.131*A*D) + (0.018*B*C) + (0.008*B*D) + (0.028*C*D) - (0.228*A^2) + (0.082*B^2) + (0.097*C^2) - (0.098*D^2) \quad Eq\ 5.2$$

Table 5.4: Optimal process conditions

Adsorbent	Temp (ºC)	Amount (g)	Time (min)	DEA %	Predicted uptake (mmol/g)	Experimental uptake (mmol/g)
ZIF-8@MCM-41	30	11.5	120	14	4.26	4.12
MCM-41/AC/Na	70	13.9	240	9	3.45	3.29

ZIF-8@MCM-41 has a model F-value of 24.88, which indicates that the model is statistically significant. Because there is a high level of agreement between the predicted R^2 value of 0.8309 and the Adjusted R^2 value of 0.9205, the fit is considered to be quite good. When compared to the actual values obtained, the fit statistics appear to be reasonable. The model F-value for MCM-41/AC/Na is 44.97, which indicates that the model is statistically significant. According to the excellent agreement between the predicted R^2 value of 0.9033 and the Adjusted R^2 value of 0.9550, the model is reasonably close to the experimental design. The standard deviation values for ZIF-8@MCM-41 and MCM-41/AC/Na were 0.22 and 0.15, respectively, for the two combinations. As shown in table 5.2, the optimized/predicted values were highly consistent with their experimental counterparts. According to the results, the RSM experimental design was successful in predicting adsorbent uptake levels within the specified parameter ranges.

5.5. Adsorption kinetics study

To gain deeper insights into the adsorption process under consideration, a thorough investigation of the kinetic regimes is crucial. Kinetic modeling plays a pivotal role in elucidating the behavior of adsorption, offering insights into whether the process is primarily physical, chemical, or a combination of both. In this study, kinetic modeling was performed under the optimal conditions determined by the RSM CCD model for both adsorbents. The pseudo-first order (PFO), pseudo-second order (PSO), Elovich kinetic, and Weber-Morris models were employed (mentioned in Chapter 2, Eq 2.1, 2.2, 2.3, 2.4 and 2.5). These models carry significant physical significance as they provide indications of specific types of adsorptions.

Table 5.5: Kinetic parameters at 25 ºC and 1 bar

Adsorbent	Kinetics Model	Temp (ºC)	Q_e exp (mmol/g)	Q_e fit (mmol/g)	k	C	α	β	R^2
ZIF-8@MCM-41	Pseudo First Order	25	3.10	3.08	0.0766				0.989
	Pseudo Second Order	25	3.10	3.28	0.0392				0.943
	Elovich	25					6.627	2.499	0.809
	Weber-Moris	25			0.1035	1.823			0.478
MCM-41/AC/Na	Pseudo First Order	25	3.24	3.22	0.0743				0.988
	Pseudo Second Order	25	3.24	3.44	0.0360				0.939
	Elovich	25					6.384	2.372	0.795
	Weber-Morris	25			0.1086	1.888			0.471

Analysis of the kinetics, as illustrated in figure 5.6, reveals that both adsorbents reached their maximum carbon capture (CC) capacity within 30 minutes, with minimal subsequent increases. The steepness of the rise after 20 minutes indicates that both adsorbents primarily exhibit

physisorption characteristics. Intriguingly, even for the MCM-41/AC/Na adsorbent, despite the presence of NaOH, physisorption emerged as the dominant mechanism. This can be attributed to the minimal retention of NaOH within the adsorbent compared to the total adsorbent volume.

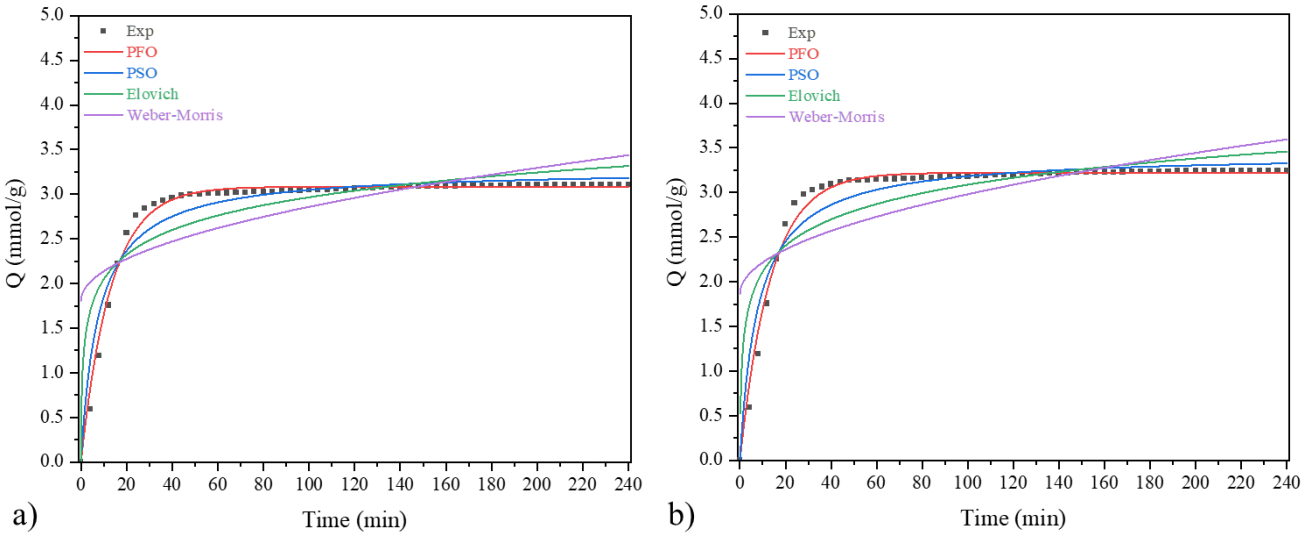

Figure 5.6: Kinetic modelling of a) ZIF-8@MCM-41 and b) MCM-41/AC/Na at 25 ºC, 33% CO_2 and 1 bar

Figure 5.6 demonstrates that the pseudo-first order model corresponds well with the experimental data for both adsorbents in this study, outperforming other tested models. Comparing the R^2 value of the PFO model to that of the PSO model (refer to table 5.5), hovering around 0.92, it is evident that the PFO model offers a reasonably good fit. This implies that physisorption is the dominant type of adsorption for these adsorbents. Furthermore, given that activated carbons, ZIF-8, and MCM-41 primarily facilitate physisorption, this alignment is consistent with the inherent nature of the base adsorbents used in the experiment. Moreover, since these adsorbents are predominantly microporous, the initial adsorption rate is fast, followed by a rapid slowdown as more pores become saturated. Particularly, the Weber-Morris model exhibited a poor fit, with R^2 values only reaching 0.477 and 0.471. In conclusion, the Pseudo-First Order model emerges as the most suitable model for fitting our experimental data when compared to other models.

5.6. Adsorption isotherm study

CO_2 concentration is one of the most important factors in determining the quantity of gaseous uptake. It also determines the time in which the adsorbent bed gets exhausted and reaches saturation/equilibrium. The amount of CO_2 present in the feed generally has an impact on the absorption capacity of the adsorbent. At 298 K, partial pressures of CO_2 were varied between 0 and 0.8 bar to investigate the effects of CO_2 concentration on the reaction. As the CO_2 concentration within the feed increased, the amount of CO_2 adsorbed also increased. This was especially noticeable as CO_2 feed percentages increased from 0 to 50. The increase in uptake values is almost three-fold within that range. After 50%, however, the increase was less substantial. From 50% to 80%, only a 20% increase was observed in uptake values. This could be because, after a certain feed percentage, the capture capacity reaches a saturation point, after which even an increase wouldn't make any difference. Even here, slight differences in the nature of adsorption could be observed between ZIF-8@MCM-41 and MCM-41/AC/Na. Beyond concentrations of 50%, ZIF-8@MCM-41 reached a flat line equilibrium. MCM-41/AC/Na, on the other hand, has a more dispersed flatline trend. The adsorption experimental data can be seen in figure 8. In their study of adsorption of CO_2 over activated carbons produced at 540 ºC to 800 ºC, Li et al. [237] also observed an increasing uptake value with an increase in CO_2 partial pressure. As with the nature of activated carbonaceous materials over a surface area of 500 m^2/g [238], the amount of increase in the uptake value with respect to the increase in CO_2 partial pressure kept decreasing. Ahmed et al. [239] also observed a similar trend with their tetraethyl pentaamine loaded Si-MCM-41 adsorbent. The reasoning given was that low CO_2 partial pressures, the pores of MCM-41 were filled rapidly and readily, whilst any subsequent increase in CO_2 partial pressure would only cause a minimal increase. This was observed in the study of Liu et al's. [240] experimental and molecular simulation studies of CO_2 adsorption over pure ZIF-8. This type of behaviour is common for materials which are predominantly

microporous in nature [240]. This is also in line with the nature of both ZIF-8@MCM-41 and MCM-41/AC/Na adsorbents as both of them showed microporous nature predominantly. Although MCM-41 is traditionally a mesoporous material by nature, the composites had predominantly microporous nature.

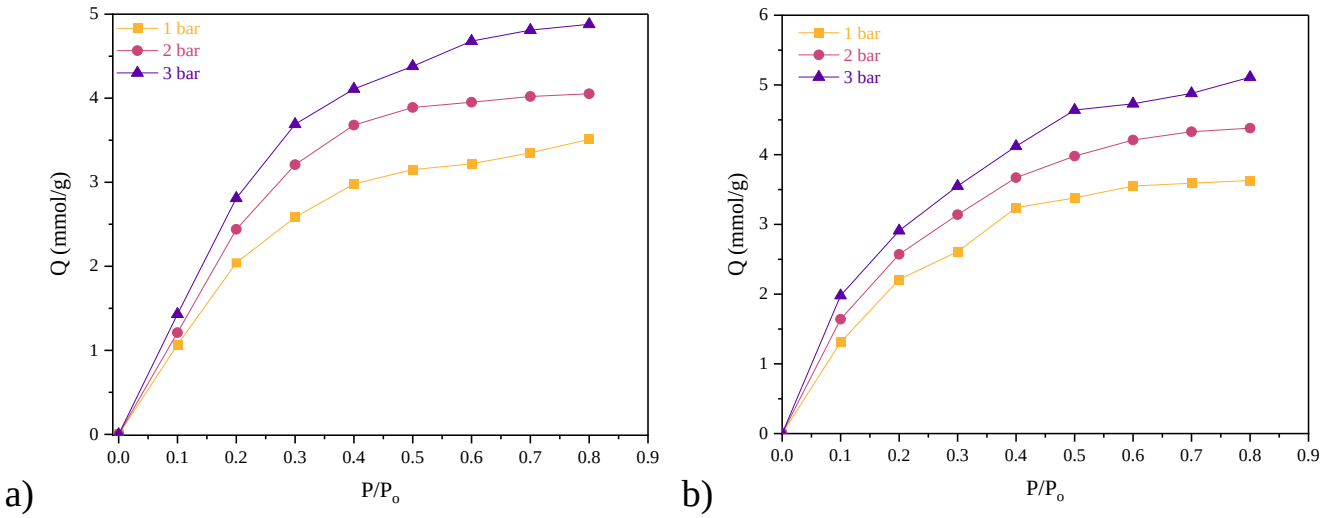

Figure 5.7: CO_2 adsorption isotherms of a) ZIF-8@MCM-41 and b) MCM-41/AC/Na at 25 ºC

Adsorption isotherms are essential for determining the nature and type of adsorption of any adsorbent. They do, in fact, shed light on the potential adsorption pattern (mentioned in Chapter 2, Eq 2.6, 2.7, 2.8 and 2.9). At 25 ºC, adsorption studies were performed on unmodified adsorbents. The system's total pressure was varied to three values: 1 bar, 2 bar, and 3 bar, with CO_2 percentages in the feed ranging from 0% to 80%.

Table 5.6: Adsorption isotherm modelling fit for Freundlich and Langmuir models at 25 ºC

Adsorbent	Total Pressure (bar)	Langmuir			Freundlich		
		k_L	Q_m (mmol/g)	R^2	k_F	n	R^2
ZIF-8@MCM-41	1	3.67	4.77	0.993	4.06	2.26	0.961
	2	3.86	5.66	0.982	4.87	2.32	0.942
	3	3.89	6.43	0.989	5.55	2.33	0.956
MCM-41/AC/Na	1	4.03	4.93	0.993	4.28	2.39	0.973
	2	3.89	5.92	0.990	5.11	2.35	0.982
	3	3.93	6.74	0.992	5.83	2.37	0.992

Table 5.7: Adsorption isotherm modelling fit for Sips and Toth models at 25 ºC

Adsorbent	Total Pressure (bar)	Sips				Toth			
		k_S	Q_m (mmol/g)	n	R^2	Q_m (mmol/g)	k_T	n	R^2
ZIF-8@MCM-41	1	14.1854	3.79	1.56	0.999	0.86	13.3286	2.24	0.996
	2	29.1501	4.32	1.89	0.998	0.21	60.7851	3.66	0.995
	3	14.4141	5.37	1.59	0.999	1.12	13.7746	2.37	0.992
MCM-41/AC/Na	1	5.3023	5.53	1.11	0.998	1.43	9.5621	1.83	0.993
	2	9.5822	4.22	1.34	0.996	3.77	5.1471	1.27	0.992
	3	3.3912	7.00	0.95	0.997	7.69	3.6619	0.93	0.998

The R^2 values from table 5.6 indicate that the Langmuir isotherm model fits well for both the adsorbents at all three process pressures. ZIF-8@MCM-41 recorded an R^2 value of 0.98 for all three pressures for the Langmuir model (table 5.4). Compared to that, the R^2 value for the same adsorbent for the Freundlich model was 0.93, 0.94, and 0.95 at 1 bar, 2 bar, and 3 bar, respectively. Similarly, for the MCM-41/AC/Na adsorbent, an R^2 value of 0.98 agreed better with the Langmuir model. The R^2 values for Sips (0.998) and Toth (0.993) models agreed the

best for both adsorbents for all pressures. The Sips model held better on the experimental data than the Toth model only slightly, as is evident from table 5.7. This indicated that the adsorption nature was mostly a mixture between monolayer and multilayer types. Furthermore, the Sips model assumes that the surface of the adsorbent is heterogenous, which is in line with the composite adsorbents. Once again, the nature of the pores decided the type of adsorption. Kapica-Kozar and their group studied CO_2 adsorption over TEPA-modified TiO_2/titanate composite nanorods and found out that Sips adsorption isotherm best fit their experimental data [213]. The study of these nanorods mainly focussed on a chemisorption process with the loading of TEPA. Similarly, Azeem et al.'s [166] study of KOH activated porous carbons, Sips model agreed exceedingly well with the isotherm data along with the Toth model. Even in Melouki et al.'s [167] study of carbons obtained from olive waste, Sips model was found to be the best suited model to describe the experimental with the Toth model being a close second best. In a comparative study done by Yongha Park et al. [168], activated carbon and zeolite-LiX were pitted against each other in terms of uptake. In that study, for both the adsorbents, the Sips model was found to the best in describing the experimental data. In contrast, graphene of average pore size 3 nm was found to obey Langmuir adsorption isotherm model in Sun et al.'s. [241] study of CO_2 adsorption. In the above-mentioned research, the adsorption behaved as if it was monolayer in nature despite having multilayer adsorption at the surface of the catalyst.

Both the adsorbents tested here are microporous in nature with Type I (a) N_2 adsorption isotherm (figure 5.4). This implies that they have long narrow pores within their structures. Adsorbents with narrow micropores often display elevated uptake values at much higher rates when exposed high process pressures. ZIF-8 being a framework with narrow pores offers much pressure difference, a driving factor necessary for adsorption at elevated pressures, at high process pressures. This is also a reason as to why MOFs and ZIFs in general are best suited for adsorption processes at high pressures. The ZIF-8@MCM-41 adsorbent also displayed

predominantly microporous nature as seen in figure 5.4. However, unlike pure ZIF-8, the composite also displayed a significant degree of meso-porosity. This explains the adsorption isotherm curve in figure 5.7. At low process pressures, the narrow micropores within the composite are filled rapidly almost in a linear fashion. But after the micropores were filled, the subsequent increase was very minimal indicating a slow filling of the existing mesopores [242]. Like ZIF-8@MCM-41, the MCM-41/AC/Na adsorbent also displayed dual textural properties. And much like the ZIF-8@MCM-41 adsorbent, it had MCM-41 mesopores with the micropores of activated carbon mainly dominating the type of pores. The MCM-41/AC/Na adsorbent had more percentage of non-microporous volume than ZIF-8@MCM-41, implying that at higher pressures, the CC values increase at lower factor than compared pure MOFs or activated carbons with nanotubes.

Heat of adsorption is another vital parameter in determining the nature and the strength of the adsorbent. In this work, heat of adsorption was calculated for unmodified adsorbents with the help of the Clausius-Clapeyron equation. Three temperatures; 25 ºC, 40 ºC and 55 ºC, were considered for a total pressure of 1 bar. A temperature difference of only 15 K was maintained for accuracy purposes. The plots of 1/T vs lnP data for both the adsorbents are displayed in figure 5.8.

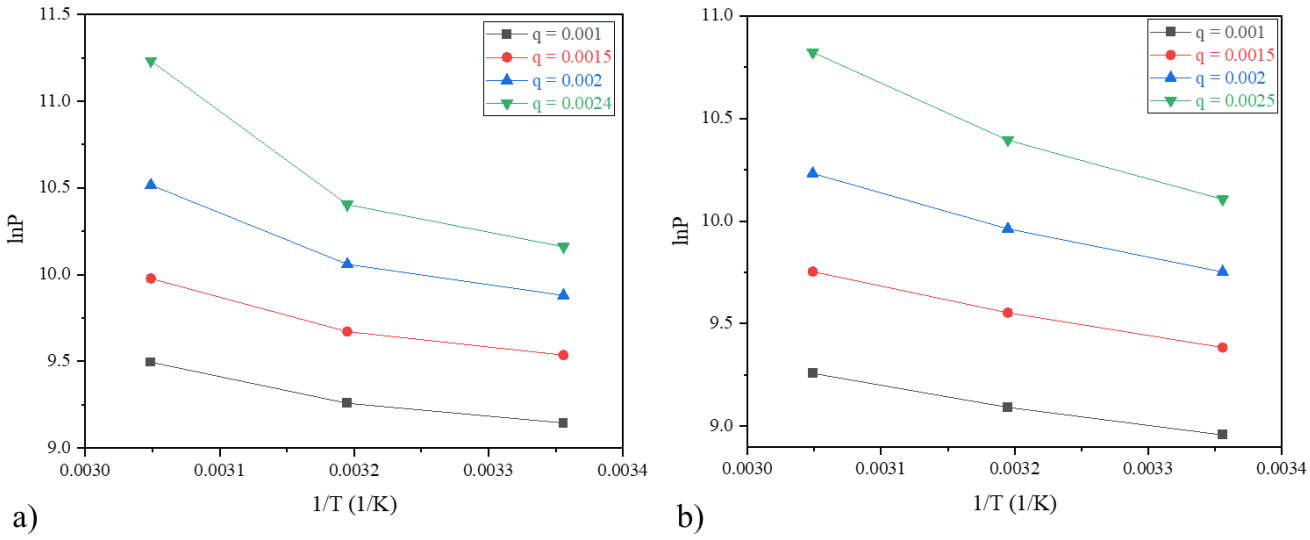

Figure 5.8: 1/T vs lnP graph for a) ZIF-8@MCM-41 and b) MCM-41/AC/Na

Four uptake values were considered in this study for ZIF-8@MCM-41. They are 0.001 kmol/kg, 0.0015 kmol/kg, 0.002 kmol/kg and finally 0.0024 kmol/kg. For these loading values, the average heat of adsorption for ZIF-8@MCM-41 adsorbent was -16.78 kJ/kmol. This is consistent with the theoretical values for pure ZIF-8. Fischer et al. [243] also confirmed that pure ZIF-8 recorded a values in between -16.0 and -19.5 kJ/mol with simulation also showing heat of adsorption values to range in between -16.0 and -17.0 kJ/mol. In their own study of low temperature CO_2 capture by ZIF-8, Russell and group [215] also found that heat of adsorption for modified ZIF-8 structures was around -18 kJ/mol. Like with ZIF-8@MCM-41, four CC loading values of 0.0010 kmol/kg, 0.0015 kmol/kg, 0.0020 kmol/kg and 0.0024 kmol/kg were considered for MCM-41/AC/Na. And the average heat of adsorption value was -12.59 kJ/mol. Compared to this, functionalized MCM-41 adsorbents in Dos Santos' study [244] obtained a heat of adsorption of around -50.0 kJ/mol signifying a domination of the functional group in the adsorption behaviour. In the present study however, the heats of adsorption for the adsorbents indicate that the adsorption is mostly physical in nature.

Since the Sips isotherm was found to be the best fit, it was considered in the calculation of the isosteric heat of adsorption. The heat of adsorption values using both Langmuir and Toth

isotherm models as well. After comparing various isotherms, the Sips isotherm was found be marginally better than other models like Langmuir and Toth and the heats of adsorption were also found to be close as per these models. The average heat of adsorption values for the ZIF-8@MCM-41 were found to be -16.63 kJ/mol, -16.78 kJ/mol and -17.13 kJ/mol for the Langmuir, Sips and Toth models respectively. The values for the MCM-41/AC/Na (for Langmuir, Sips and Toth models) were found to be -14.08 kJ/mol, -12.59 kJ/mol and -12.33 kJ/mol respectively.

5.7. Cyclic Stability studies

To properly assess the performance stability over repeated usage, cyclic stability tests were conducted. The standard sample loaded into the reactor was 5 g and carbonation for each cycle was done at a temperature of 25 ºC. The feed consisted of N_2/CO_2 with a total feed flowrate of 150 mL/min with CO_2 being around a third of the gaseous feed. After each cycle of carbonation, decarbonation or regeneration was done at 150 ºC at an inert atmosphere. The temperature was chosen so that ZIF-8 doesn't undergo too much loss in capacity. The cyclic retention is given in figure 5.9. Both the adsorbents showed exceptional stability even after 15 cycles of carbonation and regeneration. For an initial CC value of 3.03 mmol/g at 25 ºC for the ZIF-8@MCM-41 adsorbent, its uptake after 15 cycles was around 2.92 mmol/g. This is high stability considering the presence of ZIF-8 within this composite. ZIFs and MOFs in general are extremely sensitive to repeated exposure to high temperatures. The ZIF-8@MCM-41 adsorbent, however, turned into a very pale tint of yellow after the end of 15 cycles, as opposed to the usual white. The stability of MCM-41 has enhanced ZIF-8 in the case of this composite. The MCM-41/AC/Na adsorbent was even more impressive considering its higher uptake value overall. After 15 cycles, it recorded a uptake value of 3.12 mmol/g. This is around 98% retention capacity as compared to the 97% retention capacity of ZIF-8@MCM-41. A loss of three percentage points is negligible when considering a long cyclic process of 15 cycles.

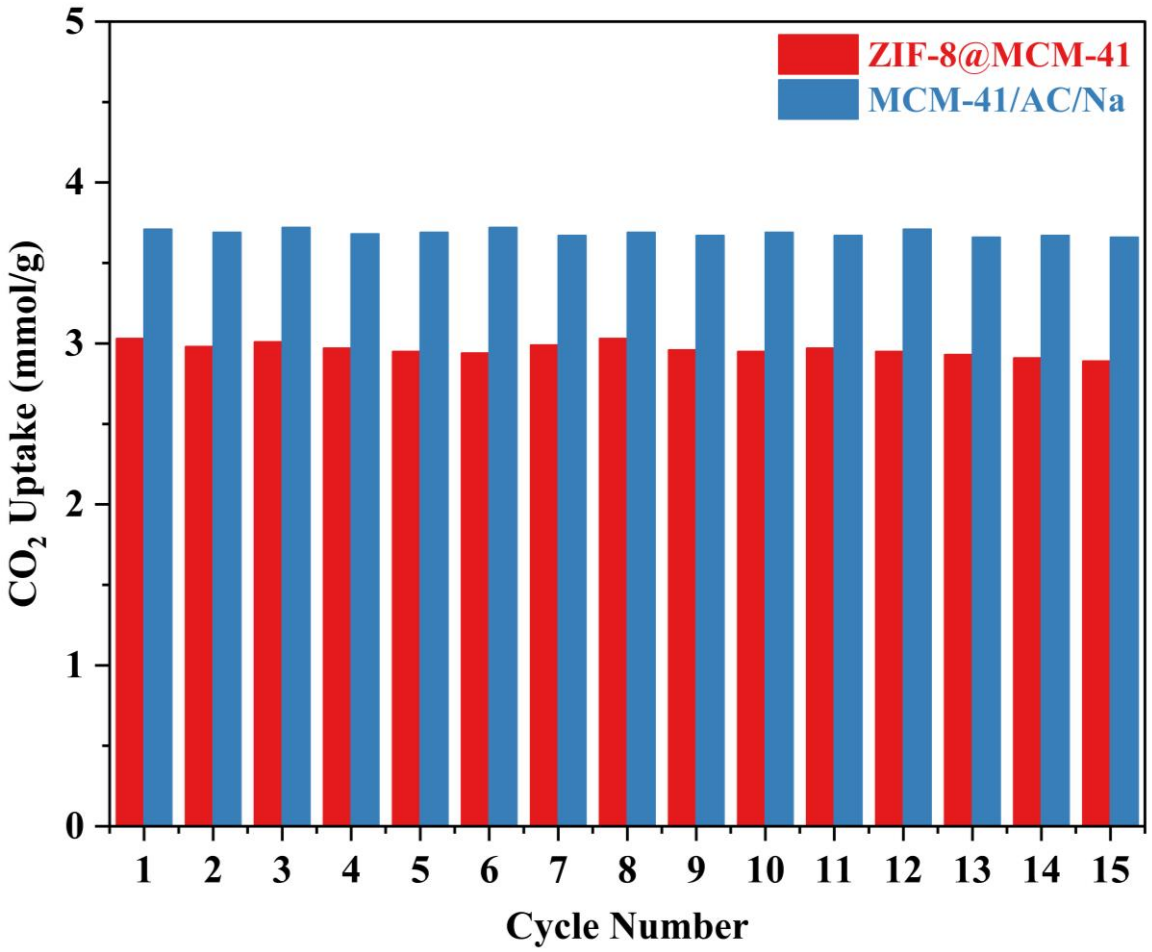

Figure 5.9: Cyclic retention capacity at 25 ºC and 1 bar

5.8. Conclusions

Two novel composites were synthesized using in situ techniques and systematically evaluated for CO_2 uptake studies. Four key parameters were considered in the experimental design. BET analysis revealed that the ZIF-8@MCM-41 adsorbent exhibited a lower surface area compared to its parent materials. SEM micrographs confirmed the presence of ZIF-8 nanocrystals within MCM-41 spheres, and similarly, the formation of MCM-41 spheres over activated carbon particles was confirmed. The adsorption temperature inversely affected the CO_2 uptake values of both adsorbents, with the highest uptake observed at 25 ºC and the lowest at 398 K. DEA loading positively influenced uptake, with 15% DEA loading yielding maximum values for both adsorbents. Mass of adsorbent and duration of feed flow had minimal influence, but both exhibited a slight positive impact on uptake. The adsorption models derived from CCD modeling aligned well with experimental data, and experiments at optimum values suggested by the CCD model fell within standard deviation values. The pseudo-first-order model effectively explained the adsorption kinetics, indicating a predominantly physisorption process, while the pseudo-second-order kinetics proved insufficient. Sips adsorption modeling revealed a combination of monolayer and multilayer adsorption types. The average heats of adsorption were -16.78 kJ/mol for ZIF-8@MCM-41 and -12.59 kJ/mol for MCM-41/AC/Na, suggesting a primarily physical nature of adsorption. Both adsorbents demonstrated excellent cyclic performance, retaining over 95% of their initial adsorption capacity. However, ZIF-8@MCM-41 exhibited slight discoloration after 15 cycles, indicating potential thermal compromise, whereas MCM-41/AC/Na showed greater stability.

Chapter 6: Carbon capture studies using CFA derived composites with ZIF 8

6. Carbon capture studies using CFA derived composites with ZIF 8

6.1. Introduction

The classification of adsorbents encompasses two overarching categories, namely physisorbents and chemisorbents. Porous metallic oxides along with other basic metallic salts are the first of four primary classes that make up the physisorbent classification [245]. The second category [246] encompasses activated carbons (ACs), biochars, and their derivatives. The extensive research and investigation of activated carbons (ACs) can be attributed to their remarkable stability and inertness. Zeolites [247] and mesoporous silicas [248] make up the third of these classes. These materials exhibit inherent properties as being natural molecular sieves and displaying a remarkable affinity towards acidic gases. Furthermore, their pH responsiveness can be precisely tailored to a desired pH value. Zeolites have garnered significant attention and are universally acknowledged as the most auspicious contenders for a multitude of commercial endeavors, particularly in the domains of CO_2 capture and conversion. Metal-organic frameworks (MOFs) [249], covalent organic frameworks (COFs) [66], and microporous organic polymers (MOPs) [250] represent a subset of materials that can be classified as the fourth category itself. The assemblage of sorbents under consideration exhibits a remarkable degree of versatility and innovation. The observed entities exhibit a notable level of adjustability and possess remarkably expansive apertures. Covalent organic frameworks (COFs) have exhibited considerable promise in the realm of CO_2 capture investigations. In contrast, it is noteworthy that these particular materials exhibit a higher degree of suitability for the purpose of membranous carbon dioxide (CO_2) separation, as opposed to direct CO_2 adsorption. Chemisorption is a phenomenon characterized by the interaction between the adsorbent and CO_2 on the surface, resulting in a more efficient entrapment of the gas. In the realm of adsorption, chemisorbents encompass a diverse array of materials, including porous metal oxides and metal salts, as well as basic compounds that are

intricately combined with solid supports. Chemisorbents, which are fundamentally basic compounds, are affixed or attached onto inactive and permeable adsorbents, such as activated carbons and mesoporous silicas. Typically, inert supports are loaded with basic materials such oxides of calcium and magnesium, amines, and hydroxides of alkali and alkaline earth metals [251]. Amines and metal hydroxides have garnered significant attention within the realm of scientific research. The rationale behind their widespread adoption stems from the inherent simplicity associated with their successful integration onto non-reactive porous substrates.

Metal Organic Frameworks (MOFs) have emerged as a pivotal class of materials in the field of carbon capture over the past two decades. This surge in their significance could be attributed to their remarkable characteristics, including but not limited to their expansive surface area, versatile functionality, modifiable pore structure, exceptional porosity, presence of accessible metal sites, and the ability to tailor their morphology [65]. In order to address certain limitations associated with metal-organic frameworks (MOFs), including thermal instability, structural degradation in the presence of moisture, and limited cyclic regeneration capability, Zeolitic imidazolate frameworks (ZIFs), a specific subclass of MOFs, have emerged as a viable alternative. ZIFs [252] have garnered significant attention in the scientific community due to their remarkable thermal stability, notable hydrophobicity, and exceptional physico-chemical characteristics.

Composites have recently garnered significant attention within the realm of adsorption and catalysis [253]. Composite materials are meticulously fabricated with the objective of synergistically amalgamating the inherent strengths of distinct classes, thereby effectively concealing any inherent weaknesses that may be present. The synthesis of a composite material consisting of metal-organic framework (MOF) and graphene oxide was done by Wang and group [254] in their investigation on the adsorption of carbon dioxide (CO_2). The composite material was designated as the Mg/DOBDC MOF@GO composite, with different ratios being

investigated. The group of composites exhibited remarkable carbon capture (CC) efficiency by synergistically leveraging the substantial surface area of the metal-organic framework (MOF) and the strong affinity of graphene oxide towards CO_2. The investigation conducted by Cheng et al. [255] focused on the examination of composites possessing a dual nature, consisting of magnesium oxide (MgO) and zinc oxide (ZnO), incorporated within zeolitic imidazolate framework-8 (ZIF-8). The composites exhibited remarkable carbon capture (CC) uptake values in comparison to ZIF-8 in its pure form, while simultaneously preserving the favorable morphological characteristics of ZIF-8. In the study conducted by Tari and team [256], an innovative composite material named Cu-BDC/MCM-41 was synthesized, combining a stable Metal-Organic Framework (MOF) with MCM-41. The composite material presented in this study exhibits a unique amalgamation of mesoporous and microporous structures, resulting in a significant enhancement of CO_2 adsorption capabilities compared to its constituent materials [256]. In our own recent investigation [189], the focus was directed towards the exploration of coal fly ash as a potential resource for the production of value-added materials. Specifically, a composite material comprising coal fly ash zeolite and ZIF-8 was synthesized and subsequently employed for the purpose of investigating its efficacy in CO_2 adsorption. The corresponding investigation yielded noteworthy findings regarding the synergistic effect of combining zeolite and ZIF-8 on the uptake of carbon dioxide. The current investigation represents a seamless extension of prior research endeavors, with a primary focus on elucidating the process of synthesizing and employing innovative composite materials.

The present study is focused upon the examination of adsorption phenomena within the confines of a fixed bed reactor system. In order to optimize the precision and effectiveness of the conducted experiments, the present study utilized the RSM with spherical type as the chosen experimental design strategy. It is important to note that the carbon capture performance of an adsorbent is subject to the influence of various factors, including but not limited to the

amine loading percentage, adsorbent weight, and temperature. It is noteworthy to acknowledge that traditional experimental designs frequently isolate these factors in order to investigate them individually, inadvertently neglecting the intricate interconnections that exist among them. RSM, however, surpasses these limitations by encompassing the simultaneous consideration of the combined effects of all the aforementioned variables. Through the utilization of regression analysis, RSM facilitates the comprehensive evaluation of the combined impact of these factors on the adsorption process. This ultimately culminates in the identification of the most favourable process conditions. The implementation of this all-encompassing methodology not only amplifies accuracy but also diminishes the necessity for a substantial quantity of trials, thus preserving precious assets such as time, financial capital, chemical substances, and energy. The primary emphasis of our investigation is centred upon three fundamental variables: temperature, duration of feed flow, and system pressure. Upon implementing the methodological framework of RSM, a comprehensive investigation into the intricate dynamics, adsorption modelling, and cyclic stability assessment of the synthesized adsorbents were investigated upon.

6.2. Characterization of adsorbents

6.2.1. Synthesis of composites

The composite material was synthesized using three methods for comparison of physical properties, CO_2 capture and ease of synthesis. The three methods are physical binding, in-situ method and simultaneous synthesis are presented in figure 6.1.

Figure 6.1: Composite synthesis protocols employed

Both ZIF-8 and Na-A were synthesized independently and were mixed in water. Then, this mixture was treated in a sonicator for uniform dispersion. After sonication for two hours, the mixture was stirred for another two hours, filtered and dried.

6.2.2. Physico-Chemical attributes

The N_2 adsorption isotherm experiments were conducted at -196 ºC and yielded information regarding the porosity and surface area characteristics of the various adsorbents under investigation. Notably, ZIF-8 emerged as the frontrunner in this study, displaying the most remarkable BET surface area at 1580 m^2/g, a clear indication of its exceptional capacity for gas

adsorption at low temperatures (table 6.1). Moreover, ZIF-8 also boasted the largest pore volume among the materials, measuring a substantial 0.79 cm^3/g, which further underscored its suitability for gas adsorption applications.

Table 6.1: BET surface areas of selected adsorbents

Adsorbent	**BET Surface area (m^2/g)**	**Pore volume (cc/g)**
ZIF-8	1584	0.79
ZIF-8@Na-A via simultaneous synthesis	78	0.12
ZIF-8@Na-A via in-situ method	354	0.32
ZIF-8@Na-A via physical binding	156	0.21

In contrast, ZIF-8 synthesized via the simultaneous method exhibited a significantly lower BET surface area, registering at only 78 m^2/g. This discrepancy highlighted the impact of synthesis methods on the resultant materials, with the simultaneous synthesis method yielding a material with comparatively lower porosity. However, it's crucial to consider the presence of Na-A in both the ZIF-8@Na-A via simultaneous synthesis and ZIF-8@Na-A via in-situ synthesis adsorbents. This addition of Na-A introduced significant mesoporous volume to these materials, enhancing their overall porosity, despite their lower BET surface areas in comparison to pure ZIF-8. The descending order of surface areas is clear: ZIF-8 leads with the highest surface area, followed by ZIF-8@Na-A via in-situ synthesis, ZIF-8@Na-A via physical binding, and finally, ZIF-8@Na-A via simultaneous synthesis with the lowest surface area. It's noteworthy that the surface area of ZIF-8@Na-A was found to be lesser than that of its parent material, ZIF-8, which can be attributed to the formation of ZIF-8 nanocrystals within the bulk pores of Na-A, effectively reducing the accessible surface area. Overall, these findings provide valuable insights into the materials' properties and their potential applications in gas adsorption

and separation processes, highlighting the intricate relationship between synthesis methods and resultant material characteristics.

Scanning electron migrographs (figure 6.2) show the topological and the morphological characteristics of ZIF-8, Na-A, ZIF-8@Na-A (in-situ method) and ZIF-8@Na-A under simultaneous method, presented in figure 6.3. Pure ZIF-8 showed ordered particle structures. The structure of ZIFs is determined by the mostly by the ratio between the ligand and the metal. The Na-A synthesized exhibited well-defined cuboid-like structures with a relatively smooth morphology. Moreover, the internally produced Na-A displayed consistent particle sizes ranging from 100 nm to 150 nm [257]. The morphology of the synthesized Na-A predominantly relied on the chemical ratio employed during synthesis. In contrast, the synthesized ZIF-8 exhibited dodecahedral structures. The successful synthesis of ZIFs also hinged on the crucial mole ratio between the metal ion and the organic linker. Notably, a Zn:Hmim ratio of 1:8 resulted in more disordered and interconnected ZIF-8 particles, while a Zn:Hmim ratio of 1:70 yielded well-ordered nano crystals. Interestingly, the simultaneous synthesis of ZIF-8@Na-A led to a distinct morphology that did not resemble either parent material's ordered structure. This departure from expected morphology might be attributed to the uneven crystal formation inherent in the simultaneous synthesis process. The resulting ZIF-8@Na-A composite showcased the characteristic cuboid particles associated with Na-A, yet it also contained meticulously ordered ZIF-8 nanocrystals, as depicted in the accompanying figure. Surprisingly, the geometry of these nanocrystals within the composite was more distinct compared to pure ZIF-8 nanocrystals.

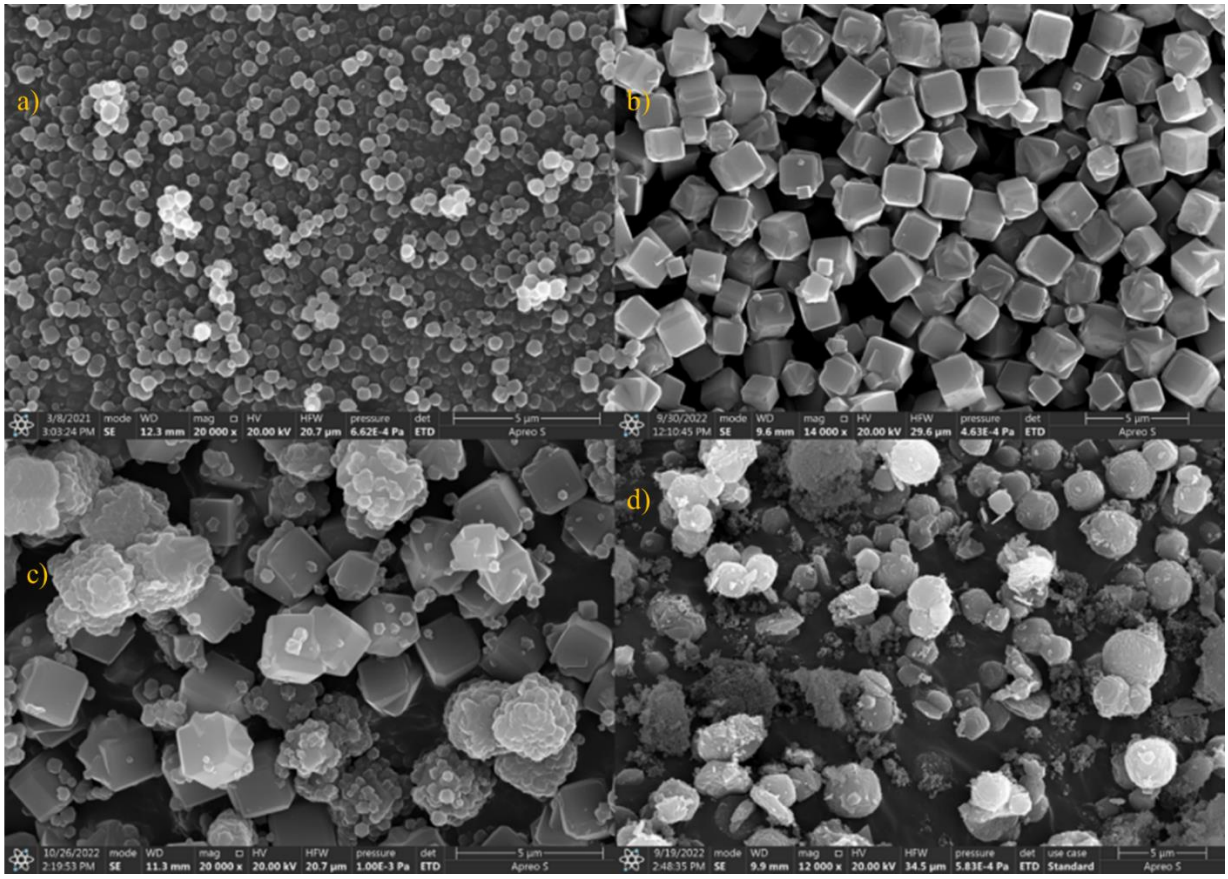

Figure 6.2: Micrographs of a) ZIF-8, b) Na-A, c) ZIF-8@Na-A (in-situ method) and d) ZIF-8@Na-A (simultaneous method)

The diffractograms presented in figure 6.3 provide valuable insights into the crystalline structures of the materials under investigation. In particular, the diffractograms reveal distinctive peaks that are characteristic of each material, shedding light on their unique structural properties. In the case of ZIF-8, a series of well-defined peaks were observed at specific angles. Notably, these peaks were detected at 7.3º, 10.3º, 12.7º, 14.7º, 16.4º, 18.0º, 23.3º, and 28.7º. These peaks correspond to specific planes within the crystal lattice structure of ZIF-8. For instance, the peak at 7.291º is indicative of the (011) plane, while the peak at 10.3º corresponds to the (002) plane. Similarly, the peak at 12.7º is associated with the (112) plane, and the peak at 16.4º is attributed to the (013) plane. Furthermore, the peak at 18.003º signifies the presence of the (222) plane [258]. However, when considering the ZIF-8@Na-A adsorbent, it was evident that these characteristic peaks shifted slightly. The diffractogram revealed peaks at angles such as 9.0º, 11.9º, 12.1º, 14.2º, 14.5º, 15.7º, 16.4º, 17.8º, 18.2º, 19.8º,

22.1º, 23.4º, 23.9º, 25.7º, 25.9º, 27.3º, 27.8º, 28.4º, 28.8º, 31.7º, 32.5º, 33.2º, 34.2º, 35.1º, and 35.9º. These shifted peaks indicate changes in the crystallographic structure compared to pure ZIF-8. The presence of Na-A in the composite is believed to influence these shifts, possibly through interactions with the ZIF-8 structure. In case of the coal fly ash-based Na-A material, its diffractogram displayed prominent peaks at angles such as 8.9º, 11.9º, 14.3º, 15.7º, 17.9º, 21.5º, 22.2º, 23.5º, 24.6º, 25.8º, 26.1º, 27.9º, 28.9º, 31.7º, 32.6º, 33.3º, 34.4º, 35.1º, and 35.9º.

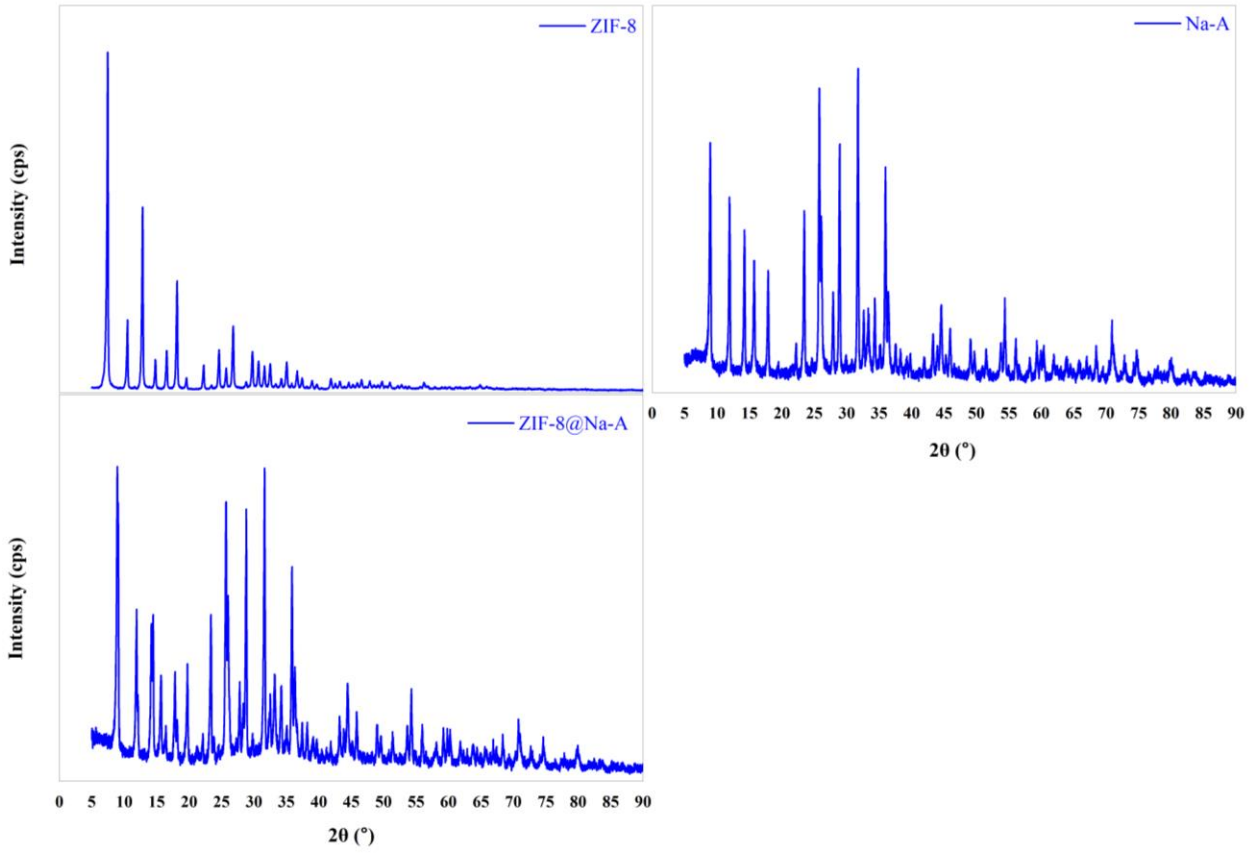

Figure 6.3: Diffractograms of a) ZIF-8, b) Na-A, and c) ZIF-8@Na-A (In situ method)

The dominance of characteristic Na-A peaks in the diffractogram of the ZIF-8@Na-A sorbent is an intriguing observation. This phenomenon can be attributed to the significant presence of Na-A within the composite material. Essentially, the abundance of Na-A appears to have played a pivotal role in shaping the diffractogram of the composite, effectively overshadowing the typical signature peaks of ZIF-8 during its synthesis process. This finding underscores the

intricate interplay between the individual components in the composite. It suggests that the presence of Na-A exerts a profound influence on the structural characteristics and crystalline properties of the composite material. The unique interactions between ZIF-8 and Na-A within the composite are evidently reflected in the diffractogram, providing compelling evidence of these structural transformations. In essence, the dominance of Na-A peaks in the diffractogram serves as a clear indication of the composite's complex and interdependent crystalline properties. This observation adds a valuable layer of understanding to the synthesis process and the resulting material's structural features. It underscores the need to consider not only the individual components but also their interactions and effects on the overall material properties, offering a deeper insight into the composite's unique crystalline characteristics.

6.3. Hierarchical optimization of the material and process

6.3.1. Adsorbent optimization based on synthesis protocol

Level I screening of adsorbents was done in this on the basis of their synthesis methods and properties. Various synthesis methods produce different kinds of morphologies for the same type of adsorbent. Often these properties could be the deciding factor in determining the uptake values. Here, three synthesis methods were compared in terms of uptake along with the BET surface areas. The results are tabulated in table 6.2. The initial experimental conditions for the carbon capture uptake studies were as follows: Temperature = 298 K, Pressure = 1 bar, CO_2 % in the feed = 16.7 % and a gas feed flowrate = 150 mL/min.

Table 6.2: Results of first level screening

Adsorbent	CO_2 Uptake (mmol/g)	BET Surface Area (m^2/g)	Pore volume (cc/g)
ZIF-8	1.12	1584	0.79
ZIF-8@Na-A via simultaneous synthesis	1.63	78	0.12
ZIF-8@Na-A via in-situ method	3.48	354	0.32
ZIF-8@Na-A via physical binding	2.38	156	0.21

From table 6.2, it is evident that pure ZIF-8 displayed high surface area and pore volume. Even when compared to the next best surface area shown by ZIF-8@Na-A synthesized via in-situ method, the difference is apparent. The ZIF-8@Na-A adsorbents synthesized via simultaneous and physical binding methods recorded values much lesser than that of the ZIF-8@Na-A via in situ method. However, when the initial uptake values are brought into the picture, the differences are obvious. Pristine ZIF-8, despite having the highest surface area, recorded the lowest uptake value (1.12 mmol/g) out of the four test adsorbents. Furthermore, the ZIF-8@Na-A via in situ method recorded the highest uptake of 3.48 mmol/g. The key point to note here is that ZIF-8 in this method has been forced to crystallized in the pores around the resident Na-A. This could have contributed to an optimal combination of the physical properties ZIF-8 to the high chemical affinity of Na-A towards CO_2 in general. ZIF-8@Na-A synthesized via simultaneous synthesis recorded the lowest of the surface area and the second lowest uptake. This could be due to the incomplete crystallization of both Na-A and ZIF-8 during the synthesis.

6.3.2. Adsorbent optimization based on ratio

Level II screening of adsorbents was done in this on the basis of the ratio between the $Zn(NO_3)_2.6H_2O$ and the Na-A during the time of synthesis. For example, an adsorbent was designated as

ZIF-8@Na-A via in-situ method 1:10, if the ratio of Zn^{2+} to Na-A was 1:10 during synthesis. Here, five such ratios were considered and were compared in terms of uptake. The results are tabulated in table. The initial experimental conditions for the carbon capture uptake studies were as follows: Temperature = 25 ºC, Pressure = 1 bar, CO_2 % in the feed = 16.7 % and a gas feed flowrate = 150 mL/min.

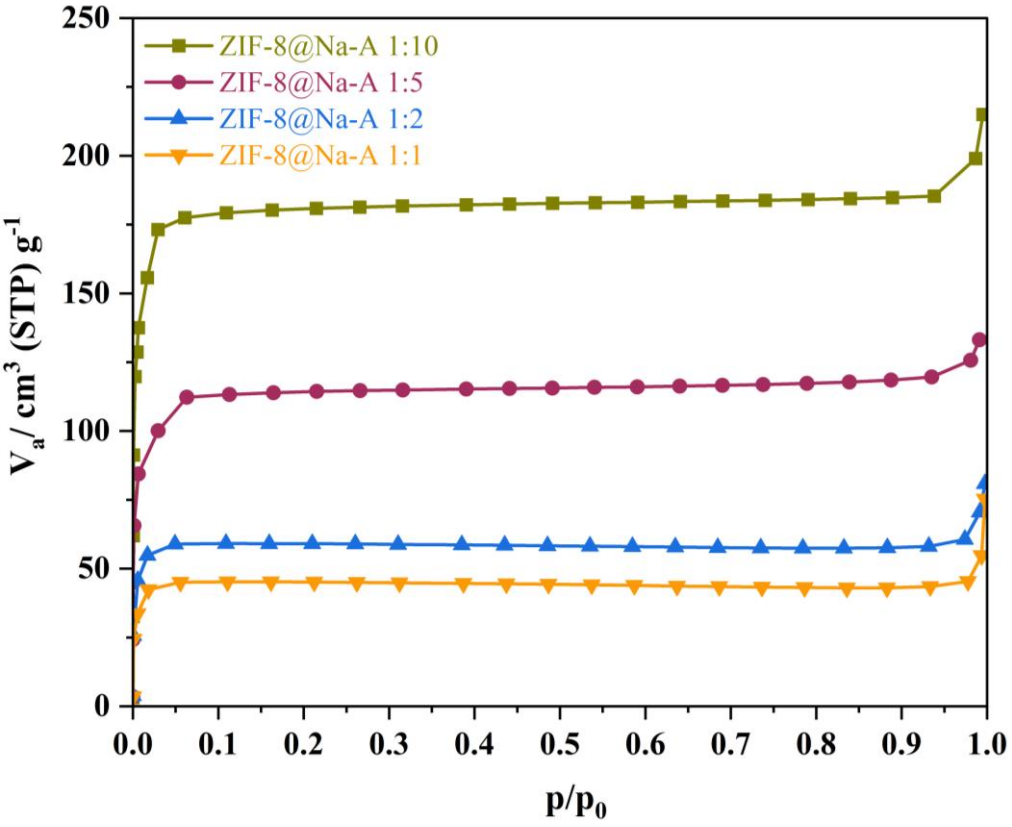

Figure 6.4: N_2 adsorption isotherms of synthesized adsorbents

Table 6.3: Results of second level screening

Adsorbent	**CO_2 Uptake (mmol/g)**	**BET Surface Area (m^2/g)**
ZIF-8@Na-A via in-situ method 1:10	3.61	711
ZIF-8@Na-A via in-situ method 1:5	3.48	388
ZIF-8@Na-A via in-situ method 1:2	2.57	212
ZIF-8@Na-A via in-situ method 1:1	2.31	110

From the tabulated results in table 6.3 and the figure 6.4, the adsorbent with the ratio of 1:10 displayed the highest uptake. It would also be interesting to note that the 1:5 adsorbent was a close second, indicating that after a certain initial synthesis ratio, the increase in uptake was nominal. Here, the increase in the quantity of ZIF-8 proved to be the deciding factor. The higher the ZIF-8 content, the higher the uptake. The content of Na-A was constant in all these adsorbents, indicating that along with the highly basic nature of Na-A, the quantity of pores and the available surface area was also a key factor in measuring the uptake. So, in line with this reasoning, the 1:1 adsorbent recorded the lowest uptake out of the four test adsorbents. Lower quantities of ZIF-8 may have deprived the CO_2 molecules of additional sites to invade and thus get trapped.

6.4. CO_2 uptake standardization

6.4.1. CO_2 uptake experimental design

In this study, Response Surface Methodology (RSM) was employed to ensure a systematic and well-structured experimental design. The study's primary focus was the investigation of three critical parameters: temperature, pressure, and aeration duration. The rationale behind this experimental design was to gain a comprehensive understanding of how these variables interplayed in the context of adsorption processes. Within the ambit of temperature variation, a spectrum of temperatures was explored, encompassing the points of 25 °C, 40 °C, 62 °C, 80 °C, and 100 °C. Notably, as the temperature was manipulated and escalated, an interesting and significant trend emerged: there was a discernible decrease in the predicted uptake values when the ZIF-8@Na-A adsorbent was employed. This temperature-dependent phenomenon sheds light on the sensitivity of the adsorption process to thermal conditions. One of the noteworthy findings of this study pertains to the comparative performance of ZIF-8@Na-A against pure ZIF-8. It is worth emphasizing that one of the inherent challenges in employing MOFs in CC tests is the tendency for the CC values obtained at lower temperatures to exhibit poor cyclic retention. However, the results of this investigation highlighted the superiority of the ZIF-8@Na-A composite adsorbent in addressing this issue. In our own previous research endeavor conducted under nearly identical conditions, pure ZIF-8 yielded an uptake value of 1.41 mmol/g. In stark contrast, the composite adsorbent developed in the present study demonstrated a remarkable twofold enhancement in CC performance, thus manifesting its efficacy as an improved adsorbent in the context of carbon capture.

Furthermore, it is noteworthy that these findings are not isolated but resonate with analogous observations from other related studies. For instance, the study conducted by Zhang and co [32] in 2014, which examined CO_2 adsorption employing biochar at elevated temperatures,

exhibited a similar temperature-sensitive behavior. In their investigation, both untreated and CO_2-treated carbonaceous sorbents displayed sorption values of 0.89 mmol/g and 1.21 mmol/g at 20°C, suggesting that temperature significantly influences the adsorption process. Similarly, another study [259], which delved into the use of zeolites for CO_2 capture, observed similar trends. Both 13-X and WE-G 592 zeolites exhibited consistent uptakes under varying conditions of CO_2 concentration and total pressure. For instance, at 30°C and 100 psi, the uptake values were approximately 5.0 mol/kg and 4.5 mol/kg, respectively. Importantly, when subjected to the same process pressure but at an elevated temperature of 120°C, these adsorbents retained a substantial portion of their uptake values, approximately 72% and 61%, respectively. This retention phenomenon was attributed to a high process pressure and the relatively high partial pressure of CO_2 within the feed gas itself, highlighting the intricate interplay of multiple factors in CC processes.

The role of temperature in influencing adsorption capacity was found to be of paramount importance, rendering it a critical factor to consider. Upon examination of the data presented, it became evident that the in-house synthesized adsorbent exhibited superior adsorption capabilities at lower temperatures (table 6.4). This observation aligned with the well-known exothermic nature inherent to physical adsorption processes. To delve further into this phenomenon, it became apparent that as temperatures increased, the interaction between solid and gas molecules at the interface intensified. This heightened interaction could be elucidated by the Boltzmann equation, which attributed it to the increased kinetic energy of the solid-gas molecules engaged in the adsorption process. Consequently, this heightened molecular interaction led to a reduction in the effective and accessible surface area available for adsorption. As a result, it could be reasonably concluded that lower sorption temperatures often yield higher sorption capacities for adsorbents optimal temperature for maximizing the adsorption capacity of each adsorbent was the lowest temperature among the available options.

Table 6.4: CO_2 adsorption studies of ZIF-8@Na-A 1:5 based on RSM design

Std	Temperature (C)	Pressure (bar)	Time of Carbonation (min)	CO_2 Uptake (mmol/g)
1	40	1.6	96	5.2
2	85	1.6	96	1.81
3	40	3.4	96	6.63
4	85	3.4	96	3.29
5	40	1.6	200	4.15
6	85	1.6	200	1.83
7	40	3.4	200	7.1
8	85	3.4	200	3.51
9	25	2.5	150	6.3
10	100	2.5	150	2.31
11	62.5	1	150	3.33
12	62.5	4	150	5.8
13	62.5	2.5	60	4.27
14	62.5	2.5	240	4.28
15	62.5	2.5	150	4.32
16	62.5	2.5	150	4.27
17	62.5	2.5	150	4.31
18	62.5	2.5	150	4.56
19	62.5	2.5	150	4.22
20	62.5	2.5	150	4.38

Process pressures were also of five parametric levels: 1.0 bar, 1.6 bar, 2.5 bar, 3.4 bar and 4 bar, as dictated by the RSM CCD spherical model. Indeed, the highest uptake of 7.1 mmol/g was observed at 3.4 bar and 40 ºC. Furthermore, at 4 bar process pressure and 62.5 ºC, the uptake was around 5.8 mmol/g indicating that process temperature also played an important role in determining the overall uptake. Nonetheless, it was a high volume of CO_2 adsorbed at that pressure. Wang et al. [260] reported that for their own rice husk synthesized Na-A, process pressure contributed to a higher CC value. K Yang et al. [183] also observed that when the process pressures increased, the uptake values of their Y1302 adsorbent increased by 300%.

Cheung and group [261] also recorded that for the nano-NaKA adsorbent, an increase in pressure saw the enhancement of the uptake value by 100%. Returning to the adsorbents in the present study, as indicated by their N_2 sorption patterns, they are all microporous in nature following the Type-I adsorption pattern. This would mean that at high process pressures, the pressure difference between the process pressure and the pressure within the narrow micropores of the sorbents would promote high volume CO_2 adsorption quickly.

In our investigation, the influence of various operational parameters on carbon capture (CC) uptake values was meticulously examined. It was apparent that temperature and pressure assumed pivotal roles in shaping the outcomes of our study. An intriguing observation was made concerning carbonation time: these factors appeared to exert a comparatively modest impact on CO_2 uptake values. In particular, when the extension of carbonation time was undertaken, a slight increment in CO_2 uptake was discerned. However, it is noteworthy that this increment did not amount to much. This is of a similar trend noted by Penchah and team in their research, which centered on the adsorption of CO_2 onto a benzene-based hyper-cross-linked polymer [262]. In their study, a marginal increase in CO_2 uptake was documented when the adsorption duration was prolonged from 2000 seconds to 3000 seconds, specifically manifesting as a shift from 75 mg/g CC after 2000 seconds to 80 mg/g after 3000 seconds. This consistent pattern of observations underscores the theory that, when the mass of the adsorbent remains constant, an extension of the contact time between gas and solid molecules tends to yield a higher gas uptake—an empirically substantiated phenomenon. Further buttressing this trend, a study by Sreenivasulu et al. in 2018 [120] reported a parallel trend. They found that longer carbonation times were linked with augmented uptake values for the adsorbents they investigated, thereby supplying additional affirmation of the affirmative correlation between prolonged contact time and an amplified efficiency in carbon capture.

In summation, while temperature and pressure were identified as fundamental drivers in influencing uptake values in our study, the effect of carbonation time and the quantity of adsorbent used, although not negligible, displayed a more subtle influence. These findings resonate with the body of related research within the field, underscoring the pivotal role of contact time in the adsorption process and shedding light on the intricate interplay of diverse parameters in the realm of carbon capture.

6.4.2. RSM model generation and verification

Table 6.5 presents the optimal conditions for the specific adsorbent under investigation, together with the ideal experimental conditions for the process, which are also included inside the same table. The equations presented in this study have successfully demonstrated a clear correlation between the experimental results and several process factors. This correlation has provided valuable insights into the relationship between CO_2 uptake values and these specific parameters. The coded CO_2 equation for ZIF-8@Na-A is presented below.

$$CO_2\ Uptake = 4.2935 - (1.4169 * A) + (0.856275 * B) - (0.0236645 * C) \quad \text{Eq 6.1}$$

Table 6.5: Model verification of optimal conditions

Adsorbent	Temp (ºC)	Pressure (bar)	Time (min)	Predicted uptake (mmol/g)	Experimental uptake (mmol/g)
ZIF-8@Na-A	55	3	120	5.12	4.88

The model F-value for ZIF-8@Na-A was recorded at 24.88, signifying the model's statistical significance. The high level of concordance observed between the predicted R^2 value, which amounted to 0.953, and the adjusted R^2 value, measuring at 0.945, provided strong evidence for a well-fitting model. A comparative analysis between these predicted values and the actual experimental results revealed reasonably favorable fit statistics. Notably, the standard deviation within the context of this experimental model for ZIF-8@Na-A was approximately 0.33. As

depicted in table 6.5, a noteworthy alignment was observed between the optimized and predicted values and their corresponding experimental counterparts. This alignment lent substantial credence to the efficacy of the RSM experimental design, underscoring its ability to accurately forecast adsorbent uptake levels within the predefined parameter ranges. The results, thus, affirm the successful application of the RSM approach in this study for precise predictions of adsorbent uptake levels within the specified parameter boundaries.

6.5. Enhancement of uptake through amine loading

6.5.1. Effect of TEPA loading on CO_2 uptake (constant temperature)

The study revealed that TEPA loading had a positive impact on the overall carbon capture (CC) uptake values, showing a distinct trend of enhanced uptake with increased TEPA loading. Notably, the CC values exhibited a substantial escalation, particularly when transitioning from 0% TEPA loading to 40% TEPA loading. For instance, the CC value of 3.75 mmol/g at 10% loading surged to 5.01 mmol/g at 40% TEPA loading. This observation is consistent with a well-established trend that an augmentation in amine loading typically leads to an increase in uptake.

This trend finds support in the research conducted by Taheri and team in their study involving TEPA-loaded mesoporous nanosilica tubes [263]. They reported a remarkable upsurge in CC, particularly when the TEPA loading was increased from 10% to 30%. Specifically, a TEPA loading of 30% resulted in a calculated CC of approximately 9 mmol/g. Similarly, Li and group observed a similar correlation when they investigated TEPA loading from 25% to 60%, which resulted in a 20% increase in CC values. In that study, the highest uptake, reaching 4.02 mmol/g, was attained for Na-A loaded with 60% TEPA [264]. An intriguing case emerged from the uptake study of TEPA loaded onto mesoporous silica gels, as conducted by Zhao and their research team [265]. They noted that as TEPA loading increased from 0% to 20%, uptake

values experienced a notable increase of 27%. However, when the TEPA loading was further elevated from 20% to 50%, the uptake displayed a contrasting trend, decreasing by 28%. This decline was attributed to the consequences of excessive amine loading. While an increase in TEPA loading initially enhances uptake due to a higher content of basic amines, an excessive rise in amine loading can lead to pore blockage, reducing the available pore volume and active adsorption sites. Furthermore, an excessive amine loading can result in an uneven dispersion of amines across the surface and pores of the parent adsorbent.

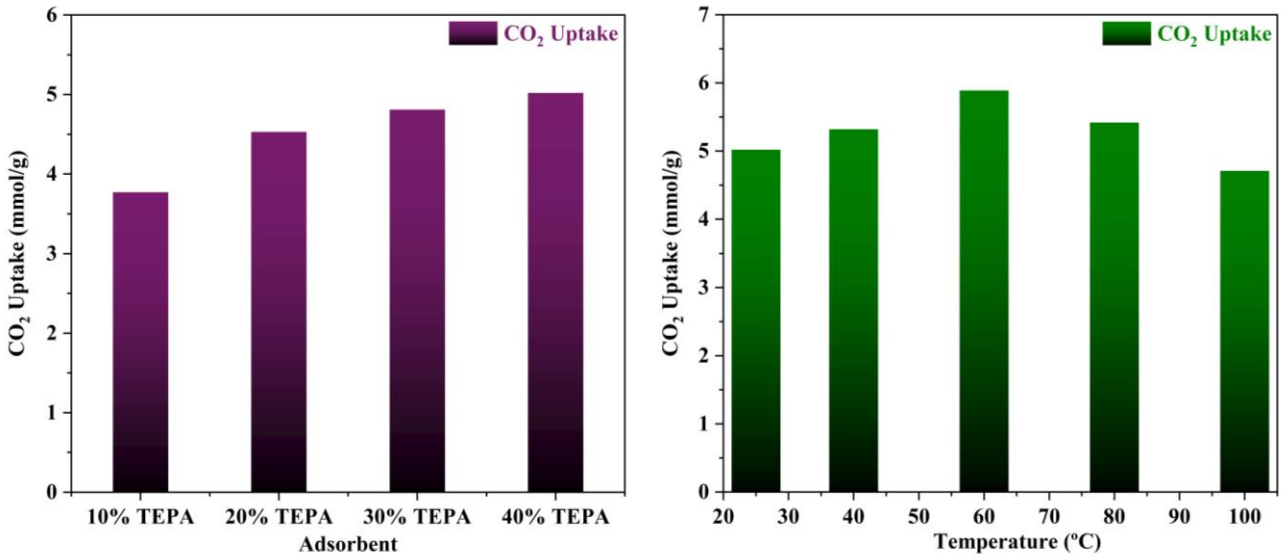

Figure 6.5: Effect of TEPA loading (at 25 ºC) and temperature (40% TEPA loading) on the uptake of ZIF-8@Na-A 1:5

6.5.2. Effect of Temperature on the uptake 40% TEPA loaded adsorbent

The effect of temperature upon uptake of the 40% TEPA loaded ZIF-8@Na-A 1:5 adsorbent is shown in figure 6.5. The TEPA loaded version of ZIF-8@Na-A gave the highest uptake value at 60 ºC. For example, the 40% TEPA loaded ZIF-8@Na-A showed an uptake value of 5.01 mmol/g at 25 ºC. It then increased considerably to 5.89 mmol/g at 60 ºC and decreased greatly to 4.71 mmol/g at 100 ºC. Liu et al. [266] conducted a thorough investigation upon the

uptake activity TEPA loaded Al-Fumarate MOF. In that study, the uptake for the 50% TEPA loaded Al-Fum MOF increased from 2.00 mmol/g at 45 ºC to 3.40 mmol/g at 60 ºC. But from 60 ºC to 100 ºC, the uptake decreased from 3.40 mmol/g to 1.50 mmol/g. This is also in line with our own study. Similarly, Zhang et al. [267] also conducted extensive studies upon the CC behaviour of amine loaded porous silica. The TEPA loaded porous silica showed a considerable increase for the 60% TEPA loaded adsorbent from 3.75 mmol/g at 30 ºC to 5.01 mmol/g at 75 ºC. However, from there it sharply decreased to 3.85 mmol at 105 ºC. Modified carbon nanotubes impregnated with TEPA also displayed the same behaviour [268]. A 75% TEPA loaded porous silica displayed an increase in CO_2 uptake from 25 ºC to 60 ºC and decreased from thence to 80 ºC. Contrary to physisorption wherein an increase in process temperature is detrimental to uptake, in amine loaded sorption processes the trend is usually hard to predict. Since some degree of chemisorption is involved in amine loaded sorbents, a short increase in temperature could result in a better uptake. This is because at optimal temperatures, 60 ºC in the present study, amine spreading across the surface of the parent sorbent would be even thus promoting high uptakes. Furthermore, an increase from this optimal temperature would result in a higher kinetic energy in CO_2 molecules thus decreasing the adsorption uptake values.

6.6. Thermo-kinetic modelling and analysis

6.6.1. Adsorption kinetics modelling

Five kinetic models were applied, encompassing the pseudo first and second orders (PSO), Avrami kinetics, Elovich model, and the Weber-Morris model (mentioned in Chapter 2, Eq 2.1, 2.2, 2.3, 2.4 and 2.5). These models bear considerable qualitative significance, as they offer valuable insights into the nature of adsorption processes. The PFO model, for instance, typically suggests a predominance of physisorption, which is generally a reversible process. Conversely, a strong concordance with the PSO model within the experimental data often signifies the prevalence of an irreversible chemisorption process governing the adsorption phenomenon. In essence, the employment of these kinetic models provides a comprehensive understanding of the adsorption mechanism at play, shedding light on the balance between physical and chemical interactions, and helping to discern the fundamental nature of the adsorption process.

Table 6.6: Kinetics models parameters at 55 ºC and 3 bar

Kinetics Model	Temp (K)	Q_e exp (mmol/g)	Q_e fit (mmol/g)	k	n	C	α	β	R^2
Pseudo First Order	55	4.88	4.92	0.0749					0.961
Pseudo Second Order	55	4.88	5.56	0.0179					0.902
Avrami	55	4.88	4.87	0.0125	1.66				0.994
Elovich	55						1.448	0.951	0.801
Weber-Moris	55			0.3468		1.809			0.605

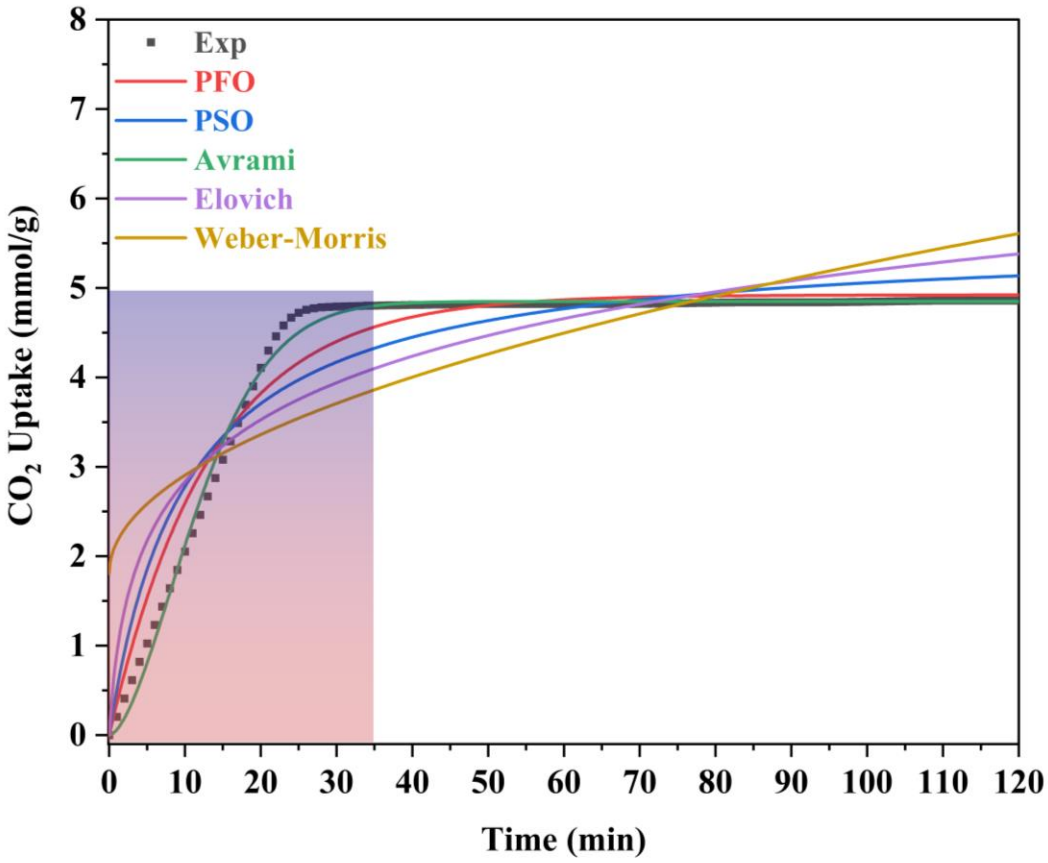

Figure 6.6: Kinetic modelling of ZIF-8@Na-A at 55 ºC, 15% CO_2 and 3 bar

Figure 6.6 and table 6.6 offer valuable insights into the kinetics of the adsorption process for the adsorbent at hand. Evident is the fact that the maximum carbon capture (CC) capacity for the sorbent is rapidly achieved within just 25 minutes, after which the increase in uptake levels off. This behavior can be attributed to the limited retention of NaOH within the adsorbents in comparison to their overall volume. Notably, among the various kinetic models assessed, the pseudo first-order (PFO) model stands out for its superior fit to the experimental data for both adsorbents, as demonstrated in the figure. When comparing the determination coefficient (R^2) of the PFO model to that of the pseudo second-order (PSO) model, both of which are presented in the table 6.6, it is evident that the PFO model provides a reasonably good fit for describing the adsorption kinetics. Surprisingly, the Avrami model emerges as the most appropriate model, with an impressively high R^2 value of 0.994, indicating a dual nature of the adsorption

process, encompassing both physisorption and chemisorption. Furthermore, it is important to consider that the predominantly microporous nature of the adsorbent resulted in a swift initial adsorption rate, followed by a sharp deceleration as the micro-pores reached saturation. The Avrami model emerged as the most suitable option for describing the experimental data in comparison to the other models tested. This underscores the significance of selecting the appropriate kinetic model to depict the complex dynamics of the adsorption process, contributing to a deeper understanding of carbon capture kinetics.

6.6.2. Adsorption isotherm modelling

The concentration of CO_2 is a crucial determinant in sorption uptake and plays a pivotal role in defining the point of adsorbent bed saturation. In Figure 6.7, we adjusted the partial pressures of CO_2 in the range of 0 to 0.8 bar while maintaining a constant temperature of 298 K to investigate the influence of CO_2 concentration on the adsorption process. Our observations revealed that an increase in the CO_2 content in the feed corresponded to a higher quantity of CO_2 being adsorbed. This trend was particularly noticeable as the CO_2 feed percentage increased from 0 to 50, resulting in a nearly threefold increase in uptake within this range. However, beyond the 50% mark, the rate of increase became less pronounced, with only a 25% increase in uptake levels from 50% to 80%. This phenomenon may be attributed to the fact that, after a certain feed percentage, the adsorption capacity reaches a saturation point, beyond which further increases in CO_2 concentration yield diminishing returns. In line with this observation, Li and group [237] noted a similar trend in their study on the adsorption of CO_2 over activated carbons produced within the temperature range of 540 ºC to 800 ºC. They found that the enhancement of uptake became increasingly marginal as the CO_2 feed percentage rose. This behaviour aligns with materials boasting available surface areas exceeding 500 m^2/g, as reported by Wilson and team [238]. Ahmed and group [239] also published findings showing a parallel trend in their investigations with TEPA loaded sorbents. They posited that at low

CO_2 partial pressures, the pores of Na-A quickly and readily become filled, while subsequent increases in CO_2 partial pressure result in only marginal additional gains. A similar trend was observed in a study of CO_2 adsorption over pure ZIF-8 [240]. Such behaviour is typical for materials predominantly characterized by microporous nature, which is consistent with the nature of the ZIF-8@Na-A adsorbent, primarily exhibiting a microporous structure.

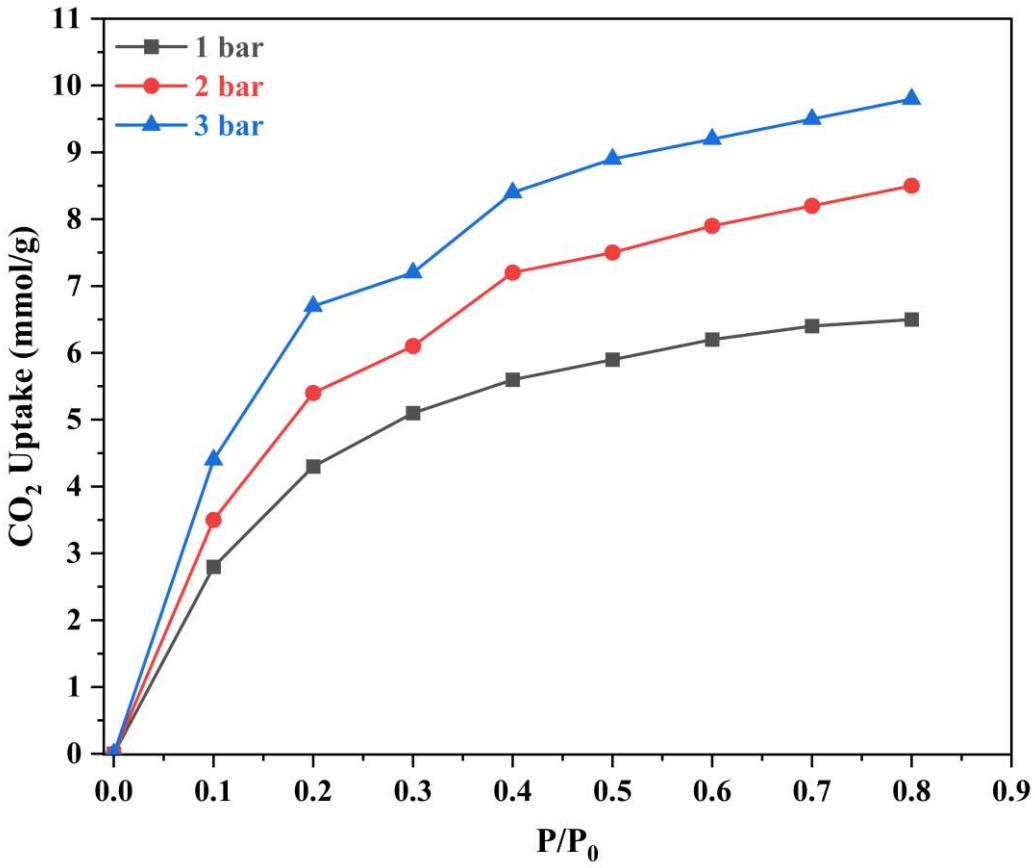

Figure 6.7: CO_2 adsorption isotherms of ZIF-8@Na-A at 25 ºC

The amount of CO_2 present is a critical factor in sorption uptake and determines when the adsorbent bed saturates. As seen in figure 6.7, partial pressures of CO_2 were adjusted between 0 and 0.8 bar while maintaining a constant temperature of 298 K to examine the impact of CO_2 concentration on the adsorption process. It was found that an increase in the feed's CO_2 content was accompanied by an increase in the amount of CO_2 adsorbed. This tendency was especially noticeable when CO_2 feed percentages rose from 0 to 50, which caused the values of uptake

within this range to nearly triple. But beyond 50%, the pace of rise became less significant. There was just a 25% rise in uptake levels from 50% to 80%. Adsorption isotherm studies were conducted of which four models were considered (mentioned in Chapter 2, Eq 2.6, 2.7, 2.8 and 2.9).

Table 6.7: Adsorption isotherm modelling fit for Freundlich at 25 ºC

Adsorbent	Total Pressure (bar)	Freundlich		
		k_F	n	R^2
ZIF-8@Na-A	1	7.38	2.86	0.981
	2	9.55	2.65	0.988
	3	10.64	2.94	0.987

Table 6.8: Adsorption isotherm modelling fit for Sips and Toth models at 25 ºC

Adsorbent	Total Pressure (bar)	Sips				Toth			
		k_S	Q_m (mmol/g)	n	R^2	Q_m (mmol/g)	k_T	n	R^2
ZIF-8@Na-A	1	8.4421	7.51	1.15	0.999	4.95	7.5638	1.25	0.998
	2	4.6015	10.75	0.98	0.998	11.77	4.6891	0.95	0.994
	3	5.2541	12.08	0.96	0.998	14.34	5.4513	0.92	0.996

The R^2 values presented in tables 6.7 and 6.8 indicate that for the ZIF-8@Na-A adsorbent, the Langmuir model did not fit at all for the considered pressures. In contrast, the Freundlich model achieved R^2 values of 0.981, 0.988, and 0.987 at 1 bar, 2 bar, and 3 bar, respectively. Although the Sips model slightly outperformed the Toth model, as shown in table 6.8, this suggests a mixed adsorption nature comprising both monolayer and multilayer characteristics. The compatibility of the Sips model with heterogeneous adsorbent surfaces aligns with the composite nature of the adsorbents. The nature of adsorption is heavily influenced by pore characteristics, as illustrated by the study on CO_2 uptake over TEPA-modified TiO_2 by Kapica-Kozar and their colleagues [213]. Similarly, in studies by Azeem et al. [166] on KOH activated porous carbons and Melouki et al. [167] on carbons derived from olive waste, the Sips model

demonstrated an excellent fit to experimental data, with the Toth model being a close second. Yongha Park et al.'s comparative study [168] involving activated carbon and zeolite-LiX for CO_2 uptake also favored the Sips model for both adsorbents. However, Sun et al.'s [241] investigation of CO_2 adsorption on graphene with an average pore size of 3 nm highlighted Langmuir adsorption behavior, despite surface multilayer adsorption. Regarding the tested adsorbents, ZIF-8@Na-A 1:5 exhibited a microporous nature indicating the presence of narrow, elongated pores within their structures. Adsorbents with such narrow micropores often exhibit heightened CO_2 uptake rates under high process pressures. ZIF-8, being a framework with these narrow pores, capitalizes on the pressure differential, a pivotal factor for adsorption at elevated pressures. This inherent property makes MOFs and ZIFs well-suited for high-pressure adsorption processes. ZIF-8@Na-A also portrays a primarily microporous character. However, unlike pure ZIF-8, this composite showcases significant decrease in microporosity. At lower process pressures, the micropores saturate rapidly, following a nearly linear trend. Subsequent increments are marginal, indicating gradual filling of existing mesopores.

6.6.3. Adsorption Thermodynamics

The heat of adsorption was calculated using the Clausius-Clapeyron equation. Three temperatures, specifically 25 ºC, 40 ºC, and 55 ºC, were considered under a process pressure of 1 bar. The resulting plots, illustrating the relationship between 1/T (reciprocal temperature) and the natural logarithm of pressure (lnP), are displayed in figure 6.8. These plots allowed valuable insights to be gained into the thermodynamics of the adsorption process and the energetics associated with CO_2 uptake on the surfaces of the adsorbent at various temperatures. The trends and variations in these plots were examined to deepen the understanding of the heat of adsorption and its temperature dependency, which played a pivotal role in assessing the feasibility and efficiency of adsorption for practical applications.

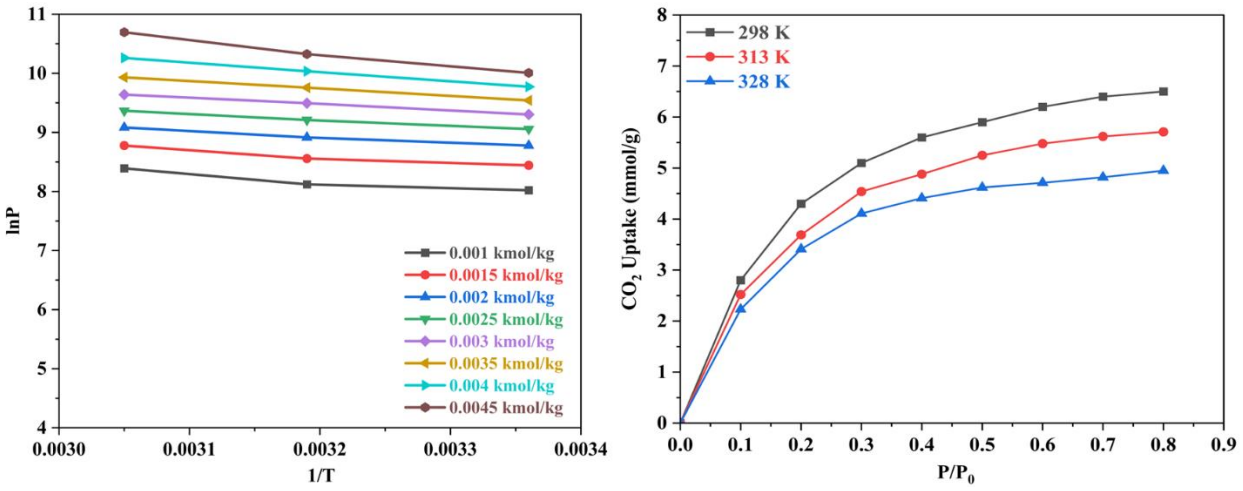

Figure 6.8: 1/T vs lnP graph for ZIF-8@Na-A and Isotherms at different temperatures

In this investigation, eight distinct carbon capture (CC) uptake values were scrutinized for ZIF-8@Na-A, encompassing a loading range from 0.001 kmol/kg to 0.0045 kmol/kg. The resulting analysis unveiled an average heat of adsorption for the ZIF-8@Na-A adsorbent at these loading levels, yielding a value of approximately -11.05 kJ/kmol. Remarkably, this figure aligns closely with the typical range observed for pure ZIF-8. Fischer and Bell [243] had previously reported heat of adsorption values for pure ZIF-8 that spanned from -12.0 to -19.5 kJ/mol, while simulations consistently indicated heat of adsorption values ranging between -14.0 and -19.0 kJ/mol. A parallel study by Russell and Migone [269], disclosed that the heat of adsorption for modified ZIF-8 structures was around -18 kJ/mol. Given the favorable fit of the Sips isotherm to our data, it was selected for the calculation of the isosteric heat of adsorption. This parameter serves as a fundamental indicator of the adsorbent's affinity for CO_2 molecules and imparts critical insights into the thermodynamics governing the adsorption process. Such information is of paramount importance in the development and assessment of carbon capture technologies, contributing to the advancement of environmentally sustainable solutions in this field.

6.7. Cyclic stability

Cyclic stability tests were carried out to thoroughly assess the durability and performance stability of the adsorbents over repeated usage. In each cycle, a standard sample weighing 5 grams was introduced into the reactor, and carbonation was conducted at a constant temperature of 25 ºC. The feed gas consisted of a mixture of N_2 and CO_2, with a total feed flowrate of 150 mL/min, and CO_2 constituted roughly one-sixth of the gaseous feed composition. Following each cycle of carbonation, the process of decarbonation or regeneration was executed at a temperature of 150 ºC within an inert atmosphere. The selection of this temperature was deliberate, aimed at preserving the capacity of ZIF-8, as it is known to be sensitive to excessive heat exposure. The cyclic retention performance is graphically represented in figure 6.9.

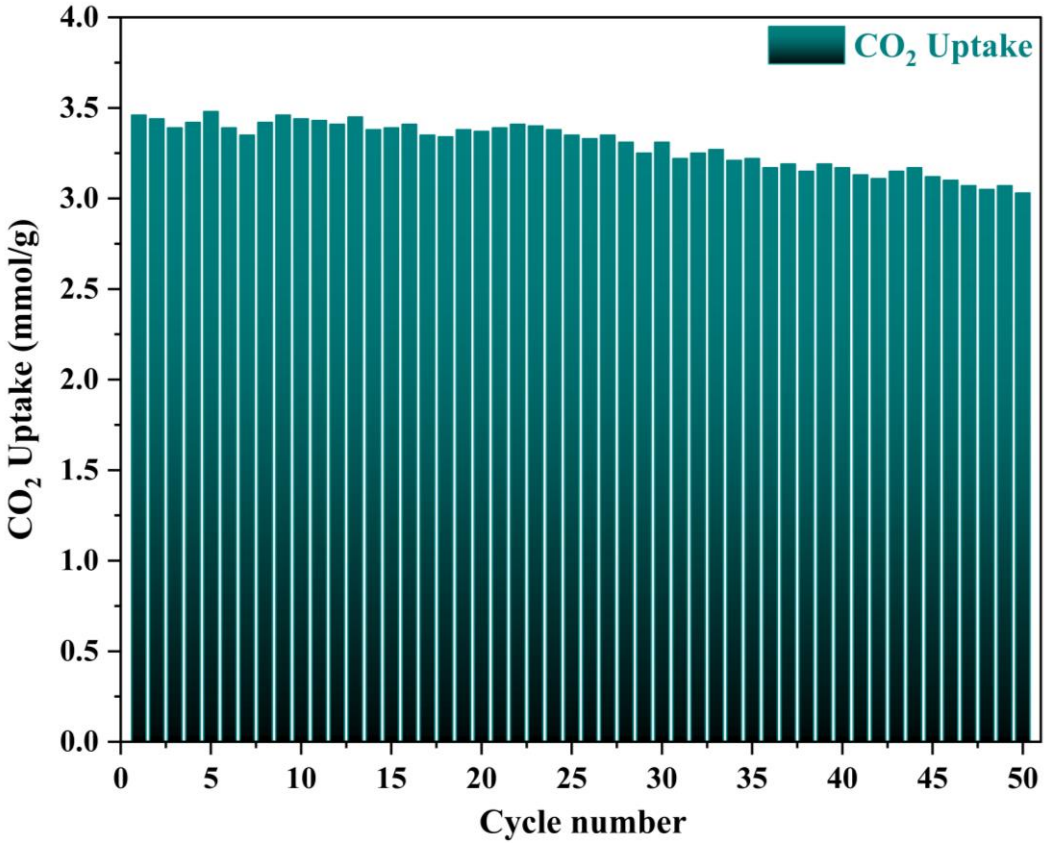

Figure 6.9: Cyclic retention capacity of ZIF-8@Na-A at 25 ºC and 1 bar

Remarkably, the adsorbent exhibited exceptional stability even after subjecting it to the rigors of 50 cycles of carbonation and regeneration. For the ZIF-8@Na-A adsorbent, which initially demonstrated a carbon capture (CC) value of 3.45 mmol/g at 298 K, its uptake after 50 cycles remained impressively high at approximately 3.03 mmol/g. This level of stability is particularly noteworthy considering the inclusion of ZIF-8 within the composite. Generally, zeolitic imidazolate frameworks (ZIFs) and metal-organic frameworks (MOFs) are known to be highly susceptible to degradation when repeatedly exposed to elevated temperatures. Notably, the ZIF-8@Na-A adsorbent exhibited a subtle change in colour, transitioning from its usual white appearance to a very pale tint of yellow after completing 50 cycles. A marginal loss of only nine percentage points over the course of 50 cyclic processes is indeed negligible. The cyclic performance of the adsorbent is visually depicted in the figure below, underscoring the remarkable stability achieved even under rigorous testing conditions.

6.8. Conclusions

Through in situ synthesis techniques, novel composites were successfully synthesized. Systematic CO_2 uptake experiments were conducted on these adsorbents, employing an RSM for process standardization. BET analysis revealed that the ZIF-8@Na-A adsorbent demonstrated a diminished surface area compared to its parent materials. This decrease in surface area was further confirmed by scanning electron microscopy (SEM) micrographs, which clearly depicted the presence of ZIF-8 embedded within the Na-A cubes. The influence of temperature on carbon capture uptake values was observed to be inversely proportional for the adsorbent. The highest uptake occurred at *25 ºC*, while the lowest was recorded at 398 K. Furthermore, an increase of TEPA loading had a positive impact on uptake, with the maximum uptake achieved at a TEPA loading of 40%. Process pressure exhibited a favorable effect on uptake, with the highest recorded uptake values occurring at 3 bar pressure. The adsorption models derived through CCD modeling were found to align exceptionally well with the experimental data. Experiments conducted at the optimal values recommended by the CCD model closely matched the standard deviation values predicted by the model, affirming the reliability of the model's predictions. The Avrami model for kinetics provided a highly effective description of the adsorption kinetics, as indicated by an R^2 value of 0.994. Sips adsorption modelling proved to be a robust method for explaining the experimental data, suggesting a combination of monolayer and multilayer adsorption mechanisms. The average heat of adsorption, calculated at -11.78 kJ/mol, underscored the predominantly physical nature of the adsorption process, revealing that it was driven primarily by physisorption interactions. Impressively, the adsorbent exhibited exceptional cyclic performance, retaining over 92% of its initial adsorption capacities even after 50 cycles. Notably, ZIF-8@Na-A exhibited a subtle change in colour, shifting to a slightly pale-yellow hue after these repeated cycles, which may indicate the possibility of thermal alteration in response to the cyclic conditions.

Chapter 7: Summary and conclusions

7. Summary and conclusions

A diverse range of adsorbents and composite materials were methodically synthesized to address the pressing need for effective carbon dioxide (CO_2) adsorption, playing a pivotal role in mitigating air pollution. The synthesis procedures were meticulously designed, prioritizing simplicity and efficiency to minimize energy consumption throughout the manufacturing process. This strategic approach not only contributes to the environmentally sustainable production of adsorbents but also underscores a commitment to developing energy-efficient solutions for combating air pollution. By employing easy synthesis protocols, the aim is to streamline the manufacturing process, making it accessible and feasible while simultaneously reducing the environmental footprint associated with energy-intensive procedures. This innovative approach holds promise not only for improving the adsorption capabilities of these materials but also for fostering a more sustainable and eco-friendlier pathway towards addressing the challenges of air pollution on a global scale.

In chapter three, utilizing coal fly ash, a zeolite-type adsorbent was synthesized and further combined with ZIF-8 through an in situ synthesis technique, resulting in the creation of a novel hybrid adsorbent. The adsorption capacity exhibited a temperature dependence, with the highest capacity recorded at 25 ºC (2.83 mmol/g), while CO_2 concentration significantly influenced the uptake, reaching around 3.6 mmol/g at higher concentrations. An increase in adsorbent loading for a given carbonation time had a slightly detrimental effect on overall uptake, whereas an increase in carbonation time had a slightly positive impact. Cyclic stability assessments indicated excellent performance of CFAZ/ZIF-8 even after five cycles of carbonation and decarbonation. The hybrid adsorbent surpassed its parent materials, suggesting a synergistic effect between ZIF-8 and CFAZ. Comparative performance with commercially available zeolites like 13X and NaX further highlighted the efficacy of CFAZ/ZIF-8. Kinetic studies revealed a combination of physisorption and chemisorption in the adsorption process,

and future investigations could explore the impact of the Zn metal ion-to-CFA weight ratio on the morphological properties and the uptake of this hybrid adsorbent.

In chapter four, two ZIF-based adsorbents, (Ce,Zn)ZIF-8 and (Ce,Co)ZIF-67, along with their amine-loaded counterparts, underwent successful synthesis and in-depth studies on CO_2 capture (CC), kinetics, and cyclic stability. The implementation of the central composite design in the response surface methodology (RSM) ensured rigorous process standardization. The superior uptake values compared to their parent ZIFs were ascribed to the introduction of crystal defects and charge, courtesy of the incorporation of cerium ions. The standard deviation values demonstrated excellent agreement with the optimal experimental conditions specified by the model, with an error percentage hovering around 7%. Further enhancement of CO_2 capacity was achieved through diethanolamine (DEA) loading. The optimized conditions for (Ce,Zn)ZIF-8 and (Ce,Co)ZIF-67, with amine loading, were identified at 15% DEA loading and 25 ºC, resulting in 4.37 and 13.6% DEA loading with 3.03 mmol/g, respectively. Cyclic stability testing revealed retention rates of 94% and 95% for the pure adsorbents after 15 cycles.

In chapter five, two novel composites were synthesized using in situ techniques and systematically evaluated for CO_2 uptake through Response Surface Methodology (RSM) standardization. Four key parameters were considered in the experimental design. BET analysis revealed that the ZIF-8@MCM-41 adsorbent exhibited a lower surface area compared to its parent materials. SEM micrographs confirmed the presence of ZIF-8 nanocrystals within MCM-41 spheres, and similarly, the formation of MCM-41 spheres over activated carbon particles was confirmed. The adsorption temperature inversely affected the CO_2 uptake values of both adsorbents, with the highest uptake observed at 25 ºC and the lowest at 125 ºC. DEA loading positively influenced the uptake, with 15% DEA loading yielding maximum values for both adsorbents. Mass of adsorbent and carbonation time had minimal influence, but both exhibited a slight positive impact on CO_2 uptake. The adsorption models derived from CCD

modeling aligned well with experimental data, and experiments at optimum values suggested by the CCD model fell within standard deviation values. The pseudo-first-order model effectively explained the adsorption kinetics, indicating a predominantly physisorption process, while the pseudo-second-order kinetics proved insufficient. Sips adsorption modeling revealed a combination of monolayer and multilayer adsorption types. The average heats of adsorption were -16.78 kJ/mol for ZIF-8@MCM-41 and -12.59 kJ/mol for MCM-41/AC/Na, suggesting a primarily physical nature of adsorption. Both adsorbents demonstrated excellent cyclic performance, retaining over 95% of their initial adsorption capacity. However, ZIF-8@MCM-41 exhibited slight discoloration after 15 cycles, indicating potential thermal compromise, whereas MCM-41/AC/Na showed greater stability.

In chapter six, through in situ synthesis techniques, novel composites were successfully synthesized. Systematic carbon capture (CC) uptake experiments were conducted on these adsorbents, employing a Response Surface Methodology (RSM) for process standardization. BET analysis revealed that the ZIF-8@Na-A adsorbent demonstrated a diminished surface area compared to its parent materials. This decrease in surface area was further confirmed by scanning electron microscopy (SEM) micrographs, which clearly depicted the presence of ZIF-8 embedded within the Na-A cubes. The influence of temperature on carbon capture uptake values was observed to be inversely proportional for the adsorbent. The highest uptake occurred at 298 K, while the lowest was recorded at 398 K. Furthermore, an increase of TEPA loading had a positive impact on uptake, with the maximum uptake achieved at a TEPA loading of 40%. Process pressure exhibited a favourable effect on CO_2 uptake, with the highest recorded uptake values occurring at 3 bar pressure. The adsorption models derived through Central Composite Design (CCD) modeling were found to align exceptionally well with the experimental data. Experiments conducted at the optimal values recommended by the CCD model closely matched the standard deviation values predicted by the model, affirming the reliability of the

model's predictions. The Avrami model for kinetics provided a highly effective description of the adsorption kinetics, as indicated by an R^2 value of 0.994. Sips adsorption modelling proved to be a robust method for explaining the experimental data, suggesting a combination of monolayer and multilayer adsorption mechanisms. The average heat of adsorption, calculated at -11.78 kJ/mol, underscored the predominantly physical nature of the adsorption process, revealing that it was driven primarily by physisorption interactions. Impressively, the adsorbent exhibited exceptional cyclic performance, retaining over 92% of its initial adsorption capacities even after 50 cycles. Notably, ZIF-8@Na-A exhibited a subtle change in colour, shifting to a slightly pale-yellow hue after these repeated cycles, which may indicate the possibility of thermal alteration in response to the cyclic conditions.

8. Recommendations for future work

The choice of water as a solvent in the synthesis of zeolitic imidazolate frameworks (ZIFs) and metal-organic frameworks (MOFs) is a strategic decision that significantly reduces the environmental impact associated with traditional organic solvents. Water is abundant, non-toxic, and easily recyclable, aligning with the principles of green chemistry. Conducting the synthesis at room temperature is a departure from traditional hydrothermal methods that often require elevated temperatures. This not only reduces energy consumption but also facilitates scalability and enhances the economic viability of the synthesis process.

The incorporation of diverse metal ions such as Zn, Ce, and Co into the framework allows for the tailoring of the structural and chemical properties of the materials. This tunability opens avenues for designing materials with specific functionalities, making them versatile for a range of applications [270,271]. The synergistic effects of combining different metal ions often result in enhanced stability and unique reactivity, providing materials that are not only diverse but also robust under various conditions.

The development of high-capacity adsorbents is crucial for addressing environmental challenges associated with increasing CO_2 levels. Modifying adsorbents with amines enhances their affinity for CO_2, making them effective tools for capturing and sequestering carbon emissions from industrial processes and power plants. The focus on optimizing these materials for practical implementation underscores a commitment to bridging the gap between laboratory-scale research and real-world applications. Understanding the stability of modified adsorbents at higher temperatures is pivotal for ensuring their effectiveness in industrial settings. Furthering this, it would also be useful in developing sorbents that can withstand even 150 cycles of carbonation and regeneration.

The potential use of recovered CO_2 for the production of clean fuels aligns with the principles of circular carbon economies [272,273]. Rather than being treated solely as a waste product, CO_2 becomes a valuable resource for fuel production, closing the carbon loop and contributing to sustainable and circular resource management. Producing clean fuels such as hydrogen and methane directly from captured CO_2 not only addresses environmental concerns but also responds to the growing demand for sustainable and renewable energy sources [274–276].

The exploration of stability at elevated temperatures, around 550ºC, positions the synthesized materials for catalytic applications, especially in reforming processes. This is a crucial parameter for considering their use in industrial catalysis, where stability under harsh conditions is essential. The presence of transition metals such as Zn, Ce, and Co in the adsorbents holds promise for catalytic transformations [277]. These metals offer catalytic sites for various reactions, presenting opportunities for cleaner and more efficient fuel production processes.

The research into bimetallic ZIFs and their applications in CO_2 adsorption and by extension in CO_2 conversion represents an exciting frontier in sustainable catalysis [278]. As the field progresses, understanding the intricate details of catalytic transformations involving these materials could lead to breakthroughs in the development of greener and more efficient catalysts. By focusing on environmentally conscious and economically viable materials, this line of research contributes to the ongoing paradigm shift towards more sustainable chemical processes. The potential applications of these materials in catalysis exemplify a holistic approach to achieving both environmental and economic sustainability [279].

Direct Air Capture (DAC) is also an interesting and obvious extension to the present work [280]. DAC is the process of capturing and removing CO_2 from the atmosphere itself. This is

an interesting prospect in the fields of purification technology, environmental engineering and materials engineering as well [152,281,282].

In summary, the synthesis methodologies and applications of bimetallic ZIFs and MOFs demonstrate a commitment to sustainability, not only in the context of reducing energy consumption and environmental impact but also in addressing pressing global challenges such as CO_2 capture and sustainable catalysis. The multifaceted approach, from synthesis to application, positions these materials as key players in the transition toward a more sustainable and circular economy.

References

[1] CO_2 emissions - Our World in Data, (n.d.). https://ourworldindata.org/co2-emissions (accessed October 10, 2023).

[2] R. Shaw, S. Mukherjee, The development of carbon capture and storage (CCS) in India: A critical review, Carbon Capture Science & Technology 2 (2022) 100036. https://doi.org/10.1016/J.CCST.2022.100036.

[3] J. Macknick, Energy and CO_2 emission data uncertainties, Carbon Manag 2 (2011) 189–205. https://doi.org/10.4155/CMT.11.10.

[4] J. Zhang, Q. Zhao, S. Wang, X. Tan, Direct capture of low concentration CO_2 using tetraethylenepentamine-grafted polyacrylonitrile hollow fibers, Sep Purif Technol 287 (2022) 120562. https://doi.org/10.1016/j.seppur.2022.120562.

[5] A. Samanta, A. Zhao, G.K.H. Shimizu, P. Sarkar, R. Gupta, Post-combustion CO_2 capture using solid sorbents: A review, Ind Eng Chem Res 51 (2012) 1438–1463. https://doi.org/10.1021/ie200686q.

[6] F. Montagnaro, A. Silvestre-Albero, J. Silvestre-Albero, F. Rodríguez-Reinoso, A. Erto, A. Lancia, M. Balsamo, Post-combustion CO_2 adsorption on activated carbons with different textural properties, Microporous and Mesoporous Materials 209 (2015) 157–164. https://doi.org/10.1016/j.micromeso.2014.09.037.

[7] D. Jansen, M. Gazzani, G. Manzolini, E. Van Dijk, M. Carbo, Pre-combustion CO_2 capture, International Journal of Greenhouse Gas Control 40 (2015) 167–187. https://doi.org/10.1016/j.ijggc.2015.05.028.

[8] F. Wu, P.A. Dellenback, M. Fan, Highly efficient and stable calcium looping based pre-combustion CO_2 capture for high-purity H_2 production, Mater Today Energy 13 (2019) 233–238. https://doi.org/10.1016/j.mtener.2019.05.013.

[9] M. Wang, A. Lawal, P. Stephenson, J. Sidders, C. Ramshaw, Post-combustion CO_2 capture with chemical absorption: A state-of-the-art review, Chemical Engineering Research and Design 89 (2011) 1609–1624. https://doi.org/10.1016/j.cherd.2010.11.005.

[10] I. Sreedhar, R. Vaidhiswaran, B.M. Kamani, A. Venugopal, Process and engineering trends in membrane based carbon capture, Renewable and Sustainable Energy Reviews 68 (2017) 659–684. https://doi.org/10.1016/j.rser.2016.10.025.

[11] A.M. Yousef, W.M. El-Maghlany, Y.A. Eldrainy, A. Attia, New approach for biogas purification using cryogenic separation and distillation process for CO_2 capture, Energy 156 (2018) 328–351. https://doi.org/10.1016/j.energy.2018.05.106.

[12] M. Johansson, T. Mattisson, A. Lyngfelt, Comparison of oxygen carriers for chemical-looping combustion, Thermal Science 10 (2006) 93–107. https://doi.org/10.2298/TSCI0603093J.

[13] A. Kumar, D.G. Madden, M. Lusi, K.-J. Chen, E.A. Daniels, T. Curtin, J.J. Perry, M.J. Zaworotko, Direct Air Capture of CO_2 by Physisorbent Materials , Angewandte Chemie 127 (2015) 14580–14585. https://doi.org/10.1002/ange.201506952.

[14] J. Ding, C. Yu, J. Lu, X. Wei, W. Wang, G. Pan, Enhanced CO_2 adsorption of MgO with alkali metal nitrates and carbonates, Appl Energy 263 (2020) 114681. https://doi.org/10.1016/j.apenergy.2020.114681.

[15] J.A. Onrubia-Calvo, A. Bermejo-López, B. Pereda-Ayo, J.A. González-Marcos, J.R. González-Velasco, Ca doping effect on the performance of $La_{1-x}Ca_xNiO_3/CeO_2$-derived dual function materials for CO_2 capture and hydrogenation to methane, Appl Catal B 321 (2023) 122045. https://doi.org/10.1016/j.apcatb.2022.122045.

[16] M. Cortazar, S. Sun, C. Wu, L. Santamaria, L. Olazar, E. Fernandez, M. Artetxe, G. Lopez, M. Olazar, Sorption enhanced ethanol steam reforming on a bifunctional Ni/CaO catalyst for H_2 production, J Environ Chem Eng 9 (2021) 106725. https://doi.org/10.1016/j.jece.2021.106725.

[17] S.L. Hsieh, F.Y. Li, P.Y. Lin, D.E. Beck, R. Kirankumar, G.J. Wang, S. Hsieh, CaO recovered from eggshell waste as a potential adsorbent for greenhouse gas CO_2, J Environ Manage 297 (2021) 113430. https://doi.org/10.1016/j.jenvman.2021.113430.

[18] Y. Xu, B. Xiao, Y. Feng, W. Yang, Y. Lv, Mn-promoted CaO-based adsorbents with enhanced CO_2 uptake performance, J Nat Gas Sci Eng 94 (2021) 104029. https://doi.org/10.1016/j.jngse.2021.104029.

[19] F. Micheli, E. Mattucci, C. Courson, K. Gallucci, Bi-functional catalyst/sorbent for a H_2-rich gas from biomass gasification, Processes 9 (2021) 1249. https://doi.org/10.3390/pr9071249.

[20] A. Hanif, S. Dasgupta, A. Nanoti, Facile Synthesis of High-Surface-Area Mesoporous MgO with Excellent High-Temperature CO_2 Adsorption Potential, Ind Eng Chem Res 55 (2016) 8070–8078. https://doi.org/10.1021/acs.iecr.6b00647.

[21] K.K. Han, Y. Zhou, Y. Chun, J.H. Zhu, Efficient MgO-based mesoporous CO_2 trapper and its performance at high temperature, J Hazard Mater 203–204 (2012) 341–347. https://doi.org/10.1016/j.jhazmat.2011.12.036.

[22] Z. Xu, T. Jiang, H. Zhang, Y. Zhao, X. Ma, S. Wang, Efficient MgO-doped CaO sorbent pellets for high temperature CO_2 capture, Front Chem Sci Eng 15 (2021) 698–708. https://doi.org/10.1007/s11705-020-1981-2.

[23] M.L.T. Triviño, V. Hiremath, J.G. Seo, Stabilization of $NaNO_3$-Promoted Magnesium Oxide for High-Temperature CO_2 Capture, Environ Sci Technol 52 (2018) 11952–11959. https://doi.org/10.1021/acs.est.8b04145.

[24] C. V. Miguel, R. Trujillano, V. Rives, M.A. Vicente, A.F.P. Ferreira, A.E. Rodrigues, A. Mendes, L.M. Madeira, High temperature CO_2 sorption with gallium-substituted and promoted hydrotalcites, Sep Purif Technol 127 (2014) 202–211. https://doi.org/10.1016/j.seppur.2014.03.007.

[25] J.M. Silva, R. Trujillano, V. Rives, M.A. Soria, L.M. Madeira, High temperature CO_2 sorption over modified hydrotalcites, Chemical Engineering Journal 325 (2017) 25–34. https://doi.org/10.1016/j.cej.2017.05.032.

[26] H. Pfeiffer, P. Bosch, Thermal stability and high-temperature carbon dioxide sorption on hexa-lithium zirconate ($Li_6Zr_2O_7$), Chemistry of Materials 17 (2005) 1704–1710. https://doi.org/10.1021/cm047897+.

[27] F.Q. Liu, G.H. Li, S.W. Luo, W.H. Li, Z.G. Huang, W. Li, F. Su, C.Q. Li, Z.B. Ding, Q. Jiang, Ultrafast Carbon Dioxide Sorption Kinetics Using Morphology-Controllable Lithium Zirconate, ACS Appl Mater Interfaces 11 (2019) 691–698. https://doi.org/10.1021/acsami.8b16463.

[28] D. Peltzer, L.A. Salazar Hoyos, B. Faroldi, J. Múnera, L. Cornaglia, Comparative study of lithium-based CO_2 sorbents at high temperature: Experimental and modeling kinetic analysis of the carbonation reaction, J Environ Chem Eng 8 (2020) 104173. https://doi.org/10.1016/j.jece.2020.104173.

[29] Y. Hu, Q. Xu, X. Zou, X. Wang, H. Cheng, X. Zou, X. Lu, MxOy (M = Mg, Zr, La, Ce) modified Ni/CaO dual functional materials for combined CO_2 capture and hydrogenation, Int J Hydrogen Energy 48 (2023) 24871–24883. https://doi.org/10.1016/J.IJHYDENE.2022.11.045.

[30] M. Amiri, S. Shahhosseini, A. Ghaemi, Optimization of CO_2 Capture Process from Simulated Flue Gas by Dry Regenerable Alkali Metal Carbonate Based Adsorbent Using Response Surface Methodology, Energy and Fuels 31 (2017) 5286–5296. https://doi.org/10.1021/acs.energyfuels.6b03303.

[31] Z. Lin, J. Wei, CO_2 adsorption on activated carbon/SBA-15 with TETA/TEPA modification, Key Eng Mater 735 KEM (2017) 164–167. https://doi.org/10.4028/www.scientific.net/KEM.735.164.

[32] X. Zhang, S. Zhang, H. Yang, Y. Feng, Y. Chen, X. Wang, H. Chen, Nitrogen enriched biochar modified by high temperature CO_2-ammonia treatment: Characterization and adsorption of CO_2, Chemical Engineering Journal 257 (2014) 20–27. https://doi.org/10.1016/j.cej.2014.07.024.

[33] W. Xie, M. Yu, R. Wang, CO_2 capture behaviors of amine-modified resorcinol-based carbon aerogels adsorbents, Aerosol Air Qual Res 17 (2017) 2715–2725. https://doi.org/10.4209/aaqr.2016.12.0597.

[34] R.R. Solís, M. del C. González, G. Blázquez, M. Calero, M.Á. Martín-Lara, Activated char from the co-pyrolysis of polystyrene and olive stone mixtures for the adsorption of CO_2, J Environ Chem Eng 11 (2023) 111370. https://doi.org/10.1016/J.JECE.2023.111370.

[35] C.H. Pimentel, L. Díaz-Fernández, D. Gómez-Díaz, M.S. Freire, J. González-Álvarez, Separation of CO_2 using biochar and KOH and $ZnCl_2$ activated carbons derived from

pine sawdust, J Environ Chem Eng 11 (2023) 111378. https://doi.org/10.1016/J.JECE.2023.111378.

[36] N. Noorani, B. Barzegar, A. Mehrdad, H. Aghdasinia, S.J. Peighambardoust, H. Kazemian, CO_2 capture in activated pyrolytic coke/metal oxide nanoparticle composites, Colloids Surf A Physicochem Eng Asp 679 (2023) 132554. https://doi.org/10.1016/J.COLSURFA.2023.132554.

[37] X. Zhao, Y. Nie, X. Yi, S. Yu, J. Zhang, X. Liu, Z. Yuan, S. Liu, J. Zhang, G. Dou, M. Wang, Design of carbonized unidirectional polyimide aerogel for CO_2 capture: Effect of pore morphology/topology on CO_2 capture, Journal of Industrial and Engineering Chemistry 128 (2023) 326–334. https://doi.org/10.1016/J.JIEC.2023.07.066.

[38] C. Minh city, L. Trung ward, T. Duc city, H. Chi Minh city, T. Thanh Nguyen, P. Toan Phan, T. Nguyen Thi, Q. Anh Nguyen Thi, T. Thich Le, S. Padungthon, N. Huy Nguyen, Ung Van Khiem street, Dong Xuyen district, Long Xuyen city, An Giang prov, International Journal 18 (2024) 71–77.

[39] C. Wu, J. Liu, Y. Wang, Y. Zhao, G. Li, G. Zhang, KCl-assisted activation of macadamia nutshell-derived carbon: Unveiling enhanced pore structure, adsorption and supercapacitor performance, Sep Purif Technol 329 (2024) 125188. https://doi.org/10.1016/J.SEPPUR.2023.125188.

[40] O.F. Cruz, J. Serafin, F.Z. Azar, M.E. Casco, J. Silvestre-Albero, D. Hotza, C.R. Rambo, Microwave-Assisted hydrothermal carbonization and characterization of Amazonian biomass as an activated carbon for methane adsorption, Fuel 358 (2024) 130329. https://doi.org/10.1016/J.FUEL.2023.130329.

[41] M. Gorbounov, E. Diaz-Vasseur, D. Danaci, S. Masoudi Soltani, Chemical activation of porous carbon extracted from biomass combustion bottom ash for CO_2 adsorption,

Carbon Capture Science & Technology 10 (2024) 100151. https://doi.org/10.1016/J.CCST.2023.100151.

[42] H. Weldekidan, H. Patel, A. Mohanty, M. Misra, Synthesis of porous and activated carbon from lemon peel waste for CO_2 adsorption, Carbon Capture Science & Technology 10 (2024) 100149. https://doi.org/10.1016/J.CCST.2023.100149.

[43] W. Zhu, Y. Wang, F. Yao, X. Wang, H. Zheng, G. Ye, H. Cheng, J. Wu, H. Huang, D. Ye, One-pot synthesis of N-doped petroleum coke-based microporous carbon for high-performance CO_2 adsorption and supercapacitors, Journal of Environmental Sciences 139 (2024) 93–104. https://doi.org/10.1016/J.JES.2023.02.008.

[44] A. Rehman, Y.J. Heo, G. Nazir, S.J. Park, Solvent-free, one-pot synthesis of nitrogen-tailored alkali-activated microporous carbons with an efficient CO_2 adsorption, Carbon N Y 172 (2021) 71–82. https://doi.org/10.1016/J.CARBON.2020.09.088.

[45] D.A. Khuong, H.N. Nguyen, T. Tsubota, Activated carbon produced from bamboo and solid residue by CO_2 activation utilized as CO_2 adsorbents, Biomass Bioenergy 148 (2021) 106039. https://doi.org/10.1016/J.BIOMBIOE.2021.106039.

[46] M. Balsamo, T. Budinova, A. Erto, A. Lancia, B. Petrova, N. Petrov, B. Tsyntsarski, CO_2 adsorption onto synthetic activated carbon: Kinetic, thermodynamic and regeneration studies, Sep Purif Technol 116 (2013) 214–221. https://doi.org/10.1016/J.SEPPUR.2013.05.041.

[47] A. Bakhtyari, M. Mofarahi, C.-H. Lee, CO_2 adsorption by conventional and nanosized zeolites, Elsevier Inc., 2020. https://doi.org/10.1016/b978-0-12-819657-1.00009-8.

[48] H. June Choi, D. Jo, S. Bong Hong, Effect of framework Si/Al ratio on the adsorption mechanism of CO_2 on small-pore zeolites: II. Merlinoite, Chemical Engineering Journal 446 (2022) 137100. https://doi.org/10.1016/J.CEJ.2022.137100.

[49] H. Tanaka, Y. Sakai, R. Hino, Formation of Na-A and -X zeolites from waste solutions in conversion of coal fly ash to zeolites, Mater Res Bull 37 (2002) 1873–1884. https://doi.org/10.1016/S0025-5408(02)00861-9.

[50] M. Kim, J.W. Lee, S. Kim, Y.T. Kang, CO_2 adsorption on zeolite 13X modified with hydrophobic octadecyltrimethoxysilane for indoor application, J Clean Prod 337 (2022) 130597. https://doi.org/10.1016/J.JCLEPRO.2022.130597.

[51] X. Chen, J. Zhou, J. Wei, X. Cui, C. Wan, M. Liu, S. Bai, J. Sun, J. Wang, Performance evaluation of bimetallic ion exchanged clinoptilolite for potential equilibrium and kinetic adsorption separations of CO_2 from CO_2/CH_4 mixture, Sep Purif Technol 331 (2024) 125563. https://doi.org/10.1016/J.SEPPUR.2023.125563.

[52] J.A. Cecilia, E. Vilarrasa-García, R. Morales-Ospino, E. Finocchio, G. Busca, K. Sapag, J. Villarroel-Rocha, M. Bastos-Neto, D.C.S. Azevedo, E. Rodríguez-Castellón, Kaolinite-based zeolites synthesis and their application in CO_2 capture processes, Fuel 320 (2022) 123953. https://doi.org/10.1016/J.FUEL.2022.123953.

[53] C. Quan, X. Jia, K. Zhang, Y. Zhang, S.R. Naqvi, N.A.S. Amin, N. Gao, Amine-impregnated silica zeolite from microalgae ash at different calcination temperatures for CO_2 capture, Int J Energy Res 46 (2022) 1220–1233. https://doi.org/10.1002/ER.7241.

[54] W. Cao, Y. Huang, D. Li, W. Chen, Z. Qie, X. Pi, Q. Du, X. Lai, Y. Li, N/S co-doped microporous zeolite-templated carbon for efficient CO_2 adsorption and separation, Journal of the Energy Institute 106 (2023) 101159. https://doi.org/10.1016/J.JOEI.2022.101159.

[55] E. Papa, M. Minelli, M.C. Marchioni, E. Landi, F. Miccio, A. Natali Murri, P. Benito, A. Vaccari, V. Medri, Metakaolin-based geopolymer – Zeolite NaA composites as CO_2 adsorbents, Appl Clay Sci 237 (2023) 106900. https://doi.org/10.1016/J.CLAY.2023.106900.

[56] D.G. Boer, Z. Asgar Pour, S. Poli, J. Langerak, B. Bakker, P.P. Pescarmona, ZSM-5/Silicalite-1 core-shell beads as CO_2 adsorbents with increased hydrophobicity, Mater Today Chem 32 (2023) 101621. https://doi.org/10.1016/J.MTCHEM.2023.101621.

[57] Z. Peng, Z. Liu, Y. Gao, J. Liu, D. Wang, H. Liu, Y. Zhang, L. Li, Synthesis and CO_2 adsorption performance of high Si/Al ratio DDR zeolites prepared from silica fume, J Environ Chem Eng 11 (2023) 110837. https://doi.org/10.1016/J.JECE.2023.110837.

[58] Y. Jin, Q. Xu, F. Zheng, J. Lu, Enhancement in CO_2 adsorption by zeolite synthesized from co-combustion ash of coal and rice husk modified with lithium ion, Journal of the Energy Institute 110 (2023) 101348. https://doi.org/10.1016/J.JOEI.2023.101348.

[59] A. Jalali, A. Ahmadpour, M. Ghahramaninezhad, E. Yasari, Hierarchical nanocomposites derived from UiO-66 framework and zeolite for enhanced CO_2 adsorption, J Environ Chem Eng 11 (2023) 111294. https://doi.org/10.1016/J.JECE.2023.111294.

[60] J. Bin Lee, I. Ahmed, G. Lee, T.W. Kim, C.U. Kim, S.H. Jhung, Synthesis of SSZ-13 zeolites using calcined rice husk as silica source for propylene production from ethylene and carbon dioxide adsorption, Journal of Industrial and Engineering Chemistry 128 (2023) 443–449. https://doi.org/10.1016/J.JIEC.2023.08.008.

[61] S.K. Wahono, J. Stalin, J. Addai-Mensah, W. Skinner, A. Vinu, K. Vasilev, Physico-chemical modification of natural mordenite-clinoptilolite zeolites and their enhanced

CO_2 adsorption capacity, Microporous and Mesoporous Materials 294 (2020) 109871. https://doi.org/10.1016/J.MICROMESO.2019.109871.

[62] H. Cheng, H. Song, S. Toan, B. Wang, K.A.M. Gasem, M. Fan, F. Cheng, Experimental investigation of CO_2 adsorption and desorption on multi-type amines loaded HZSM-5 zeolites, Chemical Engineering Journal 406 (2021) 126882. https://doi.org/10.1016/J.CEJ.2020.126882.

[63] A.A. Dabbawala, I. Ismail, B. V. Vaithilingam, K. Polychronopoulou, G. Singaravel, S. Morin, M. Berthod, Y. Al Wahedi, Synthesis of hierarchical porous Zeolite-Y for enhanced CO2 capture, Microporous and Mesoporous Materials 303 (2020) 110261. https://doi.org/10.1016/J.MICROMESO.2020.110261.

[64] S. Karka, S. Kodukula, S. V. Nandury, U. Pal, Polyethylenimine-Modified Zeolite 13X for CO_2 Capture: Adsorption and Kinetic Studies, ACS Omega 4 (2019) 16441–16449. https://doi.org/10.1021/ACSOMEGA.9B02047/ASSET/IMAGES/MEDIUM/AO9B02047_M024.GIF.

[65] R. Aniruddha, I. Sreedhar, B.M. Reddy, MOFs in carbon capture-past, present and future, Journal of CO_2 Utilization 42 (2020) 101297. https://doi.org/10.1016/j.jcou.2020.101297.

[66] Q. Gao, L. Bai, X. Zhang, P. Wang, P. Li, Y. Zeng, R. Zou, Y. Zhao, Synthesis of Microporous Nitrogen-Rich Covalent-Organic Framework and Its Application in CO_2 Capture, Chin J Chem 33 (2015) 90–94. https://doi.org/10.1002/cjoc.201400550.

[67] A. Rehman, S. Farrukh, A. Hussain, X. Fan, E. Pervaiz, Adsorption of CO_2 on amine-functionalized green metal-organic framework: an interaction between amine and CO_2 molecules, Environmental Science and Pollution Research 26 (2019) 36214–36225. https://doi.org/10.1007/s11356-019-06717-3.

[68] S. Shin, D.K. Yoo, Y.S. Bae, S.H. Jhung, Polyvinylamine-loaded metal–organic framework MIL-101 for effective and selective CO_2 adsorption under atmospheric or lower pressure, Chemical Engineering Journal 389 (2020). https://doi.org/10.1016/j.cej.2019.123429.

[69] C. Choi, R.L. Kadam, S. Gaikwad, K.S. Hwang, S. Han, Metal organic frameworks immobilized polyacrylonitrile fiber mats with polyethyleneimine impregnation for CO_2 capture, Microporous and Mesoporous Materials 296 (2020). https://doi.org/10.1016/j.micromeso.2020.110006.

[70] L. Xu, C.Y. Xing, D. Ke, L. Chen, Z.J. Qiu, S.L. Zeng, B.J. Li, S. Zhang, Amino-Functionalized β-Cyclodextrin to Construct Green Metal-Organic Framework Materials for CO_2 Capture, ACS Appl Mater Interfaces 12 (2020) 3032–3041. https://doi.org/10.1021/acsami.9b20003.

[71] S. Gaikwad, S.J. Kim, S. Han, CO_2 capture using amine-functionalized bimetallic MIL-101 MOFs and their stability on exposure to humid air and acid gases, Microporous and Mesoporous Materials 277 (2019) 253–260. https://doi.org/10.1016/j.micromeso.2018.11.001.

[72] S. Lawson, C. Griffin, K. Rapp, A.A. Rownaghi, F. Rezaei, Amine-Functionalized MIL-101 Monoliths for CO_2 Removal from Enclosed Environments, Energy and Fuels 33 (2019) 2399–2407. https://doi.org/10.1021/acs.energyfuels.8b04508.

[73] A. Koutsianos, E. Kazimierska, A.R. Barron, M. Taddei, E. Andreoli, A new approach to enhancing the CO_2 capture performance of defective UiO-66: Via post-synthetic defect exchange, Dalton Transactions 48 (2019) 3349–3359. https://doi.org/10.1039/c9dt00154a.

[74] T. He, Y. Xiao, Q. Zhao, M. Zhou, G. He, Ultramicroporous Metal-Organic Framework Qc-5-Cu for Highly Selective Adsorption of CO_2 from C_2H_4 Stream, Ind Eng Chem Res 59 (2020) 3153–3161. https://doi.org/10.1021/acs.iecr.9b05665.

[75] H.G. Zhen, H. Mao, I.U. Haq, S.H. Li, A. Ahmad, Z.P. Zhao, In-situ SIFSIX-3-Cu growth into melamine formaldehyde sponge monolith for CO_2 efficient capture, Sep Purif Technol 233 (2020). https://doi.org/10.1016/j.seppur.2019.116042.

[76] Z.S. Wang, M. Li, Y.L. Peng, Z. Zhang, W. Chen, X.C. Huang, An Ultrastable Metal Azolate Framework with Binding Pockets for Optimal Carbon Dioxide Capture, Angewandte Chemie - International Edition 58 (2019) 16071–16076. https://doi.org/10.1002/anie.201909046.

[77] Y. Chen, H. Wu, D. Lv, W. Yang, Z. Qiao, Z. Li, Q. Xia, An Ultramicroporous Nickel-Based Metal-Organic Framework for Adsorption Separation of CO_2 over N_2 or CH_4, Energy and Fuels 32 (2018) 8676–8682. https://doi.org/10.1021/acs.energyfuels.8b02287.

[78] D.K. Yoo, T.U. Yoon, Y.S. Bae, S.H. Jhung, Metal-organic framework MIL-101 loaded with polymethacrylamide with or without further reduction: Effective and selective CO_2 adsorption with amino or amide functionality, Chemical Engineering Journal 380 (2020). https://doi.org/10.1016/j.cej.2019.122496.

[79] M. Ghahramaninezhad, F. Mohajer, M. Niknam Shahrak, Improved CO_2 capture performances of ZIF-90 through sequential reduction and lithiation reactions to form a hard/hard structure, Front Chem Sci Eng 14 (2020) 425–435. https://doi.org/10.1007/s11705-019-1873-5.

[80] K. Pirzadeh, K. Esfandiari, A.A. Ghoreyshi, M. Rahimnejad, CO_2 and N_2 adsorption and separation using aminated UiO-66 and $Cu_3(BTC)_2$: A comparative study, Korean Journal

of Chemical Engineering 37 (2020) 513–524. https://doi.org/10.1007/s11814-019-0433-5.

[81] H. Molavi, A. Eskandari, A. Shojaei, S.A. Mousavi, Enhancing CO_2/N_2 adsorption selectivity via post-synthetic modification of NH2-UiO-66(Zr), Microporous and Mesoporous Materials 257 (2018) 193–201. https://doi.org/10.1016/j.micromeso.2017.08.043.

[82] S. Ullah, M.A. Bustam, A.G. Al-Sehemi, M.A. Assiri, F.A. Abdul Kareem, A. Mukhtar, M. Ayoub, G. Gonfa, Influence of post-synthetic graphene oxide (GO) functionalization on the selective CO_2/CH_4 adsorption behavior of MOF-200 at different temperatures; an experimental and adsorption isotherms study, Microporous and Mesoporous Materials 296 (2020) 110002. https://doi.org/10.1016/j.micromeso.2020.110002.

[83] H.N. Abdelhamid, Zinc hydroxide nitrate nanosheets conversion into hierarchical zeolitic imidazolate frameworks nanocomposite and their application for CO_2 sorption, Mater Today Chem 15 (2020). https://doi.org/10.1016/j.mtchem.2019.100222.

[84] X. Mu, S. Liu, Y. Chen, U.K. Cheang, M.W. George, T. Wu, Mechanistic and Experimental Study of the Formation of MoS2/HKUST-1 Core-Shell Composites on MoS2 Quantum Dots with an Enhanced CO2 Adsorption Capacity, Ind Eng Chem Res 59 (2020) 5808–5817. https://doi.org/10.1021/acs.iecr.9b06729.

[85] D. Alvarado-Alvarado, J.H. González-Estefan, J.G. Flores, J.R. Álvarez, J. Aguilar-Pliego, A. Islas-Jácome, G. Chastanet, E. González-Zamora, H.A. Lara-García, B. Alcántar-Vázquez, M. Gonidec, I.A. Ibarra, Water Adsorption Properties of $Fe(pz)[Pt(CN)_4]$ and the Capture of CO_2 and CO, Organometallics 39 (2020) 949–955. https://doi.org/10.1021/acs.organomet.9b00711.

[86] G. Han, Q. Qian, K. Mizrahi Rodriguez, Z.P. Smith, Hydrothermal Synthesis of Sub-20 nm Amine-Functionalized MIL-101(Cr) Nanoparticles with High Surface Area and Enhanced CO_2 Uptake, Ind Eng Chem Res 59 (2020) 7888–7900. https://doi.org/10.1021/acs.iecr.0c00535.

[87] Z. Hu, A. Nalaparaju, Y. Peng, J. Jiang, D. Zhao, Modulated Hydrothermal Synthesis of UiO-66(Hf)-Type Metal-Organic Frameworks for Optimal Carbon Dioxide Separation, Inorg Chem 55 (2016) 1134–1141. https://doi.org/10.1021/acs.inorgchem.5b02312.

[88] Z. Bian, X. Zhu, T. Jin, J. Gao, J. Hu, H. Liu, Ionic liquid-assisted growth of $Cu_3(BTC)_2$ nanocrystals on graphene oxide sheets: Towards both high capacity and high rate for CO_2 adsorption, Microporous and Mesoporous Materials 200 (2014) 159–164. https://doi.org/10.1016/j.micromeso.2014.08.012.

[89] W.W. Lestari, A.H. Wibowo, S. Astuti, Irwinsyah, A.Z. Pamungkas, Y.K. Krisnandi, Fabrication of hybrid coating material of polypropylene itaconate containing MOF-5 for CO_2 capture, Prog Org Coat 115 (2018) 49–55. https://doi.org/10.1016/j.porgcoat.2017.11.006.

[90] K.M. Elsabawy, A.M. Fallatah, Synthesis of newly wings like structure non-crystalline Ni^{++}-1,3,5-tribenzyl-1,3,5-triazine-2,4,6-(1H,3H,5H)-trione coordinated MOFs for CO_2-Capture, J Mol Struct 1177 (2019) 255–259. https://doi.org/10.1016/j.molstruc.2018.09.069.

[91] Y. Zhang, Y. Zhang, X. Wang, J. Yu, B. Ding, Ultrahigh Metal-Organic Framework Loading and Flexible Nanofibrous Membranes for Efficient CO_2 Capture with Long-Term, Ultrastable Recyclability, ACS Appl Mater Interfaces 10 (2018) 34802–34810. https://doi.org/10.1021/acsami.8b14197.

[92] T.A. Mulyati, R. Ediati, A. Rosyidah, Influence of solvothermal temperatures and times on crystallinity and morphology of MOF-5, Indonesian Journal of Chemistry 15 (2015) 101–107. https://doi.org/10.22146/ijc.21202.

[93] L.S. Lai, Y.F. Yeong, K.K. Lau, A.M. Shariff, Effect of Synthesis Parameters on the Formation of ZIF-8 under Microwave-assisted Solvothermal, Procedia Eng 148 (2016) 35–42. https://doi.org/10.1016/j.proeng.2016.06.481.

[94] J. Qian, F. Sun, L. Qin, Hydrothermal synthesis of zeolitic imidazolate framework-67 (ZIF-67) nanocrystals, Mater Lett 82 (2012) 220–223. https://doi.org/10.1016/j.matlet.2012.05.077.

[95] F. Zhang, T. Zhang, X. Zou, X. Liang, G. Zhu, F. Qu, Electrochemical synthesis of metal organic framework films with proton conductive property, Solid State Ion 301 (2017) 125–132. https://doi.org/10.1016/j.ssi.2017.01.022.

[96] J. Klinowski, F.A. Almeida Paz, P. Silva, J. Rocha, Microwave-assisted synthesis of metal-organic frameworks, Dalton Transactions 40 (2011) 321–330. https://doi.org/10.1039/c0dt00708k.

[97] N. Abdollahi, M.Y. Masoomi, A. Morsali, P.C. Junk, J. Wang, Sonochemical synthesis and structural characterization of a new Zn(II) nanoplate metal–organic framework with removal efficiency of Sudan red and Congo red, Ultrason Sonochem 45 (2018) 50–56. https://doi.org/10.1016/j.ultsonch.2018.03.001.

[98] W. Zhou, R. Apkarian, Z.L. Wang, D. Joy, Fundamentals of scanning electron microscopy (SEM), Scanning Microscopy for Nanotechnology: Techniques and Applications (2007) 1–40. https://doi.org/10.1007/978-0-387-39620-0_1/COVER.

[99] A.A. Bunaciu, E. gabriela Udriştioiu, H.Y. Aboul-Enein, X-Ray Diffraction: Instrumentation and Applications, Crit Rev Anal Chem 45 (2015) 289–299. https://doi.org/10.1080/10408347.2014.949616.

[100] P. Schneider, Adsorption isotherms of microporous-mesoporous solids revisited, Appl Catal A Gen 129 (1995) 157–165. https://doi.org/10.1016/0926-860X(95)00110-7.

[101] A.W. Coats, J.P. Redfern, Thermogravimetric analysis. A review, Analyst 88 (1963) 906–924. https://doi.org/10.1039/AN9638800906.

[102] L. Wang, G. Wang, X. Li, Y. Liu, Synthesis and characterization of Y-type zeolite from coal fly ash by hydrothermal method, Chinese Journal of Environmental Engineering 12 (2018) 618–624. https://doi.org/10.12030/j.cjee.201706100.

[103] J. Madhu, V. Madurai Ramakrishnan, P. Palanichamy, A. Santhanam, M. Natarajan, P. Ponnaian, K. Brindhadevi, A. Pugazhendhi, D. Velauthapillai, Rubik's cube shaped organic template free hydrothermal synthesis and characterization of zeolite NaA for CO_2 adsorption, Fuel 317 (2022) 123492. https://doi.org/10.1016/J.FUEL.2022.123492.

[104] J. Luo, H. Zhang, J. Yang, Hydrothermal Synthesis of Sodalite on Alkali-Activated Coal Fly Ash for Removal of Lead Ions, Procedia Environ Sci 31 (2016) 605–614. https://doi.org/10.1016/j.proenv.2016.02.105.

[105] C. Li, X. Li, C. Li, L. Li, Synthesis, Characterization of NaA Zeolite from Blast Furnace Slag (BFS) via Alkaline Fusion and Hydrothermal Treatment, Journal Wuhan University of Technology, Materials Science Edition 38 (2023) 401–407. https://doi.org/10.1007/S11595-023-2710-8/METRICS.

[106] T.F. de Aquino, S.T. Estevam, V.O. Viola, C.R.M. Marques, F.L. Zancan, L.B. Vasconcelos, H.G. Riella, M.J.R. Pires, R. Morales-Ospino, A.E.B. Torres, M. Bastos-

Neto, C.L. Cavalcante, CO2 adsorption capacity of zeolites synthesized from coal fly ashes, Fuel 276 (2020) 118143. https://doi.org/10.1016/j.fuel.2020.118143.

[107] Y.R. Lee, M.S. Jang, H.Y. Cho, H.J. Kwon, S. Kim, W.S. Ahn, ZIF-8: A comparison of synthesis methods, Chemical Engineering Journal 271 (2015) 276–280. https://doi.org/10.1016/j.cej.2015.02.094.

[108] T. Zhao, Y. Hui, Niamatullah, Z. Li, Controllable preparation of ZIF-67 derived catalyst for CO_2 methanation, Molecular Catalysis 474 (2019) 110421. https://doi.org/10.1016/j.mcat.2019.110421.

[109] K. Zhou, B. Mousavi, Z. Luo, S. Phatanasri, S. Chaemchuen, F. Verpoort, Characterization and properties of Zn/Co zeolitic imidazolate frameworks vs. ZIF-8 and ZIF-67, J Mater Chem A Mater 5 (2017) 952–957. https://doi.org/10.1039/C6TA07860E.

[110] L.S. Lai, Y.F. Yeong, N.C. Ani, K.K. Lau, A.M. Shariff, Effect of synthesis parameters on the formation of zeolitic imidazolate framework 8 (ZIF-8) nanoparticles for CO_2 adsorption, Particulate Science and Technology 32 (2014) 520–528. https://doi.org/10.1080/02726351.2014.920445.

[111] S. Li, S. Jia, T. Nagasaka, H. Bai, L. Yang, CO_2 Adsorption Properties of Amine-Modified Zeolites Synthesized Using Different Types of Solid Waste, Sustainability (Switzerland) 15 (2023) 10144. https://doi.org/10.3390/SU151310144/S1.

[112] A. Henrique, M. Karimi, J.A.C. Silva, A.E. Rodrigues, Analyses of Adsorption Behavior of CO_2, CH_4, and N_2 on Different Types of BETA Zeolites, Chem Eng Technol 42 (2019) 327–342. https://doi.org/10.1002/CEAT.201800386.

[113] D.S. Dao, H. Yamada, K. Yogo, L.T. Tong, H. Kiem, V. Hanoi, Response Surface Optimization of Impregnation of Blended Amines into Mesoporous Silica for High-Performance CO_2 Capture, Energy and Fuels 29 (2015) 985–992. https://doi.org/10.1021/EF502656T.

[114] H. Yan, G. Zhang, J. Liu, G. Li, Y. Wang, Highly efficient CO_2 adsorption by imidazole and tetraethylenepentamine functional sorbents: Optimization and analysis using response surface methodology, J Environ Chem Eng 9 (2021) 105639. https://doi.org/10.1016/J.JECE.2021.105639.

[115] P.A. Alaba, Y.M. Sani, I.Y. Mohammed, Y.A. Abakr, W.M.A. Wan Daud, Synthesis of hierarchical nanoporous HY zeolites from activated kaolin, a central composite design optimization study, Advanced Powder Technology 28 (2017) 1399–1410. https://doi.org/10.1016/j.apt.2017.03.008.

[116] A.Y. Aydar, Utilization of Response Surface Methodology in Optimization of Extraction of Plant Materials, Statistical Approaches With Emphasis on Design of Experiments Applied to Chemical Processes (2018). https://doi.org/10.5772/INTECHOPEN.73690.

[117] H. Yan, G. Zhang, J. Liu, G. Li, Y. Wang, Highly efficient CO_2 adsorption by imidazole and tetraethylenepentamine functional sorbents: Optimization and analysis using response surface methodology, J Environ Chem Eng 9 (2021). https://doi.org/10.1016/j.jece.2021.105639.

[118] K. Hossein, S. Shahrokh, A. Mohsen, Optimization of CO_2 capture process using dry sodium-based sorbents, Iranian Journal of Chemistry and Chemical Engineering 40 (2021) 1179–1194. https://doi.org/10.30492/IJCCE.2020.109081.3616.

[119] H.K. Lim, U.F. Md Ali, R. Ahmad, M.K. Aroua, Adsorption of carbon dioxide (CO_2) by activated carbon derived from waste coffee grounds, IOP Conf Ser Earth Environ Sci 765 (2021). https://doi.org/10.1088/1755-1315/765/1/012034.

[120] B. Sreenivasulu, I. Sreedhar, A.S. Singh, A. Venugopal, Calcination Thermokinetics of Carbon Capture Using Coal Fly Ash Stabilized Sorbent, Energy and Fuels 32 (2018) 3716–3725. https://doi.org/10.1021/acs.energyfuels.7b04147.

[121] B. Sreenivasulu, I. Sreedhar, B.M. Reddy, K. V. Raghavan, Stability and carbon capture enhancement by coal-fly-ash-doped sorbents at a high temperature, Energy and Fuels 31 (2017) 785–794. https://doi.org/10.1021/acs.energyfuels.6b02721.

[122] L.H. De Oliveira, M. V. Pereira, J.G. Meneguin, M.A.S.D. De Barros, J.F. Do Nascimento, P.A. Arroyo, Influence of regeneration conditions on cyclic CO_2 adsorption on NaA zeolite at high pressures, Journal of CO_2 Utilization 67 (2023) 102296. https://doi.org/10.1016/J.JCOU.2022.102296.

[123] R. Ezzati, Derivation of Pseudo-First-Order, Pseudo-Second-Order and Modified Pseudo-First-Order rate equations from Langmuir and Freundlich isotherms for adsorption, Chemical Engineering Journal 392 (2020) 123705. https://doi.org/10.1016/J.CEJ.2019.123705.

[124] K. Yu, W.A. Mitch, N. Dai, Nitrosamines and Nitramines in Amine-Based Carbon Dioxide Capture Systems: Fundamentals, Engineering Implications, and Knowledge Gaps, Environ Sci Technol 51 (2017) 11522–11536. https://doi.org/10.1021/ACS.EST.7B02597/ASSET/IMAGES/LARGE/ES-2017-02597D_0002.JPEG.

[125] L. Keshavarz, M.R. Ghaani, J.M.D. MacElroy, N.J. English, A comprehensive review on the application of aerogels in CO_2-adsorption: Materials and characterisation,

Chemical Engineering Journal 412 (2021) 128604. https://doi.org/10.1016/J.CEJ.2021.128604.

[126] J.G.M.S. Monteiro, H. Knuutila, N.J.M.C. Penders-van Elk, G. Versteeg, H.F. Svendsen, Kinetics of CO_2 absorption by aqueous N,N-diethylethanolamine solutions: Literature review, experimental results and modelling, Chem Eng Sci 127 (2015) 1–12. https://doi.org/10.1016/J.CES.2014.12.061.

[127] G.F. Versteeg, L.A.J. Van Dijck, W.P.M. Van Swaaij, On the kinetics between CO_2 and alkanolamines both in aqueous and non-aqueous solutions. An Overview, Chem Eng Commun 144 (1996) 133–158. https://doi.org/10.1080/00986449608936450.

[128] E.D. Revellame, D.L. Fortela, W. Sharp, R. Hernandez, M.E. Zappi, Adsorption kinetic modeling using pseudo-first order and pseudo-second order rate laws: A review, Clean Eng Technol 1 (2020) 100032. https://doi.org/10.1016/J.CLET.2020.100032.

[129] J.P. Simonin, On the comparison of pseudo-first order and pseudo-second order rate laws in the modeling of adsorption kinetics, Chemical Engineering Journal 300 (2016) 254–263. https://doi.org/10.1016/J.CEJ.2016.04.079.

[130] Y.S. Ho, Review of second-order models for adsorption systems, J Hazard Mater 136 (2006) 681–689. https://doi.org/10.1016/J.JHAZMAT.2005.12.043.

[131] A. Hartono, E.F. da Silva, H.F. Svendsen, Kinetics of carbon dioxide absorption in aqueous solution of diethylenetriamine (DETA), Chem Eng Sci 64 (2009) 3205–3213. https://doi.org/10.1016/J.CES.2009.04.018.

[132] M.A. Hubbe, S. Azizian, S. Douven, Implications of Apparent Pseudo-Second-Order Adsorption Kinetics onto Cellulosic Materials: A Review, (n.d.).

[133] J. Wang, X. Guo, Rethinking of the intraparticle diffusion adsorption kinetics model: Interpretation, solving methods and applications, Chemosphere 309 (2022) 136732. https://doi.org/10.1016/J.CHEMOSPHERE.2022.136732.

[134] Y. Deng, J.P.K. Seville, S.D. Bell, A. Ingram, H. Zhang, N. Sweygers, R. Dewil, J. Baeyens, L. Appels, Reviewing Fundamental CO2 Adsorption Characteristics of Zeolite and Activated Carbon by In-situ Measurements With Radioactively Labelled CO_2, Separation & Purification Reviews 51 (2022) 318–329. https://doi.org/10.1080/15422119.2021.1934699.

[135] M. Abbas, S. Kaddour, M. Trari, Kinetic and equilibrium studies of cobalt adsorption on apricot stone activated carbon, Journal of Industrial and Engineering Chemistry 20 (2014) 745–751. https://doi.org/10.1016/J.JIEC.2013.06.030.

[136] Y. Zhu, J. Hu, J. Wang, Removal of Co^{2+} from radioactive wastewater by polyvinyl alcohol (PVA)/chitosan magnetic composite, Progress in Nuclear Energy 71 (2014) 172–178. https://doi.org/10.1016/J.PNUCENE.2013.12.005.

[137] M.S. Shafeeyan, W.M.A. Wan Daud, A. Shamiri, A review of mathematical modeling of fixed-bed columns for carbon dioxide adsorption, Chemical Engineering Research and Design 92 (2014) 961–988. https://doi.org/10.1016/J.CHERD.2013.08.018.

[138] K. Shirzad, C. Viney, A critical review on applications of the Avrami equation beyond materials science, J R Soc Interface 20 (2023). https://doi.org/10.1098/RSIF.2023.0242.

[139] F. Yang, X. Zhu, J. Wu, R. Wang, T. Ge, Kinetics and mechanism analysis of CO_2 adsorption on LiX@ZIF-8 with core shell structure, Powder Technol 399 (2022) 117090. https://doi.org/10.1016/J.POWTEC.2021.117090.

[140] B. Guo, J. Zhang, Y. Wang, X. Qiao, J. Xiang, Y. Jin, Study on CO_2 adsorption capacity and kinetic mechanism of CO_2 adsorbent prepared from fly ash, Energy 263 (2023) 125764. https://doi.org/10.1016/J.ENERGY.2022.125764.

[141] F. Gong, Z. Huang, X. Wei, S. Liu, J. Lu, J. Ding, W. Wang, MgO promoted by Fe_2O_3 and nitrate molten salt for fast and enhanced CO_2 capture: Experimental and DFT investigation, Sep Purif Technol 307 (2023) 122766. https://doi.org/10.1016/J.SEPPUR.2022.122766.

[142] J. Zhang, S. Guo, S. Wang, X. Tan, Separation and capture of CO_2 from ambient air using TEPA-functionalized PAN hollow fibers, Sep Purif Technol 324 (2023) 124635. https://doi.org/10.1016/J.SEPPUR.2023.124635.

[143] C. Aharoni, F.C. Tompkins, Kinetics of Adsorption and Desorption and the Elovich Equation, Advances in Catalysis 21 (1970) 1–49. https://doi.org/10.1016/S0360-0564(08)60563-5.

[144] G. Skodras, I. Diamantopoulou, G. Pantoleontos, G.P. Sakellaropoulos, Kinetic studies of elemental mercury adsorption in activated carbon fixed bed reactor, J Hazard Mater 158 (2008) 1–13. https://doi.org/10.1016/J.JHAZMAT.2008.01.073.

[145] C. Goel, S. Mohan, P. Dinesha, CO_2 capture by adsorption on biomass-derived activated char: A review, Science of The Total Environment 798 (2021) 149296. https://doi.org/10.1016/J.SCITOTENV.2021.149296.

[146] E.I. Ugwu, A. Othmani, C.C. Nnaji, A review on zeolites as cost-effective adsorbents for removal of heavy metals from aqueous environment, International Journal of Environmental Science and Technology 2021 19:8 19 (2021) 8061–8084. https://doi.org/10.1007/S13762-021-03560-3.

[147] J.P. Nicot, I.J. Duncan, Common attributes of hydraulically fractured oil and gas production and CO_2 geological sequestration, Greenhouse Gases: Science and Technology 2 (2012) 352–368. https://doi.org/10.1002/ghg.1300.

[148] M. Mukherjee, S. Misra, A. Gupta, Control of pore-size distribution on CO_2 adsorption volume and kinetics in Gondwana coals: Implications for shallow-depth CO_2 sequestration potential, J Nat Gas Sci Eng 89 (2021) 103901. https://doi.org/10.1016/j.jngse.2021.103901.

[149] C. Dhoke, S. Cloete, S. Krishnamurthy, H. Seo, I. Luz, M. Soukri, Y. ki Park, R. Blom, S. Amini, A. Zaabout, Sorbents screening for post-combustion CO_2 capture via combined temperature and pressure swing adsorption, Chemical Engineering Journal 380 (2020) 122201. https://doi.org/10.1016/j.cej.2019.122201.

[150] J. Schell, N. Casas, D. Marx, R. Blom, M. Mazzotti, Comparison of commercial and new adsorbent materials for pre-combustion CO_2 capture by pressure swing adsorption, in: Energy Procedia, 2013: pp. 167–174. https://doi.org/10.1016/j.egypro.2013.05.098.

[151] S. Cavenati, C.A. Grande, A.E. Rodrigues, Separation of CH_4 / CO_2 / N_2 mixtures by layered pressure swing adsorption for upgrade of natural gas, Chem Eng Sci 61 (2006) 3893–3906. https://doi.org/10.1016/j.ces.2006.01.023.

[152] V. Stampi-Bombelli, M. van der Spek, M. Mazzotti, Analysis of direct capture of CO_2 from ambient air via steam-assisted temperature–vacuum swing adsorption, Adsorption 26 (2020) 1183–1197. https://doi.org/10.1007/S10450-020-00249-W/TABLES/5.

[153] R. Zhao, L. Liu, L. Zhao, S. Deng, S. Li, Y. Zhang, H. Li, Thermodynamic exploration of temperature vacuum swing adsorption for direct air capture of carbon dioxide in buildings, Energy Convers Manag 183 (2019) 418–426. https://doi.org/10.1016/J.ENCONMAN.2019.01.009.

[154] D. Bahamon, L.F. Vega, Systematic evaluation of materials for post-combustion CO_2 capture in a Temperature Swing Adsorption process, Chemical Engineering Journal 284 (2016) 438–447. https://doi.org/10.1016/j.cej.2015.08.098.

[155] J.A. Mason, K. Sumida, Z.R. Herm, R. Krishna, J.R. Long, Evaluating metal-organic frameworks for post-combustion carbon dioxide capture via temperature swing adsorption, Energy Environ Sci 4 (2011) 3030–3040. https://doi.org/10.1039/c1ee01720a.

[156] S. Alafnan, A. Awotunde, G. Glatz, S. Adjei, I. Alrumaih, A. Gowida, Langmuir adsorption isotherm in unconventional resources: Applicability and limitations, J Pet Sci Eng 207 (2021) 109172. https://doi.org/10.1016/J.PETROL.2021.109172.

[157] M.P. Mudoi, P. Sharma, A.S. Khichi, A review of gas adsorption on shale and the influencing factors of CH_4 and CO_2 adsorption, J Pet Sci Eng 217 (2022) 110897. https://doi.org/10.1016/J.PETROL.2022.110897.

[158] B.B. Saha, S. Jribi, S. Koyama, I.I. El-Sharkawy, Carbon dioxide adsorption isotherms on activated carbons, J Chem Eng Data 56 (2011) 1974–1981. https://doi.org/10.1021/JE100973T/ASSET/IMAGES/LARGE/JE-2010-00973T_0001.JPEG.

[159] M. Mozaffari Majd, V. Kordzadeh-Kermani, V. Ghalandari, A. Askari, M. Sillanpää, Adsorption isotherm models: A comprehensive and systematic review (2010−2020), Science of The Total Environment 812 (2022) 151334. https://doi.org/10.1016/J.SCITOTENV.2021.151334.

[160] S. Fakher, A. Imqam, A review of carbon dioxide adsorption to unconventional shale rocks methodology, measurement, and calculation, SN Appl Sci 2 (2020) 1–14. https://doi.org/10.1007/S42452-019-1810-8/TABLES/6.

[161] Gautam, R.P. Sah, S. Sahoo, A review on adsorption isotherms and kinetics of CO_2 and various adsorbent pairs suitable for carbon capture and green refrigeration applications, Sādhanā 2023 48:1 48 (2023) 1–37. https://doi.org/10.1007/S12046-023-02080-9.

[162] M. Smyrnioti, C. Tampaxis, T. Steriotis, T. Ioannides, Study of CO_2 adsorption on a commercial CuO/ZnO/Al2O3 catalyst, Catal Today 357 (2020) 495–502. https://doi.org/10.1016/J.CATTOD.2019.07.024.

[163] C. Jin, J. Sun, Y. Chen, Y. Guo, D. Han, R. Wang, C. Zhao, Sawdust wastes-derived porous carbons for CO_2 adsorption. Part 1. Optimization preparation via orthogonal experiment, Sep Purif Technol 276 (2021) 119270. https://doi.org/10.1016/J.SEPPUR.2021.119270.

[164] K. Wang, G. Wang, T. Ren, Y. Cheng, Methane and CO_2 sorption hysteresis on coal: A critical review, Int J Coal Geol 132 (2014) 60–80. https://doi.org/10.1016/J.COAL.2014.08.004.

[165] S. Ullah, M.A. Bustam, A.G. Al-Sehemi, M.A. Assiri, F.A. Abdul Kareem, A. Mukhtar, M. Ayoub, G. Gonfa, Influence of post-synthetic graphene oxide (GO) functionalization on the selective CO_2/CH_4 adsorption behavior of MOF-200 at different temperatures; an experimental and adsorption isotherms study, Microporous and Mesoporous Materials 296 (2020) 110002. https://doi.org/10.1016/J.MICROMESO.2020.110002.

[166] A. Sarwar, M. Ali, A.H. Khoja, A. Nawar, A. Waqas, R. Liaquat, S.R. Naqvi, M. Asjid, Synthesis and characterization of biomass-derived surface-modified activated carbon for enhanced CO_2 adsorption, Journal of CO_2 Utilization 46 (2021) 101476. https://doi.org/10.1016/j.jcou.2021.101476.

[167] R. Melouki, A. Ouadah, P.L. Llewellyn, The CO_2 adsorption behavior study on activated carbon synthesized from olive waste, Journal of CO_2 Utilization 42 (2020) 101292. https://doi.org/10.1016/j.jcou.2020.101292.

[168] Y. Park, D.K. Moon, Y.H. Kim, H. Ahn, C.H. Lee, Adsorption isotherms of CO_2, CO, N_2, CH_4, Ar and H_2 on activated carbon and zeolite LiX up to 1.0 MPa, Adsorption 20 (2014) 631–647. https://doi.org/10.1007/s10450-014-9608-x.

[169] Z. Yong, V. Mata, A.E. Rodrigues, Adsorption of carbon dioxide at high temperature—a review, Sep Purif Technol 26 (2002) 195–205. https://doi.org/10.1016/S1383-5866(01)00165-4.

[170] L. Giraldo, J.C. Moreno-Piraján, Study of adsorption of phenol on activated carbons obtained from eggshells, J Anal Appl Pyrolysis 106 (2014) 41–47. https://doi.org/10.1016/J.JAAP.2013.12.007.

[171] S. Choi, J.H. Drese, C.W. Jones, Adsorbent Materials for Carbon Dioxide Capture from Large Anthropogenic Point Sources, ChemSusChem 2 (2009) 796–854. https://doi.org/10.1002/CSSC.200900036.

[172] S.R. Jeong, J.H. Park, J.H. Lee, P.R. Jeon, C.H. Lee, Review of the adsorption equilibria of CO_2, CH_4, and their mixture on coals and shales at high pressures for enhanced CH_4 recovery and CO_2 sequestration, Fluid Phase Equilib 564 (2023) 113591. https://doi.org/10.1016/J.FLUID.2022.113591.

[173] K. Imawaka, M. Sugita, T. Takewaki, S. Tanaka, Mechanochemical synthesis of bimetallic Co/Zn-ZIFs with sodalite structure, Polyhedron 158 (2019) 290–295. https://doi.org/10.1016/j.poly.2018.11.018.

[174] P. Brea, J.A. Delgado, V.I. Águeda, P. Gutiérrez, M.A. Uguina, Multicomponent adsorption of H_2, CH_4, CO and CO_2 in zeolites NaX, CaX and MgX. Evaluation of performance in PSA cycles for hydrogen purification, Microporous and Mesoporous Materials 286 (2019) 187–198. https://doi.org/10.1016/j.micromeso.2019.05.021.

[175] Y. Xiao, M. Zhou, G. He, Equilibrium and Diffusion of CO_2 Adsorption on Micro-Mesoporous NaX/MCM-41 via Molecular Simulation, Ind Eng Chem Res 58 (2019) 14380–14388. https://doi.org/10.1021/acs.iecr.9b02670.

[176] B. Sreenivasulu, I. Sreedhar, B.M. Reddy, K. V. Raghavan, Stability and carbon capture enhancement by coal-fly-ash-doped sorbents at a high temperature, Energy and Fuels 31 (2017) 785–794. https://doi.org/10.1021/acs.energyfuels.6b02721.

[177] T.M.A. Mokgehle, W.M. Gitari, N.T. Tavengwa, Synthesis and characterization of zeolites produced by ultrasonication of coal fly Ash/NaOH slurry filtrates, South African Journal of Chemistry 73 (2020) 64–69. https://doi.org/10.17159/0379-4350/2020/V73A10.

[178] C. Guan, S. Liu, C. Li, Y. Wang, Y. Zhao, The temperature effect on the methane and CO_2 adsorption capacities of Illinois coal, Fuel 211 (2018) 241–250. https://doi.org/10.1016/j.fuel.2017.09.046.

[179] V.N. Le, T.K. Vo, J.H. Lee, J.C. Kim, T.H. Kim, K.H. Oh, Y.S. Bae, S.K. Kwak, J. Kim, A novel approach to prepare Cu(I)Zn@MIL-100(Fe) adsorbent with high CO adsorption capacity, CO/CO_2 selectivity and stability via controlled host–guest redox reaction, Chemical Engineering Journal 404 (2021) 126492. https://doi.org/10.1016/j.cej.2020.126492.

[180] H. Kaur, G.C. Mohanta, V. Gupta, D. Kukkar, S. Tyagi, Synthesis and characterization of ZIF-8 nanoparticles for controlled release of 6-mercaptopurine drug, J Drug Deliv Sci Technol 41 (2017) 106–112. https://doi.org/10.1016/J.JDDST.2017.07.004.

[181] A. Sayari, Q. Liu, P. Mishra, Enhanced adsorption efficiency through materials design for direct air capture over supported polyethylenimine, ChemSusChem 9 (2016) 2796–2803. https://doi.org/10.1002/cssc.201600834.

[182] C. Jin, S. Zhang, Z. Zhang, Y. Chen, Mimic Carbonic Anhydrase Using Metal-Organic Frameworks for CO_2 Capture and Conversion, Inorg Chem 57 (2018) 2169–2174. https://doi.org/10.1021/acs.inorgchem.7b03021.

[183] K. Yang, G. Yang, J. Wu, Insights into the enhancement of CO_2 adsorption on faujasite with a low Si/Al ratio: Understanding the formation sequence of adsorption complexes, Chemical Engineering Journal 404 (2021) 127056. https://doi.org/10.1016/J.CEJ.2020.127056.

[184] A. Gholidoust, J.D. Atkinson, Z. Hashisho, Enhancing CO_2 Adsorption via Amine-Impregnated Activated Carbon from Oil Sands Coke, Energy and Fuels 31 (2017) 1756–1763. https://doi.org/10.1021/acs.energyfuels.6b02800.

[185] J.T. Anyanwu, Y. Wang, R.T. Yang, Amine-Grafted Silica Gels for CO_2 Capture including Direct Air Capture, Ind Eng Chem Res 59 (2020) 7072–7079. https://doi.org/10.1021/acs.iecr.9b05228.

[186] C. Song, Q. Liu, N. Ji, S. Deng, J. Zhao, Y. Li, Y. Song, H. Li, Alternative pathways for efficient CO_2 capture by hybrid processes—A review, Renewable and Sustainable Energy Reviews 82 (2018) 215–231. https://doi.org/10.1016/j.rser.2017.09.040.

[187] J. Hu, Y. Liu, J. Liu, C. Gu, Chelation of transition metals into MOFs as a promising method for enhancing CO_2 capture: A computational study, AIChE Journal 66 (2020). https://doi.org/10.1002/aic.16835.

[188] R. Aniruddha, I. Sreedhar, R. Parameshwaran, Valorization of alkaline hydroxide modified coal fly ash to efficient adsorbents for enhanced carbon capture, Mater Today Proc 72 (2023) 74–80. https://doi.org/10.1016/J.MATPR.2022.05.557.

[189] R. Aniruddha, I. Sreedhar, Process optimization for enhanced carbon capture and cyclic stability using adsorbents derived from coal fly ash, Environmental Science and Pollution Research 1 (2021) 1–10. https://doi.org/10.1007/s11356-021-17453-y.

[190] J. Yu, L.H. Xie, J.R. Li, Y. Ma, J.M. Seminario, P.B. Balbuena, CO_2 Capture and Separations Using MOFs: Computational and Experimental Studies, Chem Rev 117 (2017) 9674–9754. https://doi.org/10.1021/acs.chemrev.6b00626.

[191] F. Marpaung, T. Park, M. Kim, J.W. Yi, J. Lin, J. Wang, B. Ding, H. Lim, K. Konstantinov, Y. Yamauchi, J. Na, J. Kim, Gram-scale synthesis of bimetallic ZIFs and their thermal conversion to nanoporous carbon materials, Nanomaterials 9 (2019) 1796. https://doi.org/10.3390/nano9121796.

[192] J. Ethiraj, S. Palla, H. Reinsch, Insights into high pressure gas adsorption properties of ZIF-67: Experimental and theoretical studies, Microporous and Mesoporous Materials 294 (2020) 109867. https://doi.org/10.1016/j.micromeso.2019.109867.

[193] J. Pokhrel, N. Bhoria, S. Anastasiou, T. Tsoufis, D. Gournis, G. Romanos, G.N. Karanikolos, CO_2 adsorption behavior of amine-functionalized ZIF-8, graphene oxide, and ZIF-8/graphene oxide composites under dry and wet conditions, Microporous and Mesoporous Materials 267 (2018) 53–67. https://doi.org/10.1016/J.MICROMESO.2018.03.012.

[194] I.U. Khan, M.H.D. Othman, A.F. Ismail, N. Ismail, J. Jaafar, H. Hashim, M.A. Rahman, A. Jilani, Structural transition from two-dimensional ZIF-L to three-dimensional ZIF-8 nanoparticles in aqueous room temperature synthesis with improved CO_2 adsorption, Mater Charact 136 (2018) 407–416. https://doi.org/10.1016/j.matchar.2018.01.003.

[195] A. Thomas, M. Prakash, Tuning the CO_2 adsorption by the selection of suitable ionic liquids at ZIF-8 confinement: A DFT study, Appl Surf Sci 491 (2019) 633–639. https://doi.org/10.1016/j.apsusc.2019.06.130.

[196] R. Kumar, K. Jayaramulu, T.K. Maji, C.N.R. Rao, Hybrid nanocomposites of ZIF-8 with graphene oxide exhibiting tunable morphology, significant CO_2 uptake and other novel properties, Chemical Communications 49 (2013) 4947–4949. https://doi.org/10.1039/C3CC00136A.

[197] R. Aniruddha, V.M. Shama, I. Sreedhar, C.M. Patel, Bimetallic ZIFs based on Ce/Zn and Ce/Co combinations for stable and enhanced carbon capture, J Clean Prod 350 (2022) 131478. https://doi.org/10.1016/j.jclepro.2022.131478.

[198] L. Li, J. Yao, P. Xiao, J. Shang, Y. Feng, P.A. Webley, H. Wang, One-step fabrication of ZIF-8/polymer composite spheres by a phase inversion method for gas adsorption, Colloid Polym Sci 291 (2013) 2711–2717. https://doi.org/10.1007/S00396-013-3024-8/FIGURES/10.

[199] X. Xu, Y. Yang, L.P. Acencios Falcon, P. Hazewinkel, C.D. Wood, Carbon capture by DEA-infused hydrogels, International Journal of Greenhouse Gas Control 88 (2019) 226–232. https://doi.org/10.1016/j.ijggc.2019.06.005.

[200] M. Sarmah, B.P. Baruah, P. Khare, A comparison between CO_2 capturing capacities of fly ash based composites of MEA/DMA and DEA/DMA, Fuel Processing Technology 106 (2013) 490–497. https://doi.org/10.1016/j.fuproc.2012.09.017.

[201] N.A.H.M. Nordin, A.F. Ismail, N. Misdan, N.A.M. Nazri, Modified ZIF-8 mixed matrix membrane for CO_2/CH_4 separation, AIP Conf Proc 1891 (2017) 20129. https://doi.org/10.1063/1.5005424.

[202] J. Ouyang, W. Gu, C. Zheng, H. Yang, X. Zhang, Y. Jin, J. Chen, J. Jiang, Polyethyleneimine (PEI) loaded MgO-SiO_2 nanofibers from sepiolite minerals for reusable CO_2 capture/release applications, Appl Clay Sci 152 (2018) 267–275. https://doi.org/10.1016/j.clay.2017.11.023.

[203] W. Henao, L.Y. Jaramillo, D. López, M. Romero-Sáez, R. Buitrago-Sierra, Insights into the CO_2 capture over amine-functionalized mesoporous silica adsorbents derived from rice husk ash, J Environ Chem Eng 8 (2020). https://doi.org/10.1016/j.jece.2020.104362.

[204] V.I. Agueda, J.A. Delgado, M.A. Uguina, P. Brea, A.I. Spjelkavik, R. Blom, C. Grande, Adsorption and diffusion of H_2, N_2, CO, CH_4 and CO_2 in UTSA-16 metal-organic framework extrudates, Chem Eng Sci 124 (2015) 159–169. https://doi.org/10.1016/j.ces.2014.08.039.

[205] D.L. Chen, H. Shang, W. Zhu, R. Krishna, Transient breakthroughs of CO_2/CH_4 and C_3H_6/C_3H_8 mixtures in fixed beds packed with Ni-MOF-74, Chem Eng Sci 117 (2014) 407–415. https://doi.org/10.1016/j.ces.2014.07.008.

[206] M. Younas, M. Sohail, L.L. Kong, M.J.K. Bashir, S. Sethupathi, Feasibility of CO_2 adsorption by solid adsorbents: a review on low-temperature systems, International Journal of Environmental Science and Technology 13 (2016) 1839–1860. https://doi.org/10.1007/s13762-016-1008-1.

[207] K. Kenyotha, K.C. Chanapattharapol, S. McCloskey, P. Jantaharn, Water based synthesis of ZIF-8 assisted by hydrogen bond acceptors and enhancement of CO_2 uptake by

solvent assisted ligand exchange, Crystals (Basel) 10 (2020) 1–23. https://doi.org/10.3390/cryst10070599.

[208] S. Mukherjee, Akshay, A.N. Samanta, Amine-impregnated MCM-41 in post-combustion CO_2 capture: Synthesis, characterization, isotherm modelling, Advanced Powder Technology 30 (2019) 3231–3240. https://doi.org/10.1016/j.apt.2019.09.032.

[209] R. Banerjee, A. Phan, B. Wang, C. Knobler, H. Furukawa, M. O'Keeffe, O.M. Yaghi, High-throughput synthesis of zeolitic imidazolate frameworks and application to CO_2 capture, Science (1979) 319 (2008) 939–943. https://doi.org/10.1126/science.1152516.

[210] M. Konni, S. Doddi, A.S. Dadhich, S.B. Mukkamala, Adsorption of CO_2 by hierarchical structures of f-MWCNTs@Zn/Co-ZIF and N-MWCNTs@Zn/Co-ZIF prepared through in situ growth of ZIFs in CNTs, Surfaces and Interfaces 12 (2018) 20–25. https://doi.org/10.1016/j.surfin.2018.04.006.

[211] A. Ghaemi, A.H. Behroozi, Comparison of hydroxide-based adsorbents of $Mg(OH)_2$ and $Ca(OH)_2$ for CO_2 capture: utilization of response surface methodology, kinetic, and isotherm modeling, Greenhouse Gases: Science and Technology 10 (2020) 948–964. https://doi.org/10.1002/ghg.2015.

[212] I.M. Saeed, P. Alaba, S.A. Mazari, W.J. Basirun, V.S. Lee, N. Sabzoi, Opportunities and challenges in the development of monoethanolamine and its blends for post-combustion CO_2 capture, International Journal of Greenhouse Gas Control 79 (2018) 212–233. https://doi.org/10.1016/j.ijggc.2018.11.002.

[213] J. Kapica-Kozar, B. Michalkiewicz, R.J. Wrobel, S. Mozia, E. Piróg, E. Kusiak-Nejman, J. Serafin, A.W. Morawski, U. Narkiewicz, Adsorption of carbon dioxide on TEPA-modified TiO_2/titanate composite nanorods, New Journal of Chemistry 41 (2017) 7870–7885. https://doi.org/10.1039/c7nj01549f.

[214] H. Wang, D. Wu, C. Yang, H. Lu, Z. Gao, F. Xu, K. Jiang, Multi-functional amorphous TiO_2 layer on ZIF-67 for enhanced CO_2 photoreduction performances under visible light, Journal of CO_2 Utilization 34 (2019) 411–421. https://doi.org/10.1016/j.jcou.2019.07.011.

[215] B. Russell, A. Migone, Low temperature adsorption study of CO_2 in ZIF-8, Microporous and Mesoporous Materials 246 (2017) 178–185. https://doi.org/10.1016/j.micromeso.2017.03.030.

[216] B. Sreenivasulu, I. Sreedhar, B.M. Reddy, K. V. Raghavan, Stability and carbon capture enhancement by coal-fly-ash-doped sorbents at a high temperature, Energy and Fuels 31 (2017) 785–794. https://doi.org/10.1021/acs.energyfuels.6b02721.

[217] S. Venet, F. Plantier, C. Miqueu, A. Shahtalebi, R. Brown, T. Pigot, P. Bordat, CO_2 capture and CO_2/CH_4 separation by silicas with controlled porosity and functionality, Microporous and Mesoporous Materials 332 (2022) 111651. https://doi.org/10.1016/J.MICROMESO.2021.111651.

[218] H. Du, L. Ma, X. Liu, F. Zhang, X. Yang, Y. Wu, J. Zhang, A Novel Mesoporous SiO2 Material with MCM-41 Structure from Coal Gangue: Preparation, Ethylenediamine Modification, and Adsorption Properties for CO_2 Capture, Energy and Fuels 32 (2018) 5374–5385. https://doi.org/10.1021/acs.energyfuels.8b00318.

[219] M. Mohamedali, H. Ibrahim, A. Henni, Imidazolium based ionic liquids confined into mesoporous silica MCM-41 and SBA-15 for carbon dioxide capture, Microporous and Mesoporous Materials 294 (2020). https://doi.org/10.1016/j.micromeso.2019.109916.

[220] J. Chang, C. Hou, D. Wan, X. Zhang, B. Xu, H. Tian, X. Wang, Q. Guo, Enhanced CO_2 adsorption capacity of bi-amine co-tethered flue gas desulfurization gypsum with water

of hydration, Journal of CO_2 Utilization 35 (2020) 115–125. https://doi.org/10.1016/j.jcou.2019.09.009.

[221] W. Huang, J. Liu, N. Rao, G. Fan, J. Yan, Q. Cheng, G. Song, Influence of surfactant on CO_2 adsorption of amine-functionalized MCM-41, Environmental Technology (United Kingdom) (2021). https://doi.org/10.1080/09593330.2021.1958012.

[222] S. Kayal, A. Chakraborty, Activated carbon (type Maxsorb-III) and MIL-101(Cr) metal organic framework based composite adsorbent for higher CH_4 storage and CO_2 capture, Chemical Engineering Journal 334 (2018) 780–788. https://doi.org/10.1016/J.CEJ.2017.10.080.

[223] A.L. Yaumi, M.Z.A. Bakar, B.H. Hameed, Melamine-nitrogenated mesoporous activated carbon derived from rice husk for carbon dioxide adsorption in fixed-bed, Energy 155 (2018) 46–55. https://doi.org/10.1016/J.ENERGY.2018.04.183.

[224] G.G. Huang, Y.F. Liu, X.X. Wu, J.J. Cai, Activated carbons prepared by the KOH activation of a hydrochar from garlic peel and their CO_2 adsorption performance, New Carbon Materials 34 (2019) 247–257. https://doi.org/10.1016/S1872-5805(19)60014-4.

[225] Y. Guo, C. Tan, J. Sun, W. Li, J. Zhang, C. Zhao, Porous activated carbons derived from waste sugarcane bagasse for CO_2 adsorption, Chemical Engineering Journal 381 (2020) 122736. https://doi.org/10.1016/j.cej.2019.122736.

[226] A.E. Ogungbenro, D. V. Quang, K.A. Al-Ali, L.F. Vega, M.R.M. Abu-Zahra, Physical synthesis and characterization of activated carbon from date seeds for CO_2 capture, J Environ Chem Eng 6 (2018) 4245–4252. https://doi.org/10.1016/j.jece.2018.06.030.

[227] N.P. Wickramaratne, M. Jaroniec, Activated carbon spheres for CO_2 adsorption, ACS Appl Mater Interfaces 5 (2013) 1849–1855. https://doi.org/10.1021/AM400112M/SUPPL_FILE/AM400112M_SI_001.PDF.

[228] J.A.S. Costa, R.A. de Jesus, D.O. Santos, J.F. Mano, L.P.C. Romão, C.M. Paranhos, Recent progresses in the adsorption of organic, inorganic, and gas compounds by MCM-41-based mesoporous materials, Microporous and Mesoporous Materials 291 (2020) 109698. https://doi.org/10.1016/j.micromeso.2019.109698.

[229] S. Loganathan, M. Tikmani, A.K. Ghoshal, Novel pore-expanded MCM-41 for CO_2 capture: Synthesis and characterization, Langmuir 29 (2013) 3491–3499. https://doi.org/10.1021/la400109j.

[230] N. Rao, M. Wang, Z. Shang, Y. Hou, G. Fan, J. Li, CO_2 Adsorption by Amine-Functionalized MCM-41: A Comparison between Impregnation and Grafting Modification Methods, Energy and Fuels 32 (2018) 670–677. https://doi.org/10.1021/acs.energyfuels.7b02906.

[231] C. Zhou, S. Yu, K. Ma, B. Liang, S. Tang, C. Liu, H. Yue, Amine-functionalized mesoporous monolithic adsorbents for post-combustion carbon dioxide capture, Chemical Engineering Journal 413 (2021) 127675. https://doi.org/10.1016/j.cej.2020.127675.

[232] W. Huang, J. Liu, N. Rao, G. Fan, J. Yan, Q. Cheng, G. Song, Influence of surfactant on CO_2 adsorption of amine-functionalized MCM-41, Environmental Technology (United Kingdom) (2021). https://doi.org/10.1080/09593330.2021.1958012.

[233] M. Sari Yilmaz, The CO_2 adsorption performance of aminosilane-modified mesoporous silicas, J Therm Anal Calorim 146 (2021) 2241–2251. https://doi.org/10.1007/s10973-020-10417-3.

[234] H.I. Meléndez-Ortiz, L.A. García-Cerda, Y. Olivares-Maldonado, G. Castruita, J.A. Mercado-Silva, Y.A. Perera-Mercado, Preparation of spherical MCM-41 molecular sieve at room temperature: Influence of the synthesis conditions in the structural properties, Ceram Int 38 (2012) 6353–6358. https://doi.org/10.1016/j.ceramint.2012.05.007.

[235] N.A.H.M. Nordin, A.F. Ismail, A. Mustafa, P.S. Goh, D. Rana, T. Matsuura, Aqueous room temperature synthesis of zeolitic imidazole framework 8 (ZIF-8) with various concentrations of triethylamine, RSC Adv 4 (2014) 33292–33300. https://doi.org/10.1039/c4ra03593c.

[236] H. Kaur, G.C. Mohanta, V. Gupta, D. Kukkar, S. Tyagi, Synthesis and characterization of ZIF-8 nanoparticles for controlled release of 6-mercaptopurine drug, J Drug Deliv Sci Technol 41 (2017) 106–112. https://doi.org/10.1016/j.jddst.2017.07.004.

[237] D. Li, J. Zhou, Y. Wang, Y. Tian, L. Wei, Z. Zhang, Y. Qiao, J. Li, Effects of activation temperature on densities and volumetric CO_2 adsorption performance of alkali-activated carbons, Fuel 238 (2019) 232–239. https://doi.org/10.1016/j.fuel.2018.10.122.

[238] S.M.W. Wilson, F. Al-Enzi, V.A. Gabriel, F.H. Tezel, Effect of pore size and heterogeneous surface on the adsorption of CO_2, N_2, O_2, and Ar on carbon aerogel, RF aerogel, and activated carbons, Microporous and Mesoporous Materials 322 (2021) 111089. https://doi.org/10.1016/j.micromeso.2021.111089.

[239] S. Ahmed, A. Ramli, S. Yusup, M. Farooq, Adsorption behavior of tetraethylenepentamine-functionalized Si-MCM-41 for CO_2 adsorption, Chemical Engineering Research and Design 122 (2017) 33–42. https://doi.org/10.1016/j.cherd.2017.04.004.

[240] D. Liu, Y. Wu, Q. Xia, Z. Li, H. Xi, Experimental and molecular simulation studies of CO_2 adsorption on zeolitic imidazolate frameworks: ZIF-8 and amine-modified ZIF-8, Adsorption 19 (2013) 25–37. https://doi.org/10.1007/s10450-012-9407-1.

[241] J. Sun, C. Chen, Y. Zhang, W. Li, Y. Song, Competitive adsorption characteristics based on partial pressure and adsorption mechanism of CO_2/CH_4 mixture in shale pores, Chemical Engineering Journal 430 (2022) 133172. https://doi.org/10.1016/j.cej.2021.133172.

[242] H.A. Patel, J. Byun, C.T. Yavuz, Carbon Dioxide Capture Adsorbents: Chemistry and Methods, ChemSusChem 10 (2017) 1303–1317. https://doi.org/10.1002/cssc.201601545.

[243] M. Fischer, R.G. Bell, Interaction of hydrogen and carbon dioxide with sod-type zeolitic imidazolate frameworks: A periodic DFT-D study, CrystEngComm 16 (2014) 1934–1949. https://doi.org/10.1039/c3ce42209g.

[244] T.C. Dos Santos, S. Bourrelly, P.L. Llewellyn, J.W.D.M. Carneiro, C.M. Ronconi, Adsorption of CO_2 on amine-functionalised MCM-41: Experimental and theoretical studies, Physical Chemistry Chemical Physics 17 (2015) 11095–11102. https://doi.org/10.1039/c5cp00581g.

[245] G.A. Mutch, S. Shulda, A.J. McCue, M.J. Menart, C. V. Ciobanu, C. Ngo, J.A. Anderson, R.M. Richards, D. Vega-Maza, Carbon Capture by Metal Oxides: Unleashing the Potential of the (111) Facet, J Am Chem Soc 140 (2018) 4736–4742. https://doi.org/10.1021/jacs.8b01845.

[246] M. Karimi, J.A.C. Silva, C.N.D.P. Gonçalves, J.L. Diaz De Tuesta, A.E. Rodrigues, H.T. Gomes, CO_2 Capture in Chemically and Thermally Modified Activated Carbons Using

Breakthrough Measurements: Experimental and Modeling Study, Ind Eng Chem Res 57 (2018) 11154–11166. https://doi.org/10.1021/acs.iecr.8b00953.

[247] C. Wang, R. Yang, H. Wang, Synthesis of ZIF-8/Fly ash composite for adsorption of Cu^{2+}, Zn^{2+} and Ni^{2+} from aqueous solutions, Materials 13 (2020). https://doi.org/10.3390/ma13010214.

[248] M. Jahandar Lashaki, H. Ziaei-Azad, A. Sayari, Insights into the Hydrothermal Stability of Triamine-Functionalized SBA-15 Silica for CO_2 Adsorption, ChemSusChem 10 (2017) 4037–4045. https://doi.org/10.1002/cssc.201701439.

[249] M.P. Suh, H.J. Park, T.K. Prasad, D.W. Lim, Hydrogen storage in metal-organic frameworks, Chem Rev 112 (2012) 782–835. https://doi.org/10.1021/cr200274s.

[250] H. Tan, Q. Chen, T. Chen, Z. Wei, H. Liu, CO_2/CH_4 separation using flexible microporous organic polymers with expansion/shrinkage transformations during adsorption/desorption processes, Chemical Engineering Journal 391 (2020) 123521. https://doi.org/10.1016/j.cej.2019.123521.

[251] M. Pardakhti, T. Jafari, Z. Tobin, B. Dutta, E. Moharreri, N.S. Shemshaki, S. Suib, R. Srivastava, Trends in Solid Adsorbent Materials Development for CO_2 Capture, ACS Appl Mater Interfaces 11 (2019) 34533–34559. https://doi.org/10.1021/acsami.9b08487.

[252] L. Valencia, H.N. Abdelhamid, Nanocellulose leaf-like zeolitic imidazolate framework (ZIF-L) foams for selective capture of carbon dioxide, Carbohydr Polym 213 (2019) 338–345. https://doi.org/10.1016/j.carbpol.2019.03.011.

[253] J.F. Saldarriaga, R. Aguado, A. Pablos, M. Amutio, M. Olazar, J. Bilbao, Fast characterization of biomass fuels by thermogravimetric analysis (TGA), Fuel 140 (2015) 744–751. https://doi.org/10.1016/J.FUEL.2014.10.024.

[254] J. Wang, S. Cui, Z. Li, S. Wen, P. Ning, S. Lu, P. Lu, L. Huang, Q. Wang, Comprehensive investigation of dynamic CO_2 capture performance using Mg/DOBDC as precursor to fabricate a composite of metallic organic framework and graphene oxide, Chemical Engineering Journal 415 (2021) 128859. https://doi.org/10.1016/j.cej.2021.128859.

[255] C.W. Chang, Y.H. Kao, P.H. Shen, P.C. Kang, C.Y. Wang, Nanoconfinement of metal oxide MgO and ZnO in zeolitic imidazolate framework ZIF-8 for CO_2 adsorption and regeneration, J Hazard Mater 400 (2020) 122974. https://doi.org/10.1016/J.JHAZMAT.2020.122974.

[256] N.E. Tari, A. Tadjarodi, J. Tamnanloo, S. Fatemi, One pot microwave synthesis of MCM-41/Cu based MOF composite with improved CO_2 adsorption and selectivity, Microporous and Mesoporous Materials 231 (2016) 154–162. https://doi.org/10.1016/j.micromeso.2016.05.027.

[257] E. Grabias-Blicharz, R. Panek, M. Franus, W. Franus, Mechanochemically Assisted Coal Fly Ash Conversion into Zeolite, Materials 2022, Vol. 15, Page 7174 15 (2022) 7174. https://doi.org/10.3390/MA15207174.

[258] Z. Zhang, S. Xian, H. Xi, H. Wang, Z. Li, Improvement of CO_2 adsorption on ZIF-8 crystals modified by enhancing basicity of surface, Chem Eng Sci 66 (2011) 4878–4888. https://doi.org/10.1016/j.ces.2011.06.051.

[259] R. V. Siriwardane, M.S. Shen, E.P. Fisher, J. Losch, Adsorption of CO_2 on zeolites at moderate temperatures, Energy and Fuels 19 (2005) 1153–1159. https://doi.org/10.1021/ef040059h.

[260] Y. Wang, T. Du, H. Jia, Z. Qiu, Y. Song, Synthesis, characterization and CO_2 adsorption of NaA, NaX and NaZSM-5 from rice husk ash, Solid State Sci 86 (2018) 24–33. https://doi.org/10.1016/J.SOLIDSTATESCIENCES.2018.10.003.

[261] O. Cheung, Z. Bacsik, Q. Liu, A. Mace, N. Hedin, Adsorption kinetics for CO_2 on highly selective zeolites NaKA and nano-NaKA, Appl Energy 112 (2013) 1326–1336. https://doi.org/10.1016/J.APENERGY.2013.01.017.

[262] H. Ramezanipour Penchah, A. Ghaemi, H. Ganadzadeh Gilani, Benzene-Based Hyper-Cross-Linked Polymer with Enhanced Adsorption Capacity for CO_2 Capture, Energy and Fuels (2019). https://doi.org/10.1021/acs.energyfuels.9b03136.

[263] F.S. Taheri, A. Ghaemi, A. Maleki, High Efficiency and Eco-Friendly TEPA-Functionalized Adsorbent with Enhanced Porosity for CO_2 Capture, Energy and Fuels33 (2019)11465–11476. https://doi.org/10.1021/ACS.ENERGYFUELS.9B02636/ASSET/IMAGES/LARGE/EF9B02636_0008.JPEG.

[264] S. Li, S. Jia, T. Nagasaka, H. Bai, L. Yang, CO_2 Adsorption Properties of Amine-Modified Zeolites Synthesized Using Different Types of Solid Waste, Sustainability 15 (2023) 10144. https://doi.org/10.3390/SU151310144/S1.

[265] P. Zhao, G. Zhang, Y. Xu, Y. Lv, Amine functionalized hierarchical bimodal mesoporous silicas as a promising nanocomposite for highly efficient CO_2 capture, Journal of CO_2 Utilization 34 (2019) 543–557. https://doi.org/10.1016/J.JCOU.2019.08.001.

[266] Q. Liu, Y. Ding, Q. Liao, X. Zhu, H. Wang, J. Yang, Fast synthesis of Al fumarate metal-organic framework as a novel tetraethylenepentamine support for efficient CO_2 capture, Colloids Surf A Physicochem Eng Asp 579 (2019) 123645. https://doi.org/10.1016/J.COLSURFA.2019.123645.

[267] G. Zhang, P. Zhao, Y. Xu, Development of amine-functionalized hierarchically porous silica for CO_2 capture, Journal of Industrial and Engineering Chemistry 54 (2017) 59–68. https://doi.org/10.1016/J.JIEC.2017.05.018.

[268] M. Irani, A.T. Jacobson, K.A.M. Gasem, M. Fan, Modified carbon nanotubes/tetraethylenepentamine for CO_2 capture, Fuel 206 (2017) 10–18. https://doi.org/10.1016/J.FUEL.2017.05.087.

[269] B. Russell, A. Migone, Low temperature adsorption study of CO_2 in ZIF-8, Microporous and Mesoporous Materials 246 (2017) 178–185. https://doi.org/10.1016/j.micromeso.2017.03.030.

[270] Y. Abdoli, M. Razavian, S. Fatemi, Bimetallic Ni–Co-based metal–organic framework: An open metal site adsorbent for enhancing CO_2 capture, Appl Organomet Chem 33 (2019) e5004. https://doi.org/10.1002/aoc.5004.

[271] R. Zou, P.Z. Li, Y.F. Zeng, J. Liu, R. Zhao, H. Duan, Z. Luo, J.G. Wang, R. Zou, Y. Zhao, Bimetallic Metal-Organic Frameworks: Probing the Lewis Acid Site for CO_2 Conversion, Small 12 (2016) 2334–2343. https://doi.org/10.1002/smll.201503741.

[272] A.A. Iordanidis, P.N. Kechagiopoulos, S.S. Voutetakis, A.A. Lemonidou, I.A. Vasalos, Autothermal sorption-enhanced steam reforming of bio-oil/biogas mixture and energy generation by fuel cells: Concept analysis and process simulation, Int J Hydrogen Energy 31 (2006) 1058–1065. https://doi.org/10.1016/j.ijhydene.2005.10.003.

[273] S. Alam, N. Lingaiah, Y. Soujanya, C. Sumana, Intensified chemical looping reforming processes with in-situ CO2 capture for high purity H_2 production from non-fuel grade bioethanol, Chemical Engineering and Processing - Process Intensification 171 (2022) 108733. https://doi.org/10.1016/j.cep.2021.108733.

[274] B. Dou, K. Wang, B. Jiang, Y. Song, C. Zhang, H. Chen, Y. Xu, Fluidized-bed gasification combined continuous sorption-enhanced steam reforming system to continuous hydrogen production from waste plastic, Int J Hydrogen Energy 41 (2016) 3803–3810. https://doi.org/10.1016/J.IJHYDENE.2015.12.197.

[275] I. Martínez, G. Grasa, J. Meyer, L. Di Felice, S. Kazi, C. Sanz, D. Maury, C. Voisin, Performance and operating limits of a sorbent-catalyst system for sorption-enhanced reforming (SER) in a fluidized bed reactor, Chem Eng Sci 205 (2019) 94–105. https://doi.org/10.1016/J.CES.2019.04.029.

[276] B. Arstad, J. Prostak, R. Blom, Continuous hydrogen production by sorption enhanced steam methane reforming (SE-SMR) in a circulating fluidized bed reactor: Sorbent to catalyst ratio dependencies, Chemical Engineering Journal 189–190 (2012) 413–421. https://doi.org/10.1016/J.CEJ.2012.02.057.

[277] M. Thomas, B.N. Nair, G.M. Anilkumar, A.P. Mohamed, K.G.K. Warrier, U.S. Hareesh, Processing of thermally stable 3D hierarchical ZIF-8@ZnO structures and their CO_2 adsorption studies, J Environ Chem Eng 4 (2016) 1442–1450. https://doi.org/10.1016/j.jece.2016.01.043.

[278] L. Chen, H.F. Wang, C. Li, Q. Xu, Bimetallic metal-organic frameworks and their derivatives, Chem Sci 11 (2020) 5369–5403. https://doi.org/10.1039/d0sc01432j.

[279] X. He, D.R. Chen, W.N. Wang, Bimetallic metal-organic frameworks (MOFs) synthesized using the spray method for tunable CO_2 adsorption, Chemical Engineering Journal 382 (2020) 122825. https://doi.org/10.1016/j.cej.2019.122825.

[280] S.M.W. Wilson, The potential of direct air capture using adsorbents in cold climates, IScience 25 (2022) 105564. https://doi.org/10.1016/J.ISCI.2022.105564.

[281] T. Deschamps, M. Kanniche, L. Grandjean, O. Authier, Modeling of Vacuum Temperature Swing Adsorption for Direct Air Capture Using Aspen Adsorption, Clean Technologies 2022, Vol. 4, Pages 258-275 4 (2022) 258–275. https://doi.org/10.3390/CLEANTECHNOL4020015.

[282] J. Elfving, C. Bajamundi, J. Kauppinen, T. Sainio, Modelling of equilibrium working capacity of PSA, TSA and TVSA processes for CO_2 adsorption under direct air capture conditions, Journal of CO_2 Utilization 22 (2017) 270–277. https://doi.org/10.1016/J.JCOU.2017.10.010.

List of publications

- **R. Aniruddha**, I. Sreedhar, B.M. Reddy, MOFs in carbon capture-past, present and future, Journal of CO_2 Utilization. 42 (2020) 101297. https://doi.org/10.1016/j.jcou.2020.101297.
- **R. Aniruddha**, V.M. Shama, I. Sreedhar, C.M. Patel, Bimetallic ZIFs based on Ce/Zn and Ce/Co combinations for stable and enhanced carbon capture, J Clean Prod. 350 (2022) 131478. https://doi.org/10.1016/j.jclepro.2022.131478.
- **R. Aniruddha**, S.A. Singh, B.M. Reddy, I. Sreedhar, Sorption enhanced reforming: A potential route to produce pure H_2 with in-situ carbon capture, Fuel. 351 (2023) 128925. https://doi.org/10.1016/J.FUEL.2023.128925.
- **R. Aniruddha**, I. Sreedhar, B.M. Reddy, Enhanced carbon capture and stability using novel hetero-scale composites based on MCM-41, Journal of CO_2 Utilization. 64 (2022) 102182. https://doi.org/10.1016/J.JCOU.2022.102182.
- **R. Aniruddha**, I. Sreedhar, Process optimization for enhanced carbon capture and cyclic stability using adsorbents derived from coal fly ash, Environmental Science and Pollution Research. 1 (2021) 1–10. https://doi.org/10.1007/s11356-021-17453-y.
- V.M. Shama, A.R. Swami, **R. Aniruddha**, I. Sreedhar, B.M. Reddy, Process and engineering aspects of carbon capture by ionic liquids, Journal of CO_2 Utilization. 48 (2021) 101507. https://doi.org/10.1016/j.jcou.2021.101507.
- **R. Aniruddha**, I. Sreedhar, R. Parameshwaran, Valorization of alkaline hydroxide modified coal fly ash to efficient adsorbents for enhanced carbon capture, Mater Today Proc. 72 (2023) 74–80. https://doi.org/10.1016/J.MATPR.2022.05.557.
- R. Aniruddha, I. Sreedhar, A comprehensive study using novel Coal fly ash-ZIF composites for enhanced and stable carbon capture, Separation and Purification Technology (submitted).

Biographies

Biography of student

Aniruddha Ramadurgam is a chemical engineer who attended SASTRA University in TN from 2011 to 2015 and graduated with a Bachelors degree in 2015. In between the duration of 2015–2017, he attended the BITS Pilani Hyderabad Campus to obtain his Masters degree in chemical engineering. He also worked for a CSIR sponsored project for three years from 2019 to 2022 under the supervision of Prof. I. Sreedhar (Scheme: 22(0783)/19/EMR-II). Aniruddha has been able to publish his works in journals that have a high degree of influence and impact factors, such as the Journal of Cleaner Production, Fuel and Journal of CO_2 Utilization. He has a total of 7 publications in the field of CO_2 capture.

Biography of supervisor

Prof. I. Sreedhar has done B.Tech in Chemical Engineering from R.E.C Warangal (Merit Scholarship), M.Tech from IIT Delhi and Ph.D from BITS Pilani. He has more than 25 years of experience in industry, academics and research. He has 82 high impact international journal publications, 4 book chapters, 1 patent, 55 conference proceedings besides a research funding of nearly 2 crores from various agencies. He has been elected as a Fellow of Telangana Academy of Sciences, Fellow of Royal Society of Chemistry, Fellow of Institute of Engineers India and a Life member of IIChE. He featured in Top 2% of World's Top Scientists as per the data curated by the Stanford University in 2021 and 2022. Ten scholars have done or are pursuing PhD under his guidance besides many ME dissertations, BE Theses and projects.